Stimulating Angiogenesis into Biomaterials through the Delivery of Growth Factors

Christian A.P. Schmidt, MD
Student number: SCHCHR 031

SUBMITTED TO THE UNIVERSITY OF CAPE TOWN

In fulfilment of the requirements for the degree
Doctor of Philosophy (Medicine)

Faculty of Health Sciences
UNIVERSITY OF CAPE TOWN

February, 2007

Supervisor: Neil H. Davies, PhD

Cardiovascular Research Unit, University of Cape Town,
South Africa

Declaration

I, Dr. Christian Alexander Peter Schmidt, hereby declare that the work on which this thesis is based is my original work (except where acknowledgements indicate otherwise) and that neither the whole work nor any part of it has been, is being, or is to be submitted for another degree in this or any other university.

I empower the University of Cape Town to reproduce for the purpose of research either the whole or any portion of the contents in any manner whatsoever.

Signed by candidate

Signature: ....

Date: 07/02/2007

Acknowledgements

It is with great pleasure that I acknowledge the support of a number of people whithout whom this thesis would not have been possible. Firstly, I would like to thank my supervisor and biology group leader Dr. Neil Davies for his generous intellectual and administrative support of my thesis, for his patience and openness for numerous discussions. Secondly, I would like to thank Prof. Zilla as Director of the Cardiovascular Reasearch Unit of the University of Cape Town. Through him I learned that even in today's struggle of many medical doctors to combine clinical work and scientific research, hard work, a clear vision and plenty of challenging ideas ultimately lead the way to success. Dr. Deon Bezuidenhout and his group of polymer scientists is thanked for the excellent collaboration between the technical specialists and us "biologists" which clearly demonstrated interaction of modern groups dealing with tissue engineering and regeneration. This is definetly a win-win situation. Furthermore, I would like to thank Dr. Paul Human as Deputy Director of the Cardiovascular Research Unit for his constant advisory support regarding any questions about the computational equipment and statistics as well as Dr. Thomas Franz as leader of the Finite Element Modelling group for becoming a working collegue and a true friend. Noel Markgraf and Raymond Michaels are thanked for their excellent help with all the animal work involved in this thesis as are all the other staff members of the Cardiovascular Research Unit for their warm welcome and friendly integration. Financial support is acknowleged from Medtronic Inc., Minneapolis, USA, which enabled me to spend this wonderful time in Cape Town and to present my scientific findings overseas. Finally I would like to thank my wife Sabine and my children Janina, Timo and Adrian for their emotional support and their enthusiasm throughout the years.

Table of Contents

List of Figures

List of Tables

Publications arising from this work

Papers

1. AAV transduction of wound cells via slow release fibrin matrix
   Christian Schmidt, Neil Davies, Peter Zilla
   In preparation

2. Heparin-coating of porous polyurethane increases angiogenesis
   Deon Bezuidenhout, Lawrence Higham, Neil Davies, Christian Schmidt, Peter Zilla
   In preparation

3. Surface bound $VEGF_{165}$ and PDGF-BB increase angiogenesis in vivo
   Neil Davies, Christian Schmidt, Deon Bezuidenhout, Lawrence Higham, PeterZilla
   In preparation

4. Hypoxia negates heparin-augmented angiogenesis: a counter- intuitive finding in porous synthetic implants
   Christian Schmidt, Neil Davies, Deon Bezuidenhout, Lawrence Higham, Peter Zilla
   In preparation

5. Sustained growth factor delivery into a synthetic polymer via osmotic pumps - a novel model to study angiogenesis
   Neil Davies, Christian Schmidt, PeterZilla, Deon Bezuidenhout
   In preparation

6. Quantification of functional neovascularisation in a porous scaffold by micro-CT, lectin perfusion, CD31 and corrosion casting
   Christian Schmidt, Mike Beck, Liz van der Merwe,
   Deon Bezuidenhout, Peter Zilla, Neil Davies
   In preparation

Published Abstracts

1. Investigations into vascular cell mobility under normoxic and hypoxic conditions"
   Christian Schmidt, Matthias Fittkau, Peter Zilla and Neil Davies
   South African Journal of Surgery, 2004 Volume 42 No.1, p 21-22

2. DNA delivery from fibrin matrices
   Christian Schmidt, Neil Davies and Peter Zilla
   South African Journal of Surgery, 2004 Volume 42 No.1, p 22

3. Matrix delivered adeno- associated virus – an update
   Christian Schmidt, Neil Davies and Peter Zilla
   South African Journal of Surgery, 2004 Volume 42 No.2, p 67

Abstract

Ischemic disease in form of ischemic heart disease (IHD), ischemic stroke and peripheral arterial disease (PAD) due to atherosclerosis represents a massive clinical and economic burden to healthcare and is currently the number one cause of death in the world. Treatment modalities for peripheral arterial disease include bypass surgery involving autologous vein or synthetic materials such as ePTFE. Long term patency of small diameter vascular grafts used for infra-inguinal reconstructions, however, is below 50 % 5 years after implantation. Therefore, novel vascular graft concepts and materials are needed. The concept of transmural in vivo endothelialisation of vascular grafts holds great promise for increasing long term patency. To achieve complete luminal endothelial cell coverage and optimal integration of the porous synthetic graft material into the host tissue, transmural ingrowth of tissue and vasa vasorum might have to be facilitated. Since $VEGF_{165}$ and PDGF-BB are growth factors known to stimulate and consolidate angiogenesis, this PhD thesis hypothesized, that neovascularisation of porous polyurethane (PU) can be increased by delivery of vascular endothelial growth factor ($VEGF_{165}$) and platelet derived growth factor (PDGF-BB). To prove this hypothesis, subcutaneous implantation of PU discs was established as a valid, reproducible, relatively simple and quantifiable neovascularisation model. Three different ways of growth factor delivery were investigated. The gene encoding for human $VEGF_{165}$ was cloned into the genome of adeno associated viruses (AAV), which served as a vector for gene transduction of autologous wound healing cells in vivo using the "Gene Activated Matrix" approach. Genetically modified matrix embedded AAV-$VEGF_{165}$ was loaded into porous PU and transduced autologous ingrowing wound cells. In contrast to the excellent transduction efficiency in myocytes, AAV showed a poor tropism for wound healing cells. The second approach to increase neovascularisation into porous PU was the surface modification of PU by covalent attachment of nitrous acid degraded heparin. Neovascularisation into the biomaterial was increased by 77 % after 10 days of subcutaneous implantation. Since certain angiogenic growth factors show a high affinity for heparin, additional loading of heparin surface modified PU with $VEGF_{165}$ increased neovascularisation even further up to 115 % at 10 days compared to control. Dual growth factor delivery of $VEGF_{165}$ and PDGF-BB not only initiated increased vascularisation of porous PU, but also created a stable vascular network 2 months after implantation. In contrast, PU loaded with $VEGF_{165}$ alone showed regression of total vascular area of 61 % compared to vascular area at 10

days. Thirdly, to study the effects of controlled, prolonged growth factor delivery, a "Neovascularisation Construct" was developed which was implanted subcutaneously in rats. The construct consisted of an osmotic mini pump and a tube of porous PU lined with ePTFE, into which a defined amount of $VEGF_{165}$ was pumped for 10 days. After implantation, granulation tissue was growing into the pores of the PU and neovascular area was increased up to 265 % compared to PBS control. Furthermore, using different growth factor concentration, a dose dependency was shown. In addition, this thesis investigated the functional perfusion of the micro vascular network growing into PU by four different vascular quantification techniques. Intravital perfusion with biotinylated lycopersicon esculentum followed by microscopical analysis, vascular corrosion casting quantified by scanning electron microscopy as well as the novel micro-CT analysis of silicone rubber perfused vessels were compared to conventional immunhistochemical analysis of endothelial cells by CD31. Interestingly, PBS perfused "Neovascularisation Constructs" showed a relatively poor perfusion; therefore CD31 immunohistochemistry "overestimated" functional neovascularisation 3 fold. All perfusion techniques indicated a strong effect of $VEGF_{165}$ delivery on vessel perfusion (10 to 20 fold increases of vascular area and volume compared to PBS control). Micro-CT scanning was shown to be an excellent tool to study micro vascular networks in a three dimensional fashion across the whole length of the sample in a limited amount of time and to provide reliable and reproducible data on vessel density, vascular volume, and connectivity. Since resolution is still limited today to about 10 µm using a commercially available bench top scanner, this new technology still needs to be complemented by immunhistochemistry and perfusion studies such as lectin perfusion and corrosion casting.

In summary, the induction of neovascularisation was achieved by heparin surface modification alone, which was even increased through additional delivery of growth factors into the biomaterial PU. The development of a stable micro vascular network at 2 months was achieved and the functionality was shown using four different, independent techniques including the novel micro-CT scanning of neovascularisation into biomaterials.

Towards the development of an in vivo, spontaneously and transmurally endothelialising vascular graft with superior long term patency further investigations are necessary. As an initial step, increased spontaneous neovascularisation of the possible graft material polyurethane was achieved. Future steps are clearly indicated to study the translation of increased neovascularisation of the biomaterial polyurethane towards increased endothelialisation in a vascular graft model.

Abbreviations

AAV	adeno associated virus
AAV-RC	adeno associated virus-repliction and capsid genes
aFGF	acidic fibroblast growth factor
AKT	protein kinase B
Ang-1	angiopoetin-1
AP	akaline phosphatase
ATCC	American Type Culture Collection
bFGF	basic fibroblast growth factor
BrdU	bromodeoxyuridine
BSA	bovine serum albumine
BW	body weight
CABG	coronary artery bypass graft
CAM	chorioallantoic membrane
CFD	computational fluid dynamics
CHO	chinese hamster ovary cells
CD	cluster of differentiation molecule
CO_2	carbon dioxide
cDNA	complementary desoxyribonucleic acid
cs	cross section
CT	computertomography
DAPI	4'-6-diamidino-2-phenylindole
DMEM	Dublecco`s modified Eagle`s medium
DMF	dimethyformamide
ds	double stranded
ECM	extracellular matrix
EDA	ethylenediamine acid
EDCI	ethylcarbodiimide hydrochloride
EDTA	ethylenediaminetetraacetic acid
EGF	epidermal growth factor
ELISA	Enzyme Linked Immunosorbent Assay
eNOS	endothelial nitric oxide synthase
EPC	endothelial progenitor cell
ePTFE	expanded poly-tetra-fluoroethylene
FACS	fluorescence-activated cell sorter

FCS	fetal calf serum
FDA	US Food and Drug Administration
FGF	fibroblast growth factor
FITC	fluorescein isothiocyanate
g	gram
GAM	gene activated matrix
GFP	green fluorescent protein
GM-CSF	granulocyte-monocyte colony-stimulating factor
GOI	genes of interest
gc	genome copies
HB-EGF	heparin binding epidermal growth factor-like growth factor
HCl	hydrochloric acid
H&E	hematoxylin and eosin
H-DMEM	HEPES buffered Dublecco`s modified Eagle`s medium
HEMA	hydroxyethylmethacrylate
HEK 293	human embryonic kidney cells
HGF	hepatocyte growth factor
HIF	hypoxia inducible factor
HSC	hematopoietic stem cells
HS-GAG´s	heparan sulfate glycosaminoglycane
HSPG	heparan sulfate proteoglycane
HU	hydroxyurea
IAV	ingrowth area vascularized
ID	internal diameter
ip	intraperitoneal
iv	intravenous
IGF-1	insulin-like growth factor
IHD	ischemic heart disease
KOH	potassiumhydroxide
KV	kilovolt
LacZ	gene encoding for β - galactosidase
LCST	lower critical solution temperature
LIMA	left internal mammary artery
MES	morpholinoethanesulfonic acid
ml	mililitre
MMP	matrix metalloproteinase
mRNA	messenger ribonucleic acid

NAD	nitrous acid degraded heparin
NADPH	nicotinamid adenine dinucleotide phosphate
NaOH	sodium hydroxide
NIH	National Institutes of Health
NO	nitrous oxide
OD	optical density
PAA	polyacrylic acid
PAD	peripheral arterial disease
PAI	plasminogen activator inhibitor
PBS	phosphate buffered saline
PCR	poymerase chain reaction
pCMV-MCS	promoter of cytomegalievirus – multiple cloning site
PDGF	platelet derived growth factor
PDGF-BB	platelet derived growth factor isoenzym BB
PDK	phosphoinositide-dependent kinase
PDS	polydioxanone
PE	polyethylene
PECAM	platelet endothelial cell adhesion molecule
PEG	polyethylene glycol
PEO	polyethylene oxide
PET	polyethylene terephthalate
PGA	polyglycolic acid
PhD	doctor of philosophy
PI	propidium iodide
PLA	poly-lactide acid
PLG	poly(lactide-co-glycolide)
PLGA	poly(lactide-co-glycolide)acid
PLDL	poly(l-lactide-co-DL-lactide)
PLGF	placental growth factor
PMSF	phenylmathanesulphonylfluoride
PNIPAAm	polyN-isopropylacrylamide
PPO	polypropylene oxide
PTA	percutaneous transluminal angioplasty
PTFE	poly-tetra-fluoroethylene
PU	polyurethane
PVA	polyvinylalcohol
PVC	polyvinylchloride

rAAV	recombinant adeno associated virus
RGD	Arginin-Glycine-Aspartat amino-acid sequence
ROS	reactive oxygen species
rpm	rotor speed per minute
SEM	scanning electron microscope
SCID	severe combined immundeficiency syndrome
ss	single stranded
TBS	tris buffered saline
TEBV	tissue engineered blood vessel
TGF	transforming growth factor
TU	transducing unit
UV	ultraviolet
uPA	urokinase type plasminogen activator
VAG	vascular access graft
VE	vascular endothelial
VEGF	vascular endothelial growth factor
VEGFR	vascular endothelial growth factor receptor
VS	vinyl sulfone
vs	versus
X-Gal	5-bromo-4-chloro-3-indolyl-beta-D-galactopyranoside

1. Introduction

1.1 Clinical impact of atherosclerosis and ischemia

Atherosclerosis is a potentially life threatening systemic disease process that affects large and medium diameter arteries throughout the arterial tree of the human body (1). Due to cardiovascular risk factors such as high cholesterol levels, diabetes or chronic arterial hypertension, cellular changes develop slowly in the arterial wall. Lymphocytes and monocyte-derived macrophages from the blood steam as well as smooth muscle cells from the underlying vessel wall accumulate within the tunica intima (2). Subsequently, an atherosclerotic plaque develops, which can lead to activation of platelets and thrombus formation. Thrombosis as a complication of atherosclerosis is characterised by an unpredictable, sudden disruption of this atherosclerotic plaque. Given the progressive, generalised nature of this disorder, the occurrence of an arterial ischemic event caused by atherosclerosis is not restricted to a single vascular bed, but is likely to affect several arterial territories (1). Three main clinical manifestations of atherosclerosis are ischemic heart disease (IHD), ischemic stroke and peripheral arterial disease (PAD), involving coronary, cerebral and peripheral vasculature, respectively (3). Atherosclerosis represents a massive clinical and economic burden to healthcare. To date, ischemic heart disease (IHD) is the number one cause of death in the world. It accounted for almost 13 million deaths in 2002 or 22 % of all deaths annually (393). In the United States, ischemic heart disease is the single largest cause of death with over 6 million deaths in 2001 and an overall prevalence of approximately 13 million people (4). Ischemic stroke is also a major health burden. Over 20 million strokes occur annually worldwide, being the third leading cause of death in industrialised countries (5.5 million in 2001), the primary cause of adult disability and the second most common cause of dementia (4), (394). Peripheral arterial disease (PAD) also contributes to the substantial morbidity and mortality of atherothrombosis. In north America and western Europe combined, PAD affects approximately 16 % of individuals over 55 years (5). There is also a strong association with increasing age. The population based "Rotterdam study" including 7715 patients revealed a prevalence of 57 % of PAD in those aged over 85 years (6). Due to the high impact of ischemic heart disease, ischemic stroke and peripheral arterial disease on morbidity and mortality, it is not surprising, that in the USA alone, it is estimated that the costs for diagnosis and treatment of cardiovascular disease are as high as 368 billion dollars annually

(4). Moreover, due to the growing percentage of the older population, an increased survival after the first event of ischemia and the changes in modern life-style, the prevalence of atherosclerosis is predicted to rise. The "Global Burden of Disease Study" predicts ischemic heart disease and cerebrovascular disease to be the first and second leading causes of death by the year 2020 (7). Although ischaemic heart disease is often perceived as a first-world problem, the World Health Organization (WHO) estimates that it will become the third most common cause of death in the developing world by 2020. The first burden of disease study for South Africa, published in 2003, estimated that 17 % of all deaths were due to cardiovascular diseases (8). It is expected that there will be a substantial increase in cardiovascular diseases especially in middle-income countries, should the risk factor profiles persist and health services fail to manage chronic conditions such as hypertension and diabetes adequately (9). There is thus a great need for effective strategies to prevent, diagnose and treat atherosclerotic and consequently ischemic disease to reduce morbidity and mortality worldwide.

1.2 Vascular grafting as treatment modality of ischemic disease

Since there is worldwide a critical need to treat ischemic disease, which leads to tissue injury, organ dysfunction and ultimately failure, effective treatment modalities need to be found. Clinical treatment of ischemic disease today involves dilatational techniques of arteries such as percutaneous transluminal angioplasty (PTA) with or without delivery of (drug-eluting) stents as well as replacement of diseased vessels by vascular grafts. In the USA alone, approximately 1.4 million arterial replacements are performed annually, most of them small caliber vascular grafts (10). Such small caliber vascular grafts are used as coronary artery bypass grafts (CABG), as vascular access grafts (VAG) for renal dialysis and as peripheral grafts (PG) to relieve lower extremity ischemia. Graft materials for peripheral grafts include autologous vein and synthetic materials such as expanded poly-tetra-fluoroethylene (ePTFE) and polyethylene terephthalate (PET, Dacron®). Up to date, autologous vein grafts are still the "Gold-standard" for bypass surgery in peripheral artery disease (PAD). There are two main reasons for this: firstly, there is a lack of autologous arterial material, which is long enough for peripheral arterial replacement. This is in contrast to cardiac bypass surgery, where at least one arterial graft, usually the left internal mammary artery (LIMA), is routinely used for bypass surgery with a 10 year patency rate of up to 89 % (11). Secondly, the available synthetic graft materials such as expanded poly-tetra-fluoroethylene

(ePTFE) and polyethylene terephthalate (PET, Dacron®) show inferior long term patency rates compared to autologous vein grafts (12). In clinical practice, the diameter and the location of the bypass for the stenosed or occluded artery influences the decision on the bypass material to choose for best long term results. For large diameter, high flow vascular bypass grafts such as aorto-femoral replacements, Dacron® is the material of choice because there usually is no autologous arterial or venous material of the required size readily available. Additionally, 93 % secondary patency rate at 10 years (13) appears to be an acceptable outcome for both patients and surgeons. ePTFE on the other hand is preferred in medium sized (6 – 12 mm diameter) bypass procedures, when autologous vein is not available or not suitable due to disease, e.g. after previous stripping of varicose veins or after previous saphenectomy for coronary artery bypass grafting (CABG). It is however clearly recognizable, that even in medium sized bypass surgery, today's available synthetic bypass materials are only the second best choice compared to autologous vein. Veith et al. showed a significantly decreased patency rate of 47 % for ePTFE femoro - popliteal grafts (including above and below knee grafts) 4 years after implantation compared to 68 % for reversed saphenous vein grafts (14). And the situation for small diameter vascular grafts (equal or less than 6 mm), implanted for example in bypass procedures with the distal anastomosis below the knee, is even worse: ePTFE grafts show patency rates between 31 % and 38 % after 4 years (15), (14). Intriguingly furthermore, the long term patency rates even of the "Gold-standard" autologous vein in small diameter replacements are relatively poor. 5 years after surgery, only 52 % - 68 % of all peripheral veingrafts are patent (16), decreasing further to a 41 % patency rate after 10 years (12). These long term results underscore that results of peripheral arterial bypass surgery with small and medium size grafts are still suboptimal, especially using synthetic materials such as ePTFE. The consequences for the patient on the other hand, are dramatic, since failure of ePTFE femoro - popliteal bypasses results after 12.2 months of bypass occlusion in an amputation rate of the ischemic limb of up to 35 % (17). In small diameter reconstructions such as venous bypass to the dorsalis pedis artery, amputation rates increase to 63 % for early graft failure (within 30 days of initial revascularisation) and 46 % for late graft failure (after 30 days of initial revascularisation) (18). Therefore, further research for alternative materials or concepts is clearly warranted.

1.3 Shortcomings of conventional vascular grafts

Conventional grafting materials such as autologous vein, ePTFE and Dacron® follow the principle of repair and replacement of function rather than real tissue regeneration. Vascular grafts materials were considered fully functional in the past, when they provided a non - leaking blood conduit with minimal thrombogenicity. Biocompatibility in this historical context, which is a material's ability to exist within a living organism without damaging adjacent cells and without creation of significant scarring, is limited mainly to physical and mechanical properties and a maximal grade of inertness. Short term biocompatibility, however, is not sufficient for bypass grafts in order to achieve sufficient long term patency rates. General reasons for early graft failure are poor patient selection, technical problems during surgery, compliance mismatch of the graft material in comparison to the native artery as well as primary thrombotic failure related to poor distal run - off (19). Reasons for late graft failure include progression of native vessel sclerosis due to underlying disease, graft degeneration as well as intimal hyperplasia leading to thrombosis and occlusion (19). Pathophysiologically autologous vein, which is subjected to supraphysiological pressures in the arterial circulation, shows excessive dilatation and intimal hyperplasia, which often results in late graft occlusion (20). Likewise, synthetic graft materials such as ePTFE and Dacron® are prone to intimal hyperplasia, thrombosis and occlusion (20). The thrombogenicity of vascular grafts can be ascribed to a persistent lack of endothelial cell coverage, even after extended implant periods. Senescent animal models such as the chacma baboon, which resembles the situation in humans most closely, show a transanastomotic pannus ingrowth of only 7.8 mm after 6 weeks (21). In humans, endothelial coverage of synthetic vascular grafts is usually limited to a few millimetres around the anastomosis (22) and only isolated, small islands of endothelium have been reported on midgraft sections of ePTFE and Dacron® prosthesis (23). These findings underscore the critical need for the development of new strategies involving biologically active materials and provide the motivation to apply tissue engineering techniques for peripheral bypass grafts. The recognition of the importance of a confluent endothelial cell lining as one aspect of vascular biology for graft patency along with advances in endothelial cell culture techniques led to the concept of endothelial cell transplantation (24).

1.4 The concept of tissue engineering of vascular grafts

Langer and Vacanti proposed the concept of tissue engineering in 1993 as a combination of the "principles of biology and engineering to the development of functional substitutes for damaged tissue" (25). The physiological response of human tissues to injury is often limited to repair, which involves the synthesis of scar tissue and is aimed at restoration of continuity in the affected organ or tissue without regeneration of its specific function. According to Williams, tissue engineering and tissue regeneration, in contrast, "aims at restoring normal structure and function through the production of new tissue that replicates what has been lost" (26). This may be achieved by "induced regeneration", which is "a strategy to enable the body to heal itself through delivery of biomolecules and supporting structures to the appropriate cellular environment" (26). Therefore, if the goal of a vascular bypass graft is not simply physical restoration of blood flow as a replacement strategy, but rather regeneration of a vascular structure, which resembles a native artery as closely as possible with respect to mechanical strength, elasticity and endothelial cell lining, then principles of tissue engineering have to be applied. Towards this end, advances in cell culture techniques allowed the first model of a blood vessel to be constructed in vitro by Weinberg and Bell in 1986 (27). This completely biological "tissue engineered blood vessel" (TEBV) was produced using cultured bovine endothelial cells, smooth muscle cells and fibroblasts as well as collagen gel as provisional matrix. Mechanical strength of the construct however, was not sufficient, even after integrating multiple layers of collagen into a Dacron® mesh (27). Similar results were obtained by L'Heureux et al. who created a tubular vascular model made of human cells and collagen (28) as well as by Hirai and Matsuda, who implanted Dacron® reinforced vascular tissue consisting of canine jugular smooth muscle cells, collagen and endothelial cells into canine posterior venae cava (29). In 1998 L'Heureux described the first "tissue engineered blood vessel" based exclusively on cultured human cells without any synthetic or exogenous biomaterial (30). Human vascular smooth muscle cells were cultured to produce a cohesive cellular sheet, which became the tunica media of the engineered blood vessel after being placed around a tubular support device. A sheet of fibroblasts was subsequently wrapped around the tunica media to provide the tunica adventitia. After maturation of the construct, the tubular support was removed and the created lumen was seeded with endothelial cells. The complete vessel was reported to show a burst strength over 2000 mmHg. The whole process however, took more than 4 months to complete. Niklason and Langer seeded bovine smooth muscle cells onto

a biodegradable synthetic scaffold of polyglycolic acid (PGA) and applied pulsatile stretch to facilitate proliferation and the contractility of cells (10). After 8 weeks of culture under pulsatile conditions, bovine aortic endothelial cells were seeded into the lumen of the construct. Mechanical properties were sufficient showing a burst strength of over 2000 mmHg, implantation into Yucatan miniature swine, however, revealed thrombotic potential of two non-pulsed grafts as well as decreased flow in one autologous graft four weeks after implantation (31).

These attempts towards a "de novo" creation of a vascular graft in vitro, following the "classic" concept of tissue engineering, offered valuable insights into the requirements of different cell lines and their dynamic interaction with a scaffold and / or a matrix. It soon became clear, however, that only highly equipped medical centres of excellence could produce such a completely biological "tissue engineered blood vessel" (TEBV) in an acceptable period of time. In parallel to research towards a TEBV, attempts have been made to endothelialise conventional vascular grafts in vitro and in vivo to increase long term patency.

1.4.1 In vitro endothelialisation

Herring et al. started to seed canine endothelial cells onto Dacron® aortic grafts using a single staged endothelial cell seeding procedure in 1978 (32). 6 weeks after aortic graft interposition in dogs he found the grafts lined with vascular endothelium supported by smooth muscle cells as well as vasa vasorum in the wall of the grafts. A few years later, clinical application of autologous endothelial cells onto femoro-popliteal bypasses implanted in 17 human patients revealed a significantly improved patency rate for the seeded group 12 months after implantation and proved the feasibility of this concept (33). Mass culture of venous endothelial cells (34) and harvest of capillary endothelial cells from fat tissue (35) were methods to overcome the previous problem of sub-optimal endothelial cell seeding density due to a relatively low cell number together with a high detachment rate of cells after restoration of blood flow. Greisler et al. have evaluated the application of endothelial cell growth factor (ECGF) onto Dacron® and polydioxanone (PDS) grafts in 1987 to stimulate the proliferation of seeded endothelial cells and to induce transmural cellular ingrowth (36), (37). To provide a matrix for endothelial cell attachment as well as a controlled local delivery system for ECGF and heparin, a self-made fibrin matrix was applied onto the graft surface (38). Using ePTFE grafts as scaffold

material, Gosselin et al. distributed fibroblast growth factor (FGF) evenly throughout the graft and endothelial cells were retained using fibrin, FGF and heparin (39).
For in vitro endothelialisation in humans, a confluent endothelial cell lining of ePTFE grafts up to a graft length of 60 cm requires an endothelial cell culture time of 4 to 5 weeks and therefore warrants a surgical two stage procedure. Zilla et al. were the first to describe the harvest of autologous endothelial cells from 4 to 5 cm of subcutaneous vein (cephalic or external jugular vein), culture for 5 weeks and subsequently the seeding onto fibrin coated ePTFE grafts in 1987 (40). Clinical data on 100 patients receiving 113 in vitro endothelialised ePTFE grafts showed a primary 9 year patency rate of 65 % for the endothelialized group versus 16 % for the control group (41). A recent study using this technique confirms excellent patency results with 83.7 % primary patency rate of infrainguinal endothelialized reconstructions after 4 years (7 mm ID grafts) (42). This data compares favourably to the 4 year patency rate of reversed autologous saphenous veins in the same position achieved by Veith et al. (14). Although in vitro endothelialisation of ePTFE grafts offers a valuable alternative to autologous vein grafts, especially when veins are not available or not suitable, the requirement of a highly specialized laboratory to culture autologous endothelial cells and the need to perform two separate operations (vein harvesting and bypass-surgery), have prevented this method from widespread clinical utilization up to now. However, the clear evidence of superiority compared to non-treated ePTFE has warranted further clinical evaluation. A multicentre clinical trial is therefore currently underway in Europe.

1.4.2 In vivo endothelialisation

Although in vitro endothelialisation of ePTFE grafts has been shown to achieve superior patency rates in comparison to non - endothelialised grafts, there is still a wide gap compared to the structure and function of a healthy native artery. Structure and function are tightly interconnected and of high complexity. If the ultimate goal is to develop a vascular graft with the patency potential rate of a native artery, then techniques of tissue engineering and tissue regeneration may have to be applied. To answer questions about possible recruitment of cells in vivo, the following considerations must be made:
There are basically three different ways to "endothelialise" vascular grafts in vivo:

1. Transanastomotic endothelialisation
2. Endothelialisation of grafts by circulating stem cells
3. Transmural endothelialisation

1.4.2.1 Transanastomotic endothelialisation

Transanastomotic endothelialisation (endothelial outgrowth) describes the growth of endothelial cells followed by smooth muscle cells from the native artery into the lumen of the vascular graft. This tissue, which also consists of platelet covered fibrin, collagen, fibroblasts and a few macrophages, is often referred to as "pannus" (21). Three major factors determine the extent of pannus outgrowth: Firstly, the extent of an initial fibrinous capsule on the graft surface. Anastomotic pannus formation seems to replicate the dimensions of the fibrin layer which it replaces (21). If there is tissue underneath this capsule as, for example, in knitted Dacron® grafts, transanastomotic outgrowth and endothelialisation occurs faster than in woven Dacron® grafts (43), where there is less tissue under the fibrous capsule (44). Secondly, porosity determines the rate of transanastomotic outgrowth. High porosity PTFE grafts externally wrapped in tissue allowed via transmural support of subfibrous tissue increased transanastomotic endothelialisation and graft healing (45). Thirdly, the animal model chosen influences the rate and extent of endothelial outgrowth. The most commonly used animal model, which is the dog, shows transanastomotic outgrowth of 2 - 3 cm within 30 days in Dacron (46) and ePTFE grafts (45). The animal model with the slowest transanastomotic healing is the senescent chacma baboon, where transanastomotic outgrowth is at least 2.1 times slower than in the dog (47). However, transanastomotic endothelialisation in humans is limited to millimeters around the anastomosis within synthetic grafts even years after implantation for unknown reasons (22), (48). Results obtained in dogs can therefore not easily be extrapolated to the human situation, where transanastomotic endothelialisation of synthetic grafts does not seem to be a successful option.

1.4.2.2 Endothelialisation of vascular grafts by circulating stem cells

Since Stumb et al. noticed in 1963, that a 4.5 cm Dacron® vascular implant in a pig was fully endothelialised within 7 days (which could not be explained by transanastomotic outgrowth), the search for a different source of endothelial cells other than those derived from the anastomosis began (49). After the construction of a small square Dacron® hub trapping device, which was implanted for 4 weeks in a dog showing endothelial coverage of the whole hub surface, the conclusion of a circulating cell source was drawn. In humans, endothelial cells were found together with myofibroblasts on a textured surface of a cardiac assist device two years after

implantation (50). It was postulated, that the source of these cells creating a "pseudo-neointima" were multipotential bone marrow stem cells. In 1994, Shi et al. demonstrated scattered islands of endothelial cells on impervious Dacron® aortic grafts 4 weeks after implantation in a dog model, which he referred to as "fallout endothelialisation" (51). Isolated putative endothelial progenitor cells that eventually differentiate into mature endothelial cells were shown to be the source of "fallout endothelial cells" (52). In a mouse hindlimb and myocardial ischemia model, the potency of these bone marrow derived endothelial progenitor cells for postnatal vasculogenesis could be shown for the first time (53). However, despite these promising results towards in vivo seeding of vascular grafts with circulating endothelial progenitor cells, three aspects need to be considered: firstly, the superior ability of dogs for rapid graft endothelialisation compared to humans, demonstrated in transanastomotic endothelialisation experiments, as mentioned above. Secondly, surface endothelialisation can be expected to decrease thrombogenicity, but complete transmural autologous tissue ingrowth is expected to resemble the morphology and dynamic behaviour of a natural artery much closer. And thirdly, even in the dog model involving bone marrow derived endothelial progenitor cells only scattered endothelial coverage was found 4 weeks after implantation (51).

1.4.2.3 Transmural endothelialisation

As transanastomotic endothelialisation of vascular grafts is limited to a few millimeters in humans and circulating stem cells are not capable of coating an entire graft in humans in an appropriate time span as yet, other possible sources of endothelial cells need to be explored. Since peripheral bypass grafts in humans are often as long as 60 cm, transmural tissue ingrowth followed by endothelialisation of the graft via connection of ingrowing capillary vessels functionally serving as vasa vasorum with the graft's surface seems to have the potential for success. Furthermore, full transmural healing could not only provide a confluent endothelium resulting in decreased thrombogenicity of the graft, but could eventually result in a full integration of the prosthetic material into the host. In the past, all studies faced the difficulty of correct determination of the source of endothelial cells on the surface of a graft. Since 89 % of all experimental studies on ePTFE and Dacron® reported on grafts, which were on average 5.5 ± 1.2 cm long with a median implantation time of 91.8 ± 17.3 days in Dacron® and 60 ± 9.36 days in ePTFE grafts, transanastomotic ingrowth was often completed before the time of explantation (21). This makes it very difficult or even impossible to determine the source of endothelial

cells as transanastomotic or transmural. In addition, obtainable data on transmural tissue ingrowth indicates, that, as with transanastomotic endothelialisation, rate and extent of transmural tissue ingrowth is influenced by graft porosity and the animal model. Low porosity of ePTFE grafts (internodal distance < 30 µm) does not allow for sufficient transmural ingrowth, since the actual spaces available for tissue ingrowth, namely the "inter-fibrillar distance", is typically in the range of 4 to 5 µm (21). Only high porosity of ePTFE grafts (internodal distance 60 µm) allows for transmural ingrowth of endothelial cells and smooth muscle cells 2 weeks after graft implantation in the young yellow baboon (54), (55). Greisler et al. reported on extensive transmural capillary ingrowth into high porosity ePTFE aortoiliac grafts in a dog model after FGF pre-treatment (56). However, untreated high porosity ePTFE grafts implanted in senescent chacma baboons, allowed only for 7.8 mm transanastomotic endothelialisation after 6 weeks without any signs of transmural ingrowth (21). The healing of Dacron® grafts is also affected by porosity. Woven (low porosity) Dacron prosthesis showed a similar tissue ingrowth pattern in the first 7 days compared to low porosity ePTFE. Nevertheless, a certain extent of transmural infiltration of fibroblasts and vasa vasorum occurs in dogs after 3 weeks (44). In humans, however, this may be absent even after years (48). In high porosity (knitted) Dacron grafts, transmurally ingrowing cells reach a compact luminal layer of fibrin after 4 weeks in the yellow baboon and rarely after 6 months or most often not at all in humans (57). In summary, most studies provide evidence, that transmural tissue ingrowth is feasible and affected by pore size. Since in humans tissue is unable to infiltrate the graft wall sufficiently with internodal distances of under 30 µm (equals 4 - 5 µm inter - fibrillar distance), spaces are recommended to be at least of the size of arterioles to allow for transmural ingrowth (21). Another inhibitory factor against sufficient transmural vascular graft tissue ingrowth is a dense inner fibrinous capsule that seems to be almost impenetrable for capillaries (58), (59). In those cases however, in which continuous transmural endothelialisation of grafts is achieved within 2 weeks after graft implantation (yellow baboon) (54), transmural tissue ingrowth is completed before the environment turns inhibitory with a dense fibinous capsule on the inside and macrophages and foreign body giant cells on the outer portion of the graft (21).

1.5 Novel vascular graft concept: facilitated transmural ingrowth

At the Cardiovascular Research Unit of the University of Cape Town, South Africa, a interdisciplinary team of researchers has focused for the last decade on the

production and evaluation of an "in vivo tissue engineered vascular graft". Bezuidenhout et al. produced a polyurethane scaffold material with a well defined 82 % porosity by a variation of the phase inversion / porogen extraction technique (47). Pores resemble open faced pentagonal dodecahedra and allow for almost uninhibited ingrowth of tissue in all dimensions. Macroporous polyurethane (157 µm pore size) was shown to decrease the inflammatory reaction of ingrowing tissue without adversely affecting the degree of neovascularisation compared to microporous polyurethane (66 µm pore size) (60). Implantation of vascular polyurethane grafts (length of 8 cm) as femoral artery replacements in the senescent chacma baboon showed transmural tissue and capillary ingrowth after 28 days. In this animal model, which resembles the human healing response more closely than other animal models, the inner fibrinous capsule was penetrated by transmurally ingrowing capillaries (47). However, since it is regarded as beneficial that this process would be completed as early as possible (21), the scope of this PhD thesis was to evaluate ways to increase transmural neovascularisation into porous polyurethane. As detailed above, it would be desirable to accelerate transmural neovascularisation and tissue ingrowth to allow endothelialisation of the grafts surface and healing of the graft wall before the inner fibrinous capsule becomes impenetrable for capillaries. This specialised form of therapeutic angiogenesis requires a thorough analysis of the present understanding of angiogenesis and its growth factors involved as well as the optimal choice of a suitable delivery method for pro-angiogenic factors and a quantifiable in vivo angiogenesis assay. These considerations are addressed in the remainder of this chapter.

1.5.1 Neovascularisation: vasculogenesis, angiogenesis, arteriogenesis and lymphangiogenesis

Blood vessel formation, also known as neovascularisation, includes the processes of vasculogenesis, angiogenesis, arteriogenesis and lymphangiogenesis (61), (62).

Vasculogenesis

Endothelial and hematopoietic cells share a common progenitor, which is called the hemangioblast. During embryonic development, the inner layers of hemangioblasts in the yolk sac develop into hematopoietic precursors, whereas the outer layers form endothelial precursor cells. Vasculogenesis is the de novo differentiation of

endothelial progenitor cells to endothelial cells to form a primitive vascular network. Endothelial progenitor cells initially aggregate and proliferate into a cordlike structure and subsequently differentiate to form a plexus of endothelial tubes (62). This early vascular network lacks pericytes and is therefore highly permeable. Once believed to occur exclusively in embryonic development, recent findings demonstrate that endothelial cells can differentiate even in adults from endothelial progenitor cells (EPC's), mesangioblasts, multipotent adult progenitor cells or side - population cells in the adult bone marrow (63), (64). Moreover it has been shown, that these bone marrow derived cells are able to incorporate into areas of neovascularisation and into vascular prosthesis (52), (65), (53). Their differentiation and mobilisation is stimulated by a myriad of growth factors and cytokines such as vascular endothelial growth factor (VEGF), basic fibroblast growth factor (bFGF), insulin - like growth factor (IGF-1) and granulocyte - monocyte colony-stimulating factor (GM-CSF) (66), (67). The VEGF homolog placental growth factor (PLGF), angiopoietin-1 (Ang-1) and inhibitor of differentiation (Id) proteins have also been shown to recruit bone-marrow derived endothelial and hematopoietic stem cells (HSC) for vasculogenesis (68), (69). Once a primitive vascular network has been established in the embryo or repair mechanisms have occurred in adults involving EPC's, further steps involving angiogenesis, arteriogenesis and lymphangiogenesis are necessary in order to meet the metabolic demands of growing tissue.

Angiogenesis

Angiogenesis as the formation of new blood vessels is a critical process in physiological tissue regeneration such as during the female reproductive cycle and in wound healing (70), (71), (72). Regulation of angiogenesis is normally well balanced, but in case of dysregulated vessel growth, it has a major impact on general health and contributes to the pathogenesis of many diseases. Historically, the best known are several types of cancer, arthritis, proliferative retinopathy of diabetics and psoriasis (71). Even disorders like asthma, obesity, infectious diseases and many inherited forms of vascular malformations are characterised or caused by abnormal or excessive angiogenesis (72), (73), (74), (75). Insufficient angiogenesis or increased vessel regression on the other hand are associated with neurodegenerative disorders like Alzheimer's disease as well as major health burdens such as stroke, arteriosclerosis, hypertension, diabetes and osteoporosis (76), (77), (78), (79), (80), (81). It has become increasingly evident, that few other processes in human physiology and pathophysiology have such an impact on health

and well-being as a fully functional vascular system. It is therefore necessary to have a sufficient understanding of the different mechanisms involved in neovascularisation.

The initial steps of angiogenesis are characterised by sprouting of new vessels from the sides and ends of preexisting ones, by bridging of endothelial cells into the lumina or by intussusception, which is the longitudinal division of preexisting vessels initiated by periendothelial cells. Sprouting , bridging and intussusception result in splitting and branching of the previously established vascular network into pre-capillary arterioles, capillaries and postcapillary venules (61), (62).
On a molecular level, the start of angiogenesis is characterised by vasodilation and an increase in permeability of preexisting vessels (82). Activated nitric oxide (NO) seems to play an important role in this process, as it directely dilates vessels and induces an increase in permeability via a transcriptional upregulation of VEGF (82). Permeability is increased through the formation of fenestrations in cell membrane structure and redistribution of the intercellular adhesion molecules platelet endothelial cell adhesion molecule-1 (PECAM-1) and vascular endothelial (VE)-cadherin (83). This in turn facilitates the extravasation of plasma proteins, which act as a provisional support structure for proliferating and migrating endothelial cells. To allow for proliferation and migration of endothelial cells in terms of sprouting, two mechanisms must run in parallel: firstly, inter - endothelial cell contacts need to be loosened and secondly, the extracellular matrix (ECM) needs to be degraded. Angiopoietin-2, which inhibits Tie-2 receptor signaling, is involved in destabilising mature vessels through the detachment of pericytes and smooth muscle cells as well as through loosening of underlying cellular matrix (84). This involves proteinases of the matrix metalloproteinase (MMP)-, the chymase-, the heparanase-, as well as members of the plasminogen activator proteinase families (85). The degradation of ECM not only provides space for sprouting of new capillaries, it also releases growth factors bound to the ECM such as VEGF, bFGF and insulin-like growth factor-1 (IGF-1), which are activated by their liberation. To date, more than 20 MMP's have been described, which play a central role in cell proliferation, angiogenesis and growth of tumors (85). It becomes evident, that a fine balance between proteinases and their inhibitors is necessary for proper physiological function, since MMP-2, MMP-3 and MMP-9 facilitate sprouting, whereas MMP-7 and MMP-9 generate angiostatin, an inhibitor of endothelial cell proliferation (86), (87). Once existing parent vessels are dilated, permeability is increased and the physical

barrier in form of extracellular matrix is degraded, endothelial cells can proliferate and migrate.

Apart from VEGF's and Ang-2, numerous additional growth factors and antagonists are involved in building a vascular network that meets the metabolic demands of the growing tissue appropriately. Fibroblast growth factors (FGF) are non-specific growth factors recruiting mesenchymal and inflammatory cells, which in response produce several angiogenic factors themselves (88). Vascular maturation after endothelial sprouting, bridging or intussusception requires stabilisation by pericytes and smooth muscle cells. Platelet derived growth factor (PDGF), which can be subdivided in five isoforms PDGF-AA, PDGF-AB, PDGF-BB, PDGF-CC and PDGF-DD (89), seems to play an important role hereby (90), (91). All different isoforms act via the two receptor tyrosine kinases PDGF receptor α and β. Insufficient recruitment of mural cells in embryos lacking PDGF-BB results in abnormal endothelial cell growth, vessel enlargement, increased permeability and impaired perfusion (92). Similar effects have been seen in tumors (93), in haemangiomas and in diabetic retinas (94). A combination of VEGF and PDGF-BB resulted in more mature vessels than therapy with either factor alone (95). PDGF-CC and PDGF-DD also promote angiogenesis, but their effect is less well characterized (96). In addition to PDGF's, Angiopoietin-1 (Ang-1) supports stabilisation of vascular networks by prevention of vascular leakage as a natural anti-permeability factor (97). Numerous additional angiogenic molecules are known and under investigation, such as hepatocyte growth factor (HGF), epidermal growth factor (EGF), erythropoietin, insulin, monocyte chemotactic protein, leptin, neuropeptides and others (98), (99). Since a vascular network shows a fine-tuned balance between vessel growth and cessation of vessel growth, there are also angiogenesis inhibitors. These include angiostatin (100), endostatin, anti-thrombin III, platelet factor 4 and interferons (101).

Arteriogenesis

Depending on the ultimate fate with respect to the type of vessel (arteriole, venule or capillary), the migrating and proliferating endothelial cells become variably surrounded by layers of periendothelial cells, also known as mural cells. This process involves activation of pericytes for capillaries and postcapillary venules as well as integration of smooth muscle cells into larger vessels, a process also referred to as "vascular myogenesis" (102). In contrast to the de novo vascular formation of vasculogenesis and the sprouting and intussusception of angiogenesis,

arteriogenesis is referred to as the in situ enlargement of muscular collateral vessels from pre-existing arteriolar anastomoses (103). Arteriogenesis occurs especially in the event of ischemia due to severe stenosis or occlusions in the vascular bed, where a sufficient compensation needs to be established quickly. Because larger collateral vessels compensate flow deficits caused by arterial lesions more efficiently than capillaries, arteriogenesis is a very important adaptive process in the vascular system (104). The driving forces for the enlargement of collaterals are pressure related arterial wall stress and fluid shear stress by the blood stream (105).

Lymphangiogenesis

Lymphangiogenesis is the generation of new lymphatic vessels from pre-existing ones, that occurs when fluid extravasated by the blood pressure needs to be reabsorbed, thereby maintaining interstitial fluid balance (106). Lymphatic vessels are furthermore essential for immune surveillance and fat absorption and are involved in the pathophysiology of inflammation and metastatic spread of tumors. The relative lack of specific molecular and cellular markers for lymphatic vessels is one of the reasons why current knowledge of lymphangiogenesis is still far behind the knowledge of angiogenesis. Recently, however, significant advances in lymphangiogenesis research have been made. VEGF-C and VEGF-D have been best studied for their role in lymphangiogenesis (107). Both growth factors bind and activate VEGFR-3 in their proforms and VEGFR-2 in their processed forms. VEGF-C has been shown to induce the growth of new functional lymphatic vessels in normal tissue (106) as well as in tumors (108). Furthermore, VEGF-C is required for VEGFR-3 specific initial steps in embryonic lymphatic development (109). VEGF-D promotes the metastatic spread of tumor cells via lymph vessels (110). Other growth factors recently related to lymphangiogenesis are Angiopoietin-1 and 2 (111), insulin-like growth factors-1 (IGF-1) and 2 (IGF-2) (112) as well as hepatocyte growth factor (HGF) (113). In summary, VEGF-C seems to be a major role player in lymphangiogenesis, but it requires other growth factors to fulfill its physiological function in regenerating tissue (114).

1.5.2 Vascular endothelial growth factor (VEGF)

As tissue grows for normal repair, remodelling and regeneration as well as under pathological situations, metabolic demands of the rapidly dividing and growing cells can only be met to a very limited extent via diffusion, usually only up to 150 µm (71).

As soon as tissue grows beyond this limit, it becomes hypoxic. This in turn activates hypoxia inducible factor-1 (HIF-1) (115). HIF-1 is a transcription factor that regulates adaptive responses to the lack of oxygen in mammalian cells. It consists of the two proteins HIF-1α and HIF-1β. Both subunits exist as a series of isoforms encoded by distinct genetic loci. HIF-1β subunits are constitutive nuclear proteins, whereas HIF-1α subunits are inducible by hypoxia. Among the three HIF-α isoforms, HIF-1α and HIF-2α appear closely related and interact with hypoxia response elements (HRE) to induce transcriptional activity of many angiogenic genes (116). In contrast, HIF-3α seems to negatively regulate the response to hypoxia (117). HIF-1 upregulates transcription of the haematopoietic growth factor erythropoietin and many angiogenic growth factors such as VEGF's and their receptors vascular endothelial growth factor receptor-1 (VEGFR1), vascular endothelial growth factor receptor-2 (VEGFR2), Angiopoietin-2 (Ang2), platelet derived growth factor-BB (PDGF-BB), transforming growth factor β-1, as well as other cytokines and enzymes such as nitric oxid synthase, cyclooxygenase-2, endothelin-1, neuropilin-1 and interleukin 8 (118). VEGF was the first endothelial cell specific, secreted, angiogenic mitogen discovered (119). In the past 15 years, there has been extensive research on VEGF's (reviewed in (120), (121), (122)) demonstrating the major role in angiogenesis (123), (124). Some applications have been translated into clinical studies already (125). Currently, the VEGF family consists of six known members: VEGF (A), VEGF-B, VEGF-C, VEGF-D, VEGF-E (also called orf virus VEGF) and placenta growth factor (PLGF) (120). These dimeric secreted glycoproteins bind in a specific manner to one or two of the VEGF receptors VEGFR-1 (FLT-1), VEGFR-2 (KDR/FLK-1) or VEGFR-3 (FLT-4) (126). Ligand binding induces receptor dimerisation and subsequent auto- or transphosphorylation. Phosphorylation of AKT by the kinase phosphoinositide-dependent kinase-1 (PDK-1) has been recently shown to be critical for the phosphorylation and activation of endothelial nitric oxide synthase (eNOS) (127). This in turn leads to nitric oxide (NO) synthesis which starts vasodilatation and upregulation of VEGF (82). The following passage descibes the various effects of the different VEGF proteins on vascular and lymphatic endothelial cells: VEGF(A) is a major regulator of both physiological and pathological neovascularisation (122). It is a relatively specific mitogen for vascular endothelial cells and elicits a pronounced angiogenic response in vitro and in vivo (128). Transcription of VEGF(A) mRNA is not only induced by HIF-1 but also by a variety of other growth factors and cytokines such as PDGF-BB, epidermal growth factor (EGF), tumor necrosis factor alpha, transforming growth factor alpha (TGFα),

transforming growth factor beta-1 (TGFβ-1) and interleukin 1β (121). VEGF(A) stimulates endothelial cell differentiation, proliferation, migration and survival. Due to it's ability to induce vascular leakage, it is also known as vascular permeability factor (129). Due to alternative exon splicing of the VEGF(A) gene there are five different VEGF(A) protein isoforms, namely $VEGF_{121}$, $VEGF_{145}$, $VEGF_{165}$, $VEGF_{189}$ and $VEGF_{206}$ (130). $VEGF_{165}$ is the predominant molecular form showing the highest mitogenic potency, possibly due to it's neuropilin-1 binding region (131), (132). In contrast, the shorter VEGF isoforms such as $VEGF_{110}$, which is generated by plasmin cleavage of longer isoforms in the extracellular matrix (ECM), and $VEGF_{121}$ are reported to show a 100 fold decreased mitotic potency compared to $VEGF_{165}$ (131). Another important feature of the different splice variants is the ability to bind heparin. $VEGF_{121}$ as a short isoform is freely soluble and does not bind to heparin, whereas a significant fraction of $VEGF_{165}$ remains bound to heparan sulfates of the cell surface and the ECM. $VEGF_{189}$ and $VEGF_{206}$ are almost completely sequestered in the ECM and act as angiogenic factors after proteolytic cleavage from the ECM (133).

VEGF-B shows 45 % identity with VEGF (A) with regards to amino acid sequence and exists as the two isoforms $VEGF\text{-}B_{167}$ and $VEGF\text{-}B_{186}$ (134). It forms heterodimers with VEGF (A) and is a selective ligand for VEGFR-1 (135). Both forms of VEGF-B are widely expressed, being most prevalent in skeletal muscle and heart (134). VEGF-B regulates expression and activity of urokinase type plasminogen activator (uPA) and plasminogen activator inhibitor 1 (PAI1) and is therefore believed to play a role in extracellular matrix degradation, cell adhesion and migration (135). Furthermore it has been shown, that $VEGF\text{-}B_{167}$ also promotes angiogenesis in association with an activation of AKT and endothelial nitric oxide synthase (eNOS) related pathways (136).

VEGF-C shows 30 % identity with VEGF (A) with regards to amino acid sequence and was cloned as a ligand for VEGFR-3 (137). It is produced as a pre-protein and stimulates migration and mitogenesis of endothelial cells (138). VEGF-C mRNA is expressed at low levels in adult heart, small intestine, thyroid, placenta and ovary (137). Since it has also been found in animals particularly in regions where lymphatic vessels develop, it seems to play a dual role as an angiogenic and lymphangiogenic factor (138). Injection of VEGF-C in a rabbit ear model of acquired lymphedema showed the induction of therapeutic lymphangiogenesis (106). VEGF-D is most closely related to VEGF-C and was initially cloned as a mitogen for fibroblasts (139). In the VEGF homology domain, VEGF-C and VEGF-D are 61 % identical. VEGF-D is a ligand and activator of VEGFR-2 and VEGFR-3, but not

VEGFR-1. VEGF-D is found in lung, heart, skeletal muscle, colon and small intestine of adult tissue and was shown to be mitogenic for vascular endothelium as well as lymphatic endothelium (140). The gene encoding the VEGF-E homologue has been discovered in the genome of a parapoxvirus, called "orf" virus that infects sheep, goats and occasionally humans and causes extensive proliferation of vascular endothelium and blood vessel dilation. Both known variants bind exclusively to VEGFR-2, stimulate endothelial cell mitogenesis and increase vascular permeability (141). PLGF was originally cloned from a human placenta cDNA library and has an amino acid sequence 46 % identical to VEGF (A) (142). Two protein isoforms, PLGF-1 ($PLGF_{129}$) and PLGF-2 ($PLGF_{152}$), are known. PLGF homodimers bind only to VEGFR-1, whereas PLGF / VEGF heterodimers bind to soluble VEGFR-2. PLGF seems to enhance angiogenesis only under pathological conditions (143) and amplifies VEGF driven angiogenesis in part through a unique cross talk between VEGFR-1 and VEGFR-2 (144). Additionally, PLGF might play an important role in collateral growth, or "arteriogenesis", which was discussed above, via it's monocyte activating properties (145).

Besides growth factors of the VEGF family, a whole variety of other growth factors such as PDGF (discussed in 1.5.1), FGF, Ang-1, Ang-2, HGF and others are involved in neovascularisation (98). It has been shown by gene knock out studies in mice however, that VEGF and it's receptors play a pivotal role in vasculogenesis and angiogenesis (123), (124). Therefore, $VEGF_{165}$ has been chosen as the main factor for neovascularisation-experiments in this PhD thesis.

1.5.3 Delivery methods of growth factors

1.5.3.1 Polypeptide delivery

The therapeutic implications of angiogenic growth factors were identified by Folkman et al. studying tumor angiogenesis as early as 1971 (146). A series of polypeptides were purified, sequenced and shown to be angiogenic in physiological as well as in pathological situations (147). The first animal experiments using recombinant basic fibroblast growth factor (bFGF) in a rabbit hindlimb ischemia model showed increased capillary density after 14 days of daily intramuscular administration of 1 to 3 µg bFGF (148). This was the beginning of the new concept of "therapeutic angiogenesis" as a possible treatment modality of ischemic disease. Pu et al. used daily intramuscular injections of 4 mg acidic fibroblast growth factor (aFGF) to create increased vascular collateral development after inducing hindlimb

ischemia in rabbits (149). Furthermore, intracoronary injection of bFGF increased the number of arterioles and capillaries in an experimental canine myocardial infarction model (150). Isner et al. reported in 1996 that single, intra-arterial injections of 0.5 to 1 mg of $VEGF_{165}$ induced significant augmentation of collateral vessel development in a rabbit hindlimb ischemia model (151). Similar results were achieved when $VEGF_{165}$ was administered via daily intramuscular injections for 10 days. These early experiments proved the concept of delivery of angiogenic growth factors as a possible mode of therapy for induced ischemic disease.

However, several issues have impeded progress in the direct use of growth factors via single or repeated injections. Firstly, the complex three dimensional structures of the proteins result in very short biological half-lifes (152). VEGF, for example, has a clearance half-life of approximately 40 minutes after injection in the human body (153). PDGF mRNA shows a serum half-life under basal conditions of 70 - 90 minutes (154). Therefore, large doses are required for a sustained and effective concentration of growth factors. This in turn carries the potential for toxicity and substantial side effects. Indeed, in human phase I clinical trials, only a limited amount of VEGF and bFGF could be administered due to the induction of severe hypotension (153). It is for these reasons that alternatives allowing the delivery of angiogenic growth factors in a sustained fashion have been searched for.

1.5.3.1.1 Sustained polypeptide delivery

In addition to direct delivery of growth factors via injection, a second tissue engineering strategy involves the sustained and controlled local delivery of angiogenic growth factors. Sustained release systems based on microspheres can be made of poly(lactide-co-glycolide) (PLG) (155), gelatin (156), alginate, or other polymeric materials (157). However, since many recombinant proteins are of large size and fragile structure and the process of generating microspheres often involves organic solvents, high temperatures and sonication, substantial protein denaturation can occur (158). Additionally, the acidic environment produced during degradation of PLGA could be responsible for the partial loss of VEGF bioactivity (159). Because of the difficulty in maintaining adaequate bioactivity, again high doses of growth factors have to be applied, which involves the danger of substantial growth factor diffusion into the circulation, an unwanted effect called "dose dumping". Furthermore, production of such a large amount of growth factors creates considerable costs (160). Recently, VEGF incorporation into synthetic bio-interactive cell ingrowth

matrices such as modified polyethylene-glycol (PEG) has shown a sustained angiogenic potential via cell demanded release (223) (1.5.4.3).

1.5.3.2 Gene transfer

1.5.3.2.1 Plasmids as gene delivery vectors

In an attempt to circumvent the above mentioned problems with "direct" delivery of growth factors to tissues and wound beds, a different strategy has been explored that involves gene therapy. The concept involves delivery of a gene encoding for a certain growth factor, rather than the recombinant protein itself, to the site requiring tissue regeneration (161). The simplest form of gene delivery is the delivery of plasmid DNA, which is a circular form of DNA, via injection. The plasmid enters the nucleus of the target cell in vivo. The cell subsequently expresses the protein of choice. Isner et al. reported 1998 on successful gene transfer for therapeutic angiogenesis in patients with peripheral artery disease (151), (162). 4 mg of naked plasmid DNA encoding for $VEGF_{165}$ injected intramuscularly into the ischemic limbs of 9 patients suffering from peripheral vascular disease, improved collateral neovascularisation clinically and on angiogram (162). To translate the concept of gene delivery to wound healing, Bonadio et al. proposed the concept of "Gene Activated Matix" (GAM) in 1999 (161). Hereby, rather than being injected directly into the wound, plasmid DNA is incorporated into a structural matrix carrier. After implantation of this "Gene Activated Matrix" carrier into a wound, autologous ingrowing cells incorporate the gene, and, after being transfected, serve as "in vivo bioreactors" producing the required angiogenic growth factor themselves. Thereby, the growth factor is produced locally in a sustained fashion. The concept of GAM, therefore, does not follow the traditional "drug delivery system", where the drug substance is delivered to the cell, but rather the opposite: the natural dynamics of granulation tissue in wound repair is maintained and ingrowing fibroblasts and other cells are directly transfected in vivo. This concept was proven by Bonadio et al. in 1999 (163). Using different matrix carriers such as collagen, alginate, cellulose, hyaluronic acid and poly(lactide-co-glycolide) for plasmid DNA (164) encoding for VEGF, PDGF-BB, bone morphogenic protein or parathyroid hormone (165), it was shown that "Gene Activated Matrix" genetically manipulates wound healing fibroblasts in vivo in a reproducible, safe and effective way (163). However, plasmid DNA was shown to be a relatively inefficient gene therapy vector with a transduction ratio of about 10 % of ingrowing wound healing cells (163). Synthetic gene delivery

vectors have been constructed to improve transduction efficiency. Cationic liposomes and condensing reagents such as poly(ethyleneimine) and poly(L-lysine) form lipoplexes and polyplexes with DNA and are the most widely used synthetic gene delivery vectors (166). Both facilitate interaction of the negatively charged DNA with the negatively charged plasma membrane, which serves as a natural barrier against insertion of foreign DNA. However, despite these attempts to increase transduction substantially, complexed DNA was found not to be substantially more efficient compared to naked DNA (167). Additionally, DNA cation complexes can disassemble shortly after in vivo gene delivery and cationic agents generally show the tendency to cause tissue necrosis. Furthermore, they show the potential for oncogenesis, can activate lymphocytes and lead to the development of pathogenic antibodies to DNA (168). Because of these drawbacks, complexed DNA has not been used in the concept of a "Gene Activated Matrix" up to now. Therefore, more efficient alternative gene delivery vehicles to naked and compexed DNA have to be found.

1.5.3.2.2 Viruses as gene delivery vectors

Viral vectors are naturally highly efficient at bypassing cellular barriers against foreign DNA insertion. Most commonly used viral vectors for gene therapy in the field of tissue engineering are recombinant herpes simplex virus, retrovirus, adenovirus and adeno-associated virus (169). All of these viruses are engineered to be replication deficient, allowing for infection of the target cell but preventing escape of the virus from the cell and therefore uncontrolled infection. Retroviruses are single stranded RNA viruses, most of which are based on the Moloney murine leukemia virus. They are able to insert themselves into the host genome semi-randomly, which has the effect of greater persistence of expression. Due to the complete removal of viral proteins, retroviruses are not immunogenic. However, they only infect actively dividing cells, which usually results in low transfection efficiency (170). Furthermore, mutagenesis may occur, which contributed to the induction of leukemia in two children being treated ex vivo with a retrovirus encoding for the common Υ_c chain of the interleucin receptor for severe combined immunodeficiency syndrome (SCID) in a recent human gene therapy trial (171).

Herpes simplex viruses are double stranded DNA viruses, which are engineered to take up foreign DNA up to 30 kilo bases (kb). $VEGF_{165}$ delivered by herpes simplex virus typ 1, which infects dividing as well as non dividing cells, has been shown to induce angiogenesis in matrigel plugs in mice (172). The vectors cytotoxicity

however, which is responsible for a whole variety of clinical diseases in humans, has hampered extensive in vivo evaluation.

For therapeutic angiogenesis, the most commonly used viral vector is adenovirus, which is capable of transducing both dividing and non-dividing cells (173). The original adenovirus is a double stranded DNA virus, which causes the common cold in humans. The recombinant, replication deficient variant shows excellent transfection efficiency and is easily produced to high titres ($1x10^{13}$ viral particles / ml) (160). Since adenoviruses remain extrachromosomal in the target cells, they do not integrate into the host genome.

Therefore, they provide only transient gene expression for 1-2 weeks in immunocompetent hosts (174). Due to their immunogenicity, adenoviruses have caused inflammatory reactions, fever and increased liver transaminases in human trials. The first gene-therapy associated death occurred in 1999 in a patient with genetic ornithine transcarbamylase deficiency, who received a high dose of adenovirus intraportally (175). Subsequently, much research has been directed towards overcoming cytotoxicity and immunogenicity of adenoviruses. This resulted in the production of "gutless" adenoviruses, from which all adenovirus genes have been removed, leaving only sequences for replication and packaging of the genome behind. The safety profile has thus been improved and the use of adenoviruses has been approved for clinical trials by the US Food and Drug Administration (FDA).

Among the alternatives, adeno-associated virus (AAV) seems to be the most promising candidate for gene therapy involved in tissue engineering (176). AAV's are single stranded, replication deficient DNA parvo-viruses, that are non pathogenic in humans. Wildtype AAV integrates specifically into chromosome 19, but this specificity has been lost in recombinant AAV (rAAV) by elimination of coding sequences, which also diminishes the immune response to viral gene products (177). Additionally, new methods of efficient production and purification of sterile rAAV titers of up to $1x10^{12}$particles / ml have become available recently (178). AAV are small viruses (20 nm), that efficiently transduce dividing as well as non-dividing cells via persistent integration into the hosts chromosomal DNA. This facilitates long-term gene expression in the absence of a cytotoxic T-lymphocyte response. Using rAAV as vector, LacZ marker genes as well as the therapeutic genes encoding for VEGF, tyroxine hydroxylase and alpha-1-antitrypsin have been transduced into mouse striated muscle, mouse ischemic myocardium, rat brain and mouse liver, respectively (177), (179), (180), (181), (182). Gene transfer and expression of factor IX in haemophilic dogs and subsequently in human trials have proven effectiveness in the absence of local toxicity, germline transmission or

immune system pertubation (183), (184). AAV therefore seems to be an attractive vector for angiogenic gene delivey in the concept of a "Gene Activated Matrix". For this reason, we chose AAV as the delivery system for VEGF to increase neovascularisation into porous polyurethane.

Since our concept of a tissue engineered vascular graft consists of the "biological" element of cells, matrices and growth factors as well as of the "mechanical" element of a porous scaffold, which provides structural support for the ingrowing tissue, different biomaterials, polymers and hydrogels as scaffold materials and matrices need to be considered. The following chapter gives an overview over different types of polymers, natural and synthetic hydrogels and matrices used in tissue engineering research.

1.5.4 Biomaterials, hydrogels and polymers as scaffold materials and matrices

Williams defined a biomaterial in 1987 as a "nonviable material used in or as a medical device intended to act with a biological system" (185). Several different groups of biomaterials have been used so far: ceramics, metals, pyrolytic carbon materials, composites and polymers. Of these, polymers represent the largest subgroup of biomaterials and can be described as macromolecules consisting of repeating monomers, which can be subdivided into natural and synthetic as well as into degradable and non-degradable polymers (186). Polymers used today in medical applications include naturally occurring materials such as cellulose and natural rubber as well as synthetic materials such as polyvinylchloride (PVC), Nylon, poly-tetra-fluoroethylene (PTFE), polyethylene terephthalate (PET), silicone rubber as well as polyurethanes (PU). All biomaterials possess three fundamental properties to a different extent:

1. Mechanical strength
2. The functional characteristic
3. Biocompatibility.

A sufficient mechanical strength of the biomaterial is necessary to maintain its physical shape in order to fulfill its proposed function. The functional characteristic is defined as a materials specific functional property to perform a required task (186). Biocompatibility finally can be subdivided into tissue compatibility (histocompatibility) and blood compatibility (hemocompatibility). Histocompatibility can be considered as a lack of toxicity and a minimal inflammatory and fibrotic response whereas hemocompatibility describes a materials potential to be non-thrombogenic and non-

complement-activating (185). The understanding of biocompatibility has evolved over decades from one of biological inertness to the insight, that a certain degree of interaction of a biomaterial with a host tissue is inevitable and can even be beneficial (186). This learning process including the improvement of functional characteristics was the prerequisite for the concept of tissue engineering and regeneration involving biomaterials, as discussed in chapter 1.4. The choice of a certain biomaterial therefore has to be made on the requirement of well defined properties for a specific application. The following sections describe the polymers and hydrogels in use in modern medicine today as well as those currently under investigation in medical research.

1.5.4.1 Hydrogels

Hydrogels are hydrophilic polymers able to absorb between 10 % and thousands of times their dry weight in water (187). Hydrogels can be derived from natural and synthetic sources. Since hydrogels provide an aqueous environment, they are able to protect cells and fragile drugs such as peptides, proteins and DNA. They are usually biocompatible and allow for a sufficient transport of nutrient to cells as well as waste products from cells. Furthermore, they can be relatively easily modified with cell adhesion ligands (188) and may be injected in vivo in a minimally invasive manner as a liquid that gels at body temperature (189). Due to all these advantageous features, hydrogels have become increasingly studied as matrices in the field of tissue engineering over the last decade (190).

1.5.4.2 Natural polymers

Natural polymers include hydrogels of collagen, fibrin, gelatin, alginate, agarose, hyaluronic acid and chitosan as well as natural rubber and cellulose. Collagen is the most widely used tissue derived natural polymer. It is the most abundant protein in mammalian tissues (191) and the main component of extracellular matrices of human tissue including ligaments, tendons, skin, bone and cartilage (190). Collagen gel is degradable by specific cell- enzymes (e.g. collagenase), thus allows cellular degradation and adhesion and meets many of the desired biological design parameters for the use of hydrogels in tissue engineering. However, collagen gels are of limited mechanical strength, potentially immunogenic and exhibit poor loading capacities for growth factors (192). Gelatin is a collagen derivative, formed by breaking the natural triple helix structure of collagen into single strands. As with

collagen, gelatin shows biologically important qualities such as cell adhesiveness and proteolytic degradability, but also limited mechanical strength (190). Fibrin is another natural polymer and plays an important role in wound healing as the major constituent of blood clots. It forms by enzymatic polymerization of fibrinogen in the presence of thrombin and serves as a provisional matrix for cellular ingrowth in the wound. Fibrin supports blood vessel formation and shows no inflammatory reaction or toxic degradation products, because it is a natural scaffold material for the generation of granulation tissue. Furthermore, fibrin has been widely used as tissue sealant and as "fibrin glue" in surgery (e.g.Tissucol, Baxter) (193). Fibrin has further been proven useful as a delivery system for angiogenic proteins (194), cells (195) and DNA of genes (196) that promote wound healing. Zisch et al. described in 2001 the covalent incorporation of $VEGF_{121}$ into fibrin by the transglutaminase activity of factor XIIIa during coagulation (197). Fibrin modified this way can be applied as an injectable gel and serve as an angiogenic ingrowth matrix. Clinical applications of "fibrin glue" containing angiogenic growth factors were described by Greisler et al. and are directed towards a confluent endothelium on the luminal surface of ePTFE bypass grafts via transmural neovascularisation (56). In vitro lining of fibrin treated ePTFE grafts prior to implantation even without additional growth factors showed superior endothelial cell retention and expansion compared to untreated control. This in turn decreases graft thrombogenicity and thus improves long term graft patency (198). However, as with most of the natural polymers, one drawback is the limited mechanical strength of fibrin gels. Additional structural support often has to be provided by a scaffold material. Alginate, another natural polymer, is an anionic polysaccharide commercially produced from marine brown seaweed (199). Due to its simple gelation under gentle conditions with divalent cations such as Ca^{2+} and Mg^{2+}, it's low cost and low toxicity, alginate is widely used as food additive, wound dressings, as well as on an experimental basis for drug, growth factor and cell delivery (200). Despite its advantageous features, alginate is not an ideal matrix for tissue engineering, since alginate hydrogels do not specifically degrade, but undergo slow, uncontrolled dissolution, which in turn results in a loss of mechanical stability. Furthermore, due to the hydrophilic character, alginate lacks cellular interaction and protein adsorption. Other natural polymers such as agarose, hyaluronic acid and chitosan are currently under investigation as matrices for the delivery of drugs, cells and growth factors (201).

1.5.4.3 Synthetic polymers

Because of the potential hazards such as immunogenicity and the risk of infectious pathogens associated with hydrogels derived from natural sources, clinical demand for synthetic replacements of biological matrices has supported research into synthetic polymers and especially synthetic hydrogels as matrices for tissue engineering (202), (203). Furthermore, synthetic polymers can be produced in a controllable and reproducible way and thus batch variation can be avoided to a large extent. Synthetic polymers can be divided in several different groups: aliphatic polyesters of lactide (PLA), of glycolide (PGA), copolymers thereof (PLGA), polypeptides, as well as hydrophilic synthetic polymers that form hydrogels such as polyvinyl alcohol (PVA), polyethylene oxide (PEO) and its copolymers such as polyethylene glycol (PEG), poly-phosphazenes as well as polyacrylic acid (PAA) and its derivates (190). Finally, polyurethanes have been used for decades for a variety of medical devices (186).

Historically, the most widely used synthetic polymers are poly-lactide acid (PLA), poly-glycolic acid (PGA) and copolymers thereof (PLGA) (204). PLGA prefabricated solid scaffolds are insoluble in water but degrade via hydrolytic attack of the ester bond. Due to its mechanical strength, PLGA copolymers have been used for many years in medical implants such as sutures and bone fixation devices and are considered safe for many applications by the FDA. Implanted PLGA scaffolds adsorb proteins from body fluids and thus are cell adhesive. This feature has lead to the integration of PLGA as scaffold material for the development of "TransCyte" and "Dermagraft", two commercially man-made skin substitutes for the treatment of burn wounds (192). Moreover, PLGA scaffolds have been used for growth factor delivery after introducing a new processing technique, which obviates high temperatures and organic solvents (205). PLGA has further been used for the controlled and sustained dual growth factor delivery of $VEGF_{165}$ and PDGF-BB to increase angiogenesis in vivo using PLGA microspheres containing pre encapsulated PDGF-BB (95). As mentioned above, a polymer's ability to absorb water and subsequently form a hydrogel shows many advantages for biological reactions involved in tissue engineering in comparison to a hydrophobic polymer. Consequently, hydrogels from synthetic polymers have received much attention recently. One of the most studied synthetic hydrogels is poly(2-hydroxyethylmethacrylate) (HEMA), which belongs to the subgroup of polyacrylic acids. Poly(HEMA) gels, which are non degradable, have been used clinically as contact lenses, as cartilage replacement and for drug delivery (206), (207), (208). Modification of poly(HEMA) gels with dextran has led to

enzymatic degradability (209). A subtype of polyacrylic acid, poly(N-isopropylacrylamide) (PNIPAAm) appears to be suitable for a minimal invasive approach of tissue engineering because it can be mixed with cells at room temperature and forms into a solid polymer-cell construct after the gel is injected and warms up to body temperature (210). This mechanism of temperature dependent phase transition has been used in vitro in cell culture assays for easy recovery of whole intact cell sheets by decreasing the temperature below the lower critical solution temperature (LCST). As the gel turns into liquid, it allows for rapid hydration and detachment of cells from the culture dish (211). However, limitations of PNIPAAm gels are its toxic, teratogenic and carcinogenic cross-linking molecules as well as its non-degradability (190). Polyvinylalcohol (PVA) is obtained from polyvinylacetate and forms non-degradable hydrogels by chemical cross-linking with glutaraldehyde. PVA hydrogels have been utilized in tissue engineering as drug delivery systems (212) as well as for bone- (213) and pancreatic cell regeneration (214). Hydrogels formed by polyphosphazenes in contrast are degradable and can be produced as ionic or water soluble, non ionic gels. They have been studied as protein drug delivery vehicles, for skeletal tissue engineering (215), as well as for encapsulation of hybridoma cells (216). Another extensively studied synthetic polymer is the group of polyethylene oxides (PEO) and the chemically similar polyethylene glycol (PEG). PEO and PEG are hydrophilic polymers that can be cross-linked into hydrogels via UV exposure (217) or by chemical Michael-type addition reactions with thiol bearing compounds (218). PEO is FDA approved for several medical applications and is one of the most frequentely used synthetic hydrogel polymers in tissue engineering research. Triblock copolymers of PEO and polypropylene oxid (PEO-bPPO-bPEO) which form a thermally reversible gel without permanent cross-links have been produced commercially (Pluronics® or Poloxamer®). A thermosensitive and biodegradable drug delivery system has been introduced by co-polymerisation of poly L-lactide with PEO (189). PEG polymer matrices on the other hand are highly hydrophilic and generally nonadhesive to proteins and cells (219). All PEG polymer matrices form from aqueous solutions containing linear or branched PEG macromers with reactive groups that can be cross linked into hydrogels. Recently, however, "intelligent" PEG matrices have been introduced via integration of bioactive sites into the PEG polymer, which allows direct molecular interaction between cells and matrix (188). Bioactive sites are combinations of synthetic cell adhesive peptide domains and peptide domains for cleavage by targeted proteases (220). Modified PEG hydrogels are therefore able to mediate specific cell adhesion and migration of ingrowing cells which produce

proteolytic enzymes, such as matrix MMP's and plasmin (221). Tissue regeneration using MMP sensitive PEG matrices has been shown to be enhanced via delivery of growth factors such as bone morphogenic protein (BMP) (222) or VEGF (223).

One limitation of all hydrogels, however, is the lack of mechanical strength. If a particular tissue engineering approach requires a substantial mechanical resistance of a material, for example in orthopaedic or vascular replacements, hydrogels may serve as a matrix which needs to be reinforced by a scaffold material. An example of a potential scaffold material showing the required mechanical behaviour is the group of polyurethanes.

Polyurethane (PU) was synthesized by Otto Bayer of I.G. Farbenindustrie, Leverkusen, Germany, as early as 1937 (224). Today, after decades of medical device production on the basis of polyurethanes, this material is still regarded as one of the best biomaterials currently available (186). It shows excellent mechanical properties, particularly tensile strength and fatigue resistance as well as good blood and tissue compatibility.

Polyurethanes consist of three basic components:

1. The polyol or so called soft segment
2. The chain extender
3. The diisocyanate compound

The combination of chain extender and diisocyanate compound is also known as "hard segment". The ability to incorporate other functional groups into the polymer network contributes to the wide range of properties of polyurethanes from soft elastomers to rigid, hard, thermosetting materials (186). Thermoplastic polyurethane, which is the most important subgroup of implantable PU devices, shows excellent tensile strength, resistance to abrasion and degradation as well as good biocompatibility. Therefore, PU has been used clinically extensively as material for cardiovascular catheters, pacemaker lead insulation, vascular prosthesis, heart valves, cardiac assist devices and wound dressings (186).

Our group has recently developed a polyurethane scaffold with well defined open porosity (82 % porosity, 157 µm pore size) by a variation on the phase inversion technique using pre-packed spherical microbeads as porogens (60). As macro-porous polyurethane with an average pore size of 157 µm this material appeared to be superior in terms of inflammatory response compared to smaller pore sizes. In contrast, the angiogenic potential appeared not to be affected by pore sizes (60).

1.5.5 Neovascularisation assays

To study the mechanisms of angiogenesis involving proliferation, migration and differentiation of endothelial cells as well as the contributions of other cell types such as pericytes and smooth muscle cells, suitable methods for assessing the effects of various growth factors and combinations thereof need to be evaluated. Ideally, this assay would be reliable, reproducible, physiologically relevant as well as technically easy to perform and to quantify. Since angiogenesis research has been growing at a rapid rate over the last ten years, valid tests to qualify and quantify angiogenesis in vitro and in vivo are becoming increasingly important (225), (226).

1.5.5.1 In vitro assays

In vitro assays provide an initial step for the evaluation of the effects of various growth factors on a single cell type or a combination of different cell types. They can be carried out rapidly, reproducibly, cost effectively and are usually easily quantifiable. Current models have focused on endothelial cell proliferation, migration and tube formation (226). Cell proliferation assays are capable of determining the number of endothelial cells in culture using a hemocytometer or an electronic counter such as a Coulter counter. Alternatively, DNA synthesis can be assayed by thymidine or bromodeoxyuridine (BrdU) incorporation as a measure of proliferation (227). Assays for endothelial cell migration include the modified Boyden chamber assays (228), phagokinetic track methods (229) as well as the endothelial cell migration assay into a denuded area (230). Differentiation assays stimulate the formation of tube-like structures (231) by culturing endothelial cells on or in matrices such as fibrin, collagen or Matrigel, which consists of extracellular and basement membrane proteins derived from the Engelbreth-Holm-Swarm mouse sarcoma. Capillary like tubules usually form within 4 to 12 hours. To resemble the physiologic situation more closely, Matrigel and fibrin clots have also been used for three dimensional tube formation studies. However, tubules grown from endothelial cell monoculture on collagen or fibrin may not have functional lumina (232). Towards this end, cocultures of endothelial cells with stromal cells such as fibroblasts and smooth muscle cells grown on Matrigel have been shown to produce tubules that contain a lumen and thus mimic a capillary bed in vivo (233). However, the matrix components produced by fibroblasts in coculture are difficult to define and interactions between cell types are likely to occur. Thus, in vitro assays in general have the advantage of a strictly determined environment with only one variable at a

specific time being changed. This however, does not represent the complexity of the in vivo situation of neovascularisation (226).

1.5.5.2 Organ culture assays

Organ culture assays are the combination of organ culture techniques with cell migration analysis. As such, these assays resemble the physiological in vivo situation more closely than any other in vitro technique because they include the surrounding non- endothelial cells such as pericytes and smooth muscle cells as well as the supporting matrix. In the most widely used assay, the rat aortic ring assay, the isolated rat aorta is cut into segments which are placed subsequentely in culture such as Matrigel (234). The outgrowth of endothelial cells is observed in relation to different test substances or growth factors. Other organ culture assays include the chick aortic arch, porcine carotid artery, human placental vein discs and fetal mouse bone (235), (236). However, it is often difficult to quantify angiogenesis using these assays since microvascular structures are often clustered together. Furthermore, in all aortic ring models, vessels grow from a large vessel towards the periphery, whereas angiogenesis is usually a microvascular event.

1.5.5.3 In vivo assays

Once a certain test substance such as a growth factor has been shown to be effective in vitro, being tested preferably in several different assays, this substance needs to be evaluated in vivo. This is of importance, because due to the complex interaction of different celltypes, matrices, hormonal and neural influences in vivo, the in vitro tested effective substance may be less or even not at all effective in vivo (237). The most widely used in vivo assay to study angiogenesis is the chick chorioallantoic membrane (CAM) assay (238), which was described by experimental embryologists more than 50 years ago (225). Briefly, the test substance or tissue is placed directly onto the CAM of 7-9 day old chick embryos, after a window has been cut in the eggshell. The angiogenic effects can be observed and measured using a stereomicroscope. In a modification of this in ovo-method, the whole embryo is transferred to a plastic culture dish after 72 hours of incubation, which allows for the quantification of blood vessels over a wider area of the CAM at any time point (239). The CAM assay is a relatively easy to perform, inexpensive angiogenesis assay suitable for large scale screening. However, since the chorioallantoic membrane itself is vascularized with an extensive capillary bed (240), it is difficult to distinguish

between the angiogenic effect of a test substance and the normal embryonic development of vascularisation. In addition, the CAM often shows an inflammation around day 8 in response to a variety of substances, which may influence angiogenesis and makes analysis of new vessels more difficult (241).

The corneal angiogenesis assay in contrast is based on a primarily avascular organ and thus allows analysis of the newly ingrown vascular network. A pocket is made in the cornea and test substances or tissues introduced into this pocket, elicit the ingrowth of blood vessels from the peripheral limbal vasculature. Initially, the method was introduced in rabbits (242), but later was used for the study of angiogenesis in mice (243). The vascular response to a test substance can be detected by perfusion of the cornea with India ink or fluorochrome-labeled dextran (244) and subsequently quantified via computed image analysis. The advantages of the corneal angiogenesis assay are: no pre-existing background vasculature, mice can be used as animal model and the process of angiogenesis can be monitored over time. On the other hand, this assay is, compared to CAM, more expensive and technically more demanding. Secondly, the cornea as avascular implantation site is for this very reason atypical for most kinds of implants. A more "physiological" type of an in vivo angiogenesis assay is the "chamber assay". The rabbit ear chamber, the mouse and rat dorsal skinfold chamber and the cranial window chamber have contributed to the study of angiogenesis (226). Once a piece of skin (skinfold chamber) or a part of the skull (cranial window chamber) is removed, the underlying tissue can be monitored microscopically with respect to angiogenesis to certain stimulatory or inhibiting substances. Neovascularisation involved in wound healing or in tumor implants may be studied. Additionally, blood flow, pH and gene expression can be measured (245).

Chamber assays allow for the three dimensional study of angiogenesis over a period of two to three weeks, but are invasive, technically demanding and may have poor optical properties due to the thickness of examined tissue. In contrast to the corneal angiogenesis assay and the chamber assays, the subcutaneous implantation of sponges and polymers is surgically a simple procedure. Natural or synthetic polymers containing test substances such as growth factors can be implanted into subcutaneous pockets in mice, rats and rabbits (246). After an implantation time of a few days, granulation tissue consisting of inflammatory cells, fibroblasts, endothelial cells and muscle cells grow around and into the porous sponges. Neovascularisation can thereby be assessed by immunohistological staining (CD31 and CD34), haemoglobin level of the sponge, or by radioactive tracer levels in blood (247). Care must be taken with interpretation of the results,

since the surgical implantation of a polymer itself can cause an inflammatory reaction that leads to an increase of angiogenesis per se (248). Furthermore, implantation, explantation and analysis of sponges has been described as time consuming and tedious (249). And unlike the corneal pocket or the chamber assay, the subcutaneous pocket assay does not allow for real time in vivo observation of angiogenesis (245). However, if a valid baseline is established by choosing the correct control groups, this assay allows for an accurate quantification of neovascularisation, since the implant is primarily avascular (249). Overall, due to the complex interplay of various biological signals, different cell types and extracellular matrix involved in angiogenesis, the optimal strategy to obtain valid and reproducible results would ideally be to combine several in vitro and in vivo assays involving different species. This, of course, is time consuming, labour intensive and therefore often impractical.

2. Hypothesis

As outlined in chapters 1.4 and 1.5, the concept of transmural in vivo endothelialisation of a vascular graft holds great promise for increased long term patency. To achieve complete luminal endothelial cell coverage and optimal integration of the porous synthetic graft into the host tissue, transmural ingrowth of tissue and vasa vasorum might have to be facilitated. VEGF and PDGF are growth factors known to stimulate and consolidate angiogenesis. This PhD thesis would like to determine, whether vascular growth factors can be delivered on and into porous polyurethane and whether these growth factors create the desired angiogenic response within the synthetic material. Therefore, three different ways of growth factor delivery are evaluated:

1. Growth factor delivery to porous polyurethane by adeno-associated viruses
2. Growth factor delivery to porous polyurethane by heparin surface modification
3. Continuous growth factor delivery by osmotic mini-pumps into a "Neovascularisation Construct"

Finally, this PhD thesis examines three different methodologies to quantify functional angiogenesis, namely lectin perfusion, micro-CT scanning and corrosion casting

The hypothesis of this PhD thesis is:

Neovascularisation of porous polyurethane can be increased by delivery of vascular endothelial growth factor (VEGF) and platelet derived growth factor (PDGF)

3. Project Aims

In order to prove or disprove this hypothesis, four main project aims were identified, which are as follows:

1. A valid, reproducible, simple and quantifiable neovascularisation model has to be established.

2. Different ways of growth factor delivery including different matrices to induce neovascularisation of porous polyurethane need to be investigated.

3. The induction as well as the stability of neovascularisation into porous polyurethane through delivery of VEGF and PDGF-BB as well as a combination thereof has to be investigated.

4. The relative proportion of perfused neovessels (vessel functionality) needs to be investigated using different analytical tools of quantification.

4. Growth factor delivery by adeno-associated viruses

4.1 Introduction

Since rAAV has been shown to efficiently transduce LacZ and VEGF genes into striated and myocardial muscle cells, we wished to investigate whether rAAV is also capable of transducing cells that form granulation tissue growing into subcutaneously implanted porous polyurethane discs. The approach utilized was to deliver AAV from a matrix, a novel modification of the "Gene Activated Matrix" (GAM) method (as described in the main introduction). Up to now, mainly plasmids have been used as gene delivery vectors in GAM's (163), (250). Chandler et al. were the first to utilize a viral vector, namely adenovirus encoding for PDGF to enhance tissue formation (251). AAV has, so far, never been used as gene delivery vector using the GAM approach. AAV may transduce granulation tissue growing into a porous scaffold, thus allowing for localized and sustained production of angiogenic growth factors. This could improve transmural neovascularisation of porous polyurethane as a possible scaffold material for vascular grafts providing the basis for rapid integration into the host tissue and ultimately sufficient surface endothelialisation for improved long term patency.

Therefore, replication deficient adeno-associated virus (AAV) was genetically modified in our laboratory to integrate a gene of interest into the genome of autologous cells. Following the concept of GAM, AAV was embedded into a matrix and was expected to transduce autologous cells growing into the matrix after implantation in vivo. To provide structural stability, the matrix was inserted into porous polyurethane as a possible vascular graft material. As it is known of subcutaneous implants, autologous wound repair cells consist of inflammatory cells, myofibroblasts, fibroblasts and endothelial cells. As these cells migrate into the porous polyurethane scaffold, they become infected by the virus, the "therapeutic gene" is transferred and wound cells therefore act after AAV transduction as "Bioreactor". Before in vivo experiments on the transduction efficacy could be started, three "in vitro" questions had to be answered:

1. How stable is AAV in serum?
2. What is the release kinetics of AAV using different matrices within the polyurethane scaffold?
3. How can release kinetics and transduction efficiency be improved?

Since the ability of viral vectors to transduce autologous cells is dependent on the amount of infectious virus present at the time of cellular ingrowth into the "bioreactor" model, an ideal matrix or a biomaterial would be one which shows excellent AAV-LacZ retention for at least 7 to 10 days. It is well known, that AAV shows high affinity to the negatively charged heparin molecule (259), and this is the reasoning behind the heparin column AAV-LacZ purification method, which was used for the production of AAV-LacZ (254). Furthermore, the use of this high heparin-affinity of AAV-LacZ was explored, whether it increases AAV-LacZ retention within the porous PU disc. To this end, polyurethane discs were surface coated with heparin (4.2.1.2) and assayed with regards to viral retention (4.2.4.2).

4.2 Materials and Methods

4.2.1 Polyurethane (PU) discs

4.2.1.1 Production of PU discs

Polyurethane (PU) discs with a diameter of 5.4 mm and a thickness of 2 mm with well-defined open porosity (82 % porosity, 157 ± 1 µm pores) were produced by a variation on the phase inversion technique using pre-packed spherical micro beads as porogens in our laboratory as described previously (60) (Figure 1).

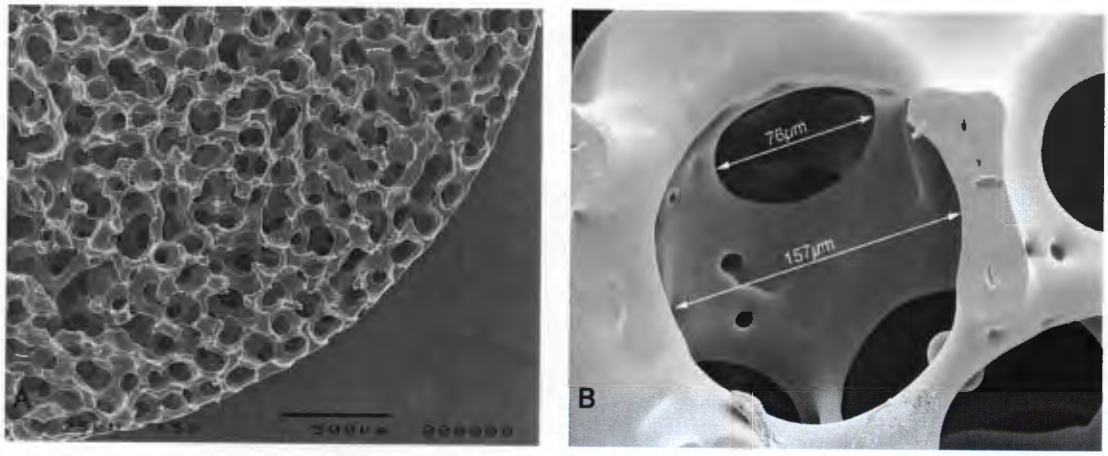

Figure 1: Scanning Electron Microscopic (SEM) picture of a porous polyurethane disc with a diameter of 5.4 mm and a thickness of 2 mm (50 x magnification) (A). Discs show well-defined open porosity of 82 %, a pore size of 157 ± 1 µm and interconnected windows of 76 ± 1 µm (SEM, 500 x magnification) (B). Discs were produced and pictures taken by Bezuidenhout et al., with permission.

4.2.1.2 Heparin coating of PU discs

For certain experiments, PU discs were coated with heparin by Mr. Lawrence Higham, polymer scientist at the Cardiovascular Research Unit of the University of Cape Town, via a three step process:

1. Cerium-ion initiated graft copolymerization with acrylic acid and acrylamide
2. Covalent attachment of ethylene diamine
3. Immobilization of nitrous acid degraded (NAD) heparin via reductive amination

PU discs were washed in isopropanol (Sigma Aldrich Chemie, Steinheim, Germany) for 20 minutes and then rinsed in distilled water for 20 minutes, replacing the distilled water every 5 minutes. The grafting solution, consisting of 4 M acrylic acid (Sigma Aldrich Chemie, Steinheim, Germany), 1 M acrylamide (Sigma Aldrich Chemie, Steinheim, Germany), 0.015 M cupric nitrate (Merck Chemicals, Saarchem, Gauteng, South Africa) and 0.006 M cerium ammonium nitrate (Merck KgmA, Darmstadt, Germany) was purged of oxygen by bubbling argon gas at a rate of 5 liters / minute for 5 minutes. Discs were added to this solution and reacted for 40 minutes at room temperature, while being sonicated to ensure even coverage. Upon completion of the reaction, discs were rinsed for 30 minutes in distilled water and then washed in PBS (pH 7.4) overnight on a platform shaker. Washed discs were immersed in a 1 M 2 - morpholinoethanesulfonic acid monohydrate / ethylenediamine (MES / EDA solution, 0.5 M MES, 0.5 M EDA, pH 5.0) containing 0.05 M N - (3 dimethylaminopropyl) – N -ethylcarbodiimide hydrochloride (EDCI) (both Fluka Chemie GmbH, Switzerland) for 2 hours at room temperature and sonicated. Discs were rinsed in distilled water and washed overnight in PBS (pH 7.4).

Heparinisation was achieved by reacting the discs in a 0.4 M acetate buffered solution (0.2 M sodium acetate) (Saarchem - Holpro Analytic, Krugersdorp, South Africa), 0.2 M glacial acetic acid, pH 4.6 (Merck Chemicals, Saarchem, Gauteng, South Africa) containing sodium cyanoborohydride (1 mg / ml) (Sigma Chemicals, St.Louis, USA) and nitrous acid degraded heparin (2 mg / ml, MW 6483, Celsus Laboratories Inc., Cincinnati, Ohio, USA) at 50°C in a sonic bath for 2 hours. Treated PU discs were rinsed in distilled water, washed overnight in PBS (pH 7.4), sterilized by immersion in 70 % ethanol for 12 hours and air dried under sterile conditions until loading with $VEGF_{165}$ or PBS (Figure 2).

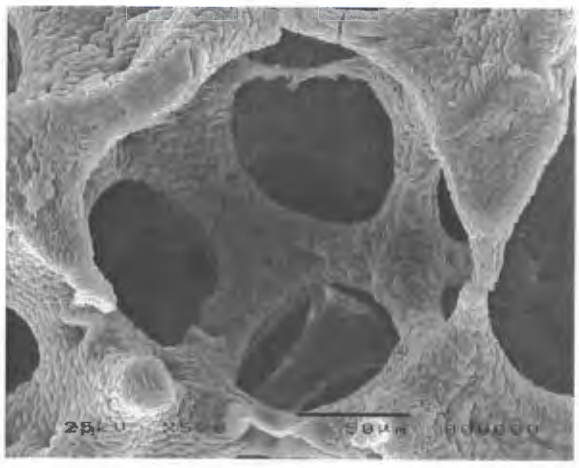

Figure 2: SEM picture of a heparin coated PU disc. Discs were heparin surface modified by L. Higham by cerium-ion initiated graft copolymerization with acrylic acid and acrylamide, covalent attachment of ethylene diamine and immobilization of nitrous acid degraded (NAD) heparin via reductive amination. The picture was taken at 500 x magnification by Bezuidenhout et al., with permission

4.2.2 Matrices: fibrin, collagen, polyethylene glycol (PEG)

4.2.2.1 Fibrin matrix

For matrix cellular ingrowth studies as well as for AAV elution studies, fibrin matices were produced in three different concentrations: 10 mg / ml, 25 mg / ml and 50 mg / ml using commercially available fibrin (Tisseel™ Kit 2.0H, Baxter, USA). To produce a stock solution, fibrinogen was dissolved in Nanopure® water (Barnstead International Dubuque, Iowa, USA) to a concentration of 80 - 120 mg / ml. The exact concentration was determined by UV absorption at 280 nm with an extinction coefficient of 1.55. For 50 µl of fibrin at a concentration of 10 mg / ml, 5 µl fibrinogen 100 mg / ml was added to 44 µl of PBS in one well of a 96 well plate (Costar® E.I.A., Cambridge, MA, USA). 0.5 µl of 100 mmol / l $CaCl_2$ (Sigma Aldrich Chemie, Steinheim, Germany) as well as 0.5 µl of 200 I.E. / ml thrombin (Tisseel™ Kit 2.0 H, Baxter, USA) were added, mixed and aspirated into the PU disc immediately by squeezing the disc at least three times with a plunger of a 1 ml syringe (Codan Medical Apl., Rodby, DK) to remove all trapped air inside the disc and to efficiently load the fibrin matrix.

A concentration of 25 mg / ml of fibrin (50 µl) was achieved by mixing 12.5 µl of fibrinogen 100 mg / ml with 36.5 µl PBS, 0.5 µl $CaCl_2$ and 0.5 µl thrombin (200 I.E. / ml). 50 µl of fibrin in the highest concentration of 50 mg / ml was produced by mixing 25 µl of fibrinogen 100 mg / ml with 24 µl PBS, 0.5 µl $CaCl_2$ and 0.5 µl thrombin (200 I.E. / ml). All fibrin loaded discs were incubated at 37°C for 60 minutes to allow for adequate polymerization before implantation for cell invasion and tissue ingrowth studies.

4.2.2.2 Collagen matrix

Collagen matices were produced at a final concentration of 0.5 % for tissue ingrowth and 0.4 % for AAV transduction studies. First, a 0.6 % collagen solution was made by dissolving 6 mg of lyophilised collagen type I from calf skin (Fluka Chemie, Sigma Aldrich Chemie, Germany) in 1ml of 1 mM hydrochloric acid (HCL) (Merck Chemicals Ltd, South Africa) at 4°C overnight. After gentle vortexing, 1 ml of a 0.5 % collagen gel was produced the following way: 830 µl collagen 0.6 % was added to 100 µl 10 x PBS (Gibco, Paisley, UK), to 11.5 µl 1 M sodiumhydroxide (NaOH) (Saarchem - Holpro Analytic, Krugersdorp, South Africa) and to 58.5 µl Nanopure ® water. All solutions were kept at 4°C. Finally, pH was adjusted, if necessary, to 7.0 by pipetting 1 M NaOH. Aspiration of the collagen solution into the PU discs was done as described in 4.2.2.1. Thereafter, the collagen solution inside the PU disc was allowed to gel at 37°C for at least 2 hours. Cross linking was facilitated using a CO_2 free incubator.

4.2.2.3 Polyethylene glycol matrix

PEG matrices were produced at concentrations of 3 % and 5 %. In order to obtain 50 µl of a 3 % final concentration, 15 µl of a 10 % m / v 20 kDa 4 arm PEG vinyl sulfone (PEG 20 - 4 VS) (20kg/mol) produced in our laboratory as per Lutolf et al. (221) was incubated with 1.8 µl mono-cysteine cell adhesion peptide GCGYGRGDSPG (RGD) at 6.6 mg / ml and 20.7 µl PBS pH 7.4 for 30 minutes at 37°C. Then 12.5 µl of a di-cysteine enzymatically cleavable, cross linking peptide GCREGPQGIWGQERCG (MMP-1) at 21 mg / ml was added to the solution. A 5 % final concentration solution was produced in an analogous fashion but 25 µl 10 % PEG 20-4 VS was mixed with 3 µl 6.6 mg / ml RGD peptide and 9.5 µl PBS followed by 12.5 µl 35 mg / ml MMP-1 peptide. The PEG solutions were aspirated into the PU discs as described in 4.2.2.1. Furthermore, all PEG loaded discs were incubated at 37°C for 60 minutes to allow for adequate polymerization before implantation for cell invasion and tissue ingrowth studies.

MMP-1 peptide was a gift from Dr. M. Lutolf, Stanford University, California, USA. The RGD peptide was synthesized in our laboratory by Mrs. Mona Bracher.

4.2.3 Recombinant adeno-associated virus (rAAV)

In the following chapters AAV is used as a synonym for recombinantly produced single stranded AAV serotype 2 (rAAV - 2), unless stated otherwise.

4.2.3.1 Production of single stranded AAV-LacZ, AAV-VEGF and double stranded AAV-GFP

AAV vectors were produced by Mrs. Ronett Seldon, technician at the Cardiovascular Research Unit, without helper adenovirus using the "AAV helper-free system" of Stratagene, (Stratagene, La Jolla, USA), based on the methodology described previously by Matsushita et al. (252). The vector production process involved co-transduction of human embryonic kidney cells (HEK 293) (American Type Culture Collection ATCC, Manassas, VA, USA) using the calcium phosphate method with the following three plasmids:

1. The recombinant AAV vector plasmid containing the gene of interest, in our case the gene encoding for LacZ and $VEGF_{165}$, respectively
2. The AAV helper plasmid, which carries adenovirus-derived E2A, E4 and VA regions and mediates AAV vector replication
3. The AAV-RC plasmid, which carries AAV replication and capsid genes

The pAAV-lacZ plasmid was supplied with the "helper free kit". The gene for $VEGF_{165}$ was subcloned into the pCMV - MCS vector supplied with the Stratagene AAV helper free kit from pCi - $VEGF_{165}$ (kind gift from J. Dulak, Jagellonian University, Krakow, Poland) by Ronnett Seldon. It is recommended by the manufacturers that genes of interest (GOI) that are shorter than 1000 base pairs, should have "stuffer" DNA added to increase total length cloned to greater than 1 kb. Therefore, as the $VEGF_{165}$ gene has a length of 450 bp it was subcloned between the ECoR I and Xba I sites of a modified pCMV - MCS vector, pCMV-stuffer. This vector had a non-coding region of DNA of 740 bp inserted between the Pst I and Bgl II of pCMV - MCS. The $VEGF_{165}$ gene plus the relevant flanking regions was then subcloned into pAAV - MCS (a vector containing the inverted terminal repeats of AAV-2) following the manufacturer's instruction. The resultant pAAV - $VEGF_{165}$ was used to generate AAV - $VEGF_{165}$ virus via the "helper-free system". All restriction

enzymes were obtained from Promega, Madison, WI, USA and digestions were carried out as per the manufacturer's instructions.

Double stranded AAV encoding for green fluorescent protein (dsAAV-GFP) was produced as follows: again, the triple plasmid co-transduction method was used to produce recombinant viral stocks (253). In contrast to the AAV helper- and the AAV-RC plasmid which were used in exactly the same way as for the co-transduction of single stranded AAV, the AAV vector plasmid was double stranded under the control of the cytomegalie virus promoter (a kind gift of Dr. X. Xiao, University of Pittsburgh, Pittsburgh, USA). Green fluorescent protein (GFP) served as the gene of interest. Single stranded AAV - GFP was purchased from Stratagene (Stratagene, La Jolla, USA). For graphical illustration of vector production, see Figure 3, which was reproduced from Stratagene's instruction manual "AAV helper-free system", (Stratagene, La Jolla, USA).

4.2.3.2 Vector harvesting and purification

AAV vectors were harvested and purified by a single step, heparin gravity flow column, which was described by Auricchio et al. in 2001 (254). Shortly, HEK 293 cells from one 15 cm dish were harvested 3 days after transduction and resuspended in 2.5 ml of Dulbecco's modified Eagle's medium (DMEM) (Gibco, Paisley, UK). After two cycles of freezing and thawing, cells from 25 plates were pooled and incubated with 0.1 mg of DNase I and RNase A (Roche Biochemicals, Mannheim, Germany) per plate for 30 minutes at 37°C. After centrifugation at 3000 rpm for 15 minutes, deoxycholic acid (Sigma, St.Louis, MO, USA) was added to the supernatant to a final concentration of 0.5 % and incubated for 30 minutes at 37°C. The crude lysate was sequentially filtered through a 5 µm and a 0.8 µm pore size filter (Millipore, Bedford, MA, USA) and then applied to a heparin column as follows: 8 ml of a 50 % heparin - agarose suspension (Sigma, St.Louis, MO, USA) was added to a 2.5 cm diameter plastic column (Sigma, St.Louis, MO, USA). After flow through, a filtration membrane (Sigma, St.Louis, MO, USA) was placed on top of the column which was then equilibrated with 25 ml phosphate buffered saline (PBS), pH 7.4. A Luer-Lock controlled the flow speed of the crude lysate, which was added to the column, to about 1 drop per second. The matrix was washed twice with 25 ml of PBS, pH 7.4 containing 0.1 M NaCl. Afterwards, AAV was eluted with 15 ml of PBS, pH 7.4 containing 0.6 M NaCl. Finally, the eluate was concentrated to 1 ml by centrifugation in a Biomax filter device (Millipore, Bedford, MA, USA).

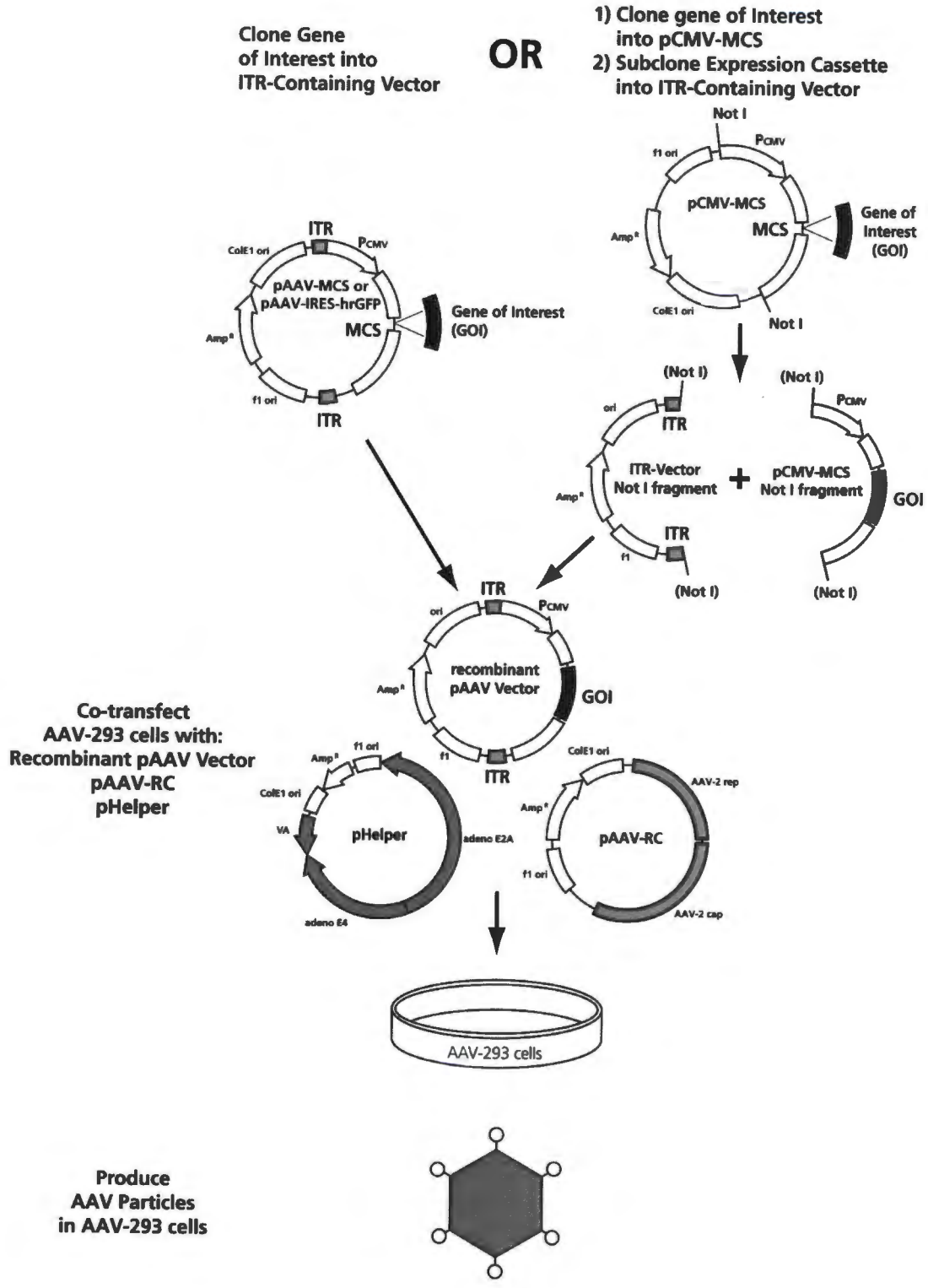

Figure 3: AAV helper-free, triple plasmid co-transduction method: AAV production involves the recombinant AAV vector plasmid carrying the gene of interest, the AAV - RC plasmid (AAV replication and capsid genes) and a helper plasmid. The plasmids co-transduce HEK-293 cells and produce replication deficient, non pathogenic AAV. This graph is reproduced from Stratagene's instruction manual "AAV helper-free system", (Stratagene, La Jolla, USA).

4.2.3.3 Quantification of AAV by PCR

Purified vectors were quantified for genome copies (gc) by real time polymerase chain reaction (PCR). PCR was performed using the Quantitect SYBR Green PCR kit (Qiagen, Southern Cross Biotechnology (Pty) Ltd - South Africa). PCR amplification was carried out using primers that annealed to regions in the multiple cloning sequence that spanned the gene of interest (see below). 1 µl of left and right primer each, 3 µl RNase free water, 5 µl sample and 10 µl SYBR green were added to a final volume of 20 µl. PCR was performed using a Light Cycler® 2.0 (Roche, Basel, Switzerland) with a 15 minutes activation time at 95°C, followed by 35 cycles of 15 seconds at 94°C for denaturation, 20 sections at 55°C for annealing and 15 seconds at 72°C for amplification. The 5 µl sample was taken from a 100 µl preparation, which consisted of 10 µl original AAV sample, 10 µl 10 x DNase buffer, 76 µl nuclease free water and 4 µl DNase I - RNase free. The 100 µl solution was overlayed with mineral oil, incubated for 1 hour at 37°C, boiled for 5 minutes and then cooled immediately on ice. PCR products were subjected to melting curve analysis using the light cycler system to assay for the amplification of non - specific products. Furthermore, in each PCR run, a standard curve was generated using a 5 log spanning serial dilution of the vector plasmid pAAV from 10^3 to 10^8 copies. A standard curve was plotted using Microsoft Excel software (Microsoft, USA) with the threshold cycle on the x - axis and the logarithm of the copy number on the y - axis. A logarithmic regression was performed and the equation was used to determine the genome copies present in the AAV samples. Regression coefficients for the standard curves ranged from 0.995 - 1.

AAV primer sequences used were:
AAV MCS left 5' CAA GTA CGC CCC CTA TTG AC 3'
AAV MCS right 5' TAT CCA CGC CCA TTG ATG TA 3'

Materials used for Light Cycler quantification:
10 x DNase buffer – (50 mM Tris - HCL pH 7.5, 10 mM $MgCl_2$)
Nuclease free water – (0.1 % Depc treated water)
DNase I - RNase free (Roche, Basel, Switzerland)
Mineral oil (Promega, Madison, WI, USA)
Quantitect SYBR Green PCR kit (Qiagen, Southern Cross Biotechnology (Pty) Ltd - South Africa)

Light Cycler® 2.0 (Roche, Basel, Switzerland)
Light Cycler® capillary holder and cooling block (Roche, Basel, Switzerland)
Light Cycler® capillaries (Roche, Basel, Switzerland)

4.2.3.4 Infectivity of AAV

An assay that allows the quantification of the number of infective AAV-LacZ units in a sample was established according to the protocol given in the "Stratagene manual" (Stratagene, La Jolla, USA). HT 1080 fibrosarcoma cells (passage 7) were obtained from the European Collection of Cell Cultures (ref. 85111505 ECACC). Cells were maintained in Dulbecco's modified Eagle's medium (DMEM growth medium, Gibco, Paisley, UK) supplemented with 10 % fetal calf serum (FCS, Delta Biologics, South Africa), 1 % 200 mM L-glutamate (Sigma Aldrich Chemie, Steinheim, Germany), and 1 % penicillin and streptomycin (p / s) (Sigma Aldrich Chemie, Steinheim, Germany).

Preparation of HT 1080 permissive cells

HT1080 cells were plated at a density of 1.5 x 10^5 per well in 1 ml of DMEM growth medium in 12 well tissue culture plates and incubated overnight at 37°C. At approximately 70 % cell confluence, 0.2 ml of AAV permissive medium (recipe given below) was added per well for final concentrations of 40 mM hydroxyurea (HU) (Sigma Aldrich, Steinheim, Germany) and 1 mM sodium butyrate (Sigma Aldrich, Steinheim, Germany) in the medium. Plates were returned to 37°C after thorough swirling for 6 hours. Finally, medium was aspirated and cells were washed once with 1 ml of pre-warmed L - DMEM (DMEM supplemented with 2 % (v / v) heat-inactivated FCS and 2 mM L - glutamine).

Viral stock dilution and application

AAV - LacZ viral stocks were diluted in 2 ml volumes over a 10 - fold series from 10^{-2} to 10^{-5} in L - DMEM. Next, 0.5 ml of each virus dilution was added to separate wells of the 12 well plate in duplicate. Plates were incubated for 2 hours at 37°C, being swirled gently at 30 minute intervals. Finally, 0.5 ml of pre-warmed H - DMEM (DMEM supplemented with 18 % (v / v) heat-inactivated FCS and 2 mM

L-glutamine) was added per well and the 12 well plate was further incubated for 48 hours at 37°C.

Detection of transduced cells by X-gal (5-bromo-4-chloro-3-indolyl-beta-D-galactopyranoside) staining

Transduced cells were detected using a standard technique described by Mercer et al. (255). H - DMEM medium was aspirated from each well and rinsed once with 1 ml PBS (pH 7.3). Next, 1 ml of fixative (recipe given below) was added to each well on ice for 5 minutes. After aspiration of the fixative, cells were rinsed three times with PBS for 4 minutes each and stained with 500 µl staining solution (recipe given below) at 37°C overnight. Finally, the next morning, cells were rinsed once with PBS and analyzed as described in 4.2.7.

Detection of transduced tissue by X-gal staining

To detect transgene expression of LacZ in transduced tissue such as muscle samples or granulation tissue, the following standard protocol for X-gal staining was used (255): Freshly removed tissue was fixed in 5 ml of 4 % paraformaldehyde / PBS (pH 7.0 - 7.5) (Saarchem, Kruegersdorp, South Africa) for 1 hour at 4°C. Tissue was rinsed three times with 5 ml of rinse buffer (recipe given below) at room temperature for 30 minutes each. Thereafter, tissue was stained using 5 ml of X-gal staining solution overnight (recipe given below) at room temperature. Finally, tissue was post-fixed overnight in 5 ml 10 % formalin (Merck Chemicals, Gauteng, South Africa) at 4°C.

Infectivity assay on Chinese Hamster Ovary (CHO) cells

To determine infectivity and transgene expression of GFP delivered by AAV, CHO cells (kind gift of Prof. Iqbal Parker, Department of Microbiology, University of Cape Town, South Africa), were used according to the following protocol:
CHO cells were trypsinised, counted and seeded into a 24 well plate. 75000 cells were seeded in MCDB (Sigma Aldrich, Steinheim, Germany) and 10 % Fetal calf serum (FCS) (Delta Biologics, South Africa) and allowed to settle for 5 hours. 2 µl of ssAAV-GFP or 2 µl of dsAAV-GFP (8×10^6 gc) of the virus preparations were added and re-incubated for 48 hours.

Materials used for AAV titer measurements in cells and tissues

All used chemicals were purchased from Sigma Aldrich, Steinheim, Germany, unless stated otherwise.

PBS:
100 mM sodium phosphate (pH 7.0 - 7.5)
150 mM NaCl

AAV permissive medium:
DMEM Growth Medium
(containing 10 % (v / v) heat-inactivated FCS and 2 mM L-glutamine)
240 mM hydroxyurea (HU)
6 mM sodium butyrate.
Prepare stock of 1 M HU in PBS, filter sterilize, add 240 µl stock per ml AAV permissive medium. Prepare stock of 0.5 M sodium butyrate in PBS, filter sterilize, add 12 µl per ml AAV permissive medium.

Fixative for cells:
2.7 ml of 37 % formaldehyde
0.4 ml glutaraldehyde (25 %)
add to 50 ml with cold PBS (pH 7.3)

X-gal staining solution for cells:
1 ml X-gal stock (25 mg / ml in DMF)
50 µl magnesium chloride ($MgCl_2$)
41 mg potassium ferricyanide
53 mg potassium ferrocyanide
add to 25 ml with PBS (pH 7.3)

Rinse buffer for X-gal staining of tissue
100 mM sodium phosphate (pH 7.3)
2 mM $MgCl_2$
0.01 % sodium deoxycholate
0.02 % NP - 40 (by volume)

X-gal staining solution for tissue

Rinse buffer plus:

5 mM potassium ferricyanide, from 0.5 M stock

5 mM potassium ferrocyanide, from 0.5 M stock

1 mg / ml X-Gal, from 25 mg / ml stock in dimethylformamide (DMF)

4.2.4 AAV in vitro studies

4.2.4.1 AAV elution studies from different matrices

In order to achieve best results of AAV transduction of granulation tissue growing into the porous polyurethane discs loaded with different matrices ("Gene Activated Matrix" approach), we first sought to determine the ability of different matrices to retain AAV. Three different concentrations of fibrin matrices, namely 10 mg / ml, 25 mg / ml and 50 mg / ml were evaluated. Furthermore, collagen 0.4 % was tested for its AAV retention abilities as a single matrix as well as in combination with PEG 3 %. The different matrices were produced as described in chapters 4.2.2.1, 4.2.2.2, and 4.2.2.3. For elution studies, AAV was integrated into matrices in the following manner:

AAV-LacZ elution from fibrin matrices

Fibrin matrices were produced using the Baxter Tisseel™ Kit (Tisseel™ Kit 2.0 H, Baxter, USA). For AAV elution studies from different fibrin concentrations, PU discs were loaded with fibrin containing AAV as follows:

1. Fibrin 10 mg / ml: 5 µl fibrinogen (100 mg / ml)
   0.5 µl thrombin (200 IE / ml)
   0.5 µl $CaCl_2$ (100 mmol / l)
   10 µl AAV-LacZ (2.23×10^{10} gc / ml)
   34 µl PBS

2. Fibrin 25 mg / ml: 12.5 µl fibrinogen (100 mg / ml)
   0.5 µl thrombin (200 IE / ml)
   0.5 µl $CaCl_2$ (100 mmol / l)
   10 µl AAV-LacZ (2.23×10^{10} gc / ml)

26.5 µl PBS

3. Fibrin 50 mg / ml: 25 µl fibrinogen (100 mg / ml)
0.5 µl thrombin (200 IE / ml)
0.5 µl $CaCl_2$ (100 mmol / l)
10 µl AAV-LacZ (2.23 x 10^{10} gc / ml)
14 µl PBS

After addition of thrombin, PU discs were immediately squeezed at least three times with a plunger of a 1 ml syringe (Codan Medical Apl, Rodby, DK) to mix and load the fibrin solution thoroughly and to remove all air trapped inside the disc.

AAV-LacZ elution from collagen matrices

As described in chapter 4.2.2.2 "Collagen matrix", a 0.6 % collagen solution was produced by dissolving 6 mg of lyophilised collagen type I from calf skin (Fluka Chemie, Sigma Aldrich Chemie, Germany) in 1 ml of 1 mM hydrochloric acid (HCL) (Merck Chemicals Ltd, South Africa) at 4°C overnight. After gentle vortexing the next morning, 1 ml of a 0.5 % collagen gel was produced the following way:

830 µl collagen 0.6 %
100 µl 10 x PBS (Gibco, Paisley, UK)
11.5 µl 1 N sodium hydroxide (NaOH) (Saarchem - Holpro Analytic, Krugersdorp, South Africa)
58.5 µl Nanopure® water (Barnstead International Dubuque, Iowa, USA)

All solutions were kept at 4°C. Finally, the pH was adjusted to 7, by pipetting extra 1N NaOH, if necessary. To obtain a collagen 0.4 % solution, 40 µl of collagen 0.5 % were added to 10 µl of AAV-LacZ (2.23 x 10^{10} gc / ml) per well. PU disc were squeezed at least three times with a plunger of a 1 ml syringe (Codan Medical Apl, Rodby, DK) to mix and load the collagen solution thoroughly and at the same time to remove all trapped air inside the disc.

AAV-LacZ elution from PEG matrices

To evaluate the ability of PEG 3 % to sufficiently retain AAV for a prolonged period of time, a PEG 3 % matrix was produced, as described in chapter 4.2.2.3. This

matrix was loaded with AAV-LacZ and integrated into PU discs in the following fashion:

40 µl of the above mentioned PEG / RGD / MMP - 1 solution was added to 10 µl of AAV-LacZ (2.23 x 10^{10} gc / ml) per well. PU disc were squeezed at least three times with a plunger of a 1 ml syringe (Codan Medical Apl, Rodby, DK) to mix and load the PEG solution thoroughly and at the same time to remove all trapped air inside the disc. In order to study the ability of a combined PEG 3 % and collagen 0.4 % matrix to retain AAV-LacZ more efficiently, 10 µl AAV-LacZ (2.23 x 10^{10} gc / ml) were embedded into 45 µl of a collagen 0.5 % matrix, loaded into the PU disc, lyophilized overnight and coated subsequently with 50 µl of PEG 3 % (described in 4.2.2.3). After loading of the PU discs with the different matrices containing AAV-LacZ, discs were incubated at 37°C for at least 2 hours to allow for adequate polymerization. Thereafter, PU discs were submersed in 5 ml PBS + 0.5 % BSA (Merck Chemicals Ltd, Gauteng, South Africa) + 0.02 % NaN_3 (Merck Chemicals Ltd, Gauteng, South Africa) for 8 days at 37°C under continuous agitation. 100 µl aliquots were taken at 6 hours, 24 hours, 48 hours, 3 days and 7 days and subsequently stored at –80°C until quantification of AAV-LacZ genome copies using real time PCR, as described in 4.2.3.3. Results were expressed as total number of genome copies (gc) eluted or as percentage of eluted related to loaded AAV-LacZ.

4.2.4.2 AAV-LacZ elution from heparin coated PU discs

To determine the ability of heparin surface modified PU to retain AAV, heparin-coated PU discs were loaded with 45 µl AAV-LacZ (4.15 x 10^{11} gc / ml), without addition of any matrix. All discs were left overnight at 4°C, to allow for adsorption of the virus to the heparin coated PU surface. The next day, all discs were washed in 10 ml PBS for one hour at 37°C under continuous agitation to eliminate non-bound AAV-LacZ from PU discs. Thereafter, all discs were taken into a fresh 10 ml PBS containing tube and shaken gently for the next 8 days at 37°C. 100 µl aliquots were taken of the wash at 6 hours, 20 hours, 50 hours, 100 hours and 190 hours and subsequently stored at –80°C until quantification of AAV-LacZ genome copies using PCR, as described in 4.2.3.3. Results were expressed as number of genome copies per total loading dose. To evaluate the reversibility of the AAV-LacZ binding to heparin-coated PU discs, AAV-LacZ was "salt eluted" at the end of the experiment (after 190 hours). After AAV was loaded, the heparin coated PU discs had been submersed for 8 days (190 hours) in 10 ml PBS and the last aliquot had been taken,

PU discs were transferred to 1 ml of 250 mM NaCl for one hour. Then discs were transferred to the next dilution of 350 mM NaCl for one hour and so forth, until the highest concentration of NaCl (650 mM) was reached. 100 µl aliquots were taken of all different dilutions and stored at -80°C until quantification of AAV-LacZ genome copies using PCR, as described in 4.2.3.3. Furthermore, infectivity was evaluated using the HT 1080 assay, as described above in 4.2.3.4.

4.2.5 AAV in vivo studies

Animals

All animal experiments including surgical procedures complied with the "principles of laboratory care" and the guidelines for the care and use of laboratory animals (NIH publication no. 86-23). Approval was obtained from the "Animal Research and Ethics Committees of the University of Cape Town, South Africa". Male Wistar rats were used for in vivo studies and were bred and kept at the University of Cape Town Animal Unit. Rats were housed in standard cages and received water and standard pelleted diet ad libitum.

Injection of ink and AAV into tibialis anterior muscles

As an indicator of local distribution of injected solutions, 100 µl ink (Kandahar Black Indian Ink, Daler-Rowney, Bracknell, UK), diluted 1:2 in PBS, (50 µl ink plus 50 µl PBS) was injected directly into the tibialis anterior muscle of male wistar rats, as described previously (256). Therefore, rats (250 g – 300 g body weight (BW)) were anaesthetized with a standard anesthetic mixture of 10 % ketamine hydrochloride (Anaket - V®, Centaur Labs, Bayer AG, Germany) plus 2 % xylazine (2 % Rompun®, Bayer AG, Germany) in a ratio of 9 to 5 v / v i.m. (approx. 0.05 - 0.1 ml / 100 g BW). After shaving and iodine disinfection of one lower hindlimb of a wistar rat, a 0.5 cm skin incision was made directly above the tibialis anterior muscle of each leg. 100 µl ink was injected under visual control using a 1 ml 29 G single use syringe with integrated needle (Omnican 100, Braun, Melsungen, Germany) in each tibialis anterior muscle. 5 minutes after injection, the rat was killed by CO_2, the tibialis anterior muscles were excised and analyzed macroscopically and microscopically after sectioning and eosin staining. The same technique was used

thereafter to inject 100 µl AAV-LacZ (1.1×10^{10} gc) as well as AAV-$VEGF_{165}$ (1.1×10^{10} gc) into tibialis anterior muscles as positive controls for further studies.

Subcutaneous and intramuscular implantation of PU discs

To evaluate ingrowth of granulation tissue consisting of inflammatory cells, fibroblasts and endothelial into porous polyurethane discs, a subcutaneous implantation model was established. In addition, this model was used for the studies on neovascularisation and angiogenesis as well as for evaluation of the "Gene Activated Matrix", consisting of AAV-LacZ or AAV-$VEGF_{165}$, matrices and PU discs. The anaesthesiological and surgical procedure for implantation of up to six round, flexible PU discs with a diameter of 5.4 mm and a thickness of 2 mm was as follows: Male wistar rats were anaesthetized with a standard anaesthetic mixture of ketamine hydrochloride plus 2 % xylazine as desribed above. After shaving and disinfection of the skin with iodine (10 % Povidone Iodine, Dismed Pharma, Johannesburg, South Africa), up to three longitudinal skin incisions of one centimeter length each were made by the use of a scalpel (blade size 11, Swann-Norton®, Sheffield, UK) on either side of the dorsal paramedian skin to create six subcutaneous pouches in total, large enough for one PU disc to be implanted in each pocket. Pockets were created inserting a small surgical mosquito into each incision allowing for gentle spreading of the subcutaneous tissue. Care was taken to avoid any hemorrhage, since this would have negative effects on the animal and inhibit tissue ingrowth into the PU disc through hematoma formation. Discs were implanted using a rotational algorithm to ensure an equal distribution of different groups at each implant position. The wounds were subsequently closed by placing one or two single stiches of non-absorbable prolene 4-0 (Ethicon, Johnson & Johnson Professional Products (Pty.) Ltd., Gauteng, South Africa). For postsurgical analgesia, buprenorphine (Temgesic® Bayer AG, Germany) was injected intramuscularly (approx. 0.1 ml / 70 g BW) in the back leg after the animal started to recover from anaesthesia. PU discs were left implanted subcutaneously for 3 to 28 days. To compare this subcutaneous approach with an intramuscular approach in terms of tissue ingrowth and effectivity of gene delivery, latissimus dorsi muscle of male wistar rats was used as implantation site in the following way:
Anaesthetic and analgesic drugs were given in the same dosage as described above. After sterile washing and draping of the rat dorsal midline an incision of the skin of about 2 cm was made with the scalpel followed by dissection of the subcutaneous and connective tissue to reach the spinal part of the latissimus dorsi

muscle. The incision of its tendon of about 1 cm and careful elevation of the latissimus dorsi muscle from the serratus anterior and the intercostal muscles was followed by the creation of a small pouch underneath the latissimus dorsi muscle. Up to two PU discs were implanted into one pouch on either side. After inspection for any signs of bleeding, the pouch was closed by re-fixation of the tendon of the latissimus dorsi muscle to the spine with several single prolene 7-0 stitches. Finally, the skin was closed with prolene 4-0 in a continuous way. PU discs were left implanted between 3 days and 28 days.

Explantation and processing of PU discs and muscles

After rats were killed by CO_2 inhalation, discs and surrounding tissue were explanted en bloc and cut in half. One half of the disc was fixed in 4 % formalin (40 % formalin diluted in PBS, pH 7.4) (Merck Chemicals LTD, Gauteng, South Africa) overnight at 4°C for Eosin as well as Hematoxylin & Eosin (H&E) staining to quantify tissue ingrowth. For evaluation of LacZ gene expression by X-gal staining, the second half of the disc as well as freshly removed tibialis anterior muscles were fixed in 5 ml of 4 % paraformaldehyde / PBS (pH 7.0 - 7.5) (Saarchem, Kruegersdorp, South Africa) for 1 hour at 4°C. Tissue was further processed as described in 4.2.6.

For evaluation of GFP gene expression, PU discs and muscle samples were explanted, frozen immediately in melting n-pentane, pre-cooled by liquid nitrogen (Merck Chemicals LTD, Gauteng, South Africa), and cryo-sectioned at a thickness between 10 µm and 20 µm.

$VEGF_{165}$ detection in PU discs and muscles

AAV-$VEGF_{165}$ transduced tibialis anterior muscles as well as AAV-$VEGF_{165}$ loaded PU discs were protein extracted after explantation. Furthermore, $VEGF_{165}$ was measured using an enzyme linked immunosorbent assay (Duo Set ELISA Development System for human VEGF), (R&D, Minneapolis, MN, USA). For protein extraction and ELISA, we used the following protocol:

1. Tibialis anterior muscles and PU discs were excised (10 x 5 mm), cut into several small pieces, and frozen immediately in liquid nitrogen
2. The samples were homogenized manually first, using mortar, pestle and tin foil under constant cooling with liquid nitrogen. Afterwards, the samples were

homogenized further using the "X Press Homogenizer XPII" (Tekniva, Gauteng, South Africa). Therefore, samples were added to a 2 ml cryogenic vial "Bio One" (Greiner bio one, Cape Town, South Africa) including two metal balls. Muscle samples were shaken for 10 seconds with two metal balls, PU discs only 1 second with 1 metal ball.

Protein isolation

Unless stated otherwise, all chemicals for protein isolation were purchased from Sigma Aldrich Chemie, Steinheim, Germany.

1. 1 ml PBS with 1 % Triton - X100 + 0.5 M EDTA + 1 mM PMSF + Aprotinin (1000 units / ml, cooled to 4°C) was added to each vial holding a muscle sample. 150 µl PBS with 1 % Triton - X100 + 0.5 M EDTA + 1 mM PMSF + Aprotinin (1000 units / ml, cooled to 4°C) was added to each vial holding a PU disc sample.
2. The sample was incubated on ice for 10 minutes (in rotor shaker), transferred to a fresh tube removing the metal balls and centrifuged at 10000 rpm for 10 minutes at 4°C.
3. The supernatant was transferred to a fresh tube (yield typically 100 µl out of 150 µl for the disc and 600 µl out of 1000 µl for the muscle sample)
4. VEGF ELISA was performed on samples.

VEGF ELISA

VEGF ELISA was performed according to the manufacturer's protocol using the "Duo Set ELISA Development System for human VEGF" (R&D, Minneapolis, MN, USA).

Shortly, a monoclonal antibody specific for $VEGF_{165}$ was pre-coated onto a 96 well micro plate overnight. Standards and samples were pipetted into the wells and any $VEGF_{165}$ present was bound by the immobilized antibody. After washing away any unbound substances, an enzyme-linked polyclonal antibody specific for $VEGF_{165}$ was added to the wells. Following three washes, a substrate solution was added to the wells and color developed in proportion to the amount of $VEGF_{165}$ bound in the initial step. The color development was stopped after 30 minutes and the intensity was measured using a "Benchmark® Microplate Reader" (Biorad, Japan) at 450 nm.

Manufacturer's protocol (Quantikine® Immunoassay, R&D, Minneapolis, MN, USA) for the detection of VEGF:

1. Prepare all reagents and standards
2. Add 100 µl assay diluent RD1W to each well
3. Add 100 µl standard, control or sample to each well
4. Incubate for 2 hours, aspirate and wash 3 times
5. Add 200 µl conjugate to each well and incubate for 2 hours
6. Aspirate and wash 3 times
7. Add 200 µl substrate solution to each well and protect from light.
8. Incubate for 25 minutes, add 50 µl stop solution and read at 450 nm within 30 minutes.

The zero standard optical density was subtracted from all readings. Thereafter, a standard curve was constructed by blotting the absorbance for each standard on the y - axis against the concentration of growth factor on the x - axis. A best fit curve was drawn through the points on the graph and a regression equation was obtained using Microsoft Excel software (Microsoft, USA). This way, a growth factor concentration could be calculated for each sample.

4.2.6 Histology and immunohistochemistry

Hematoxylin & Eosin (H&E) staining

Eosin as well as Hematoxylin & Eosin (H&E) staining was performed on muscle and on granulation tissue ingrown into PU discs for tissue ingrowth studies as well as in addition to X-gal staining for transduction efficiency studies. After being stained with X-gal, muscle tissues and PU discs were paraffin embedded, cut in 5 µm sections and stained with a light eosin stain. A standard procedure was applied for H&E and Eosin stains including dewaxing, hydrating, staining and mounting as described by Gamble et al. (257).

Protocols:

Fixation in 4 % formalin for H&E

1. Dilute 40 % formalin (Merck Chemicals, Gauteng, South Africa) 1:10 in deionized H_2O
2. Fix samples overnight at 4°C

Hematoxylin & Eosin

All chemical used were purchased from Merck Chemicals, Gauteng, South Africa, unless stated otherwise

Mayers Hematoxylin

1. Add 2 g hematoxylin to 50 g potassium aluminium and to 0.2 g sodium iodate
2. Dissolve in 1 L distilled water using gentle heat or at 37°C incubator or water bath.
3. Add 1 g citric acid and 50 g chloral hydrate, dissolve well.
4. Boil for 5 minutes, cool and filter

Eosin

1. Dissolve 10 g eosin in 1000 ml H_2O
2. Add a few drops of acetic acid

Staining Method:

1. Dewax slides for 20 minutes in 2,2,4 tri-methylpentane as the solvent
2. Hydrate in 3 x 100 %, 2 x 96 % and 2 x 70 % alcohol followed by distilled water.
3. Place in hematoxylin for 5 minutes, and then into running tap water for 5 minutes.
4. Place in eosin for 30 seconds, dip in distilled water and dehydrate through the graded alcohols to 3 x solvent.
5. Place a drop of Entellan® (Merck, Darmstadt, Germany) onto a cover slip and place the slide on top of it with the section facing downwards. Wipe around it and allow drying.

4.2.7 Image analysis

To obtain an overview of transduced muscle and PU disc samples, X-gal stained specimen were analysed after explantation by the use of a stereo microscope (Leica MZ 7.5 Stereomicroscope, Leica Microsystems GmbH, Wetzlar, Germany) attached to an external light source (Leica LZ) and camera system (Leica DFC 280). Pictures were taken between 6.3 x and 45 x magnification and processed using "Leica IM 500 Image Manager Software".

To evaluate AAV-LacZ transduction efficiency on HT 1080 cells, the cells were visualized at 50 x magnification (Leica DM IRBE 541000, Leica, Germany). X-gal positive cells were counted manually in a 12 well plate in two different dilutions in duplicate using a cell counter. On muscle tissue and PU disc cross sections, 100 x magnification was adequate for image analysis. Images were taken of one whole muscle or PU disc cross section (12 optical fields) and analysed using Leica Q-win software (Leica Microsystems GmbH, Wetzlar, Germany). The PU disc cross section as well as the muscle section was taken at the largest diameter of the specimen. Total number of transduced cells per cross section was counted manually on Eosin stained slides at each time point and expressed as total number of transduced cells per cross section. The area of lacZ transduced muscle cells on muscle samples was analyzed as well by Leica Q-win image analysis system and was expressed as total area in μm^2. GFP positive cells and tissues were analyzed using a "Zeiss Fluorescent Microscope" (Zeiss Axiovert 200M, Jena, Germany). Images were captured with a high resolution "Zeiss Axiocam" with the help of "Axiovision Software" 3.1. Cells expressing GFP were counted on a whole cross section manually at 100 x magnification. Results on GFP positive cells were given as percentage of total number of cells per cross section. Tissue ingrowth was measured on H&E stained cross sections and is expressed as per cent tissue ingrowth of the total porous disc area.

4.2.8 Statistical evaluation

All data obtained on body weight, tissue ingrowth as well as number and area of transduced cells is expressed as mean values including standard error of mean. Differences between groups were compared by student's two-tailed t-test. A value of $p < 0.05$ was considered significant.

4.3 Results

4.3.1 AAV in vitro

4.3.1.1 Production of AAV

Using the "AAV helper-free system" of Stratagene (Stratagene, La Jolla, USA) (252), co-transduction of human embryonic kidney cells (HEK 293) with 3 plasmids and a novel heparin-column purification method (254), 8 different AAV-LacZ batches were produced (4.2.3.1 and 4.2.3.2). As assessed by the HT 1080 infectivity assay, transducing levels reaching up to 4.5 x 10^9 transducing units / ml were achieved (1.99 ± 0.3 x 10^9 transducing units AAV-LacZ / ml on average) (Figure 4). Real time PCR analysis of the batch of virus with the highest level of transducing units per ml (4.5 x 10^9 transducing units / ml of AAV-LacZ) yielded 5.4 x 10^{11} genome copies AAV / ml (4.2.3.3). This translates to a ratio of 1:120 (transducing units / genome copies), indicating the production of highly infective virus.

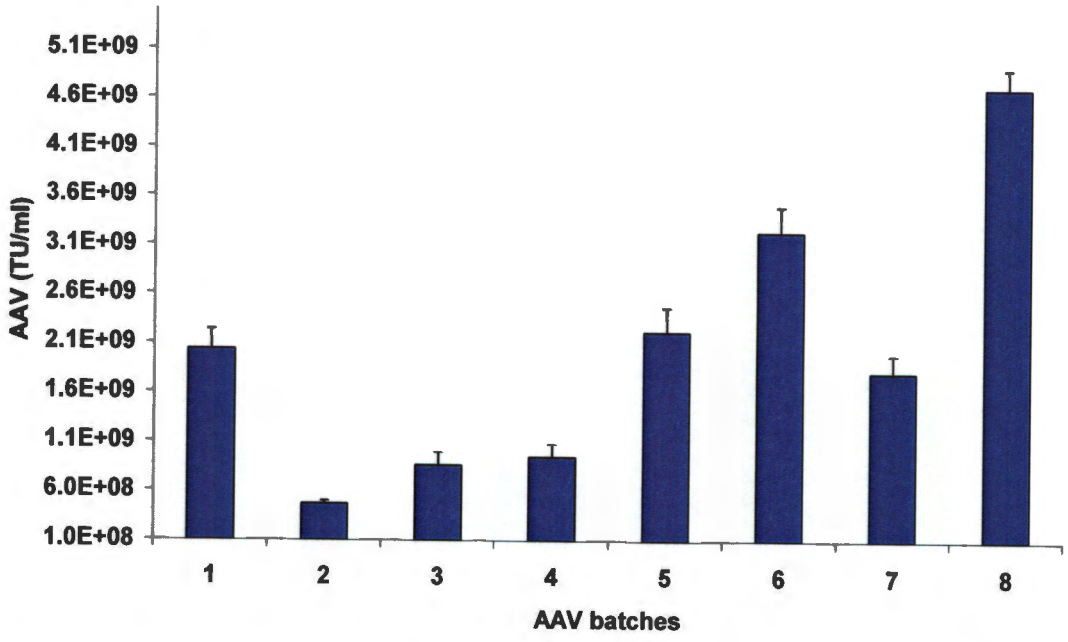

Figure 4: Production of 8 different batches of AAV-LacZ using the "AAV helper free system" and a novel heparin column purification method. Virus titers between 4.6 x 10^8 and 4.5 x 10^9 transducing units / ml (1.99 ± 0.3 x 10^9 transducing units AAV / ml on average) were produced (counted in triplicate).

4.3.1.2 Stability of AAV-LacZ

AAV-LacZ survival in 50 % FCS, 50 % PBS

To determine long term survival and infectivity, 20 µl (equals 4.46 x 10^9 gc) of AAV-LacZ (AAV stock 2.23 x 10^{11} gc / ml) were diluted in 10 ml L-DMEM and incubated in 50 % fetal calf serum (FCS) and 50 % phosphate buffered saline (PBS) for 34 days at 37°C. Samples of 500 µl each were taken at 24 hours and 7, 14, 21 and 34 days in duplicate. Infectivity of AAV-LacZ was tested using HT 1080 fibrosarcoma cells, as described above (Chapter 4.2.3.4). Results are given as number of transducing units / ml (TU) of AAV in relation to time. Throughout the experimental period, there was a quasi linear decline of infective virus starting at 100 % of initial AAV-LacZ loaded at 24 hours to 65.95 % at 7 days, 72.34 % at 14 days and 27.66 % at 21 days (Figure 5). At 34 days, AAV-LacZ was not infectious anymore. However, it was anticipated that autologous wound healing cells would grow into the porous polyurethane within 7 to 10 days after implantation and would therefore be sufficiently transduced by infective AAV-LacZ at the initial stage of wound healing.

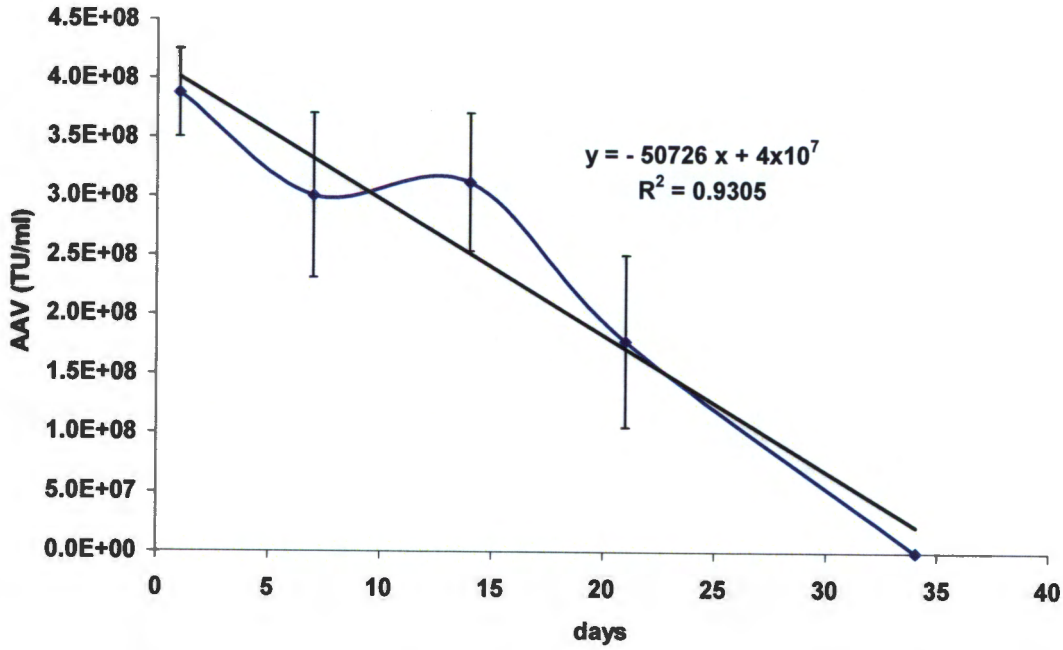

Figure 5: AAV-LacZ infectivity in 50 % FCS / 50 % PBS over 34 days at 37°C: Linear decline of infective virus from 100 % at 24 hours to 65.95 % at 7 days, 72.34 % at 14 days, 27.66 % at 21 days and finally to no detectable infectivity of initially loaded virus at 34 days, as assessed by HT1080 infectivity assay described in chapter 4.2.3.4 (n=2).

4.3.1.3 AAV-LacZ elution from PU discs

AAV-LacZ elution from fibrin

AAV-LacZ elution from fibrin matrices of different concentrations embedded in polyurethane discs was evaluated, as described in chapter 4.2.4.1. Distribution of AAV was considered uniform as it was gelled from solution. AAV-LacZ was quantified by real time polymerase chain reaction (PCR) (chapter 4.2.3.3) (258) and showed a characteristic behavior: AAV-LacZ retention was superior in higher fibrin matrix concentrations. The lowest concentrated fibrin matrix (10 mg / ml) eluted 98.24 % of the initially loaded virus after 4 days, whereas only 67.92 % was eluted at the same time point from fibrin 25 mg / ml. The highest concentrated study group, fibrin 50 mg / ml eluted only 36.52 % of the initially loaded virus after 4 days. In all concentrations, an initial burst release could be recognized, which leveled off to a saturation point with no further virus elution (Figure 6).

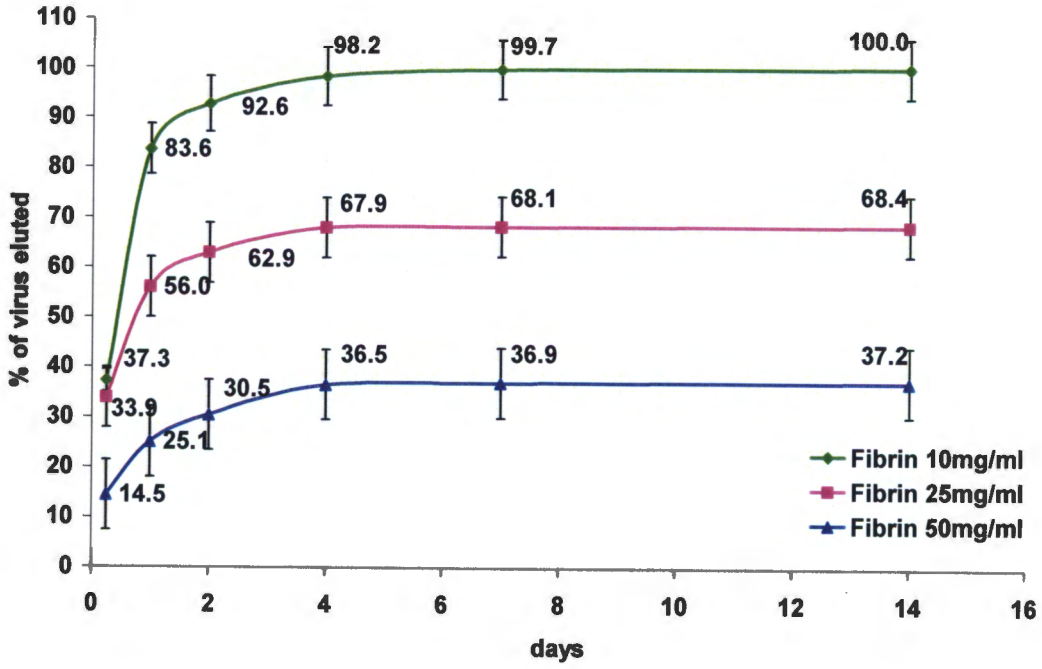

Figure 6: AAV-LacZ elution from fibrin loaded PU discs (n=1). AAV-LacZ was embedded in fibrin 10, 25 and 50 mg / ml matrices for 14 days, respectively. Elution into 37°C PBS + 0.5 % BSA + 0.02 % NaN_3 under continuous agitation. After 4 days, 98.24 % of the initial virus load was eluted from fibrin 10 mg / ml (green line), 67.92 % from fibrin 25 mg / ml (pink line) and only 36.52 % from fibrin 50 mg / ml (blue line).

AAV-LacZ elution from collagen and PEG

To compare AAV-LacZ retention abilities of different hydrogels, we tested collagen at a concentration of 0.4 %, PEG 3 % and fibrin 50 mg / ml embedded in porous PU discs, as described in chapter 4.2.4.1. Collagen showed a substantial burst release of 73.74 % of the initial virus load at 7 days. This release was very similar to the medium concentration fibrin matrix (68.14 % at 4 days) of the previous experiment and thus offered no advantage to fibrin from the perspective of virus retention. PEG 3 % showed even less AAV retention with 87.72 % elution at 6 hours and 89.14 % at 24 hours. Because of this very high initial burst release of virus embedded in PEG 3 % matrix, measurements of further time points was discontinued for the PEG 3 % study arm. High concentration fibrin (50 mg / ml) hydrogel, on the other hand, proved excellent consistency of previous results with 37.54 % elution after 7 days (previously 37.18 %) and was shown to be superior in terms of AAV retention compared to collagen 0.4 % and PEG 3 % (Figure 7).

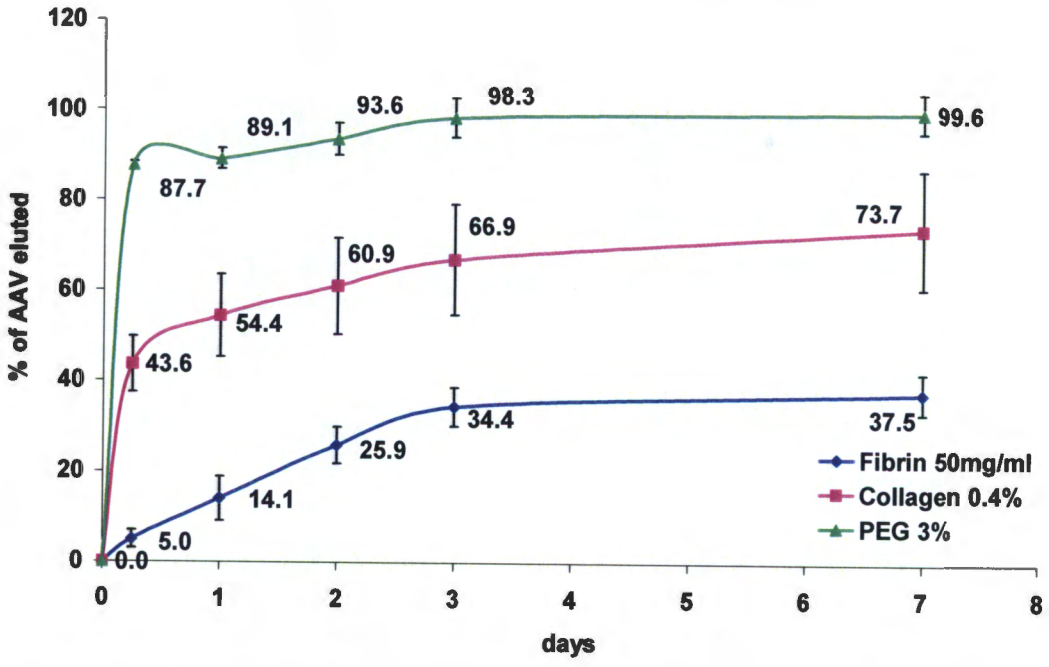

Figure 7: AAV-LacZ elution from collagen 0.4 %, fibrin 50 mg / ml and PEG 3 % matrices loaded into PU discs (n=2). Elution into PBS + 0.5 % BSA + 0.02 % NaN_3 under continuous agitation was evaluated for 7 days at 37°C. PEG 3 % showed a rapid elution of 89.14 % of the initial virus loaded (green line). After 7 days, fibrin 50 mg / ml showed superior AAV-LacZ retention (37.54 %, blue line) in comparison to collagen 0.4 % (73.74 %, pink line).

AAV-LacZ elution from PEG 3 % after collagen 0.4 % preloading

Since fibrin 10 mg / ml and PEG 3 % did not show sufficient AAV-LacZ retention on its own, combinations of matrices were tested to evaluate potentially superior virus retention. AAV-LacZ was embedded in collagen 0.4 %, polymerized within PU discs, and lyophilized overnight (preloading). The next day, fibrin 10 mg / ml and PEG 3 % gels were polymerized around the lyophilisate, as described in chapter 4.2.4.1. Results indicated a substantial drop of AAV-LacZ elution, if AAV-LacZ was preloaded with collagen 0.4 %, lyophilized overnight and finally coated with PEG 3 % in comparison to fibrin 10 mg / ml or PBS. After 48 hours, 76.77 % of the fibrin 10 mg / ml coated AAV-LacZ and 76.59 % of the PBS control group was eluted, but only 3.41 % of PEG 3 % coated collagen preloaded AAV-LacZ was eluted (Figure 8). After 6 days, 88.08 % of AAV-LacZ was eluted in the PBS and 99.9 % in the fibrin 10 mg / ml group, but only 4.65 % AAV-LacZ was eluted in the PEG 3 % group. Therefore, PEG 3 % after collagen preloading promised to be even more efficient than high dose fibrin (50 mg / ml) as gene activated matrix in terms of AAV-LacZ retention. Lyophilisation had no influence on AAV infectivity (personal communication: Neil Davies).

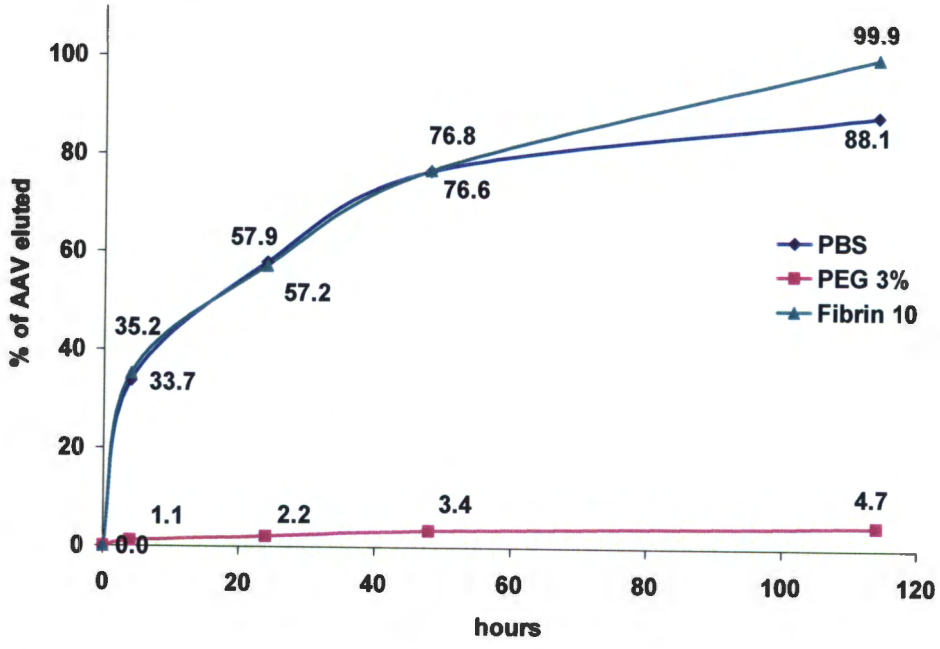

Figure 8: AAV-LacZ elution from PEG 3 %, fibrin 10 mg / ml and PBS loaded PU discs after collagen 0.4 % preloading. AAV-LacZ was embedded in a collagen 0.4 % matrix, lyophilized overnight and subsequently coated with PEG 3 %, fibrin 10 mg / ml or PBS as control. Elution in PBS + 0.5 % BSA + 0.02 % NaN_3 for 6 days at 37°C showed that fibrin coated, collagen preloaded PU had a similar release of AAV-LacZ as PBS control after 2 days (76.78 % vs.76.59 % of initial AAV loading green and blue line, respectively). AAV-LacZ embedded

in PEG 3% after collagen preloading, however, showed substantially less release at 2 days (3.41 % of initial AAV-LacZ loading, pink line) (n=1).

AAV-LacZ elution from heparin coated PU discs

Uniformity of heparin distribution on the PU surface was achieved as shown by scanning electron microscopy (Figure 2). In addition to the morphologic aspect, a strong, reversible binding of AAV-LacZ onto the heparin coated PU surface was proven by our elution studies. The elution of AAV-LacZ from heparin coated polyurethane was only 1.15 % of the AAV-LacZ elution of the non-coated control PU sample after 8 days. Whereas non coated PU elutes 99.4 % of loaded AAV in the wash with only minimal amount of virus being eluted subsequently, the heparin coated polyurethane retains the virus for at least 8 days (Figure 9). To prove the reversibility of the binding of AAV-LacZ to the surface modified PU and to evaluate the amount of virus still present, we subjected the PU discs at the end of the experiment after 8 days to increasing concentrations of NaCl, starting with 0.25 M NaCl, as described in 4.2.4.2. At 0.35 M NaCl, 56.25 % of the initially loaded virus could be recovered (Figure 10). After being reversed from heparin binding by 0.35 M NaCl, increasing the salt concentration stepwise to 0.65 M showed almost no additional effect on AAV elution. The percentage of AAV-LacZ, which was still infective after the salt elution, was determined by the HT 1080 infectivity assay, as described in chapter 4.2.3.2. This assay showed that only 7.54 % of initially loaded virus was still infective after 8 days of heparin-binding and salt elution using 0.35 M NaCl.

These results indicate that although there is excellent retention of virus due to presumably electrostatic binding of AAV-LacZ to heparin-coated PU, AAV-LacZ seems to retain only minor infective potential, at least after 0.35 M NaCl elution at 8 days.

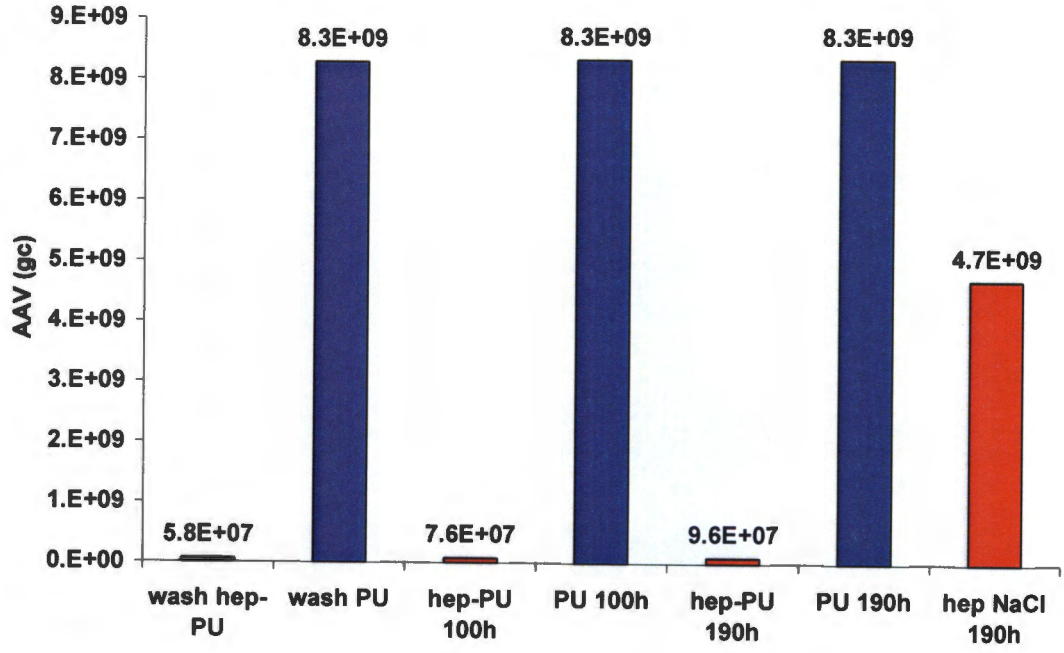

Figure 9: AAV-LacZ elution from heparin coated PU (red) vs. uncoated control PU (blue) shown for the wash, at 4 days and at 8 days. Only 1.15 % of the AAV elution from non-coated control PU sample was released from heparin surface modified PU discs after 8 days. 0.35 M NaCl recovered 56.25 % of loaded AAV-LacZ from heparin coated PU after 8 days (hep NaCl 190 h), (n=1).

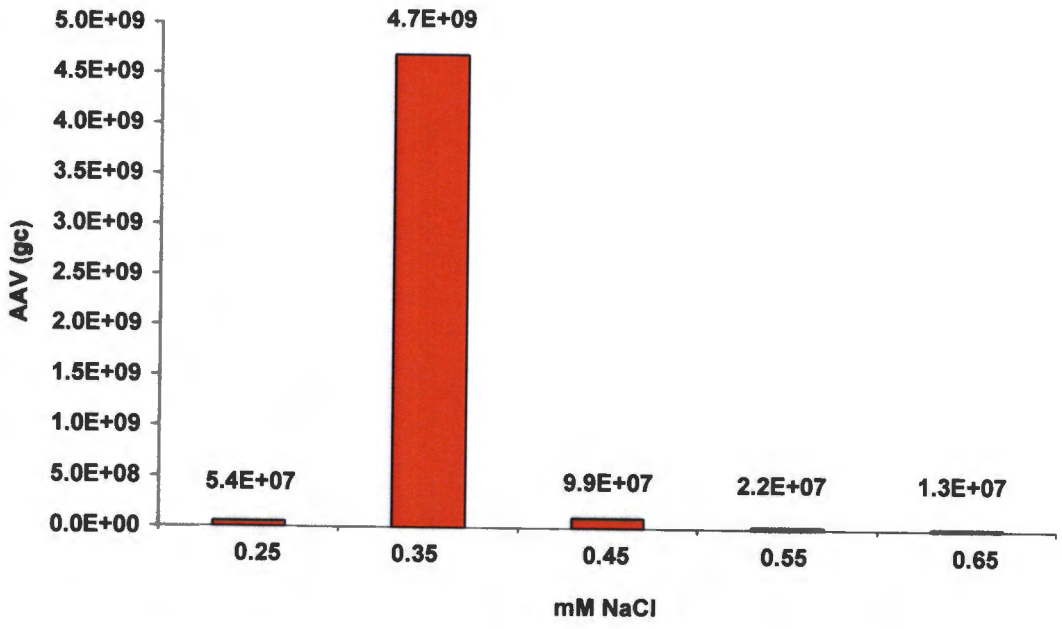

Figure 10: Salt elution of AAV-LacZ from heparin coated PU. 0.35 M NaCl recovered 56.25 % of the initially loaded AAV-LacZ, higher salt-concentration has minimal effect on additional AAV-LacZ elution (n=1).

4.3.2 AAV in vivo

4.3.2.1 Tissue ingrowth into fibrin and PEG matrix embedded PU discs implanted subcutaneously

After having evaluated the above mentioned matrices as potential candidates for the "Gene Activated Matrix" and heparin surface coating on the ability to efficiently retain AAV-LacZ, it was also necessary to determine the rate of cellular ingrowth into these matrices. Only a reasonably fast ingrowth into the matrix containing the virus can provide the basis for sufficient transduction, as AAV-LacZ was only stable for a limited period of time. Therefore, the first set of in vivo experiments included subcutaneous PU disc implant studies in rats to evaluate the rate of tissue ingrowth. Tissue ingrowth in a wound healing situation created by subcutaneous PU disc implantation consists mainly of inflammatory cells as well as fibroblasts, myofibroblasts and endothelial cells and is referred to as "granulation tissue". To evaluate the rate of tissue ingrowth into different matrices, PU discs were loaded with different concentrations of fibrin and PEG, implanted subcutaneously in rats for 10 days and analyzed, as described in chapters 4.2.6 and 4.2.7. Image analysis showed an equally fast tissue ingrowth into fibrin 10 mg / ml and fibrin 25 mg / ml loaded PU after 10 days (61.8 ± 2.83 % vs. 70.85 ± 4.88 %, n= 4, difference n.s.). High dose fibrin at a concentration of 50 mg / ml however, inhibited cellular ingrowth into porous polyurethane compared to fibrin 10 mg / ml and 25 mg / ml. (32 % ± 3.11 of the total disc area) (n=4, $p<0.05$). The two tested concentrations of PEG (3 % and 5 %) inhibited tissue ingrowth even further at 10 days in a concentration dependent way (17 ± 2.26 % vs. 8.85 ± 0.78 %, n=4, $p<0.05$) (Figure 11A).

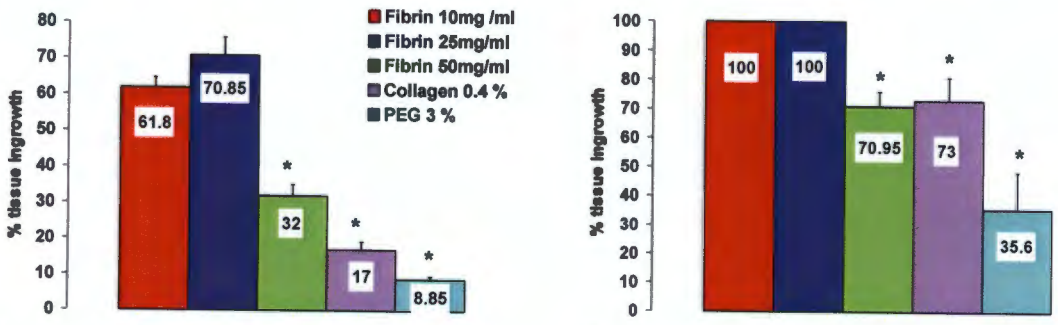

A B

Figure 11: Tissue-ingrowth in fibrin 10, 25 and 50 mg / ml as well as in PEG 3 % and 5 % at 10 days (A) and 20 days (B) subcutaneous implantation in rats. * indicates decreased tissue ingrowth in fibrin 50 mg / ml compared to fibrin 10 and 25 mg / ml (n=4, $p<0.05$). ** indicates decreased tissue ingrowth in PEG 5 % compared to PEG 3 % (n=4, $p<0.05$). No significant difference between PEG 3 % and PEG 5 % at 20 days (n=4, $p=0.07$).

At 20 day implantation time, fibrin 10 mg / ml and 25 mg / ml matrices achieved a complete tissue ingrowth within the PU discs, whereas with fibrin 50 mg / ml, tissue ingrowth was still incomplete (70.95 % ± 5.02) (n=4, $p<0.05$) (Figure 11B). PEG 3 % and 5 % still inhibited tissue ingrowth in comparison to fibrin 10 and 25 mg / ml significantly (n=4, $p<0.05$), but due to high variability, there was no significant difference between PEG 3 % and PEG 5% concentrations at 20 days (73 % ± 7.92 % and 25.6 % ± 12.73 %, respectively) (n=4, $p=0.07$) (Figure 11B).

4.3.2.2 Tissue ingrowth into fibrin matrix embedded PU discs implanted intramuscularly

Since the concept of a "Gene Activated Matrix" using AAV would be enhanced by a fast ingrowth of cells into the matrix, different implantation sites for the PU discs were assessed for their effect on the amount of tissue ingrowth per time. Intramuscular implantation of fibrin 10 mg / ml loaded PU discs for 10 days in the latissimus dorsi muscle of wistar rats (4.2.5) showed a 41.5 % increased tissue ingrowth relative to subcutaneous implants (90 ± 12.68 % vs. 63.6 ± 9.8 %, $p<0.05$). The same pattern of tissue ingrowth could be shown for PU discs loaded with collagen 0.5 % as matrix. Intramuscular disc implantation increased tissue ingrowth by 36.3 % at 10 days (62.83 ± 6.18 % vs. 85.6 ± 5.9 %, $p<0.05$) (Figure 12).

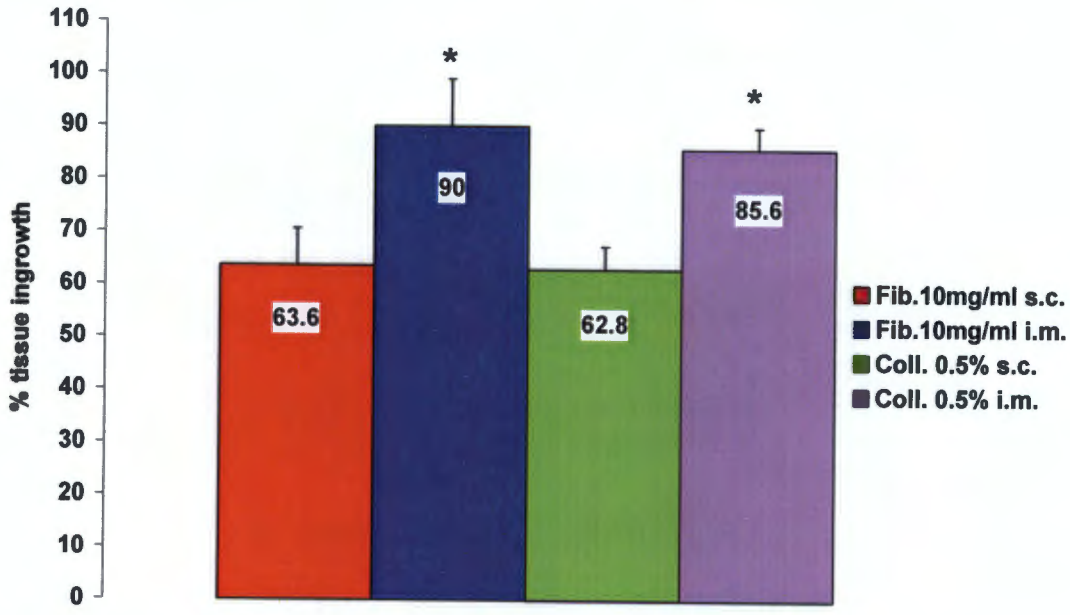

Figure 12: Tissue ingrowth into PU discs after 10 days intramuscular implantation. Comparison between subcutaneous and intramuscular implantation sites using fibrin 10 mg / ml and collagen 0.5 % matrices. * indicates a significant difference relative to its counterpart implantation site (n=4, $p<0.05$).

4.3.2.3 Determination of AAV-LacZ infectivity in vivo

After having evaluated AAV-LacZ survival, AAV-LacZ elution from and tissue ingrowth into different matrices within a porous polyurethane scaffold, the next step was to check transduction efficiency of AAV-LacZ in different tissues. Transduction efficiency was evaluated first using lacZ as reporter gene. Since it is well known, that AAV shows an excellent tropism for muscle cells (177), (260), AAV-lacZ was injected directly into the tibialis anterior muscle of rats to determine the degree and the time-course of gene delivery (4.2.5). To evaluate the technical feasibility of an injection into the tibialis anterior muscle and the distribution of a 100 µl injection, ink was used as a tracer. 100 µl in total (50 µl ink plus 50 µl PBS) was injected each into the tibialis anterior muscle of both legs of one wistar rat. Macroscopic and histologic analysis revealed an even distribution of ink throughout the muscle with the ink well confined within the fascia surrounding the muscle (Figure 13).

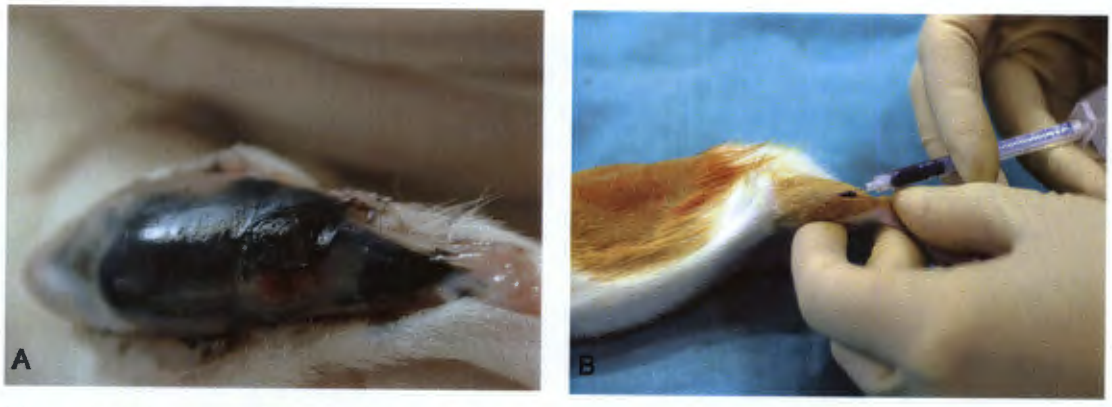

Figure 13: Macroscopic aspect of a tibialis anterior muscle of a wistar rat after direct injection of 100 µl diluted ink (50 µl ink, 50 µl PBS). The ink appears to be well confined within the fascia surrounding the muscle (A). Demonstration of surgical technique of injection under direct visualization, as described in 4.2.5 (B).

Having shown the efficiency and confinement of the intramuscular injection with ink, AAV transduction of striated muscle cells using lacZ as reporter gene was evaluated. Injection of 100 µl AAV-LacZ (1.1×10^{10} gc) in tibialis anterior muscles of rats showed macroscopically signs of transduction as early as 3 days after injection (Figure 14). Microscopic cross sections of X-gal stained tibialis anterior muscle are shown in Figure 15. Negative control muscle samples, which were stained for X-gal, but did not have AAV-LacZ injected, did not show signs of β-galactosidase activity. Image analysis of cross sections taken at 4 different time points revealed that transduction of muscle cells peaked at day 14 and was detectable as long as 28 days after injection (Figure 16).

Figure 14:
Macroscopic aspect of a LacZ transduced tibialis anterior muscle after direct injection of AAV-LacZ. X-Gal staining indicates successful transduction of myocytes as blue color. The picture was taken with a stereo microscope at 10 x magnification.

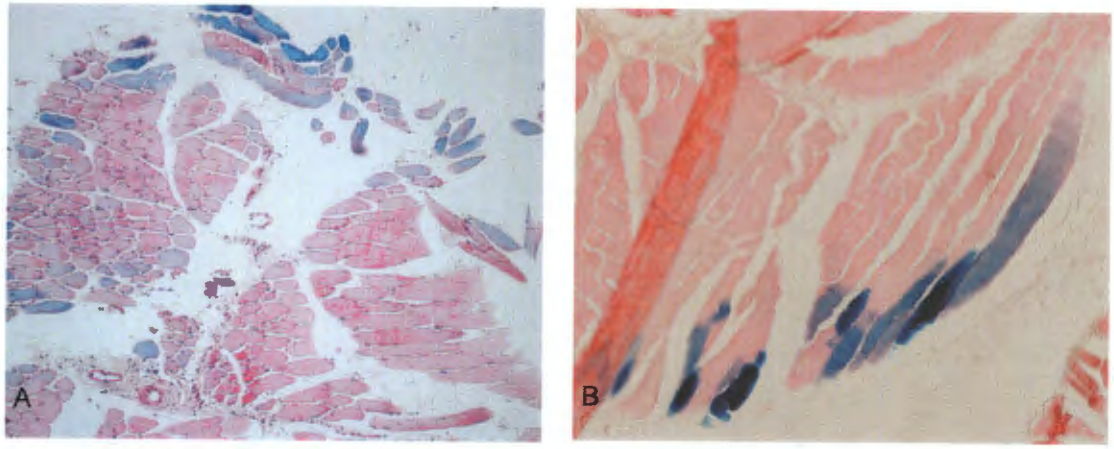

Figure 15: Microscopic cross section of X-Gal stained tibialis anterior muscle 14 days after direct injection of 100 µl AAV-LacZ at a magnification of 100 x (A) and 250 x (B). Blue cells express β-galactosidase and indicate efficient gene delivery.

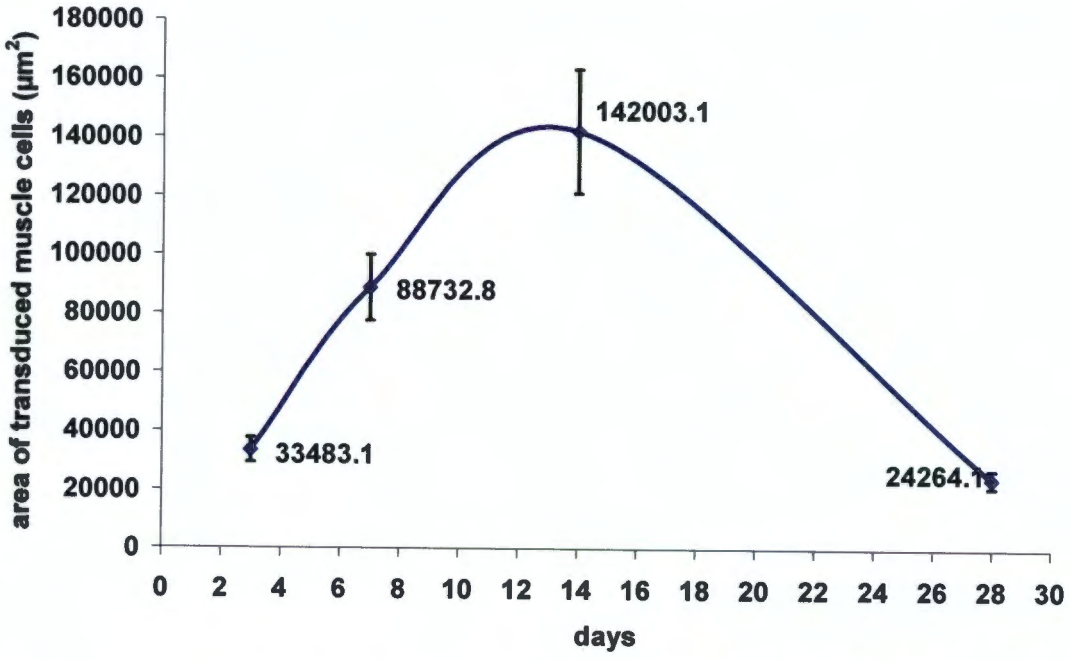

Figure 16: Time curve of AAV–LacZ transduction of striated muscle, as evaluated by X-gal staining. Transduction is seen as early as 3 days after injection, peaking at 14 days and still present at a lower level at day 28. Area of transduced muscle cells is expressed as μm^2 (n=3).

These results were the basis for the next experiments using the "Gene Activated Matrix" approach to deliver genes to granulation tissue. To this end, PU discs were filled with AAV-LacZ embedded in a matrix of fibrin 10 mg / ml (n=8). Discs were implanted subcutaneously for 3, 7, 14, 20 and 28 days, as described in chapter 4.2.5. Granulation tissue growing into the porous PU and microscopically identified as myocytes, fibroblasts and macrophages showed transgene expression (Figure 17). Compared to muscle tissue, a similar time course was achieved by AAV-LacZ transduction of granulation tissue. LacZ protein expression was evident from day 7 onward showing highest expression at day 10 and leveling off until day 28 (Figure 18). Due to the experimental setup, with cells growing actively into the matrix loaded scaffold, there was no sign of transduction at 3 days because tissue just started to infiltrate the matrix at this time. However, the amount of transduction was limited.

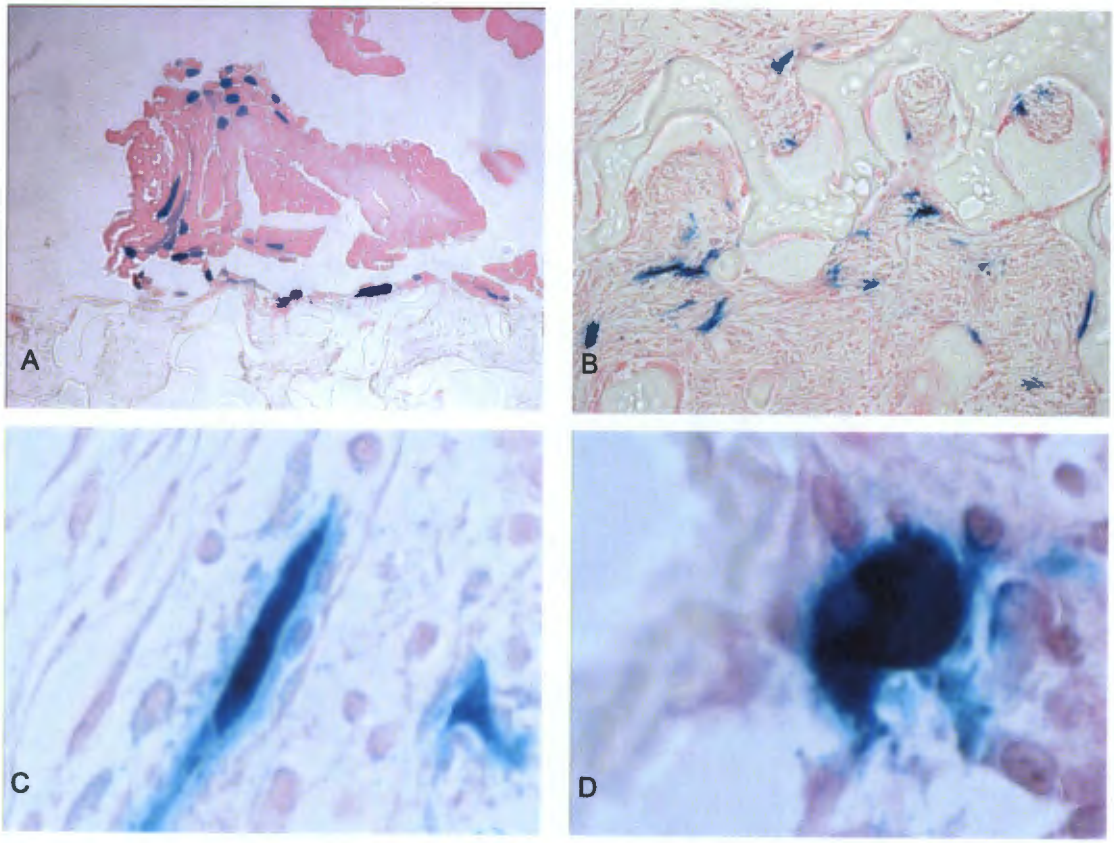

Figure 17: Microscopic images of transgene expression of β-galactosidase mediated by AAV-LacZ using the "Gene Activated Matrix approach". AAV-LacZ has been embedded in fibrin 10 mg / ml matrix, which was supported by porous PU. After X-gal staining, blue color indicates β-galactosidase production. (A): Transduction of myocytes surrounding the PU implant (100 x magnification). (B): Transduction of cells resmbling fibroblasts and macrophages inside the PU disc (250 x magnification). Histological detail of a transduced fibroblast (C) and a macrophage (D) at 400 x magnification.

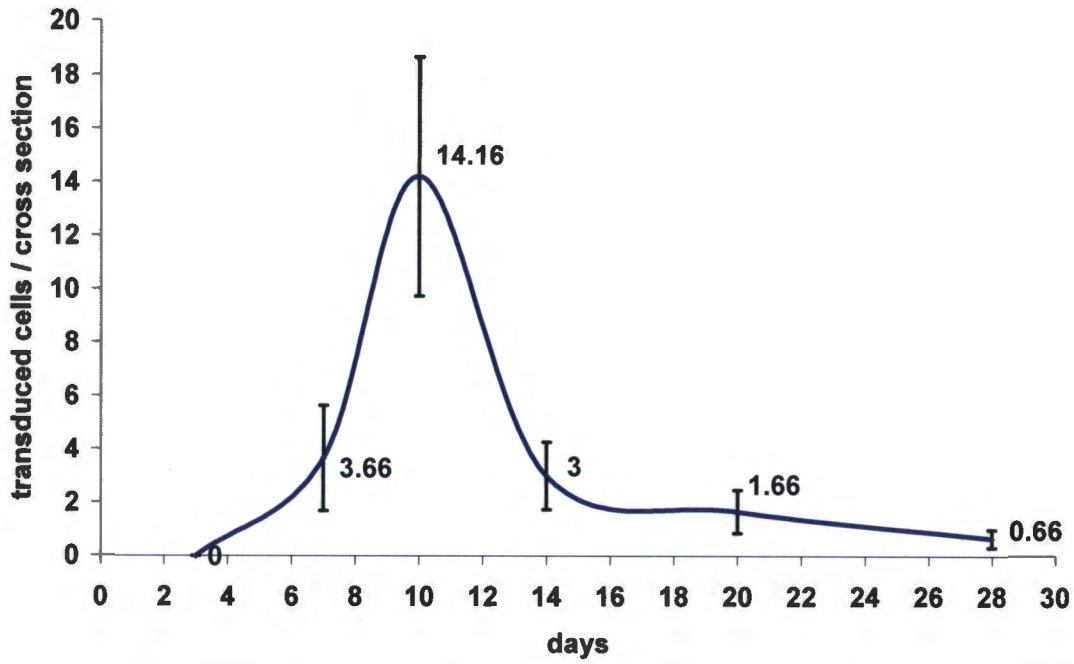

Figure 18: Time curve of AAV–LacZ transduction of granulation tissue (cells morphologically identified as myocytes, fibroblasts and macrophages). Cells growing into porous PU loaded with fibrin 10 mg / ml for up to 28 days expressed β-galactosidase as early as day 7 after implantation of the "Gene Activated Matrix" and was still present at day 28 , peaking at day 10 (n=4).

These results indicated effectiveness of the concept of gene delivery from matrix embedded AAV supported by porous PU as a scaffold material.

Since fibrin 50 mg / ml indicated superior AAV-LacZ retention capabilities compared to medium (25 mg / ml) and low (10 mg / ml) fibrin concentrations in the in vitro experiments, we were interested to evaluate, if fibrin 50 mg / ml offers an advantage compared to fibrin 10 mg / ml and 25 mg / ml as "Gene Activated Matrix" in terms of in vivo transduction. Indeed, after 10 days of AAV-LacZ embedded in fibrin matrices of different concentrations, transduction of granulation tissue was best achieved in the 50 mg / ml fibrin matrix (51.33 ± 10.6 transduced cells / cross section (cs) vs. 20.33 ± 4.51 / cs in fibrin 25 mg / ml and 14.67 ± 4.51 / cs in fibrin 10 mg / ml) (Figure 19). The difference between high dose fibrin and medium or low dose fibrin was significant ($p<0.05$). Control discs without fibrin and without AAV did not show signs of transduction.

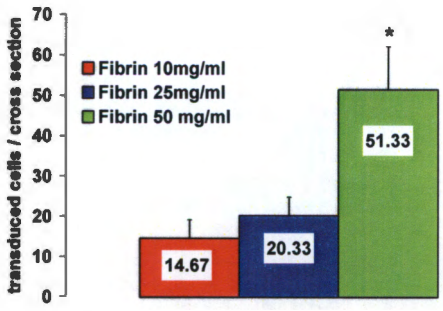

Figure 19:
Transduction of granulation tissue with AAV-LacZ from different matrices at 10 days. PU discs loaded with fibrin 10 mg / ml (red column), 25 mg / ml (blue column) or 50 mg / ml (green column) embedded AAV-LacZ were implanted subcutaneously in rats. The graph shows the number of transduced cells, as assessed by X-gal staining, per cross section. * indicates $p < 0.05$ compared to fibrin 10 mg / ml and 25 mg / ml (n=3).

In order to optimize transduction efficiency not only by increasing AAV-LacZ retention by the use of fibrin 50 mg / ml, but additionally by accelerating tissue ingrowth, the intramuscular implantation site was compared to the subcutaneous approach. Previous experiments using fibrin 10 mg / ml suggested accelerated tissue ingrowth by 41.5 %, if PU disc were implanted in an intramuscular compared to a subcutaneous fashion. Therefore, it was necessary to evaluate, if accelerated tissue ingrowth in a dense fibrin hydrogel translates as well to higher transduction efficiency of AAV-LacZ. However, after 10 days implantation time, there was no significant difference between the subcutaneous and intramuscular approach in terms of AAV-LacZ transduction efficiency (86 ± 16.25 versus 90 ± 15.13 transduced cells / cs, n=4, p=n.s.).

4.3.2.4 AAV-LacZ delivery from heparin coated PU discs

Since in vitro experiments indicated, that heparin coating of polyurethane discs improved AAV-LacZ retention within the disc to such an extent, that only 1.15 % of AAV-LacZ compared to non-coated control discs was released after 8 days, it was of interest to determine the efficiency of AAV-LacZ transduction of granulation tissue from heparin coated PU discs. After 10 days of subcutaneous implantation of PU discs, microscopic analysis showed an increase in transduction from 0.5 ± 0.29 cells / cs in the non-coated PU control group to 6.33 ± 3.84 cells / cs in the heparin-coated PU group (n=4). Due to the variation of results, the increase was, however, not statistically significant (p=0.13).

4.3.2.5 Transduction efficiency of AAV-VEGF$_{165}$ on muscle tissue

After proof of concept of AAV transduction of striated muscle cells and transduction of granulation tissue growing into matrix loaded polyurethane, the coding sequence for VEGF$_{165}$ was cloned into the AAV genome. To evaluate transgene delivery intramuscular as a tissue with high susceptibility to transduction, rats were injected with 1.6 x 10^9 genome copies of AAV-LacZ as well as 1.6 x 10^{10} genome copies of AAV-VEGF$_{165}$ into tibialis anterior muscles. After 10 days, VEGF$_{165}$ ELISA showed 109.7 ± 31.02 pg / ml VEGF$_{165}$ in VEGF$_{165}$ transduced legs compared to 19.05 ± 0.58 pg / ml VEGF$_{165}$ in LacZ transduced legs ($p<0.05$, n=3) (Figure 20 A). This result indicated successful gene delivery of VEGF$_{165}$ by AAV-VEGF$_{165}$.

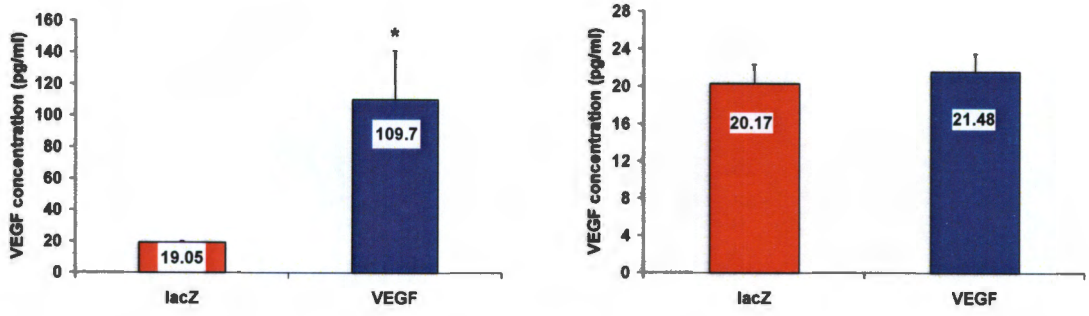

A B

Figure 20: AAV-VEGF$_{165}$ transduction of muscle (A) and granulation tissue (B). A: More than 5-fold increase of VEGF$_{165}$ production of myocytes by direct AAV-VEGF$_{165}$ injection into the right tibialis anterior muscle (blue column) compared to VEGF$_{165}$ production of myocytes injected with AAV-LacZ (red column) as control ($p<0.05$) (n=3, 10 days after injection). B: PU discs loaded with fibrin 50 mg / ml embedded AAV-VEGF$_{165}$ (blue column) or AAV-LacZ (red column), respectively, were implanted intramuscularly for 10 days (n=6). No significant transgene expression of VEGF$_{165}$ was detectable above LacZ levels using VEGF$_{165}$ ELISA in granulation tissue (p=n.s.)

4.3.2.6 Transduction efficiency of AAV-VEGF$_{165}$ on granulation tissue

Since AAV was capable of delivering the gene encoding for VEGF$_{165}$ into muscle cells, the question arose, if AAV would also be able to transduce the VEGF$_{165}$ gene into the cells of granulation tissue. PU discs containing AAV-LacZ in fibrin 50 mg / ml were compared to discs containing AAV-VEGF$_{165}$ in fibrin 50mg / ml after intramuscular implantation for 10 days. The level of VEGF$_{165}$ measured in intra-porous granulation tissue from PU discs was very low. Furthermore, the level of VEGF$_{165}$ measured in the AAV-VEGF$_{165}$ (21.48 ± 1.97 pg / ml) loaded PU discs was

not significant compared to AAV-LacZ loaded control discs (20.17 ± 2.14 pg / ml, n=6, n.s.) (Figure 20 B).

4.3.2.7 Transduction efficiency of double stranded (ds) AAV-GFP on muscle and granulation tissue

Since double stranded (ds) AAV has been reported to show superior and accelerated transduction in vitro and in vivo (261), its ability to transduce granulation tissue growing into porous polyurethane using the concept of "Gene Activated Matrix" was evaluated. Firstly, in vitro transduction experiments of dsAAV-GFP on Chinese Hamster Ovary (CHO) cells were performed, which resulted in superior gene delivery in comparison to single stranded AAV-GFP (Figure 21). Secondly, dsAAV-GFP (4×10^{11} gc / ml) was embedded in fibrin matrices of 10 mg / ml, 25 mg / ml and 50 mg / ml and loaded into uncoated as well as heparin-coated PU discs. PU discs were implanted subcutaneously in wistar rats for 10 days (n=3). Additionally, 100 µl dsAAV-GFP (4×10^{9} gc) was injected into the left tibialis anterior muscle of each rat.

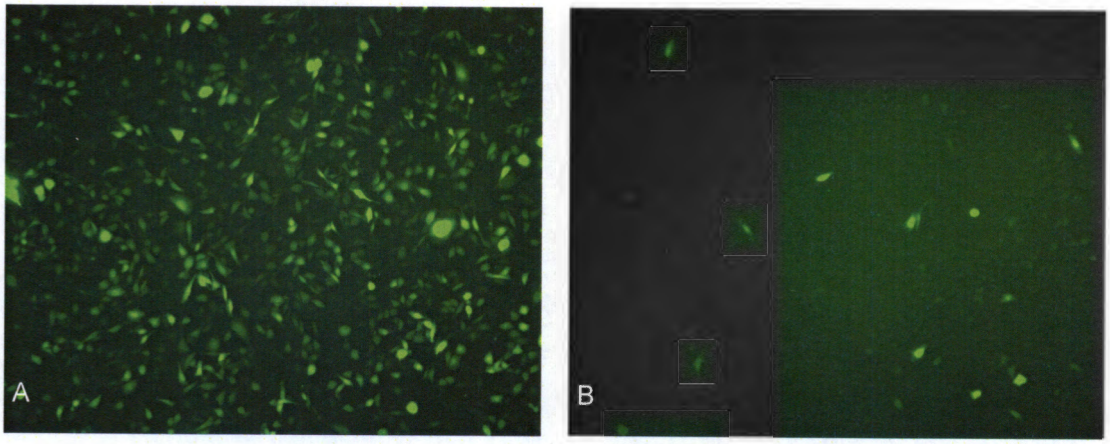

Figure 21: Superior transduction efficiency of double stranded (ds)AAV-GFP on Chinese Hamster Ovary (CHO) cells (A) compared to single stranded (ss)AAV-GFP (B). Green cells indicate successful gene delivery and Green Fluorescent Protein expression (magnification 50 x). Cells were transduced with 1000 gc per cell for both AAV types.

Microscopic analysis of dsAAV-GFP injected tibialis anterior muscles showed strong signs of transgene expression (Figure 22 A). On image analysis, 37.4 ± 5.2 % of all myocytes were positive for expression of GFP. Granulation tissue, however, did not show significant signs of GFP expression inside the PU discs (Figure 22 B).

Therefore, in our model of "Gene Activated Matrix", even double stranded AAV encoding for GFP could not increase transduction efficiency.

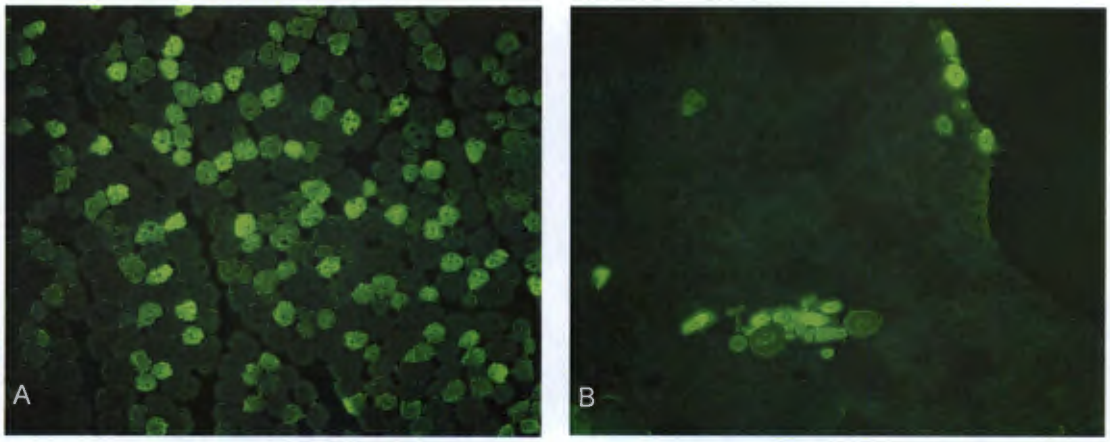

Figure 22: Strong GFP expression of myocytes 10 days after direct dsAAV-GFP injection into tibialis anterior muscle in rats (A)(37.4 ± 5.2 % of all muscle cells transduced, n=3). In contrast, dsAAV delivery of GFP to granulation tissue results in significantly reduced transduction relative to muscle using the "Gene Activated Matrix" approach after 10 days (B), (magnification 100 x). GFP positive cells in (B) are myocytes surrounding the PU disc.

An overview on all different modes of agent delivery within different matrices to the specific delivery sites as well as the evaluated endpoint is given in table 1.

Mode of delivery	Agent delivered	Delivery site	Tissue examined for
Direct injection	Ink	Tib. ant. muscle	Distribution of ink
Direct injection	AAV-LacZ	Tib. ant. muscle	Transduction efficiency
Direct injection	AAV-gfp	Tib. ant. muscle	Transduction efficiency
Direct injection	AAV-VEGF	Tib. ant. muscle	VEGF Protein expression
PU+ fibrin 10 mg/ml embedded AAV	AAV-LacZ	Subcutaneously	Transduction efficiency
PU+ fibrin 25 mg/ml embedded AAV	AAV-LacZ	Subcutaneously	Transduction efficiency
PU+ fibrin 50 mg/ml embedded AAV	AAV-LacZ	Subcutaneously	Transduction efficiency

PU+ fibrin 50 mg/ml embedded AAV	AAV-LacZ	Latissimus dorsi muscle	Transduction efficiency
PU+ fibrin 50 mg/ml embedded AAV	AAV-gfp	Subcutaneously	Transduction efficiency
PU+ fibrin 50 mg/ml embedded AAV	AAV-VEGF	Subcutaneously	VEGF Protein expression
Heparin coated PU	AAV-LacZ	Subcutaneously	Transduction efficiency

Table 1: Modes of AAV and ink delivery within different matrices to specific delivery sites. Tissue was either examined for distribution of ink, transduction efficiency including LacZ, gfp and VEGF Protein expression.

4.4 Discussion

Local angiogenic growth factor delivery seems to be desirable for a variety of clinical situations such as impaired wound healing in diabetic ulcers as well as in peripheral artery disease to create a functional collateral vascular network as soon as possible to improve oxygen delivery to the affected tissues. Furthermore, neovascularisation is regarded as the rate limiting step for functional integration of biomaterials into a living organism. Direct injection of angiogenic growth factors however, requires large doses to be effective due to short biological half life's (152), (153). This in turn, carries the potential for toxicity, substantial side effects such as severe hypotension and high costs (153). The need for a sustained growth factor delivery led to the concept of gene therapy for tissue regeneration. The concept involves the delivery of a gene encoding for angiogenic growth factors, rather than the recombinant protein itself, to the site requiring tissue regeneration (161). This gene can be delivered by plasmid DNA (250), synthetic gene delivery vectors such as lipoplex- and polyplex-DNA (166) or viruses (169). In order to achieve a sustained, localized and controllable growth factor production, Bonadio et al. proposed the concept of a "Gene Activated Matrix" (GAM) in 2000 (161). This approach embeds the vector in form of a plasmid or a virus carrying the gene encoding for the growth factor into a matrix. This matrix can be structurally supported by a scaffold material and delivers the gene of interest after implantation to wound healing cells, such as inflammatory cells, myofibroblasts, fibroblasts, and endothelial cells. These cells take up the gene, and serve as in vivo bioreactors after transduction, producing the required angiogenic growth factor themselves. This concept has been shown to be effective

by Shea et al. who provided evidence for the successful delivery of PDGF from a poly(lactide-co-glycolide) (PLG) matrix into a wound healing situation, creating enhanced matrix deposition and blood vessel formation (250). The "Gene Activated Matrix" approach was further successful in stimulating bone growth using p-MAT-1 plasmid embedded in a collagen matrix in a dog model (163). Doukas et al. immobilized adenovirus encoding for PDGF in a collagen matrix and showed enhanced granulation tissue deposition after subcutaneous implantation of GAM loaded polyvinyl alcohol (PVA) sponges in rats (262). So far, adenoviruses are the only viral vectors that have been used in GAM (160). Since adenoviruses, however, show particular disadvantages in gene therapy such as transient gene expression and a substantial immune response (263), it appeared useful to evaluate, whether the GAM approach might be effective in a porous polyurethane scaffold, using different matrices and adeno-associated viruses as vectors.

Production of AAV

The production of up to 4.5×10^9 transducing units of AAV / ml ($1.99 \pm 0.3 \times 10^9$ TU AAV / ml on average), as assessed by the HT 1080 infectivity assay, appears to be well in accordance with literature. Matushita et al. reported on 1.4×10^{11} transducing units / ml of AAV using the "AAV helper free" production method (252). Other authors produced between 5×10^8 (260) and 1.8×10^{11} transducing units / ml (256), (254). Production of AAV often differs by more than 100 times for unknown reasons (254), (256) and our own variability in AAV production of almost 10 times (4.6×10^9 up to 4.6×10^9 transducing units / ml) is well within the acceptable range. The determination of genome copies of AAV by real-time PCR (264) has been shown to be a fast and reliable method for the quantification of AAV (258). Furthermore, it allowed the calculation of the "infectivity ratio" between transducing units and genome copies. In our own experiments, a batch of AAV-LacZ with a concentration of 4.5×10^9 transducing units / ml resulted from 5.4×10^{11} genome copies / ml. This translates to an infectivity ratio of 1:120, proving the production of highly infective viruses. This is in excellent agreement with data from Auricchio et al., who reported an infectivity ratio of 1:99 (254). The high infectivity ratio of 1:120 is most likely the result of the novel heparin gravity flow purification method, which substantially increased the amount of infectious virus after purification in comparison to conventional purification methods such as Cesium-Chloride ($CsCl_2$), where infectivity ratios typically range between 1:100 and 1:1000 (254), (265). In conclusion, using the "AAV helper-free system" of Stratagene coupled with the

single step heparin purification protocol, it was possible to produce a high number of AAV with an excellent infectivity ratio.

In vitro results

The first two AAV-LacZ elution studies clearly showed increasing virus retention with increasing matrix concentrations. At 24 hours in PBS / BSA, fibrin 50 mg / ml (25.08 % AAV-LacZ release) showed superior AAV-LacZ retention in comparison to fibrin 25 mg / ml (56.03 % AAV-LacZ release), and fibrin 10 mg / ml (83.62 % AAV-LacZ release). This parallels results by Doukas et al., who showed increased retention of adenovirus from collagen matrices, when the concentration was increased from 0.15 % (17 % Adenovirus release after 24 hours) to 2.6 % (3 % Adenovirus release after 24 hours) (262). Chandler et al. reported on 20 % adenovirus release from collagen 0.15 % after 48 hours compared to 10 % release from collagen 2.6 % after 48 hours (251). Our own results using collagen 0.4 % (54.38 % release after 24 hours and 60.93 % release after 48 hours) showed a 3-4 fold higher elution of virus. A possible reason might be the different size of viruses, with AAV (30 nm) being one of the smallest known viruses and about three times smaller than adenoviruses (260), which might result in decreased physical entrapment in the matrix. In terms of AAV-LacZ elution, PEG 3 % matrix showed inferior AAV retention after 24 hours (89.14 % elution) compared to collagen 0.5 % (54.38 % elution) and fibrin 50 mg / ml (8.85 % elution). Despite the high density of PEG gels, which allows for production of mesh sizes (distance between crosslinks) between 50 nm to 1 µm (221), AAV-LacZ (30 nm) was not sufficiently retained within the PEG matrix. This might be due to small structural defects that allowed expulsion of AAV-LacZ by the swelling of the PEG gel after it was placed in buffer.

Shea et al. showed, however, that even retention of only 10 % - 45 % of a plasmid encoding for PDGF from PLG matrix after 4 days was sufficient to increase vascularisation and to build up granulation tissue (250). Our best results in terms of AAV retention were achieved by coating the porous PU disc with PEG 3 % after preloading and AAV embedding in Collagen 0.5 % (4.65 % AAV release after 5 days) as well as by heparin binding of AAV (1.15 % AAV release after 8 days). We could show that AAV lost its infectivity in 50 % FCS / 50 % PBS over time (100 % of initial AAV-LacZ loaded at 24 hours to 65.95 % at 7 days and 27.66 % at 21 days). The phenomenon, that no additional AAV was released from different matrices after 7 days might be due to little additional AAV release and a parallel decrease in infective numbers over time. Therefore, as assessed on HT 1080 infectivity assay,

there was no additional AAV elution after 7 days. Another explanation might be that AAV got bound at higher levels by transglutaminase in the PBS + 0.5 % BSA solution.

Efficiency of the "Gene Activated Matrix" (GAM)

Tissue ingrowth

The efficiency of the GAM is influenced by the type of vector, the matrix and the cells involved. The matrix thereby not only serves as a vehicle for the retention of the vector such as a virus, but also as an ingrowth matrix for target cells. It was therefore important to look at tissue ingrowth characteristics of different matrices as well as their ability to allow for efficient transduction. The results indicate a strong relationship between matrix density and tissue ingrowth for fibrin as well as for PEG matrices: the denser the matrix, the slower the cellular ingrowth. After 10 days subcutaneous implantation, fibrin 25 mg / ml loaded discs showed 70.85 %, whereas fibrin 50 mg / ml showed 32 % tissue ingrowth. At 20 days, fibrin 25 mg / ml loaded discs were completely ingrown (100 %), whereas discs loaded with fibrin 50 mg / ml still had incomplete tissue ingrowth (70.95 %). A concentration and time dependent cellular ingrowth was similar for PEG 3 % and 5 % matrices, as it was also shown by Lutolf et al. (221). Since the highly porous PU discs showed a remarkable mechanical stability as well as a certain degree of elasticity at explanation, sectioning of discs was relatively easy and did not result in any major cutting artifacts despite the small size of 5.4 mm in diameter.
In terms of AAV retention, the highest concentration of fibrin (50 mg / ml) showed a AAV-LacZ retention of 62.46 % after 7 days and compared favorably in terms of cellular ingrowth (32 % of PU disc) to polyvinyl alcohol (PVA) discs loaded with 0.15 % collagen (26 % ingrowth), as described by Doukas et al. (262). By the described technique of intramuscular PU disc implantation into the latissimus dorsi muscle, we could increase the tissue ingrowth at 10 days from 62.8 % (subcutaneous) to 85.6 % for collagen 0.5 % and from 63.6 % (subcutaneous) to 90 % for fibrin 10 mg / ml loaded PU discs. Interestingly, a technique involving the excision of the latissimus dorsi muscle was originally described for the creation of a seroma model (266). The technique of implanting discs under the latissimus dorsi muscle, however, did not show any measurable amount of fluid collection and lead to increased cellular ingrowth in discs.

In an attempt to accelerate tissue ingrowth into PVA sponges, growth factor delivery has been described by Chandler et al. (251). He achieved 70 % tissue ingrowth in PVA sponges at 10 days by adenovirus mediated delivery of PDGF and bFGF. Using our model of fibrin and collagen matrices integrated in PU discs, tissue ingrowth into the plain matrices was sufficient at 10 days for gene transfer studies. The data on tissue ingrowth obtained on healthy, young rats can of course only be extrapolated to the clinical setting involving aged and infirmed humans with great caution. Tissue ingrowth can be expected to be much slower in human patients.

Gene transfer into skeletal muscle

As AAV's tropism for muscle tissue is well known (177), (267), our first step towards gene transfer of granulation tissue was to prove AAV's infectious ability on muscle tissue. After an initial experiment using India-ink to evaluate the feasibility of an intramuscular injection into the rat's tibialis anterior muscle, which has been described previously (256), striated muscle cells were successfully transduced by intramuscular injection of AAV-LacZ. In accordance with experiments described by Richter et al. for the transduction of vascular smooth muscle cells using AAV-LacZ (260), as well as by Deodato et al. (268) and Galeano et al. (269) for the transduction of "panniculus carnosus", a layer of skeletal muscle underlying the dermis in rodents, LacZ transgene expression in our own experiments started as early as 3 days after injection and lasted for at least 28 days. Long term transduction of muscle cells up to 1.5 years using AAV has been described by Xiao et al. (177). By the use of the same intramuscular injection technique, AAV was also capable of $VEGF_{165}$ gene transfer in vivo in our hands. A 5.75 fold increase in $VEGF_{165}$ concentration was measured by ELISA in muscle tissue 10 days after AAV-$VEGF_{165}$ injection compared to AAV-LacZ control (109.7 vs.19.05 pg / ml $VEGF_{165}$). Galeano et al. measured $VEGF_{165}$ levels in mice burn wounds (270) and in wounds of diabetic and normal mice (269) after direct injection of approximately 1×10^{11} gc AAV-$VEGF_{165}$. $VEGF_{165}$ was hereby produced almost exclusively within the subdermal muscle layer "panniculus carnosus". After 7 days, 72 pg / ml $VEGF_{165}$ was detected in wounds of normal mice (80 pg / ml in diabetic mice) (269). This increased to 104 pg / ml $VEGF_{165}$ in burn wounds 14 days after injection of 1×10^{11} gc AAV-$VEGF_{165}$ into the wound (270). By injection of 1.6×10^{10} gc AAV-$VEGF_{165}$ (6.25 x less than Galeano) into the tibialis anterior muscle, we measured 109.7 pg / ml after 10 days, which proved the high infectivity of our AAV-$VEGF_{165}$. Shimpo et al. reported on 1 ng / g tissue of $VEGF_{165}$ via ELISA 10 weeks after direct

intramuscular injection of 1.8 x 10^{13} gc AAV / injection site (256), which would translate to about 600 pg / ml $VEGF_{165}$ (tibialis anterior muscle weight about 600 mg of 300g rats). These high $VEGF_{165}$ levels might be due to extraordinary high AAV titers reported by Shimpo et al. or the later time points evaluated (256). Taken together, AAV-LacZ and AAV-$VEGF_{165}$ produced in our laboratory to high titers and high infectivity in vitro proved to translate its ability for LacZ and $VEGF_{165}$ gene transfer into the intramuscular in vivo situation well in accordance with literature.

Gene transfer into granulation tissue

LacZ transgene delivery by AAV vectors in the setting of a "GAM" was effective. Muscle cells, fibroblasts and occasionally macrophages expressed β-galactosidase and were stained positive by X-gal indicating highest transgene expression 10 days after PU disc implantation. Gene expression in our model was first seen after 3 days and was followed up for 28 days. Experiments involving different matrices showed that the most concentrated matrix (fibrin 50 mg / ml) with its superior AAV-LacZ retention abilities and sufficient tissue ingrowth at 10 days was the matrix of choice in terms of transduction efficiency. Fibrin 50 mg / ml was superior to fibrin 25 mg / ml, to fibrin 10 mg / ml as well as to collagen 0.4 % matrices. However, the overall intensity of gene expression using the "Gene Activated Matrix" model was limited in our hands (maximum 90 cells per PU cross section) and did not reach the 30 % - 50 % transduction efficiency of granulation tissue reported by Bonadio et al., who delivered plasmid genes from collagen sponges (163). Bonadio reported, that "most transfected cells were judged to be fibroblasts by morphologic criteria" (163). AAV vectors have recently been tested for efficiency in a variety of different cell types with variable success. Cells, which have been found to be highly permissive for AAV infection, originate from muscle (267), brain (271) and liver (181). On the other hand, vascular endothelial cells (272), (273) fibroblasts (274) and macrophages (263) have been found to show low transduction efficiency. The reason for the displayed specificity was found in AAV's biology recently: by making contact with the cell membrane, AAV binds to the negatively charged heparan sulfate proteoglycan (HSPG) as a receptor for AAV (259). This attachment is enhanced by fibroblast growth factor receptor 1 binding (275). AAV interacts with $\alpha_v\beta_5$ integrins, enters the cell via endocytosis and reaches the nucleus via AAV containing endosomes. The viral genome is finally integrated into the host cell genome (276). Hansen et al. has revealed impaired intracellular trafficking of AAV as one reason for inefficient transduction of murine fibroblasts (274). The generally low levels of transduction of

vascular endothelial cells (EC's) by all 8 known serotypes of AAV was explained by deficiencies in EC binding, virion degradation by the proteasome as well as by virion sequestration into the extracellular matrix (277). Furthermore, the extracellular matrix of EC's contains large deposits of HSPG, which compete as matrix bound AAV receptors for virus binding and transduction of EC's (273). These findings could explain our own results with AAV delivery from heparin coated PU discs. Despite excellent AAV retention on heparin surface modified PU discs (1.15 % AAV release after 8 days), AAV-LacZ transduction of granulation tissue was not increased after 10 days. However, the studies showing no significant effect of heparin ($p=0.13$) were based on a population size of four. Since a larger population size might have yielded significance, further studies in this respect are indicated. Furthermore, the use of double stranded AAV-GFP, which circumvents the rate-limiting step for transgene expression, namely the conversion of single stranded (ss)DNA to double stranded (ds)DNA, by a mutation of the inverted terminal repeat (261), was not efficient. Since only myocytes are highly permissive for AAV transduction in contrast to fibroblasts, EC's and macrophages, the overall low transduction rate of granulation tissue is explainable. Additionally, neutrophil peptides as products of inflammation have been shown to inhibit AAV transduction in bronchial secretions from cystic fibrosis patients (278). Since the wound healing situation in the PU disc initially shows a certain degree of inflammation involving neutrophils and macrophages, these peptides may well inhibit AAV transduction of granulation tissue as well. The only reports on enhanced wound healing after AAV-$VEGF_{165}$ delivery so far, refer to the "panniculus carnosus" as the transduced cell type (268), (269). The future direction of AAV gene delivery leads towards a genetically altered tropism of AAV to generate vectors that are more efficient, and even selective for specific tissues, such as vasculature (272), (279), (280).

In summary, efficient LacZ and $VEGF_{165}$ transduction mediated by AAV could only be achieved in muscle cells. Granulation tissue growing into porous polyurethane was visibly transduced by AAV-LacZ, the amount of $VEGF_{165}$ expression following AAV-$VEGF_{165}$ transduction was, however, not detectable by VEGF ELISA after protein extraction from PU discs. Therefore, we looked into modalities other than AAV to increase neovascularisation into porous polyurethane.

5. Growth factor delivery from heparin modified porous polyurethane surfaces

5.1 Introduction

5.1.1 Heparin surface modification

Heparin and heparan sulfate glycosaminoglycans (HS-GAG's) are acidic complex polysaccharides found on cell surfaces and in the extracellular matrix (281). They were discovered by McLean in 1916 (282). HS-GAGs are characterized by a linear chain of 10 - 200 disaccharide units of N-acetyl-D-glucosamine that is linked to D-glucuronic acid and are not only the most acidic but also amongst the functionally most diverse biopolymers found in nature. Besides it's well known key role in anticoagulation (283), it has become increasingly clear, that HS-GAGs are also of importance in cell growth and development (284), in viral invasion (285) as well as in angiogenesis and inflammation (286). The fact, that heparin influences angiogenesis was shown 1983 by Folkman et al., who demonstrated that heparin had anti-angiogenic and anti-tumor effects in combination with corticosteroids (287). This in turn, lead to the identification of bFGF as the first heparin-binding, angiogenic growth factor discovered in 1984 (147). Over time, various other growth factors have been discovered and a strong affinity for heparin has, for example, been shown for vascular endothelial growth factor ($VEGF_{165}$ and $VEGF_{189}$) (288), the fibroblast growth factor (FGF) family (289), platelet derived growth factor (PDGF), heparin binding epidermal growth factor-like growth factor (HB-EGF) (290), keratinocyte growth factor (KGF) (291) and transforming growth factor beta (TGF-beta) (292). The exact mechanisms of heparin derivates influencing the angiogenic response to growth factors is subject to ongoing research. As for bFGF, the most intensely investigated growth factor, there is evidence, that syndecan 4, a cell surface heparan-sulfate-proteo-glycane (HSPG), serves as a low-affinity bFGF receptor, which bFGF must first bind to, before it activates the FGF receptor (293). Likewise, heparin has been shown to enhance $VEGF_{165}$ induced phosphorylation of VEGFR-2 by 1.7 fold because a heparin like domain of heparan sulfate forms a complex with $VEGF_{165}$ and VEGFR-2 (294). As a result of these interactions of heparin with various growth factors, several authors evaluated the potential of heparin for therapeutic angiogenesis using different matrices and biomaterials. So far, mainly

growth factor delivery from heparin enriched collagen matrices has been reported (295), (296), (297), but alginate (298) and fibrin (299) has also been used.
Since our group recently developed the covalent binding of deaminated heparin onto a highly porous PU (47), we were interested to investigate, if heparin coating of PU discs loaded with angiogenic growth factors such as VEGF and PDGF-BB sustains their release to achieve increased neovascularisation. Therefore, the pro-angiogenic effect of heparin with and without growth factors, a combination thereof as well as growth factors without heparin coating have been evaluated.

5.1.2 Heparin surface modification and hypoxia

Since neovascularisation into synthetic materials used as scaffolds for organ or tissue replacement often occurs under hypoxic conditions, special attention needs to be paid to the mechanisms involved in integration of these materials into hypoxic tissue. Surgical implantation of biomaterials creates an environment of wound healing. Cells involved in the healing response such as macrophages and fibroblasts have been found to be characteristically hypoxic (300). A variety of angiogenic growth factor genes such as VEGF (128), bFGF (301), PDGF (302), angiopoietin-1 (303) and angiopoietin-2 (304) are known to be up regulated under hypoxic conditions in vitro. Furthermore, up regulation of VEGF in vivo has been shown in several organs of mice and rats including brain, heart, lungs, liver, kidney, and muscle under hypoxic conditions (305) (306). VEGF upregulation in vivo leads to increased neovascularisation in rat and mouse brain (307), (308) , (309), (310), rat heart, skeletal muscle (311) and rat pulmonary circulation under hypoxic conditions (312). The effect of VEGF up regulation on angiogenesis, however, has to our knowledge not yet been investigated under chronic hypoxic situations involving biomaterials such as porous polyurethane in a wound model. The question in this context was, whether chronic whole body hypobaric hypoxia would have an effect on heparin induced angiogenesis into heparin coated polyurethane discs in a wound model.

5.2. Materials and methods

5.2.1 Production and heparin binding of PU discs

Polyurethane discs were produced and subsequently surface modified via covalent binding of deaminated heparin (4.2.1.1, 4.2.1.2).

5.2.2 Production of recombinant $VEGF_{165}$

Human $VEGF_{165}$ was produced in our laboratory using recombinant DNA. The protocol for the recombinant production of VEGF was kindly provided by Dr. A. Zisch, University of Zürich, Switzerland. Briefly, the cDNA of human $VEGF_{165}$ was cloned into the expression plasmid pRSET T7 (Novagen, Madison, WI, USA) between restriction sites Nde1 and BamHI. The pRSET-$VEGF_{165}$ was introduced into the E.coli expression host BL21 (DE3) pLysS. Once the transformed bacteria had reached an OD 600 of 0.8, isopropyl-β-D1-thiogalactopyranoside was added to 1 mM to induce protein expression for 3 hours. The bacterial cells were then pelleted and frozen at -20°C. The pellet was then resuspended in a tenth of the original culture volume in lysis buffer (50 mM Tris, pH 7.5, 150 mM NaCl, 5 mM EDTA), followed by incubation with lysozyme at 0.1 mg / ml suspension for 20 minutes at room temperature. Benzonaze (Merck KGA, Darmstadt, Germany) was then added at 50 units / ml suspension, and incubated overnight at 4°C. Inclusion bodies were collected by centrifugation at 30 000 g for 30 minutes. The pellets were then washed in washing buffer (4 M urea, 20 mM Tris, pH 8.0, 150 mM NaCl, 2 mM EDTA) with stirring overnight at 4°C. After re-pelleting of the insoluble inclusion bodies, they were solubilised in extraction buffer (8 M urea, 20 mM Tris, pH 8.0, 150 mM NaCl, 10 mM dithiothreitol) with stirring overnight at 4°C. The supernatant was dialysed sequentially for 24 hours against 6, 4 and 2 M urea in 20 mM Tris, pH 8.0, 150 mM NaCl, 2mM EDTA at 4°C. The monomeric proteins were then dimerized over a period of 48 hours at 4°C in the presence of oxidized and reduced glutathione (Sigma, Darmstadt, Germany) at 0.5 and 5 mM respectively. The dimerized solution was then dialysed extensively against 20 mM Tris, pH 8.0, 150 mM NaCl, 2mM EDTA at 4°C. The dialysed solution containing dimerized $VEGF_{165}$ was then passed over a heparin agarose column (Applichem, Darmstadt, Germany). The column was washed with 10 column volumes of 20 mM Tris, pH 8.0, 150 mM NaCl and the bound $VEGF_{165}$ eluted with 0.75 M NaCl, 20 mM Tris, pH 8.0. The

eluted $VEGF_{165}$ was then dialysed against 20 mM Tris, pH 8.0, 150 mM NaCl. A standard yield of about 5 mg $VEGF_{165}$ in a volume of 20 ml was obtained.

Porous PU discs were loaded with PBS, $VEGF_{165}$ or PDGF-BB according to the following protocol:

After pipetting 40 µl of PBS (control), PDGF-BB or $VEGF_{165}$ into one well of a 96 well plate, heparin-coated PU discs were dropped into the solution and squeezed at least three times with a plunger of a 1 ml syringe (Codan Medical Apl., Rodby, DK) to remove all trapped air inside the discs and to efficiently load the growth factor containing solution, or control PBS, into the discs. The growth factor was allowed to passively adsorb overnight onto the heparinised surface at 4°C. Non-heparin-coated PU control discs were loaded with 40 µl of PBS or 40 µl of PDGF-BB or $VEGF_{165}$ the same way and left overnight at at 4°C.

5.2.3 Recombinant PDGF-BB

Recombinant human platelet derived growth factor isoform BB (PDGF-BB) was purchased from Pepro Tech® (Pepro Tech Inc., Roxy Hill, NJ, USA) and diluted according to the manufacturer's protocol with sterile PBS to a concentration of 1 mg / ml. To achieve the desired concentration and volume for the elution studies and in vivo angiogenesis assays, 1 mg / ml was further diluted in sterile PBS before PU discs were loaded, as described in chapter 5.2.2.

5.2.4 Elution assays

To determine the time course of growth factor elution from uncoated and heparin coated PU discs loaded with $VEGF_{165}$, PDGF-BB or a combination of $VEGF_{165}$ and PDGF-BB, PU discs were submersed in 5 ml PBS + 0.5 % BSA (Merck Chemicals Ltd, Gauteng, South Africa) + 0.02 % NaN_3 (Merck Chemicals Ltd, Gauteng, South Africa) for 8 days at 37°C under continuous agitation (n=3) after 3 washing steps in 1 ml PBS + 0.5% BSA + 0.02% NaN_3 for 1 hour each to eliminate any unbound growth factor. 100 µl aliquots were taken at various time points between 2 hours and 8 days. $VEGF_{165}$ and PDGF-BB Enzyme-Linked Immunosorbent Assay (ELISA) was performed to determine the amount of $VEGF_{165}$ and / or PDGF-BB released from discs (Quantikine® Human VEGF Immunoassay and Quantikine® Human PDGF-BB Immunoassay, R&D, Minneapolis, MN, USA). ELISA's were performed according to the manufacturer's protocol, as described below. Shortly, a monoclonal

antibody specific for $VEGF_{165}$ or PDGF-BB was pre-coated onto a microplate. Standards and samples were pipetted into the wells and any $VEGF_{165}$ or PDGF-BB present was bound by the immobilized antibody. After washing away any unbound substances, an enzyme-linked polyclonal antibody specific for $VEGF_{165}$ or PDGF-BB was added to the wells. Following a wash, a substrate solution was added to the wells and color developed in proportion to the amount of $VEGF_{165}$ or PDGF-BB bound in the initial step. The color development was stopped after 30 minutes and the intensity was measured using a "Benchmark® Microplate Reader" (Biorad, Japan) at 450 nm.

Manufacturer's protocol (Quantikine® Immunoassay, R&D, Minneapolis, MN, USA) for the detection of $VEGF_{165}$ and PDGF-BB:

Prepare all reagents and standards

1. Add 100 µl assay diluent RD1W to each well
2. Add 100 µl standard, control or sample to each well
3. Incubate for 2 hours, aspirate and wash 3 times
4. Add 200 µl conjugate to each well and incubate for 2 hours
5. Aspirate and wash 3 times
6. Add 200 µl substrate solution to each well and protect from light.
7. Incubate for 25 minutes, add 50 µl stop solution and read at 450 nm within 30 minutes.

The zero standard optical density was subtracted from all readings. Thereafter, a standard curve was constructed by blotting the absorbance for each standard on the y-axis against the concentration of growth factor on the x-axis. A best fit curve was drawn through the points on the graph and a regression equation was obtained using Microsoft Excel software (Microsoft, USA). From this equation a growth factor concentration could be calculated for each sample.

5.2.5 In vivo angiogenesis assay

All animal experiments using the "in vivo angiogenesis assay" were approved by the "University of Cape Town's Animal Research Ethics Committees".

To study the effects of heparin surface modification of porous polyurethane, the "subcutaneous pocket" approach in rats was chosen. Up to six PU discs were implanted in anaesthetized Wistar rats, as described in chapter 4.2.5 "AAV in vivo studies". In addition to the normal environment provided for the rats, one set of experiments included the use of a hypobaric hypoxic chamber.

5.2.6 Hypobaric hypoxic chamber

Rats were kept under controlled conditions (12:12 hours light–dark cycle) with access to a commercially fabricated pelletted diet and water ad libitum. For the hypoxia experiments, rats were housed in a lexan hypobaric chamber (SciTech®, Cape Town, South Africa). Rats were exposed to the hypobaric hypoxic stimulus (45 kPa at 11 % ambient O_2) for 10 days. After 5 days, the hypoxic chamber was opened for 10 minutes to replace food and water and to clean the cages. Appropriate age and sex matched normoxic controls were used for all experiments. After 10 days in hypoxic vs. normoxic environment, the rats were killed with CO_2 gas and the PU discs were explanted, cut in half and fixed in 4 % formalin for H&E and DAPI staining and in zinc fixative for CD31 staining.

5.2.7 Histology

To assess tissue ingrowth and angiogenesis, half a PU disc was fixed in 4 % formalin for Hematoxylin & Eosin (H&E) and DAPI staining. A standard procedure was applied for H&E stains on 5 µm sections including dewaxing, hydrating, staining and mounting as described previously (257) (chapter 4.2.6). Reagents and procedures are described below. The remaining half PU disc was fixed in 10 % zinc fixative for staining with anti-CD31 antibody using the following protocol, described by Beckstead in 1994 (313):

Zinc fixative

Prepare 0.1 M tris buffer, pH 7.4, in the following fashion:

1. Trisma-Base 12.1 g (Sigma Aldrich Chemie GmbH, Steinheim, Germany)
2. 1.0 N HCL 81.5 ml (Merck Chemicals, Gauteng, South Africa)
3. Deionized H_2O 900 ml

Prepare zinc fixative as follows:

1. 0.1 M Tris buffer, pH 7.4 recipe above (1000 ml)
2. Add 0.5 g calcium acetate (Merck Chemicals, Gauteng, South Africa)
3. Add 5.0 g zinc acetate (Merck Chemicals, Gauteng, South Africa)
4. Add 5.0 g zinc chloride (Sigma Aldrich Chemie GmbH, Steinheim, Germany)
5. Mix to dissolve. The final pH will be approximately 6.5 - 7.0.

PU discs were fixed in zinc fixative overnight at room temperature, followed by stepwise dehydration in 70 %, 90 %, 95 % and 100 % ethanol (2 changes) (Merck Chemicals, Gauteng, South Africa). Discs were then cleared in 2 changes of xylene (Merck Chemicals, Gauteng, South Africa) for 50 minutes each at room temperature, followed by paraffin (Merck, Darmstadt, Germany) embedding.
To allow for accurate quantification of angiogenesis inside the PU discs, CD31 antibody staining for endothelial cells was used. CD31 staining was done on zinc fixed samples, which showed best antigenicity and results on rat tissue (313).

Endothelial marker CD 31

1. Fix tissue in 10 % zinc overnight, as per protocol given above.
2. Process overnight through graded alcohols, but replace xylene with 2,2,4 tri-methylpentane as the solvent (because PU in the samples is dissolved by Xylene). Embed in wax.
3. Cut 5 µm sections on un-coated slides
4. Incubate overnight at 37°C.
5. Dewax using 4 changes of 2,2,4 tri-methylpentane, and 2 changes of cycolhexanone, then take through graded alcohol to water.
6. Rinse for 10 minutes in PBS with 0.1 % tween.
7. Apply Primary Antibody Mouse Anti-Rat from RDI-RTCD31 (RDI Research Diagnostics Inc., Flanders, NJ) dilution 1:50 in 1 % BSA / PBS, for 40 minutes
8. Rinse 2 x in PBS + 0.1 % tween.
9. Apply DAKO LSAB 2 alkaline phosphatase kit (DAKO, A/S, Glostrup, Denmark). Apply link antibody for 10 minutes, wash in 2 x PBS + 0.1 % tween. Apply streptavidin AP for 10 minutes, and wash in 2 x PBS + 0.1 % tween.
10. Add chromogen / substrate, BCIP/NBT DAKO (DAKO, A/S, Glostrup, Denmark), until colour development is complete.
11. Rinse in running tap water.
12. Dehydrate, clear in 2,2,4 tri-methylpentane, and mount in Entellan (Merck, Darmstadt, Germany)

To assess the density of cellular ingrowth on heparin coated PU discs, cell nuclei were stained with DAPI on formalin fixed sections following this protocol:

Nuclear marker DAPI

1. Dehydrate sections through graded alcohols and take down to H_2O.
2. Mount sections in DAPI Vector Shield Mounting Medium (Vector Laboratories Inc. Burlinghame, CA, USA)
3. Seal with nail varnish (Reflon, SA)

5.2.8 Microscopy and image analysis

Light microscopy

A Leica light microscope at a magnification of 100 times was used for image aquisition (Leica DM IRBE 541000 light microscope, Germany). Images were taken of the whole PU disc cross section using Leica Q-win software, which added up to 12 optical fields at 100 times magnification (Leica Microsystems GmbH, Wetzlar, Germany). Images were analysed with respect to tissue ingrowth (Leica Q-win image analysis program) on H&E stained cross sections and expressed as per cent tissue ingrowth of the porous disc area. Total vessel counts were carried out on CD31 stained cross sections. Again, at 100 times magnification, 12 optical fields added up to a whole PU disc cross section. Vessels were circled manually using the Leica Q-win image analysis program, which resulted in the total vessel number per disc (normalized to vessels / mm^2) as well as the total area of all vessels per disc (mm^2). Data on total vascular area is furthermore presented as percentage of ingrowth area, calculated on the basis that 16 % of total area in a disc is occupied by PU (personal communication D. Bezuidenhout). Vessels were defined as CD31 positive structures within the area of interest, that either showed a transparent lumen or erythrocytes within. Due to the high magnification used and the strict definition of a vessel, the probability of artifacts resulting from counting a single capillary multiple times, as it weaves in and out the field of a two-dimensional slide, was minimized. The area of interest was defined as the porous area within the polyurethane.

Fluorescence microscopy

Cellular density of cross sections stained with DAPI was assessed using a Fluorescence Microscope (Nikon Eclipse 90i, Nikon, Japan) attached to the X-Cite® 120 Fluorescence Illumination system (Nikon, Japan). At 100 times magnification,

12 optical fields were taken by a digital camera (Nikon Digital Camera DXM 1200 C, Nikon, Japan) and stitched automatically with minimal overlap using "NIS-Elements AR Software" (Nikon, Japan). Cells stained positive for DAPI were subsequently quantified after downsizing the stitched image size by 75 % (Adobe Photoshop 7.0, Adobe, USA). The DAPI nuclei were counted in the downsized image using the "Visiopharm" image analysis system (Visiopharm Integrator System, Kopenhagen, Denmark). Data for cellular density is expressed as cells / mm^2 / ingrowth area.

5.2.9 Statistical evaluation

All data obtained on body weight, tissue ingrowth as well as number and area of cells and vessels are expressed as mean values including standard error of mean. Differences between groups were compared by student's two-tailed t-test. A value of $p < 0.05$ was considered significant.

5.3 Results

5.3.1 In vitro studies

To provide evidence that $VEGF_{165}$ was indeed immobilized on the heparin coated PU surface, 12 µg of $VEGF_{165}$ was loaded in heparin coated PU and plain PU and elution was measured over 4 days (n=2). 1192.14 ± 167 ng of $VEGF_{165}$ (9.91 % of the initial VEGF loading dose) was eluted from the heparin coated disc after 4 days. (Figure 23). In contrast, only 81 ng of $VEGF_{165}$ (6.75% of the initial VEGF loading dose) was released from uncoated PU after 4 days and the initial washing steps.

5.3.1.1 $VEGF_{165}$ and PDGF-BB elution from heparin coated PU discs

$VEGF_{165}$ and PDGF-BB elution from heparin coated PU discs loaded with 12 µg $VEGF_{165}$ plus 1.8 µg PDGF-BB was measured over 7 days in triplicate. $VEGF_{165}$ ELISA showed that in the "$VEGF_{165}$ only" group, 2878.8 ± 96.5 ng $VEGF_{165}$ (23.03 % of loading dose) was eliminated in the first washing step. Over the next 48 hours, 1026.4 ± 79.7 ng of $VEGF_{165}$ (8.21 % of the initial VEGF loading dose), was eluted from the disc (Figure 24). 1 M NaCl salt elution for 1 hour released 62.7 ± 3.7 ng $VEGF_{165}$ (0.5 % of the initial $VEGF_{165}$ loading dose). VEGF elution of the combined 12.5 µg $VEGF_{165}$ plus 1.8 µg PDGF-BB group showed similar results: 4172.5 ± 374 ng $VEGF_{165}$ (33.38 % of loading dose) was eliminated in the first washing step. Over

the next 48 hours, 899.9 ± 243.2 ng of $VEGF_{165}$ (7.2 % of the initial VEGF loading dose), was eluted from the disc (Figure 24). 1 M NaCl salt elution for 1 hour released 57 ± 0.7 ng $VEGF_{165}$ (0.46 % of the initial $VEGF_{165}$ loading dose).

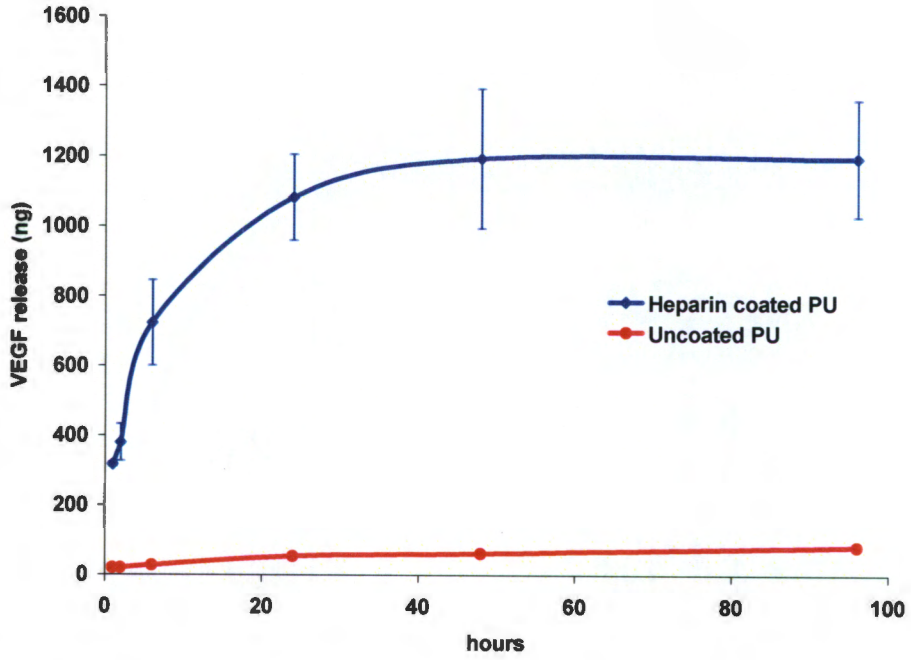

Figure 23: VEGF-ELISA: $VEGF_{165}$ elution from heparin coated PU discs loaded with 12 µg $VEGF_{165}$ (blue line) compared to uncoated PU discs loaded with 12 µg VEGF $_{165}$ (red line) respectively (n=2). Evidence for $VEGF_{165}$ immobilisation and sustained release.

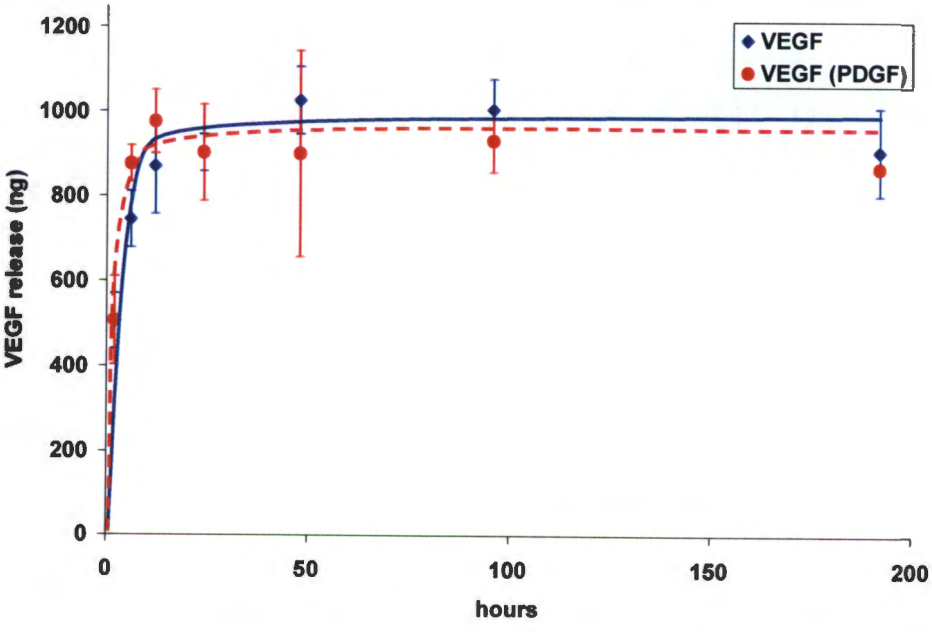

Figure 24: VEGF-ELISA: $VEGF_{165}$ elution from heparin coated PU discs loaded with 12 µg $VEGF_{165}$ (blue line) compared to heparin coated PU discs loaded with 12 µg VEGF $_{165}$ plus 1.8 µg PDGF-BB (red line), respectively (n=3). 1.8 µg PDGF-BB does not affect $VEGF_{165}$ elution from PU discs.

PDGF-BB ELISA was used to evaluate the release of 1.8 µg PDGF-BB compared to 1.8 µg PDGF-BB plus 12 µg $VEGF_{165}$ loaded to heparin coated PU discs over 7 days (n=3). In the 1.8 µg "PDGF-BB only" group, 32 ± 1.9 ng PDGF-BB (1.45 % of loading dose) was eliminated in the first washing step. Over the next 7 days, 66.9 ± 2.3 ng PDGF-BB (3.04 %) was eluted from the disc (Figure 25). 1 M NaCl salt elution for 1 hour released 1687.4 ± 47.9 ng PDGF-BB (94.9 % of the initial loading dose). PDGF-BB elution of the combined 12.5 µg $VEGF_{165}$ plus 1.8 µg PDGF-BB group showed similar results: 37.1 ± 2.1 ng PDGF-BB (1.69 % of loading dose) was eliminated in the first washing step. Over the next 7 days 59 ± 1.9 ng of PDGF-BB (2.68 %), was eluted from the disc (Figure 25). 1 M NaCl salt elution for 1 hour released 1748 ± 17.8 ng PDGF-BB (99.14 % of the initial PDGF-BB loading dose). In summary, $VEGF_{165}$ and PDGF-BB elution studies revealed 12 µg $VEGF_{165}$ and 1.8 µg PDGF-BB as efficient loading of the heparin surface modified PU discs with minimal displacement between $VEGF_{165}$ and PDGF-BB. From an in vivo point of view, this dual growth factor concentration should allow enough $VEGF_{165}$ to be released during the first 48 hours for the initiation of an angiogenic response, while thereafter release of PDFG-BB should allow for stabilization of the newly created vascular network.

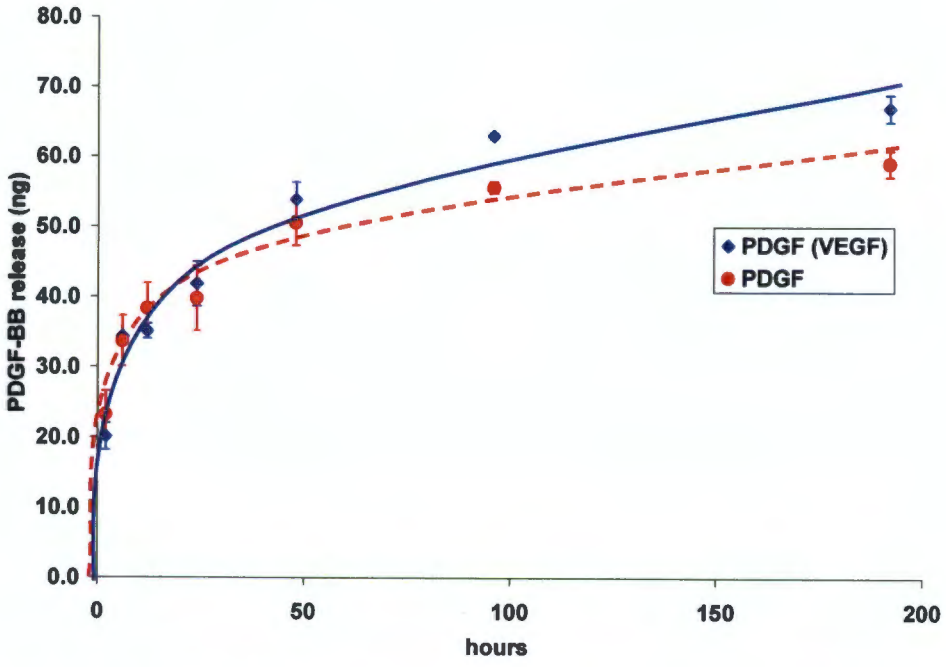

Figure 25: PDGF-BB-ELISA: PDGF-BB elution from heparin coated PU discs loaded with 1.8 µg PDGF-BB (red line) compared to heparin coated PU discs loaded with 12 µg $VEGF_{165}$ plus 1.8 µg PDGF-BB (blue line), respectively (n=3). 12 µg $VEGF_{165}$ does not affect PDGF-BB elution from PU discs.

5.3.2 In vivo studies

5.3.2.1 Effect of immobilised $VEGF_{165}$, PDGF-BB and a combination thereof on neovascularisation in heparin coated PU discs at 10 days

Because the in vitro elution studies showed, that $VEGF_{165}$ and PDGF-BB bound to heparin coated PU with different affinities and were released in a characteristic, time dependent fashion over 48 hours ($VEGF_{165}$) and more than 7 days (PDGF-BB), the angiogenic potential of the heparin immobilized growth factors alone and in combination were evaluated in a rat subcutaneous model. PU discs were implanted in a subcutaneous fashion in the following groups (n=8):

1. Plain PU (uncoated PU)
2. Heparin coated PU without growth factors
3. Heparin coated PU with 1.8 µg PDGF-BB
4. Heparin coated PU with 3.6 µg PDGF-BB
5. Heparin coated PU with 12 µg $VEGF_{165}$
6. Heparin coated PU with 1.8 µg PDGF-BB + 12 µg $VEGF_{165}$

Vessel density

Surface modification with heparin alone increased average vessel density by 77.64 % compared to uncoated control PU (144.23 ± 24 vessels / mm^2 vs. 81.19 ± 6.06 vessels / mm^2, $p<0.05$). Except 1.8 µg PDGF-BB, all other growth factor loaded discs increased vessel density significantly compared to heparin coated PU without growth factors. PDGF-BB 3.6 µg increased vessel density by 17.13 % (168.94 ± 16.43 vessels / mm^2 vs. 144.23 ± 24 vessels / mm^2, $p<0.05$), 12 µg of $VEGF_{165}$ increased vessel density by 19.32 % (172.1 ± 20.95 vessels / mm^2 vs. 144.23 ± 24 vessels / mm^2, $p<0.05$) and the combination of 12 µg $VEGF_{165}$ plus 1.8 µg PDGF-BB increased vessel density by 26.24 % (182.08 ± 39.65 vessels / mm^2 vs. 144.23 ± 24 vessels / mm^2, $p<0.05$). 3.6 µg PDGF-BB further increased vessel density in comparison to 1.8 µg PDGF-BB by 25.92 % (168.94 ± 16.43 vessels / mm^2 vs. 134.16 ± 26.46 vessels / mm^2, $p<0.05$) (Figure 26). Histological sections stained with CD31 antibody of uncoated PU, heparin coated PU and 12 µg $VEGF_{165}$ loaded PU discs are shown in Figure 27.

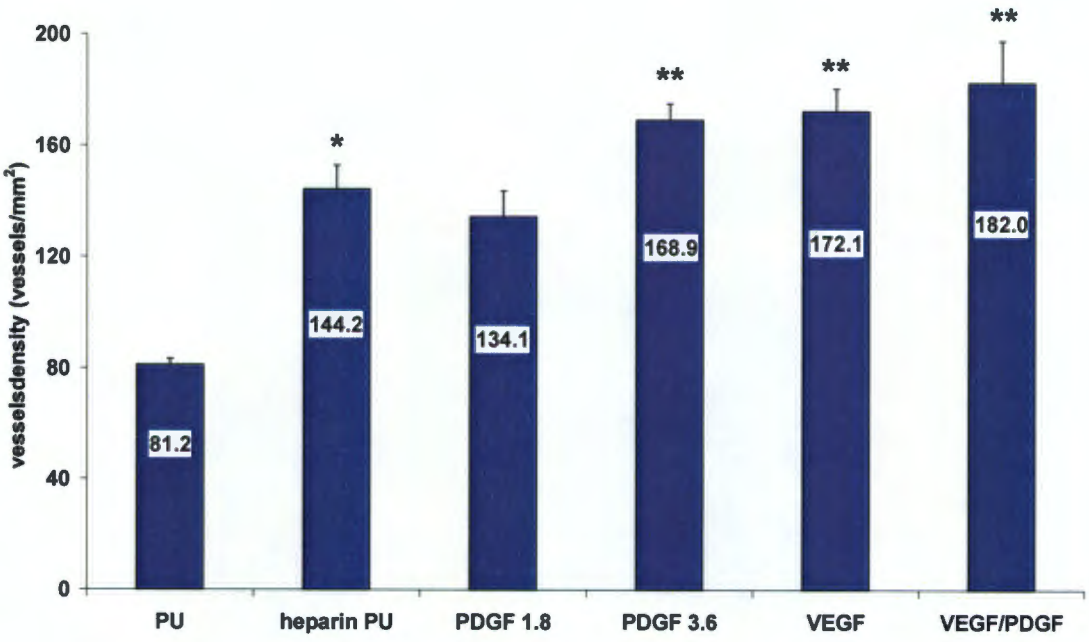

Figure 26: Vessel density of $VEGF_{165}$/PDGF-BB heparin surface modified PU: after 10 days subcutaneous implantation, vessel density of heparin coated PU increased by 77.64 % compared to uncoated control PU (144.23 ± 24 vessels / mm^2 vs. 81.19 ± 6.06 vessels / mm^2), 3.6 µg PDGF-BB increased vessel density by 17.13 % (168.94 ± 16.43 vessels / mm^2), 12 µg $VEGF_{165}$ by 19.32 % (172.1 ± 20.95 vessels / mm^2), and the combination of 12 µg $VEGF_{165}$ plus 1.8 µg PDGF-BB increased vessel density by 26.24 % (182.08 ± 39.65 vessels / mm^2) compared to heparin coated PU (144.23 ± 24 vessels / mm^2). * indicates $p<0.05$ vs. PU control, ** indicates $p<0.05$ compared to heparin coated PU (n=8).

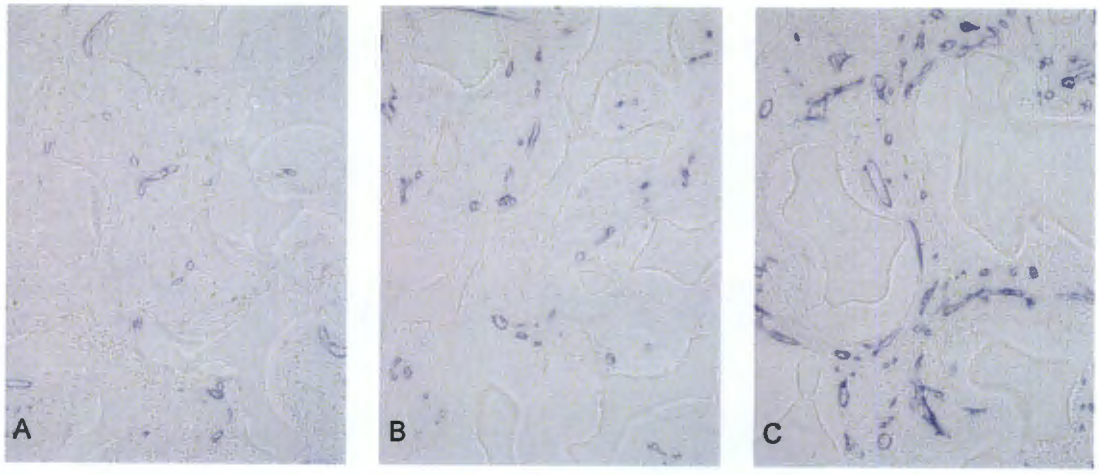

Figure 27: Representative immunhistological sections of CD31 stained uncoated PU (A), heparin coated PU (B), and heparin coated plus 12 µg $VEGF_{165}$ loaded PU (C) after 10 days subcutaneous implantation in rats (100 x magnification). Increased neovascularisation (blue tubelike structures) of heparin coated PU dics is clearly visible (B) (77.64 % compared to uncoated PU, $p<0.05$), which is further enhanced by additional $VEGF_{165}$ (C) (111.97 % compared to uncoated PU, n=8, $p<0.05$).

Vascular area

Since the extent of neovascularisation is often not sufficiently characterized by vessel count alone as a particular treatment may generate small vessels and thus potentially not increase vascular area, we analysed total vascular area per PU disc cross section as well. Data is presented as % ingrowth area vascularized (IAV). In parallel to vessel number, surface modification with heparin alone increased average vascular area by 74.89 % compared to uncoated control PU (4.25 ± 0.17 % IAV vs. 2.43 ± 0.33 % IAV, $p<0.05$). Vascular area was further increased by 12 µg $VEGF_{165}$ in comparison to heparin coated PU without growth factors by 42.82 % (6.07 ± 0.37 % IAV vs. 4.25 ± 0.17% IAV, $p<0.05$). 12 µg $VEGF_{165}$ in addition to 1.8 µg PDGF-BB finally increased vascular area by 45.64 % compared to heparin coated control PU (6.19 ± 0.34 % IAV vs. 4.25 ± 0.17 % IAV, $p<0.05$) (Figure 28).

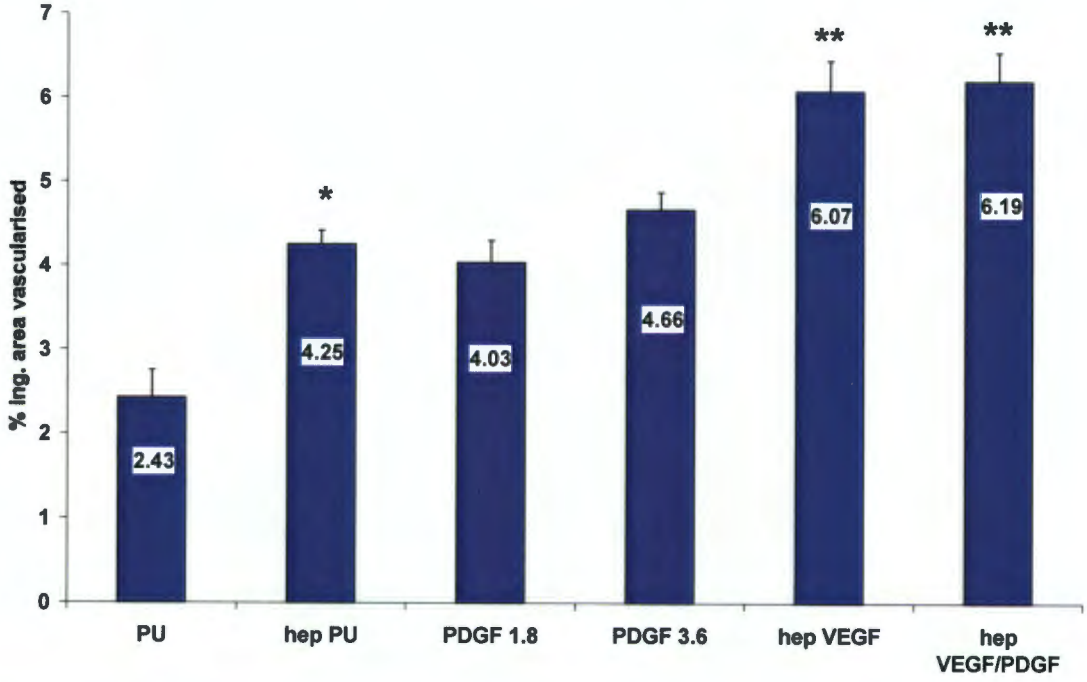

Figure 28: Vascular area of $VEGF_{165}$ / PDGF-BB heparin surface modified PU: Surface modification with heparin alone increased average vascular area by 74.89 % compared to uncoated control PU (4.25 ± 0.17 % vs. 2.43 ± 0.33, $p<0.05$, indicated by *). Vascular area was further increased in 12 µg $VEGF_{165}$ loaded PU by 42.82 % in comparison to heparin coated PU (6.07 ± 0.37 % vs. 4.25 ± 0.17 %, $p<0.05$). 12 µg $VEGF_{165}$ in addition to 1.8 µg PDGF-BB finally increased vascular area by 45.64 % compared to heparin coated control PU (6.19 ± 0.34 % vs. 4.25 ± 0.17 %, $p<0.05$). ** indicates $p<0.05$ compared to heparin coated PU (n=8).

5.3.2.2 Effect of immobilised $VEGF_{165}$, PDGF-BB and a combination thereof on neovascularisation in heparin coated PU discs at 2 months

In parallel to the growth factor delivery experiment on a 10 day short term basis, we were interested to evaluate the angiogenic potential of heparin coated PU with and without growth factor addition on a long term basis. Therefore, PU discs were implanted in a subcutaneous fashion for 2 months in the following groups (n=8).

1. Plain PU (uncoated PU)
2. Heparin coated PU without growth factors
3. Heparin coated PU with 1.8 µg PDGF-BB
4. Heparin coated PU with 12 µg $VEGF_{165}$
5. Heparin coated PU with 1.8 µg PDGF-BB + 12 µg $VEGF_{165}$

Vessel density

Heparin surface modification increased mean vessel density after 2 months implantation time by 41.91 % in comparison to non coated control PU (101.57 ± 40.07 vessels / mm^2 vs. 59 ± 13.20 vessels / mm^2, $p<0.05$). Addition of 1.8 µg PDGF-BB to the heparin coated PU discs showed a further 40.82 % increase in vessel density (171.64 ± 49.13 vessels / mm^2 vs.101.57 ± 40.07 vessels / mm^2, $p<0.05$). Addition of $VEGF_{165}$ to heparin coated discs failed to increase vessel density at 2 months compared to heparin coated discs. There was however, still a 52.46 % vessel increase against non coated control PU (124.1 ± 40.07 vessels / mm^2 vs. 59 ± 13.20 vessels / mm^2, $p<0.05$). In general, the increasing importance of PDGF-BB over time in comparison to $VEGF_{165}$ was evident since 1.8 µg PDGF-BB loading on heparin coated PU discs was as efficient as a combination of 12 µg $VEGF_{165}$ and 1.8 µg PDGF-BB in creating vessels at 2 months (171.64 ± 49.13 vessels / mm^2 vs. 173.75 ± 41.54 vessels / mm^2) (Figure 29). If the treatment groups at 10 days are compared with the same groups at 2 months, the following becomes apparent: the uncoated control PU discs showed a decrease in vessel density of 27.33 % (81.19 ± 6.06 vessels / mm^2 vs. 59 ± 13.21 vessels / mm^2, $p< 0.05$). Heparin coated PU discs decreased in vessel density by 29.58 % at 2 months (144.23 ± 24 vessels / mm^2 vs. 101.58 ± 35.05 vessels / mm^2, $p<0.05$), as did $VEGF_{165}$ loaded heparin coated PU discs (27.89 % decrease, 172.10 ± 20.95 vessels / mm^2 vs. 124.1 ± 20.95 vessels / mm^2, $p<0.05$). Only 1.8 µg PDGF-BB loaded heparin coated PU discs showed an increase in vessel density by 27.93 % at

2 months, (134.16 ± 26.46 vessels / mm^2 vs. 171.64 ± 49.13 vessels / mm^2, $p<0.05$). If PDGF-BB was bound additionally to $VEGF_{165}$, PDGF-BB had a stabilizing effect on neovascularisation by neutralizing the decrease in vessel density observed in the $VEGF_{165}$ alone group (Figure 29).

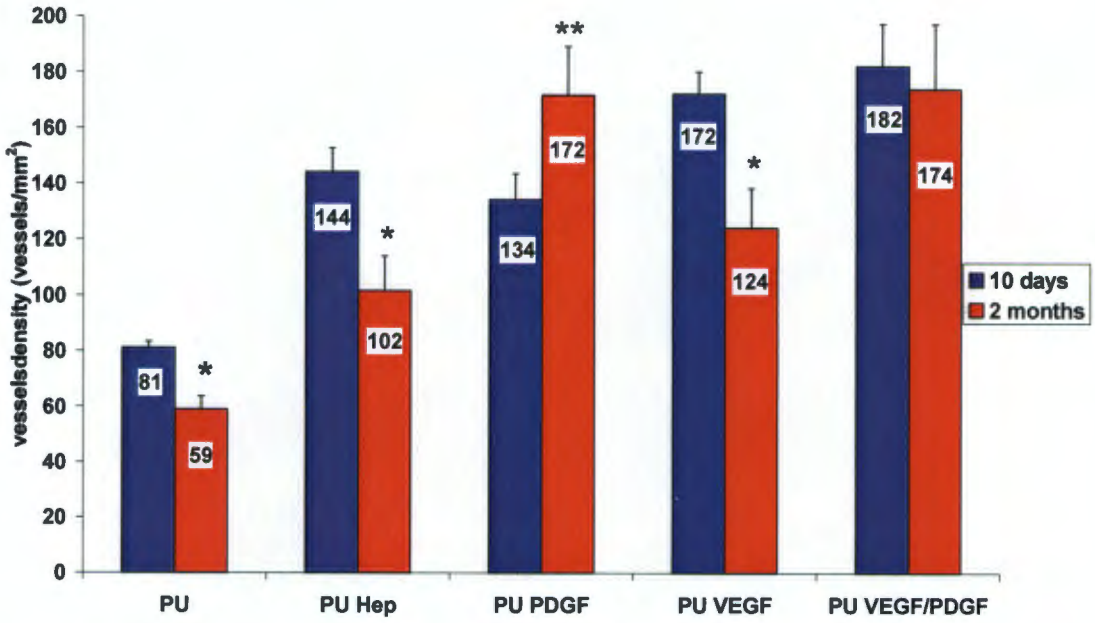

Figure 29: Vessel density of $VEGF_{165}$ / PDGF-BB heparin surface modified PU after 10 days (blue column) and 2 months (red column) implantation time (n=8). * indicates decrease of vessel density at 2 months compared to 10 days in the uncoated PU group by 27.33 % (81.19 ± 6.06 vessels / mm^2 vs. 59 ± 13.21 vessels / mm^2, $p< 0.05$), in the heparin coated PU group by 29.58 % (144.23 ± 24 vessels / mm^2 vs. 101.58 ± 35.05 vessels / mm^2, $p<0.05$) and in the PU $VEGF_{165}$ group by 27.89 % (172.10 ± 20.95 vessels / mm^2 vs. 124.1 ± 20.95 vessels / mm^2, $p<0.05$). The stabilizing effect of PDGF-BB on neovascularisation at 2 months was shown by the increase in vessel density of 27.93 % at 2 months (134.16 ± 26.46 vessels / mm^2 vs. 171.64 ± 49.13 vessels / mm^2, $p<0.05$, as indicated by **). The combination of $VEGF_{165}$ / PDGF-BB stabilized neovascularisation at 2 months at the level of 10 days.

Vascular area

Heparin surface modification of PU discs increased vascular area by 44.94 % at 2 months compared to control PU, but failed to reach statistical significance (1.97 ± 0.84 % ingrowth area vascularised (IAV) vs. 1.36 ± 0.35 % IAV, $p= 0.078$). Addition of 1.8 µg PDGF-BB and the combination of 12 µg $VEGF_{165}$ and 1.8 µg PDGF-BB increased vascular area significantly by 42.11 % (1.97 ± 0.84 % IAV vs. 2.8 ± 0.57 % IAV, $p<0.05$) and 43.25 % (1.97 ± 0.84 % IAV vs. 2.82 ± 0.7 % IAV, $p<0.05$), compared to heparin coated PU discs without growth factors, respectively. $VEGF_{165}$ on heparin coated PU discs failed to increase vascular area in comparison to

heparin coated PU discs, but increased the area by 71.97 % (1.36 ± 0.35 % IAV vs. 2.34 ± 0.42 % IAV, $p<0.05$) compared to uncoated PU (Figure 30).

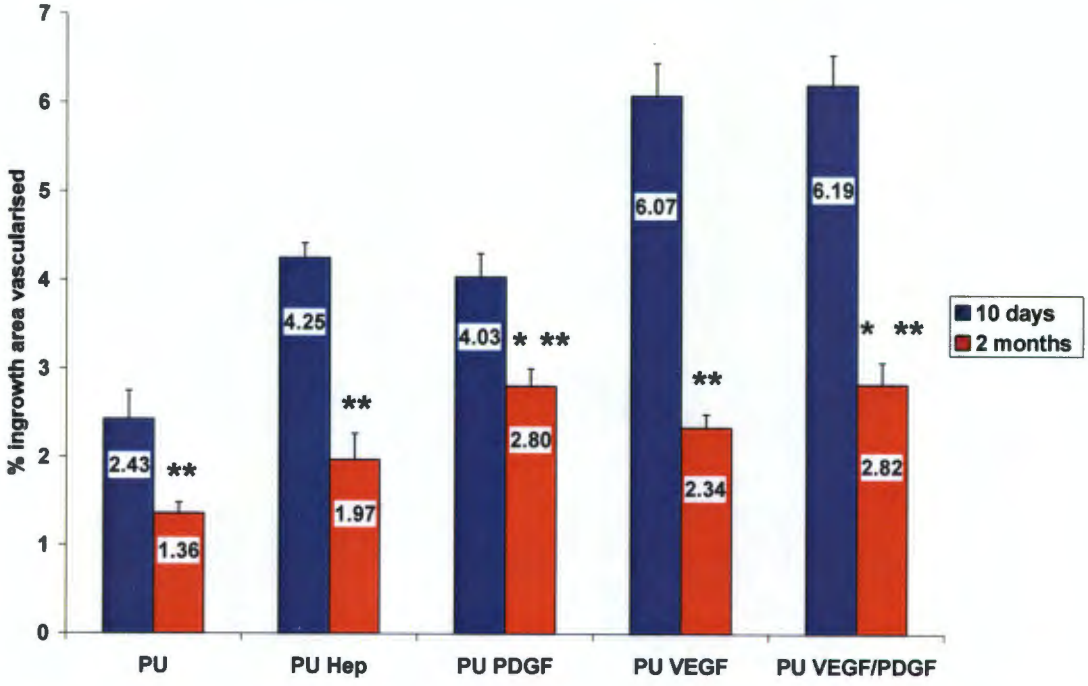

Figure 30: Vascular area of $VEGF_{165}$ / PDGF-BB heparin surface modified PU at 10 days (blue columns) and 2 months (red columns) (n=8). * indicates increase of vascular area at 2 months of the PU PDGF-BB group by 42.11 % (1.97 ± 0.84 % IAV vs. 2.8 ± 0.57 % IAV, $p<0.05$) as well by 43.25 % in the PU $VEGF_{165}$ / PDGF-BB group (1.97 ± 0.84% IAV vs. 2.82 ± 0.7 % IAV, $p<0.05$) compared to the heparin coated group without growth factors. ** indicates significant vessel regression in all groups at 2 months compared to the same groups at 10 days ($p<0.05$).

In comparison to the vascular area at 10 days implantation time, however, it was evident, that all treatment groups showed significant vascular regression, ranging from 30.53 % for the PDGF-BB 1.8 µg treated group to 61.47 % for the 12 µg $VEGF_{165}$ treated group (Figure 31). Overall, after 2 months of subcutaneous implantation, neovascularisation regressed in the $VEGF_{165}$ supplemented group compared to 10 days in terms of vessel density and vascular area (Figures 29 and 30). PDGF-BB on the other hand, seems to have stabilized neovascularisation in terms of vessel density and showed the least regression of vascular area (Figure 31).

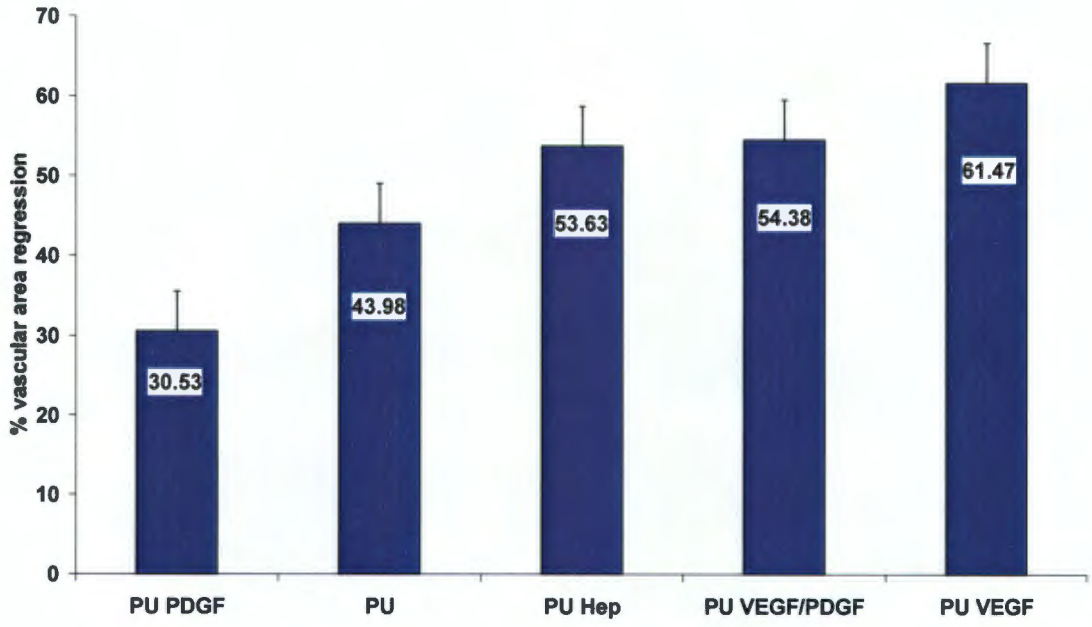

Figure 31: Regression of neovascularisation at 2 months compared to 10 days. The highest vessel regression was seen in the PU $VEGF_{165}$ group (61.47 %), whereas the PU PDGF-BB group showed only a regression of only 30.53 % (n=8).

5.3.3 Surface modification in chronic hypoxia

As described in 5.1.2, the following studies would like to clarify, whether chronic whole body hypobaric hypoxia has an effect on heparin-induced angiogenesis into heparin coated polyurethane discs in a wound model. PU discs were implanted in a subcutaneous fashion for 10 days in the following groups (n=8):

1. Plain PU (uncoated PU)
2. Heparin coated PU
3. Heparin coated PU with 12 µg $VEGF_{165}$

Rat weight as a marker for efficient hypoxia

Rats were subjected to whole body hypobaric hypoxia for 10 days, as described in chapter 5.2.6. Rat weights were used as a marker of efficient whole body hypobaric hypoxia, as described previously by La Manna et al. (309). The ability to gain weight differed significantly between the normoxic and the hypoxic study groups. Normoxic rats gained 68.2 % weight (135.25 ± 5.26 g at implantation vs. 227.5 ± 10.93 g at explantation, n=8) during the 10 day period. Hypoxic rats increased their weight only

by 36.33 %, (142 ± 5.29 g at implantation vs. 193.6 ± 10.62 g at explantation) ($p<0.05$).

Cellular density of heparin coated PU discs implanted in hypoxic rats

In order to evaluate neovascularisation of heparin surface modified PU discs with and without addition of 12.5 µg $VEGF_{165}$ under hypoxic conditions, sufficient tissue ingrowth into the porous discs after 10 days implantation time was a prerequisite. On light microscopical analysis of H&E stained sections, as described in chapters 4.2.6, 5.2.7 and 5.2.8, all samples showed 100 % tissue ingrowth. Since possible differences in cellular densities needed to be investigated, we used DAPI nuclear stain to allow for automated image analysis of cellular density as a marker for tissue density inside PU discs.

In the normoxic group, surface modification with heparin alone increased cellular density compared to uncoated PU control discs by 39.76 % (2066.24 ± 330.33 cells / mm^2 vs. 1478.36 ± 215.39 cells / mm^2, $p<0.05$). Addition of $VEGF_{165}$ to heparin surface modified PU revealed as well an increased tissue density inside PU discs (2192.8 ± 185.17 cells / mm^2, $p<0.05$) (Figure 32). In the hypoxic treatment group however, heparin surface modification failed to increase cellular density compared to PU control discs (1689.14 ± 250.76 cells / mm^2 vs. 1592.56 ± 168.38 cells / mm^2, p=n.s., n=8). Only if $VEGF_{165}$ was added to heparin surface modified PU discs, the tissue density increased in the hypoxic group compared to PU control by 20.66 % (1921.64 ± 271.63 cells / mm^2 vs. 1592.56 ± 168.38 cells / mm^2, $p<0.05$). If the hypoxic subgroups are compared against the normoxic subgroups, the heparin surface modified subgroup showed a significantly lower cellular density under hypoxic conditions (1689.14 ± 250.76 cells / mm^2 vs. 2066.24 ± 330.33 cells / mm^2, $p<0.05$). Taken together, heparin surface modification alone increased cellular density under normoxic, but not under hypoxic conditions, where additional external $VEGF_{165}$ is required to show this effect.

Neovascularisation of heparin coated PU discs implanted in hypoxic rats

Evaluation of the neovascularisation into PU control discs, heparin surface modified PU discs and $VEGF_{165}$ supplemented heparin coated PU discs after 10 days subcutaneous implantation under normoxic and hypoxic conditions showed the following results:

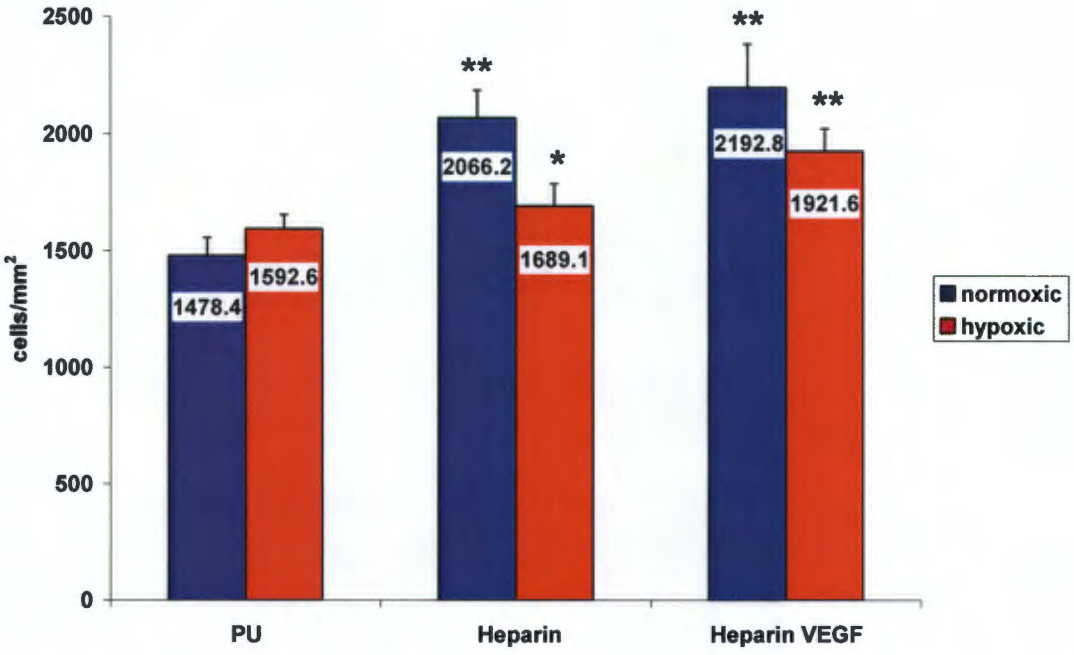

Figure 32: Cellular density of $VEGF_{165}$ loaded, non-heparin coated PU control discs (PU), heparin coated PU discs (Heparin) and the combined heparin coated and $VEGF_{165}$ loaded PU discs (Heparin VEGF). Implantation subcutaneously in wistar rats, which were kept under normoxic (blue columns) (n=8) or hypobaric hypoxic conditions (11 % O_2) (red columns) for 10 days (n=8). Automated image analysis was used for quantification after DAPI nulclear staining. * indicates $p<0.05$ between normoxic and hypoxic conditions (1689.14 ± 76.15 cells / mm^2 vs. 2066.24 ± 116.79 cells / mm^2). ** indicates $p<0.05$ in same O_2 concentration (2066.24 ± 116.79 cells / mm^2, in the heparin coated group as well as 2192.8 ± 185.17 cells / mm^2 in the heparin VEGF coated group vs. 1478.36 ± 76.15 cells / mm^2 in the control PU group for normoxia) ** also indicates increased cellular density in hypoxic group after external addition of $VEGF_{165}$ (1921.64 ± 96.04 cells / mm^2 vs. 1592.56 ± 59.53 cells / mm^2.

In the normoxic group, heparin surface modification increased vascular density in PU discs after 10 days compared to uncoated PU control discs by 61.25 % (130.31 ± 13.7 vessels / mm^2 vs. 80.81 ± 2.93 vessels / mm^2, $p<0.05$) (Figure 33). Addition of $VEGF_{165}$ to the heparin coated PU discs further increased vascular density by 31.29 % (171.09 ± 12.56 vessels / mm^2 vs. 130.31 ± 13.7 vessels / mm^2, $p<0.05$). Under hypoxic conditions however, heparin coating alone failed to increase vascular density compared to PU control discs. Only after addition of $VEGF_{165}$ to heparin coated PU discs, vascular density increased by 27.99 % compared to heparin coated PU (103.93 ± 4.83 vessels / mm^2 vs. 81.20 ± 2.93 vessels / mm^2, $p<0.05$) (Figure 33). If subgroup neovascularisation is directly compared in normoxic vs. hypoxic conditions, the following becomes evident:

1. No difference between normoxic and hypoxic control PU discs

2. 37.69 % reduced vascular density in the hypoxic heparin coated PU group compared to the normoxic heparin coated PU group (81.20 ± 8.48 vessels / mm^2 vs. 130.31 ± 13.7 vessels / mm^2, $p<0.05$)
3. 39.25% reduced vascular density in the hypoxic $VEGF_{165}$ supplemented heparin coated PU group compared to the normoxic $VEGF_{165}$ supplemented heparin coated PU group (103.93 ± 4.83 vessels / mm^2 vs. 171.09 ± 12.56 vessels / mm^2, $p<0.05$).

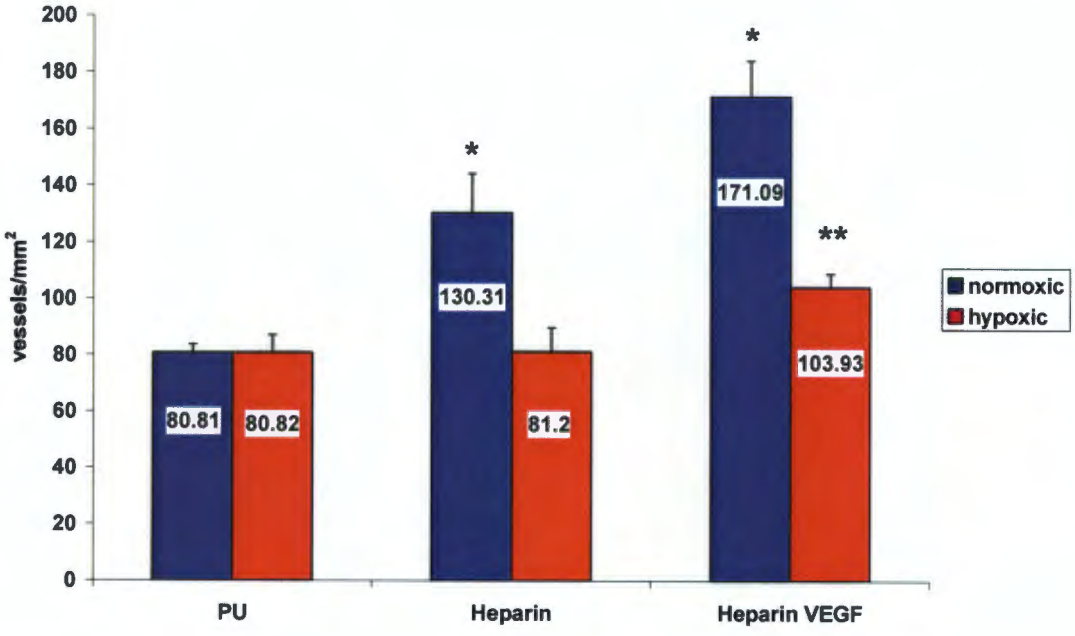

Figure 33: Neovascularisation of normoxic (blue columns) and hypoxic (red columns) (11 % O_2) surface modified PU discs. * indicates a 61.25 % increase in neovascularisation in heparin surface modified PU discs after 10 days compared to $VEGF_{165}$ loaded, uncoated PU control discs under normoxic conditions (130.31 ± 13.7 vessels / mm^2 vs. 80.81 ± 2.93 vessels / mm^2, $p<0.05$) as well as further 31.29 % increase by addition of $VEGF_{165}$ to heparin coated PU (171.09 ± 12.56 vessels / mm^2 vs. 130.31 ± 13.7 vessels / mm^2, $p<0.05$). ** indicates a 27.99 % increased vascular density by $VEGF_{165}$ loaded, heparin coated PU discs under hypoxic conditions compared to heparin coated PU (103.93 ± 4.83 vessels / mm^2 vs. 81.20 ± 2.93 vessels / mm^2, $p<0.05$). Note the failure of heparin coated PU discs without $VEGF_{165}$ to increase neovascularisation under hypoxic conditions.

Overall, results of the neovascularisation study paralleled results of the cellular density study indicating, that heparin surface modification alone was able to increase cellular and vascular density at 10 days in normoxia. Under hypoxic conditions, however, this was not the case. Only after addition of $VEGF_{165}$ to the heparin coated PU was the vessel density as well as the cellular density increased. A hypoxic environment decreased neovascularisation of heparin surface modified PU with or without $VEGF_{165}$ by approximately 40 %.

5.4 Discussion

We could show, that covalent attachment of heparin onto porous polyurethane increased neovascularisation after subcutaneous implantation in rats for 10 days by 77.64 % compared to non coated controls. This effect can even be enhanced by the addition of angiogenic growth factors such as $VEGF_{165}$ and PDGF-BB, which in combination showed an overall increase in vascular density of 124.26 %. Heparin as a pro-angiogenic matrix as well as a delivery system for the controlled release of heparin binding growth factors has also been reported by other investigators. Fujita and Ishihara incorporated heparin passively via electrostatic bonding into chitosan hydrogel matrices (314), (315). Fibroblast growth factor-2, which was added to the chitosan / heparin hydrogel, showed a controlled release of about 20 % of the loading dose within the first day in an in vitro elution experiment. Neovascularisation into this chitosan hydrogel was increased by the addition of heparin in a mouse subcutaneous model. This effect was potentiated by the incorporation of FGF-2 into the heparin loaded chitosan hydrogel, whereas FGF-2 without heparin showed only a minor effect (314). Other authors described the use of different matrices, such as fibrin, alginate and collagen for heparin modified release of growth factors. Sakiyama and Hubbell immobilized heparin by electrostatic interactions within a modified fibrin matrix and achieved the release of heparin binding growth factors such as FGF in response to cellular activity during wound healing (299). A sustained release of FGF was further shown by Tanihara et al. using a covalently cross linked gel of heparin and alginate (298). FGF, which was added to the alginate / heparin hydrogel, showed a controlled in vitro elution of about 25 % of the loading dose within the first 24 hours, which continued delivering FGF for about one month. As a consequence, increased angiogenesis was achieved into the gel after two weeks of subcutaneous implantation in rats (298). Wissink et al. covalently attached heparin to a collagen matrix and decreased thereby the initial burst release of FGF from 60 % to 18 % after 48 hours compared to non-heparinised control (295). In vivo delivery of FGF in combination with heparin within a gelatin gel has been previously reported by Doi et al. (316), $VEGF_{165}$ in the same model was tested by Masuda et al. (317). In each case, growth factor plus heparin resulted in increased endothelial coverage of a micro-porous PU graft after aortic replacement in rats for 4 weeks. In contrast to FGF, $VEGF_{165}$ facilitated even transmural tissue ingrowth into the heparin / gelatin treated graft substantially (317). $VEGF_{165}$ immobilized in a heparin containing collagen matrix was described recently by Steffens et al. (318). He reported on an increased angiogenic potential of a collagen matrix implanted into

chorio-allantoic membranes in chicken embryos, if the matrix was pretreated with heparin. $VEGF_{165}$ added to collagen without heparin only showed minor effects, whereas $VEGF_{165}$ in combination with heparin revealed a strong angiogenic response (318). Our own approach was the direct, covalent attachment of heparin onto the biomaterial polyurethane without addition of an external ingrowth matrix. In vitro results showed a sustainable, controlled release of $VEGF_{165}$ (899.9 ± 243.2 ng at 48 hours) as well as of PDGF-BB (66.9 ± 2.3 ng at 7 days). In vivo, the strong angiogenic potential of heparin immobilization alone was demonstrated in terms of vessel density and vascular area in excellent agreement with literature, as discussed above. Therefore, a simple, heparin based staged growth factor delivery was achieved. A technically more demanding staged growth factor delivery model was described recently by Richardson et al. (95) and Chen et al. (319) for $VEGF_{165}$ delivery from a poly(lactide-co-glycolide) (PLG) scaffold and PDGF-BB delivery from pre-encapsulated microspheres. The exact mechanisms of heparin derivates influencing the angiogenic response to growth factors are still not completely understood. So far, heparin has been shown to enhance $VEGF_{165}$ –induced phosphorylation of VEGFR-2 by 1.7 fold because a heparin-like domain of heparan sulfate forms a complex with $VEGF_{165}$ and VEGFR-2 (294). Soker et al. have shown, that variations in the size and sulphatation of heparin influence its $VEGF_{165}$ binding capacity (288). Furthermore, endogenous heparin binding growth factors could be "trapped" by the heparin coated surface and contributed as well to the increased neovascularisation observed.

Our results on single and dual growth factor delivery in vivo at 10 days and 2 months emphasized the importance of a long term study. At 10 days, vessel density was increased by PDGF-BB, $VEGF_{165}$ and a combination thereof. At 2 months, however, PDGF-BB could still increase vessel density, whereas $VEGF_{165}$ induced vessels regressed. The level of vascular area regression at 2 months, however, was lowest in PDGF-BB delivered and highest in $VEGF_{165}$ delivered samples. The combination of both growth factors showed a stable level of vessel density. Overal vascular area decreased significantly even in the dual growth factor delivery group after 2 months because vessel size decreased substantially. Dual growth factor delivery has been described as a preferred way to achieve neovascularisation of biomaterials compared to single growth factor delivery, because it mimics the physiological situation with spatially and temporarily controlled delivery of growth factors more closely. Richardson et al. reported on increased neovascularisation by the controlled, dual growth factor release of $VEGF_{165}$ and PDGF-BB (95), whereas Cao et al. used a combination of PDGF-BB and FGF to induce angiogenesis and

even long term vascular stability for more than one year (320). Since $VEGF_{165}$ is well known to initiate angiogenesis (128), (321), (72) and PDGF-BB has been shown to recruit pericytes and thus to stabilize vascular networks (322) (323) (324), we chose this growth factor combination to induce stable, functional neovascularisation into heparin surface modified PU. $VEGF_{165}$ alone showed a clear angiogenic response in our model at 10 days with respect to increased vessel density and vascular area. At 2 months, there was significant regression of $VEGF_{165}$ induced neovascularisation, since $VEGF_{165}$ was delivered only for a period of a few days, as indicated by our elution studies. Overall vascular density and area was however, at 2 months still higher compared to control. Vessel regression after cessation of $VEGF_{165}$ delivery has been described by Benjamin and Keshet (325), (326) and other authors (327), (328). 3.6 µg PDGF-BB as pericyte recruiting and therefore stabilizing factor showed angiogenic potential in terms of increased vessel density at 10 days. PDGF has been shown to be angiogenic (96), (329) including the development of functional vascular anastomoses (330), mainly through the recruitment of pericytes (322). Betzholtz suggests, that one of the most essential roles of pericytes might be the formation of endothelial tubes with a uniform diameter to ensure optimal perfusion (331).

With regards to the dual growth factor delivery, the following becomes apparent:

At 10 days, $VEGF_{165}$ / PDGF showed the strongest angiogenic response without difference to sole $VEGF_{165}$ delivery. There was no additive effect of the combination of growth factors. At 2 months, vessel density and vascular area were highest in the dual growth factor group followed by sole PDGF-BB delivery. As mentioned earlier, sole $VEGF_{165}$ delivered vessels regressed to 61.47 %. Very similar results were reported recently by Chen et al. using a porous PLG scaffold for the sustained and controlled delivery of $VEGF_{165}$ and pre-encapsulated PDGF-BB. Using less $VEGF_{165}$ (1.5 µg), but more PDGF-BB (3 µg) alone and in combination, they found an equal angiogenic potential of PDGF-BB, $VEGF_{165}$ and a combination thereof after 2 weeks implantation in ischemic tissue (319). After 6 weeks, only the treatment groups involving PDGF-BB remained stable with a two fold increased vessel area compared to control and $VEGF_{165}$ delivered polymers. This indicates a angiogenic as well as a stabilizing effect of PDGF-BB, which was shown by increased α- SMA (smooth muscle actin) staining at 6 weeks in the PDGF-BB delivered groups (319). In our model, actin staining was not sufficient to discriminate sufficiently between perivascular smooth muscle cells and myofibroblasts, which were numerous throughout the whole PU disc. In summary, the staged growth factor delivery including $VEGF_{165}$ and PDGF-BB is useful to create increased neovascularisation

into a biomaterial for an implant period of up to two months, since overall vascular area was increased two fold compared to control. With the approach of dual growth factor delivery, we generated elevated levels of vessels for the entire implant period. $VEGF_{165}$ increased neovascularisation at earlier stages whereas PDGF-BB increased neovascularisation later on and stabilized $VEGF_{165}$ induced vessels. Therefore, dual growth factor delivery of $VEGF_{165}$ and PDGF-BB seems to be a useful tool for future applications in the field of tissue engineering.

Since neovascularisation into synthetic materials used as scaffolds for organ or tissue replacement often occurs under hypoxic conditions we were interested to investigate, whether chronic whole body hypobaric hypoxia would have an effect on heparin-induced angiogenesis into heparin coated polyurethane discs in a wound model. As an unexpected finding, whole body hypobaric hypoxia (11 % O_2) did not increase neovascularisation into porous PU discs implanted subcutaneously in rats, but rather had a distinctive counter-effect on the angiogenic efficiency of covalent heparin coating. In accordance with our previous results, heparin surface modification increased vessel density by 61.25 % compared to baseline under normoxic conditions. Addition of $VEGF_{165}$ had an additive effect up to 111.71 %. In hypoxia, however, the pro-angiogenic effect of heparin was completely absent, and additional $VEGF_{165}$ was necessary to increase vessel density by 28.59 % compared to control (as shown in Figure 32). Possible explanations for these findings are:

1. A direct effect of chronic hypoxia on the angiogenic effect of heparin.
2. Chronic hypoxia counteracts the angiogenic effect of heparin via other mechanisms such as reduced growth factor levels

In the literature, there is some evidence for a direct alteration of heparin by hypoxia. In vitro studies by Humphries et al. have shown that endogenous production of heparan sulfate of endothelial cells is significantly reduced by 31.11 % under hypoxic conditions (332). A reduction in proteoglycans under hypoxia has also been shown in fibroblasts (333). At this point, however, it is only speculation, if there is an additional alteration on the functional level of heparin under hypoxic conditions, which leads to a decreased binding capacity of heparin binding growth factors such as $VEGF_{165}$, PDGF-BB and bFGF.

More evidence exists for an anti-angiogenic effect of chronic hypoxia that counteracts the pro-angiogenic effects of heparin surface modification of PU. While upregulation of angiogenic genes such as genes encoding for $VEGF_{165}$ (128), bFGF (301), PDGF-BB (302), Angiopoietin-1 (303) and Angiopoietin-2 (304) was clearly shown under acute hypoxic conditions in vitro and is generally accepted, much more controversy exists regarding the in vivo effects of chronic hypoxia on different

tissues (306). Firstly, there is an important difference between acute and chronic hypoxia. Angiogenic genes encoding for $VEGF_{165}$, PDGF-BB and bFGF are up-regulated in acute hypoxia with a maximum stimulation at about 48 hours after induction of the systemic hypoxic stimulus (128), (302), (301). Thereafter, up-regulation of genes often returns to baseline levels within 4 - 7 days. Chronic hypoxia exceeding 7 days on the other hand often fails to increase growth factor levels and as a result, there is either no angiogenesis at all or the vascular network is unstable. Ruscher et al. (334) and Levy et al. (335) showed that prolonged exposure to hypoxia for weeks down-regulates transcriptional activation of $VEGF_{165}$ in cells and tissues as a result of decreased HIF-1 binding activity. While acute hypoxia initiates angiogenesis, chronic hypoxia often cannot sustain it (336). Secondly, increased angiogenesis as a physiological adaptive mechanism to chronic hypoxia seems to occur mainly in vital organs like the brain (308), (309), the heart, lung, liver, kidney and pulmonary circulation (312), (306). Marti and Risau noticed, that the response to hypoxia in vivo is differentially regulated at the level of specific cell types in certain organs resulting in increased VEGF gene expression in some tissues while others show no change in VEGF expression or even a down regulation (306). Conflicting data exists for example for skeletal muscle, where Smith and Marshall evaluated an increase in number of small arterioles in rats exposed to 12 % hypoxia for 18 days (311), whereas most studies showed no change in capillary to fiber ratio in skeletal muscle eliminating the influence of a decreased muscle fibre size (337), (338). In a recent human study, acclimatization to 4100 meters above sea level did not change capillary density in skeletal muscle (339).

To complicate matters even further, wound healing, as evaluated in our subcutaneous disc implant model, is a very complex situation involving inflammatory cells and is generally thought to have a local hypoxic environment on its own (340), (341). However, recent data suggests, that the traditional cascade of hypoxia, increased growth factor levels and therefore increased angiogenesis might not be as simple as previously thought, at least not for a wound healing situation. Haroon et al. reported on high $VEGF_{165}$ expression in a rat punch biopsy wound model at day 1 without any signs of hypoxia, as assessed on a cellular basis using pimonidazole adducts as a hypoxia marker (342). He concluded that induction of angiogenic cytokines in the early wound healing phase may be triggered by other mechanisms than hypoxia. This data was supported by Howdieshell et al., who found high $VEGF_{165}$ levels in a surgically created hernia in a pig without the wound fluid being hypoxic (343). Therefore, in a wound model at normoxic breathing conditions,

angiogenic cytokines may be present without hypoxia. In accordance with this theory, several authors reported, that wound angiogenesis is facilitated by normoxia or even by hyperoxia (344), (345). Elevated VEGF levels have been found in wounds treated by hyperbaric oxygen treatment (346). The important role of O_2 for wound healing and angiogenesis on a molecular level has been elucidated recently (336). Sen et al. showed, that Reactive Oxygen Species (ROS) like H_2O_2 and superoxide, which require oxygen in the presence of NADPH oxidases, are present in vivo in wounds and facilitate wound healing and angiogenesis (347). H_2O_2 hereby potently induced VEGF expression in human keratinocytes (348). Angiogenesis in this case is accomplished via a hypoxia-inducible factor (HIF) independent activation of VEGF. Using subcutaneously implanted viscose-cellulose sponges in rats, Niinikoski showed as early as 1969, that collagen production and angiogenesis was decreased in parallel to the level of hypoxia in wounds (349). PO_2 in the sponges were found to be hypoxic between 8 - 15 mmHg between day 7 and 15 using direct fluid aspiration and tonometry. Since the Km for collagen production is 19 mmHg , he concluded, that the wound pO_2 of 7 to 15 mmHg appeared to be suboptimal for collagen production at a normoxic breathing environment for the rat (340). Lower oxygen levels impaired wound healing by ineffective neutrophil killing of bacteria, decreased collagen production, epithelialisation and angiogenesis (349). Taking the above mentioned results and conclusions into consideration, our own results are explainable as follows: the vessel density of about 80 vessels / mm^2 might constitute a baseline level of vascularisation, which is required to meet the metabolic demands of the tissue grown into the porous PU 10 days after implantation under normoxic as well as under hypoxic conditions. After an initial upregulation of angiogenic genes, which initiate angiogenesis, chronic systemic hypoxia acts in a counter productive way, for example by a lower level of ROS and consequently less VEGF expression. Therefore, after 10 days in a hypoxic environment, no change in vascularisation was seen even in the heparin coated group. Only after supplemental $VEGF_{165}$, the vessel density was increased. However, the additional $VEGF_{165}$ induced increase in vessel density occurred at a much lower level than under normoxic conditions. Clearly, this complex issue needs further investigations on a molecular level to fully understand the mechanisms involved in wound healing and thus create the basis for applied research into wound / biomaterial interactions.

6. Growth factor delivery via an osmotic mini-pump into a "Neovascularisation Construct"

6.1 Introduction

The third approach towards increasing angiogenesis within porous polyurethane focused on the controlled and sustained delivery of $VEGF_{165}$. Since various growth factors such as $VEGF_{165}$ and PDGF-BB only have short biological half life's between 30 and 70 minutes (154), clinical angiogenic efficiency even of repeated single injections is limited (152). Continuous $VEGF_{165}$ delivery in contrast, has been shown to have a superior angiogenic effect compared to repeated single injections (350). To study the effects of various growth factor levels over different time periods up to several months, a controlled and sustained delivery system is necessary. Such a system could be based on osmotic mini-pumps. "Alzet Osmotic Mini-Pumps" have been implanted in animals as a drug delivery device since 1995, initially to eliminate the need for frequent animal handling and repetitive injection schedules (351). A continuous drug delivery system into polyvinyl alcohol sponges has been successfully introduced in a wound healing model in 2001 (352). The usefulness of this controlled delivery device soon became clear and osmotic pumps have been used thereafter in a variety of cardiovascular and neurosurgical animal experiments. To study the effects of growth factors in a wound model, we developed a novel "Neovascularisation Construct". Hereby, $VEGF_{165}$ would be pumped for an extended period of time (in our experiments up to 10 days) into a tube made of porous polyurethane. After subcutaneous implantation in rats, granulation tissue was supposed to grow into the pores and angiogenesis could be increased by the constant delivery of $VEGF_{165}$. Furthermore, by terminating growth factor delivery at a specific time point, the impact of growth factor concentrations on vessel regression could be studied.

6.2 Materials and methods

6.2.1 Production of "Neovascularisation Constructs"

Polyurethane (PU) with well-defined open porosity (82 % porosity, 157 ± 1 µm pores) was produced in our laboratory by a variation on the phase inversion technique using pre-packed spherical microbeads as porogens, as described

previously (47) and as mentioned in chapter 4.2.1.1. Subsequently, PU tubes were formed with an inner diameter of 2.5 mm, length of 12 mm and a wall thickness of 0.5 mm. To allow tissue ingrowth into the porous PU, but to eliminate ingrowth into the lumen, PU tubes were lined with 350 µm of expanded poli-tetra-fluoroethylene (ePTFE) (Zeus, Orangeburg, SC, USA). An ePTFE plug (1.8 mm x 3 mm) (Zeus, Orangeburg, SC, USA) was attached to each end of the tube, one with a central hole of 1.2 mm diameter, where a 10 mm polyethylene catheter with an inner diameter of 0.9 mm was inserted (Scientific commodities Inc., Lake Havasu, AZ, USA). Finally, osmotic mini pumps of different sizes were attached, as described below. In total, 56 "Neovascularisation Constructs" were produced with the help of Dr. Deon Bezuidenhout and Mr. Johann Eygelaar, polymer scientists at the Cardiovascular Research Unit of the University of Cape Town (Figures 34 A and B).

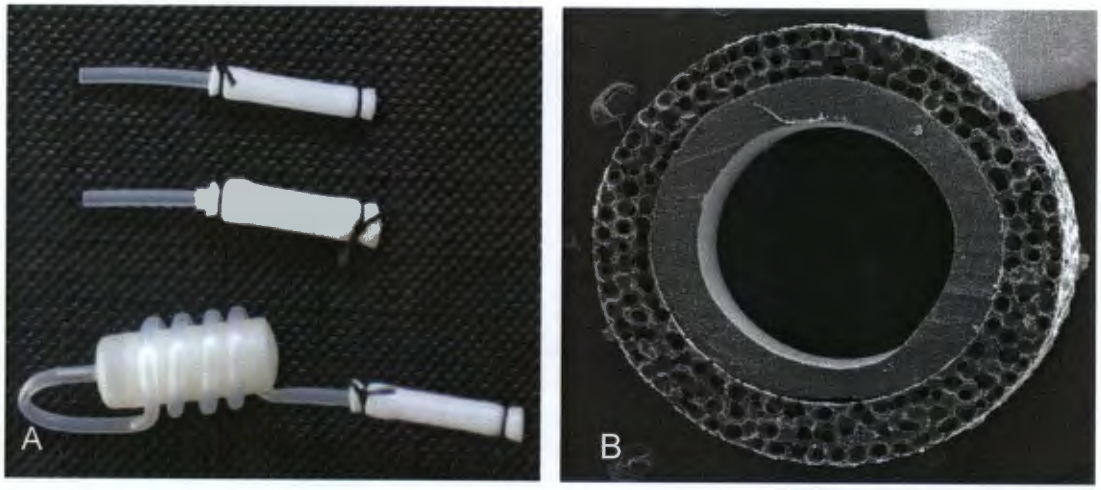

Figure 34: (A): Photograph of a "Neovascularisation-construct" consisting of polyethylene (PE) connection and polyurethane (PU) tissue ingrowth tube (top). Lined with ePTFE (middle) and whole construct including Alzet ® osmotic mini-pump (bottom). (B): Cross section of a "Neovascularisation Construct" shows ePTFE inner lining (350 µm) surrounded by 500 µm porous PU to allow tissue ingrowth from the outside after subcutaneous implantation. SEM picture at 25 x magnification.

6.2.2 Prolonged $VEGF_{165}$ delivery into PU by an osmotic mini-pump

$VEGF_{165}$ was produced in our laboratory using standard recombinant DNA technology resulting in a concentration of 250 µg /ml, as described in detail in chapter 5.2.2. Osmotic mini-pumps were purchased from Alzet® (Durect Corporation, Cupertino, CA, USA) In order to achieve a continuous delivery of $VEGF_{165}$, for at least 10 days, the model "1002", with a pump rate of 0.22 µl / h, a maximum pumping duration of 14 days and a filling volume of 108 µl was chosen.

Pumps were filled either with $VEGF_{165}$ (250 µg / ml) or an equal amount of PBS (Gibco, Paisley, UK) (n=7) using the sterile filling needle provided by the manufacturer. According to the manufacturer's protocol, pumps were incubated in Nanopure® water (Barnstead International Dubuque, Iowa, USA) at 37°C overnight. After sterilization in 70 % ethanol (Sigma, Steinheim, Germany) for 12 hours, the ePTFE-lined PU tubes were permeabilized subsequently by flushing with 10 ml of 97 % ethanol (Sigma, Steinheim, Germany) followed by 10 ml of PBS. PU tubes were filled with 20 µl of $VEGF_{165}$ or PBS, respectively, and attached to the pumps via a flexible 10 mm long polyethylene catheter (0.9 mm inner diameter) (Scientific commodities Inc., Lake Havasu, AZ, USA), which was pre-filled with 8 µl of $VEGF_{165}$ or PBS, respectively. Pump-tube constructs were kept in 37°C PBS until subcutaneous implantation on the same day. To verify PBS and $VEGF_{165}$ delivery at explantation, osmotic pumps were compressed manually to complete emptiness. The rest volumes were measured and mean pump rates were calculated.

6.2.3 Subcutaneous rat implantation model

Male wistar rats (234 g - 254 g body weight) were anaesthetized with a standard anesthetic mixture of 10 % ketamine hydrochloride (Anaket-V®, Centaur Labs, Bayer AG, Germany) plus 2 % xylazine (Rompun® Bayer AG, Germany), (ratio 9 to 5 v/v) i.m. (approx. 0.05 - 0.1 ml / 100 g BW). A longitudinal skin incision of one centimeter length was made on each side in the dorsal paramedian skin to create a subcutaneous pouch large enough for one "Vascularisation Construct" to be implanted on each side of each rat. Care was taken not to bend or kink the flexible polyethylene catheter between the osmotic pump and the polyurethane tube. The different groups of constructs were implanted using a rotational algorithm to ensure an equal distribution of groups at each implant position. Each rat received one construct delivering PBS and one construct delivering $VEGF_{165}$ to the polyurethane tube. Wounds were subsequently closed by placing two single stitches of prolene 4-0. For post surgical analgesia we injected buprenorphine (Temgesic®, Bayer AG, Germany) i.m. (approx. 0.1 ml / 70 g BW) in the back leg after the animal started to recover from anaesthesia. Constructs were implanted for 10 days. Rats were kept in standard cages and had access to a commercially fabricated pelletted diet and water ad libitum. At the end of the implantation periods, rats were killed with CO_2 gas and constructs were explanted. All animal experiments were approved by the "University of Cape Town's Animal Research Ethics Committees".

6.2.4 Histology

Pumps still attached to the polyethylene catheter were separated from the polyurethane tubes, which were cut in half and fixed in 4 % formalin for H&E and 10 % zinc fixative for CD31 staining, respectively, as described in detail in chapter 5.2.7 "Histology".

6.2.5 Image analysis

Images of H&E and CD31 stained cross sections were taken at 100 x magnification using a digital microscope (Nikon Cool Scope, Nikon, Japan). One complete cross section taken from the central part of the "Neovascularisation Construct" was analyzed. Therefore, between 45 and 60 single frames at 100 x magnification were taken in an automated fashion and the separate frames were stitched together without overlap by the use of "EclipseNet" software (Nikon, Japan). Tissue ingrowth was assessed on H&E cross sections and expressed as percentage tissue ingrowth of the porous space within the polyurethane. Furthermore, in constructs without ePTFE lining, the area of tissue growing into the lumen of the PU construct was assessed and expressed as percentage of the total luminal area. Vessels were counted semi-automatically using the Visiopharm® image analysis program (Visiopharm® Integrator System, Kopenhagen, Denmark). Vessels were defined as CD31 positive structures within the area of interest, that either show a transparent lumen or erythrocytes within. The area of interest was defined as the porous area within the polyurethane. Vascular density was reported as vessels / mm^2. Because neovascularisation created by $VEGF_{165}$ appeared to be irregular in shape on histological cross sections lacking typically rounded, clearly defined shapes, vascular area rather than vessel density was used to quantify neovascularisation from the second study onwards. Vascular area was defined as vessel area per tissue ingrowth area and was quantified as % IAV (ingrowth area vascularized). Furthermore, the mean vascular diameter was determined and reported in µm.

6.2.6 Statistical analysis

All data given on vessel density and vascular area is expressed as mean values ± standard error of mean. Differences between groups were compared by student's two-tailed t-test. A value of $p<0.05$ was considered significant.

6.3 Results

6.3.1 Osmotic mini-pumps deliver PBS and VEGF safely and effectively

"Neovascularisation Constructs" consisting of an osmotic mini-pump, the polyethylene catheter and the polyurethane tube lined on the inside with ePTFE as well as non ePTFE lined constructs, were implanted into subcutaneous pockets of wistar rats (n=6) (Figures 35 A and B). The surgical approach was relatively simple and all animals gained weight appropriately without signs of discomfort or behavioral abnormalities (321.5 ± 9.18 g after 10 days vs. 249.67 ± 6.46 g at implantation date, $p< 0.05$).

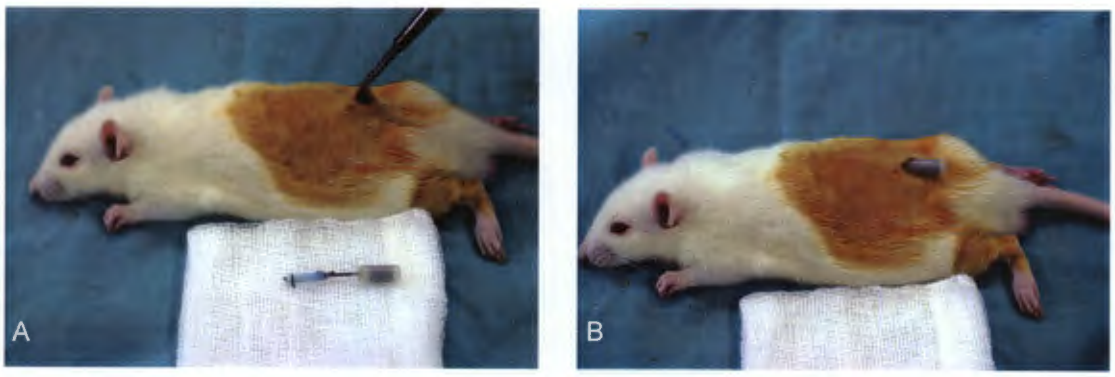

Figure 35: Demonstration of surgical implant technique: 5 mm skin incision at the back paramedian (A), followed by careful insertion of the "Neovascularisation construct" (here a straight model) into the subcutaneous pocket (B). For continuous $VEGF_{165}$ delivery, an Alzet® osmotic mini-pump (Durect Corporation, Copertino, CA, USA), model "1002", with a pump rate of 0.22 µl / h for a maximum pumping duration of 14 days and a filing volume of 108 µl was chosen.

At explantation, all constructs were found connected and macroscopically functional without signs of kinking in any parts. Tissue reaction in terms of vascularisation and capsule formation appeared to be localized within approximately 5 mm around the polyurethane tube. After 10 days of subcutaneous implantation, measured osmotic pump rest volume, as described in chapter 6.2.2, was 53.67 ± 2.08 µl in the PBS group, 51.67 ± 2.89 µl in the ePTFE lined PBS group, 57.67 ± 3.05 µl in the $VEGF_{165}$ group and 55 ± 4.58 µl in the ePTFE lined $VEGF_{165}$ group. Differences between groups were non significant. Mean calculated pumprates were 0.226 ± 0.01 µl / h for the PBS filled pumps, 0.235 ± 0.01 µl / h for the ePTFE lined PBS filled pumps, 0.21 ± 0.01 µl / h for the $VEGF_{165}$ filled pumps and 0.221 ± 0.02 µl / h for the ePTFE lined $VEGF_{165}$ filled pumps (Figure 36). Therefore, given a loading volume of 108 µl,

51.67 ± 3.78 µl $VEGF_{165}$ (250 µg / ml) was delivered on average in the VEGF groups, which equals to 12.92 ± 0.94 µg of $VEGF_{165}$.

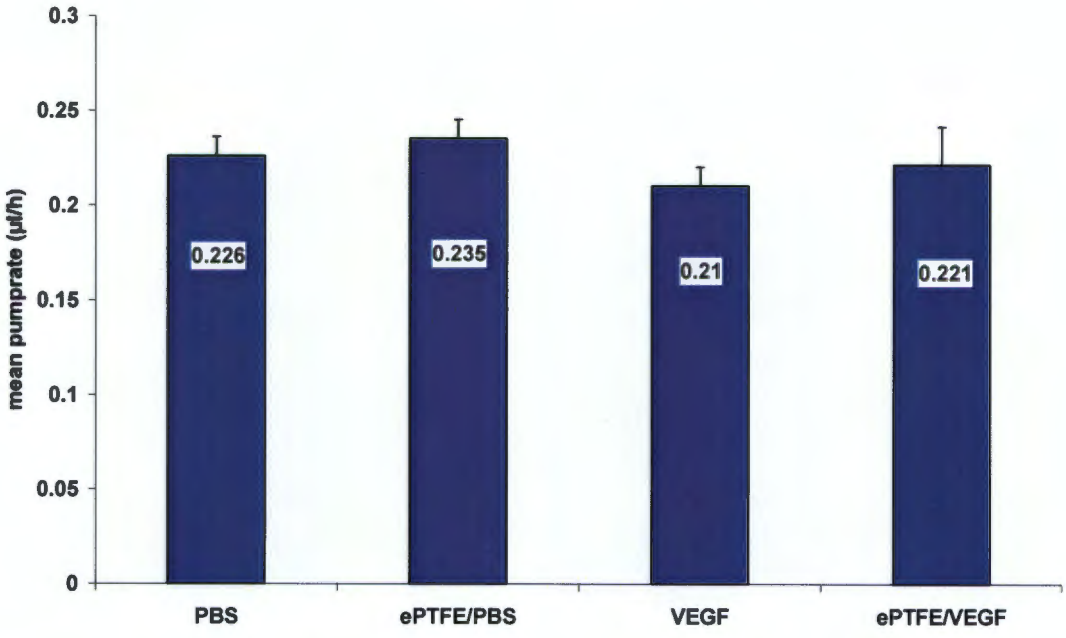

Figure 36: mean calculated pump rates in µl / h of osmotic pumps pumping PBS into non-lined PU constructs (PBS), PBS into ePTFE lined PU constructs (ePTFE / PBS), $VEGF_{165}$ into non-lined PU constructs ($VEGF_{165}$) and $VEGF_{165}$ into ePTFE lined PU constructs (ePTFE / VEGF) (all subgroups n=3). No significant difference in pump rates after 10 days subcutaneous implantation between subgroups.

These measurements were in excellent agreement with the manufacturers dates which specify a mean pumping rate of 0.22 ± 0.05 µl / h at 37°C (initial volume of 108 µl). Measurements of the residual pump volume together with the intact macroscopic appearance of the construct were regarded as sufficient evidence for the efficient delivery of PBS and $VEGF_{165}$, respectively, to the polyurethane tubes. Furthermore, no effect of the ePTFE lining on the rest volume and thus on the pumprate was observed.

6.3.2 EPTFE lining prevented tissue ingrowth into the lumen

Image analysis showed a 100 % tissue ingrowth into the pores of the PU construct after 10 days in all four different groups studied. Tissue ingrowth into the luminal space of PBS filled, non-lined "Neovascularisation Constructs" was 64.12 ± 13.81 % on average after 10 days of subcutaneous implantation and almost complete in some samples (Figure 37 A) Luminal lining with ePTFE prevented tissue ingrowth at

the inner surface of the PU effectively and only allowed minimal ingrowth into the lumen of PBS delivered constructs (1.7 ± 1.7 % tissue ingrowth) ($p<0.05$) (Figure 37 B and C). $VEGF_{165}$ filled, non lined constructs showed a tissue ingrowth of 60.66 ± 12.65 %, which was reduced to 1.8 ± 1.8 % for the $VEGF_{165}$ filled, ePTFE lined constructs ($p<0.05$) (Figure 38).

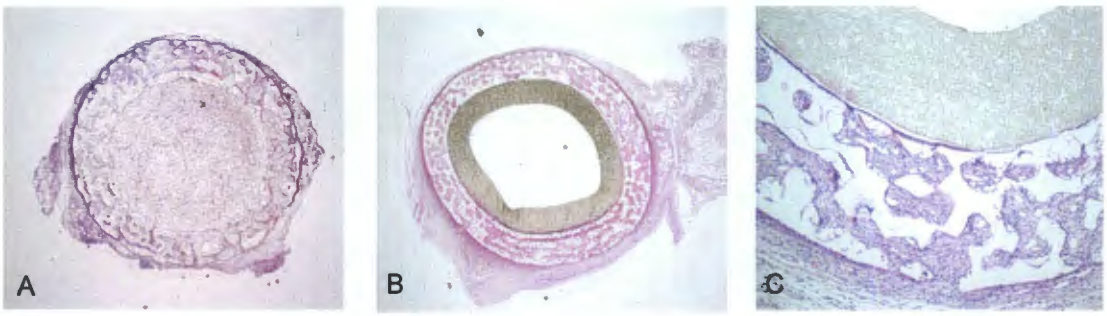

Figure 37: Histological analysis of tissue ingrowth into "Neovascularisation Constructs" after 10 days subcutaneous implantation (H&E staining of cross sections). Without ePTFE lining, there was substantial intraluminal tissue ingrowth (A, 25 x magnification). EPTFE lining prevented intraluminal tissue ingrowth effectively (B, 25 x magnification and C, 100 x magnification)

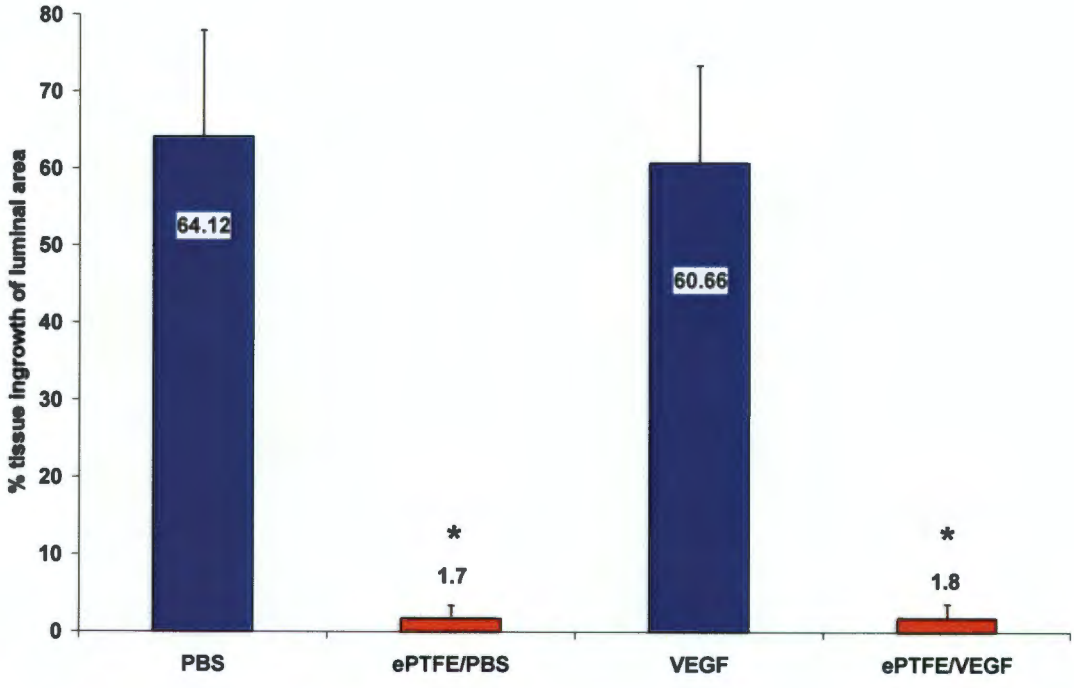

Figure 38: Effect of ePTFE lining on intraluminal tissue ingrowth: Non-lined PBS delivered constructs showed 64.12 ± 13.81 % tissue ingrowth, whereas $VEGF_{165}$ delivered non-lined constructs showed 60.66 ± 12.65 % tissue ingrowth (blue columns). In contrast, ePTFE lined constructs (red columns) showed a minimal 1.7 ± 1.7 % tissue ingrowth for PBS and 1.8 ± 1.8 % for $VEGF_{165}$ delivered constructs. * indicates significant reduction of intraluminal tissue ingrowth by ePTFE lining in each subgroup. ($p<0.05$).

Since prevention of intraluminal tissue ingrowth represented a prerequisite for further studies involving growth factor delivery for extended time periods, all "Neovascularisation Constructs" used after the initial study were lined with ePTFE.

6.3.3 $VEGF_{165}$ delivery increased vessel density and vascular area of "Neovascularisation Constructs"

Vessel density increased significantly after 10 days of continuous $VEGF_{165}$ (250 µg / ml, 1µg / day) by 75.19 % (146.9 ± 24.6 vessels / mm^2 for $VEGF_{165}$ pumped vs. 83.8 ± 8.3 vessels / mm^2 for PBS pumped constructs, $p<0.05$) (Figure 39 A). In parallel, vascular area increased significantly by 154.21 % (9.57 ± 1.7 % IAV for $VEGF_{165}$ pumped constructs vs. 3.76 ± 0.2 % IAV for PBS pumped constructs, $p<0.05$) by continuous delivery of $VEGF_{165}$ for 10 days (Figure 39 B).

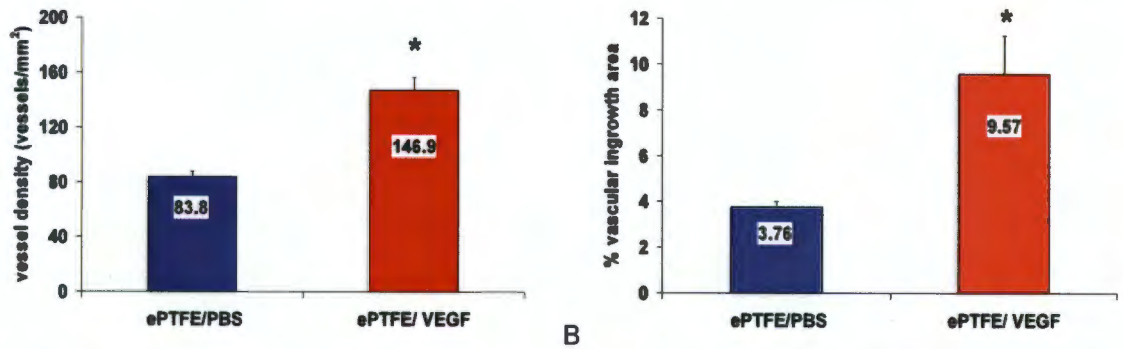

Figure 39: (A): Vessel density of PBS vs. $VEGF_{165}$ (250 µg / ml, 1 µg / day) delivered "Neovascularisation Constructs" after 10 days. * indicates significantly increased vessel density of $VEGF_{165}$ delivered constructs (red columns) compared to PBS (blue columns) delivered constructs (146.9 ± 24.6 vessels / mm^2 vs. 83.8 ± 8.3 vessels / mm^2, $p<0.05$) (n=4) (B): Vascular area of PBS vs. $VEGF_{165}$ (250 µg / ml, 1 µg / day) delivered "Neovascularisation Constructs". * indicates significantly increased vascular area of $VEGF_{165}$ delivered construct compared to PBS delivered construct (9.57 ± 1.7 % IAV (ingrowth area vascularized) for $VEGF_{165}$ delivered constructs vs. 3.76 ± 0.2 % IAV for PBS delivered constructs, $p<0.05$) (n=4).

For graphical illustration, Figure 40 shows representative CD31 stained sections of PBS delivered PU (40 A) including graphical image analysis (40 B) as well as $VEGF_{165}$ delivered PU (40 C) including graphical image analysis (40 D). Overall, the "Neovascularisation Constructs" including internal lining of ePTFE appeared to be a suitable method to study the effect of $VEGF_{165}$ on porous biomaterials such as polyurethane.

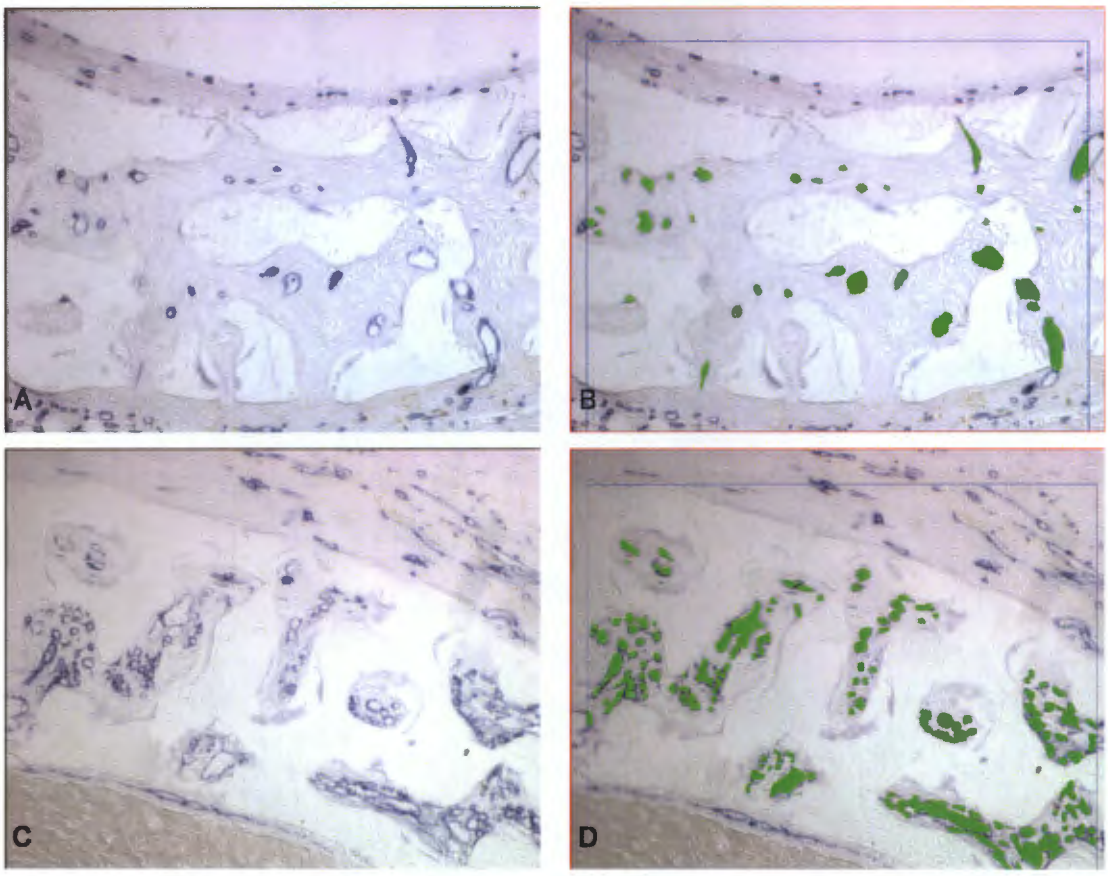

Figure 40: Representative light microscopical images (100 x magnification) of PBS and $VEGF_{165}$ (250 µg / ml) delivered cross sections of the "Neovascularisation Construct". All samples were stained with CD31 endothelial marker (blue color). (A) section after 10 day delivery of PBS showed moderate vascularisation, which was quantified semi-automatically for vessel density and vascular area, which is shown in green color in (B). Increased vascularisation after 10 day delivery of $VEGF_{165}$ (250 µg / ml) (C), which was quantified in (D) (green color indicates identified vessels within the area of interest).

6.3.4 $VEGF_{165}$ dosage study

Since the model for the prolonged, continuous delivery of $VEGF_{165}$ into porous polyurethane was established and increased neovascularisation in comparison to PBS control treatment was proven, the effect of different $VEGF_{165}$ dosages was evaluated. $VEGF_{165}$ was delivered by Alzet® osmotic mini pumps (model 1002, 0.22 µl / h pump rate, 14 days, 108 µl volume) in three different concentrations into "Neovascularisation Constructs", implanted subcutaneously for 10 days: $VEGF_{165}$ 2.5 µg / ml (250 µg / ml diluted 1:100 in PBS), which equals to 10 ng $VEGF_{165}$ per day, $VEGF_{165}$ 25 µg / ml (250 µg / ml diluted 1:10 in PBS), which equals to 100 ng $VEGF_{165}$ per day and $VEGF_{165}$ 250 µg / ml, which equals to 1 µg $VEGF_{165}$ per day (n=4). PBS, which was also pumped for 10 days, served as control (n=4).

Results indicated that 10 days of continuous PBS delivery induced a vascular area of 2.4 ± 0.13 % IAV within the porous polyurethane of the "Neovascularisation Construct". $VEGF_{165}$ 10 ng / day showed no increase of vascular area (2.11 ± 0.56 % IAV). $VEGF_{165}$ 100 ng / day and $VEGF_{165}$ 1 µg per day, in contrast, increased vascular area by 144.9 % (5.88 ± 0.73 % IAV) and 265.1 % (8.76 ± 1.37 % IAV) compared to PBS, respectively ($p<0.05$ in both cases) (Figure 41). No significant difference was seen between medium and high $VEGF_{165}$ dose ($p=0.11$).

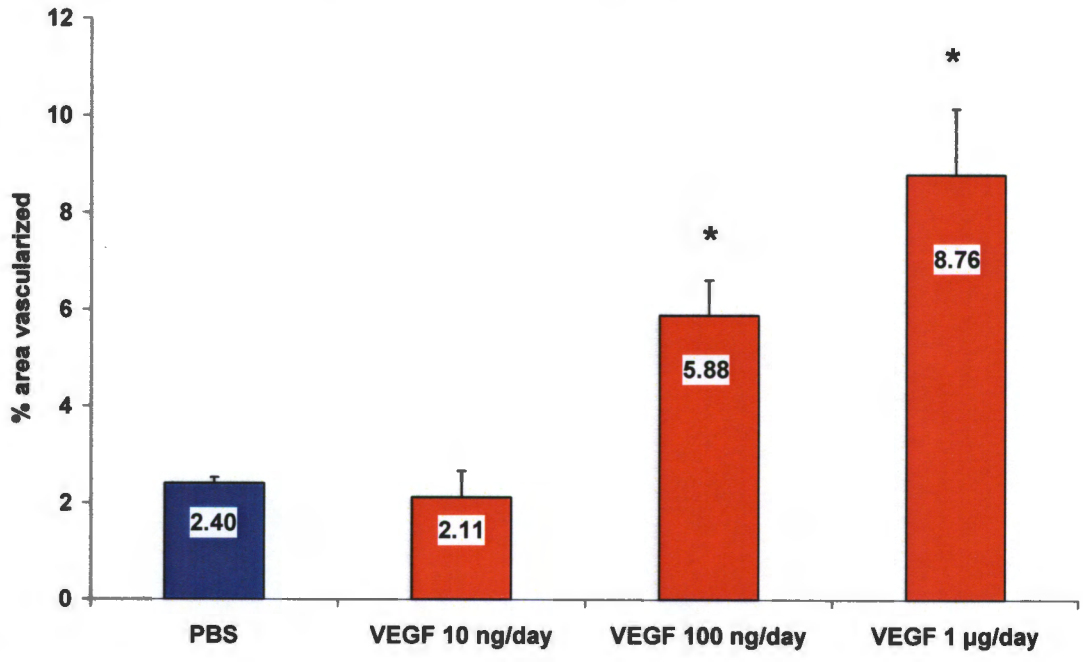

Figure 41: Ingrowth area vascularized (IAV) of newly formed vascular network within the porous polyurethane of the "Neovascularisation Construct" induced by 10 day continuous delivery of PBS, $VEGF_{165}$ 10 ng / day, 100 ng / day or 1 µg / day (n=4). $VEGF_{165}$ 10 ng / day showed no increase of vascular area (2.11 ± 0.56 % IAV) compared to PBS (2.4 ± 0.13 % IAV). $VEGF_{165}$ 100 ng / day and $VEGF_{165}$ 1 µg per day, however, increased vascular area by 144.9% (5.88 ± 0.73 % IAV) and 265.1 % (8.76 ± 1.37 % IAV) compared to PBS, respectively. * indicates significant difference to PBS ($p<0.05$ in both cases).

6.4 Discussion

Continuous delivery of $VEGF_{165}$ for 10 days resulted reproducibly in 2 - 3 fold dose-dependent increase of neovascularisation into the porous PU construct. Growth factor delivery was efficient and well in accordance with literature. Croll et al. delivered $VEGF_{164}$ directly to the cortex of adult rats at different dosages (30 ng / day up to 240 ng / day) for 7 days using osmotic mini pumps (353). She found no effect on vascular density delivering 30 ng / day and a minimal effect of 60 ng / day. Using 120 ng / ml and 240 ng / day however, Croll et al. noticed increased vessel

density (141.1 %), tortuosity and diameters (140.8 %) compared to PBS infused brains (353). Similarly, in our studies, there was no difference between $VEGF_{165}$ 10 ng / day and PBS, but $VEGF_{165}$ 100 ng / day increased vascular area by 144.9 % and 1000 ng / day even by 265.1 % in a subcutaneous model. Therefore, a dose dependency could be shown, as described by other groups (354), (353). Continuous delivery of $VEGF_{165}$ by the use of osmotic mini pumps has been reported for a wound model recently: Ward et al. found a two to three fold increased neovascularisation (vessel density) using a rat subcutaneous wound model delivering 450 ng / day $VEGF_{165}$ via an osmotic pump 1 mm around a biosensor (355). The effect of $VEGF_{165}$ delivery was localized and restricted to 13 mm around the sensor, where vessel density was still 50 - 100 % higher compared to PBS control. No significant angiogenesis was measured 25 mm from the delivery site of $VEGF_{165}$. Furthermore, repeated serum measurements of $VEGF_{165}$ up to 6 weeks revealed no elevated $VEGF_{165}$ levels in the systemic circulation (355). In the aforementioned continuous $VEGF_{165}$ delivery study to brain parenchyma, neovascularisation and $VEGF_{165}$ delivery (240 ng / day), as assessed by immunostaining, was restricted to 1.5 mm around the canula tip (353). In our own experiments, $VEGF_{165}$ was not delivered directly into subcutaneous granulation tissue, but rather into the "Neovascularisation Constructs". Therefore local neovascularisation appeared to be very localized within the 0.5 mm thick porous PU and a surrounding granulation tissue layer of 2 - 3 mm. Macroscopically, there was no sign of a distant or systemic angiogenic response. Therefore, continuous delivery of $VEGF_{165}$ into the porous PU "Neovascularisation Construct" appeared to be a reliable and safe model to induce neovascularisation within a biomaterial. Future experiments are indicated to study long term growth factor delivery as well as mechanisms involved in vessel regression. Furthermore, since we were able to induce such a rigorous angiogenic response into polyurethane, it appeared necessary to investigate structure and function of the newly formed micro- vascular network.

7. Quantification of functional neovascularisation in a porous scaffold by micro-CT, lectin perfusion, CD31 and corrosion casting

7.1 Introduction

Tissue engineering as a therapeutical approach to regenerate lost or diseased tissues and organs via delivery of cells, constructs and biomolecules to the appropriate site requires a functional vascular network for adequate integration (26). Therefore, research using tissue engineering strategies has recently focused more and more on mechanisms involved in angiogenesis into biomaterials. It is generally accepted today that vascularisation of cell engrafted matrices and scaffolds is of utmost importance for the survival and proper function of tissue engineered constructs (356), (357), (358). In order to evaluate and quantify neovascularisation in biomaterials, a variety of different techniques has been used up to now. Standard histology including immunohistochemical staining for endothelial markers such as CD31, CD34 and von Willebrand factor is commonly employed to quantify vessels. Due to the high resolution of modern microscopes of less than 1 µm, vascular parameters such as micro vascular density and area are readily obtainable on cross-sections using appropriate image analysis programs. However, conventional histology as a two dimensional cross section technique is suboptimal in providing informations about a three dimensional vascular network with its loops and branches. Serial sections are very laborious and even computed confocal microscopy allows only for a limited three dimensional quantification of 100 µm. Furthermore, non-translucent biomaterials such as bone, ceramics and many synthetic polymers reduce the optical penetration of light for the study of micro vascular networks into these materials to a great extent. Additionally and importantly, vessel morphology including measurements of vessel density and vessel area on endothelial cell immuno-stained sections provide insufficient information about vessel perfusion. Luminal erythrocytes are generally not accepted as a reliable marker for perfusion (359). Historically, there have been several different techniques to evaluate and quantify three dimensional vascular networks as well as to determine vascular perfusion. As a three dimensional morphological method, vascular corrosion casts have been used as early as 1842 by Bowman to study the architecture of vascular networks in the kidney (360). In order to quantify

vessel dimensions, branching features and inter-vascular distances by light or scanning electron microscopy, the surrounding tissue needs to be cleared or corroded in total from the casting material, which is usually methyl-methacrylate, silicon rubber or gelatin (361). As a functional, physiological analysis, Lectin perfusion has been introduced recently to study perfused micro vascular networks (362). Thereby, plant lectins bind to endothelium of perfused vessels after injection into the circulatory system. Species specificity has been demonstrated for different lectins, Bandeirea simplicifolia agglutinin-I (BS-I), for example, stains vascular endothelium in all species but human, while Ulex europeus agglutinin-I (UEA-I) stains only human endothelium (362). As a quantitative perfusion method, Color Doppler imaging is a real time assessment of vascular flow. It has been used for example in a mouse hindlimb ischemia model to quantify vascular perfusion (363), (364). Due to its low penetration depth however, this technique is only suitable for relatively superficial blood flow and is unable to penetrate into hydrophobic scaffold materials (365). Additionally, with an optical resolution of about 200 µm it does not reflect the anatomical situation of capillaries and small vascular networks precisely enough (365). Magnetic resonance angiography (MRA) and positron emission tomography (PET) are methods used in clinical medicine and research to evaluate blood flow and blood volume, but again, the resolution of 200 µm and 1.5 mm respectively, are not suitable for micro vascular imaging up to now (366), (367).

Micro-computed tomography (micro-CT) in contrast is a recently developed technique to study vascular networks in great detail in a three dimensional fashion. Originally described by Feldkamp et al. to investigate the microstructure of bone (368), it soon appeared that by perfusing the circulation with contrast agents such as barium sulfate or lead chromate containing silicone rubber, even small vascular structures almost down to the capillary level can be quantified with sufficient resolution. Subsequently, in addition to bone tissue, micro-CT has been used to study the microvasculature of rat kidney (369), heart (370), (371), coronary arteries (372), lung (373) and vasa vasorum of coronary arteries (374). Furthermore the vascular network of liver (375), tumors (376), and collateral vessel development after ischemic injury in a mouse model has been reconstructed (377). A review on microvasculature in small rodents using a synchrotron source for micro-CT, which allows a resolution of a few microns, was published by Ritman et al. in 2002 (378). Only very recently however, was micro-CT used to characterize scaffold materials. Guldberg et al. characterized porous poly(L-lactide-co-DL-lactide) (PLDL) scaffold micro-architecture and related it to compressive mechanical properties (379). Further research quantified mineralisation into PLDL scaffolds in vitro using micro-

CT (380). In vivo bone regeneration was demonstrated with calcium phosphate as biomaterial via micro-CT and compared to scanning electron microscopy (381). Ho and Hutmacher reviewed the current role of micro-CT in the characterization of scaffold materials in 2006 (382). To our knowledge however, this new technique of three dimensional visualization combined with the ability to exactly quantify vascular structures has not been used to study microvascular networks grown into biomaterials. Since we have recently developed an in vivo "Neovascularisation Construct", as described earlier in chapter 6, we were interested to quantify the three dimensional neovascularisation of porous polyurethane by means of micro-CT. The studies should assess the possibilities as well as its limitations of this new image modality. Data obtained by micro-CT was compared to conventional morphological CD 31 immunhistochemistry, to scanning electron microscopic data on vascular corrosion casts as well as to functional data of vessel perfusion using biotinylated lycopersicon esculentum lectin (362), (383).

7.2 Materials and methods

Production of "Neovascularisation Constructs", the prolonged $VEGF_{165}$ delivery via osmotic mini pumps as well as the subcutaneous rat implantation model has been described in chapters 6.2.1, 6.2.2 and 6.2.3.

7.2.1 Lectin perfusion and CD31

For initial proof of concept, the circulatory system of rats was perfused with fluorescein isothiocyanate (FITC) labeled lycopersicon esculentum lectin (Vector Laboratories, Inc. Burlinghame, USA). For quantification of the functional neovascularisation into subcutaneously implanted porous polyurethane tubes, we subsequently used biotinylated lycopersicon esculentum lectin (Vector Laboratories, Inc. Burlinghame, USA). Therefore, rats were perfused using a slight variation of a standard protocol, as described previously by Thurston et al. (384). Briefly, 10 days after implantation, 500 µg of lycopersicon esculentum lectin was injected in 500 µl of 0.9 % NaCl into the left femoral vein of anaesthetized rats (n=4). After the skin was incised over the left groin to visualize the left femoral vein, lectin was injected slowly using a 1 ml 29 Gauge single-use syringe with an integrated needle (Omnican 100, Braun, Melsungen, Germany) and a stereo-microscope at a magnification of 16 to 25 times (Leica MS 5, lightsource intralux 5000-1, vopi, Switzerland). After 3 minutes, the chest was opened via a midline sternotomy and the aortic lumen was entered via the left ventricular chamber using an 18 Gauge intravenous canula (Abbocath-T 18 G x 51mm, Abbocath Ireland LTD). The right atrium was incised to allow for the exsanguination of the animal while the circulatory system was perfused with 100 ml 1 % paraformaldehyde in PBS at 37°C at 120 mmHg. The "Neovascularisation Constructs" at the back of each animal were explanted as well as the left kidney as a control for perfusion. Pumps still attached to the polyethylene catheter were separated from the polyurethane tubes, which were cut in half and fixed in 1 % paraformaldehyde / PBS for the detection of biotinylated lectin (n=4) and 10 % zinc fixative for CD31 staining (n=4) at room temperature for 24 hours. All samples were further processed and stained with anti-CD31 antibody using a standard protocol (313), as described in chapter 5.2.7 "Histology". For the detection of biotinylated lectin, 1 % paraformaldehyde / PBS fixed, dewaxed sections were equilibrated in tris buffered saline (TBS) for 10 minutes. Streptavidin / alkaline phosphatase (K0610-11 DAKO, A/S, Glostrup, Denmark) was applied for 10

minutes at room temperature, rinsed in TBS and detected by applying BCIP/NBT for 8 minutes incubation. Samples were washed in water, dehydrated in increasing concentrations of alcohol and mounted in Entellan (Merck, Darmstadt, Germany).

7.2.2 Micro-CT perfusion technique

In order to visualize the neovascularisation into the polyurethane tube by micro-CT, the vascular system of rats was perfused with a radiopaque contrast medium (n=4). To this end, animals were injected with 700 I.U. heparin / kg body weight i.p. 30 minutes before perfusion. Immediately after the rats have been killed with CO_2 gas, an abdominal midline incision was made and the descending aorta was exposed. A polyethylene catheter (PE 100 Intramedic Clay Adams, Becton Dickinson, USA, 0.86 mm I.D.) was inserted into the descending aorta, which has been tied off distally. After severing the inferior vena cava next to the aorta, the circulatory system was flushed with 60 ml of 0.9 % NaCl at 37°C containing 10 units of heparin per ml of NaCl at a pressure of 120 mmHg. During this time 10 ml of lead chromate containing radiopaque silicone rubber (Microfil® MV-122, Flow Tech; Carver, MA, USA) was prepared and infused immediately afterwards at a pressure of 120 mmHg into the abdominal aorta "retrograde" following the NaCl perfusion. Once the silicone rubber started to gel, the infusion was stopped and allowed to further solidify for 1 hour until subcutaneous "Neovascularisation Constructs" were explanted. Implants were stored at 4°C in 10 % neutral buffered formalin until they were scanned.

7.2.3 Micro-CT imaging

Neovascularisation in the $VEGF_{165}$ or PBS perfused polyurethane tubes was imaged using a commercially available, high resolution (6 µm nominal resolution) desktop micro-CT scanner (µ-CT 40, Scanco Medical AG, Bassersdorf, Switzerland). The scanning time for 1000 sections of each sample was 288 minutes at 55 kV and 114 µA. To be able to analyze the fine vascular network including arterioles, capillaries and venules, we used the highest resolution of 6 µm, which created images of 2048 x 2048 pixels. A threshold of 220, which is the equivalent of 22 % of the maximal grey scale value, was chosen to visualize the vessels in the specified area of interest. The area of interest was defined as the layer of polyurethane within the "Neovascularisation Construct" without the adjacent ePTFE on the inside and without incoming and outgoing vessels on the outside of the construct. In order to

study the three dimensional vascular architecture, Feldkamp's cone-beam reconstruction algorithm was used (385). To quantify three dimensional histo-morphometric values such as vessel thickness, distribution of vessel thickness, vascular volume and connectivity , a method previously employed for the analysis of trabecular bone (386), was used (387). Recently, this method was also applied for the study of collateral vessel development (377). Vessel thickness and distribution of vessel thickness was calculated using a method independent of the model for assessing thickness in three dimensional images (387). Vascular volume was calculated by computing voxel size and voxel number in 3D images after application of the threshold. Connectivity was defined according to Odgaard and Gunderson as the number of interconnections within a network that can be devided before two separate networks are created (388).

The semi automated software, which is provided with the micro-CT 40, is capable of generating histograms of the distribution of vessel sizes. Color coding highlights the micovasculature within the area of interest and subdivides different vessel diameters. Micro CT scanning as well as image analysis and calculations was provided by Mr. Marcus Burkhardt (Scanco Medical AG, Bassersdorf, Switzerland).

7.2.4 Histology of Microfil® perfused samples

After micro-CT scanning, formalin fixed Microfil® perfused samples (n=4) were evaluated microscopically. After alcohol dehydration, samples were embedded in wax and 10 µm thick sections were cut and mounted unstained on un-coated slides. Microfil® perfused microvessels were quantified using a digital automated microscope (Nikon Cool Scope, Nikon, Japan), as described in 7.2.7.

7.2.5 Corrosion casting perfusion technique

"Neovascularisation Constructs" were implanted in rats for 10 days subcutaneously, as described in 6.2.3. Standard methods were used for vascular corrosion casting (361). Shortly, heparinised rats (700 I.U. heparin / kg BW i.p.) were anaesthetized with a standard anaesthetic mixture of ketamine hydrochloride 10 % (Anaket-V®, Centaur Labs, Bayer AG, Germany) plus 2 % xylazine (Rompun® Bayer AG, Germany), (ratio 9 to 5 v / v) i.m. (approx. 0.05 - 0.1 ml / 100 g BW). The chest was opened via a midline sternotomy and the aortic lumen was entered via the left ventricular chamber using an 18G i.v. canula (Abbocath-T 18G x 51 mm, Abbocath

Ireland LTD). The rats circulatory system was subsequently perfused with 100 ml phosphate buffered saline (PBS) at 37°C at 120 mmHg after an incision in the right atrium was made to allow for exsanguination of the animal. Immediately afterwards, 15 ml of a mixture of 10 / 0.3 v / v Mercox Red /Catalyst (Ladd Research, Williston, Vermont, USA) was infused at the same rate. After complete resin curing (1-2 days at room temperature), the "Neovascularisation Constructs" at the back of each animal were explanted and soft tissue was macerated in 10 % KOH (Sigma Aldrich, Steinheim, Germany) for 2 - 4 hours. Subsequently, casts inside and around the porous polyurethane were rinsed with hot water, dissected and air dried overnight.

7.2.6 Scanning electron microscopic analysis of corrosion casts

Dry samples consisting of the casting material and the PU tubes lined with ePTFE were cut in half, mounted on metal stubs using double-sided gluing tape and colloidal silver to achieve conductivity. Samples were further sputter coated with gold (Polaron Range SC 7640 Sputter Coater) at 1.5 kV for 3 minutes and examined using a Scanning Electron Microscope (Jeol SEM, JSM 5200, Japan) at 15, 35, 50, 100, 150, 200, 350, 500, 750 and 1000 times magnification. Images were captured by the use of "Orion 5 for Windows" control systems high resolution image software (Jeol, Japan). After images have been taken of the outside of the construct, 5 mm cross sections were cut, mounted, sputter coated and scanned again. Image analysis of vascular area inside the polyurethane pores was carried out using "Leica Q Win for Windows" (Leica, Wetzlar, Germany), whereby the whole area of a 5 mm cross section (12 frames at 150 x magnification) was analyzed. Total vascular area of a cross section was reported as μm^2.

7.2.7 Image analysis

For initial experiments to evaluate lectin perfusion of tracheal capillary networks of rats, fluorescein isothiocyanate (FITC) labeled lycopersicon esculentum lectin was detected by UV light using a Fluorescent Microscope (Nikon Eclipse 90i, Nikon, Japan) equipped with a fluorescent illumination system (Nikon X-Cite® 120, Nikon, Japan) attached to a digital camera (Nikon DXM 1200 C, Nikon, Japan). Images of biotinylated lycopersicon esculentum lectin, CD31 stained cross sections as well as unstained Microfil® perfused sections were taken at a 100 x magnification using a digital automated microscope (Nikon Cool Scope, Nikon, Japan). One complete

cross section taken from the central part of the "Neovascularisation Construct" was analyzed. Therefore, between 45 and 60 single frames were taken in an automated fashion and the separate frames were stitched together without overlap by the use of "EclipseNet" software (Nikon, Japan). Vessels were counted semi-automatically using the Visiopharm® image analysis program (Visiopharm® Integrator System, Kopenhagen, Denmark). Vessels were defined as lectin or CD31 positive structures within the area of interest, that either show a transparent lumen or erythrocytes within. The area of interest was defined as the porous area within the polyurethane. The outside of the construct was excluded from analysis, as was the luminal area of the construct and the ePTFE. Vascular density was reported as total vessels per cross section and vascular area was quantified as total vascular area in μm^2 per cross section. Furthermore, the mean vascular diameter was calculated from the measured circumference divided by Π and reported in µm, assuming roundness of vessels.

7.2.8 Statistical analysis

All data obtained on vessel sizes, distributions of vessel sizes, vascular areas, vascular volumes and connectivity is expressed as mean values ± standard error of mean. Differences between groups were compared by two-tailed student's t-test. A value of $p<0.05$ was considered significant.

7.3 Results

7.3.1 CD31 immunohistchemistry of $VEGF_{165}$ stimulated neovascularisation

Histo-morphometrical analysis of the "Neovascularisation Constructs" via endothelial staining with anti CD31 antibody confirmed the strong angiogenic effect of $VEGF_{165}$ on the construct, as described in 6.3.3. Prolonged delivery of 1 µg / day $VEGF_{165}$ (250 µg / ml) for 10 days showed an increase in vessel number, size and area in comparison to PBS treated controls (n=4). Mean vessel density increased significantly from 376.25 ± 108.48 vessels / cross section to 820.5 ± 92.34 vessels / cross section (increase of 118.07 %, $p<0.05$) (Table 2). Mean vascular area increased from $67.12 \times 10^3 \pm 14.37 \times 10^3$ μm^2 to $216.37 \times 10^3 \pm 37.28 \times 10^3$ μm^2 (increase of 222.36 %, $p<0.05$) (Table 3 and Figure 42 A) and mean vessel

diameter increased from 23.75 ± 1.39 µm to 30.49 ± 1.55 µm (increase of 28.38 %, $p<0.05$) (Table 4 and Figure 42 B).

	PBS	$VEGF_{165}$	p-value
CD31	376.25 ± 108.48	820.5 ± 92.34	$p<0.05$
Lectin	53.25 ± 3.64	389 ± 51.73	$p<0.05$
Corrosion cast	55.75 ± 10.51	230.5 ± 30.17	$p<0.05$
Micro-CT	0.93 ± 0.1	3.37 ± 0.58	$p<0.05$

Table 2: Analysis of vessel density of micro-vascular network created in "Neovascularisation Constructs" by PBS vs. $VEGF_{165}$ delivery for 10 days. Assessed by CD31, Lectin perfusion, SEM analysis of vascular corrosion casts and by Micro-CT scanning. Data is presented as total vessel number per cross section or vessels/ mm (Micro-CT). The p-value indicates the comparison of PBS vs. $VEGF_{165}$ within each analysis subgroup.

	PBS	$VEGF_{165}$	p-value
CD31	23.75 ± 1.39	30.49 ± 1.55	$p<0.05$
Lectin	28.12 ± 4.44	32.46 ± 8.9	p = n.s.
Corrosion cast	16.58 ± 0.75	31.73 ± 1.87	$p<0.05$
Micro-CT	44.5 ± 1.73	65.6 ± 4.03	$p<0.05$

Table 3: Analysis of vessel diameters (µm) of micro-vascular network created in "Neovascularisation Constructs" by PBS vs. $VEGF_{165}$ delivery for 10 days. Assessed by CD31, Lectin perfusion, SEM analysis of vascular corrosion casts and by Micro-CT scanning. The p-value indicates the comparison of PBS vs. $VEGF_{165}$ within each analysis subgroup.

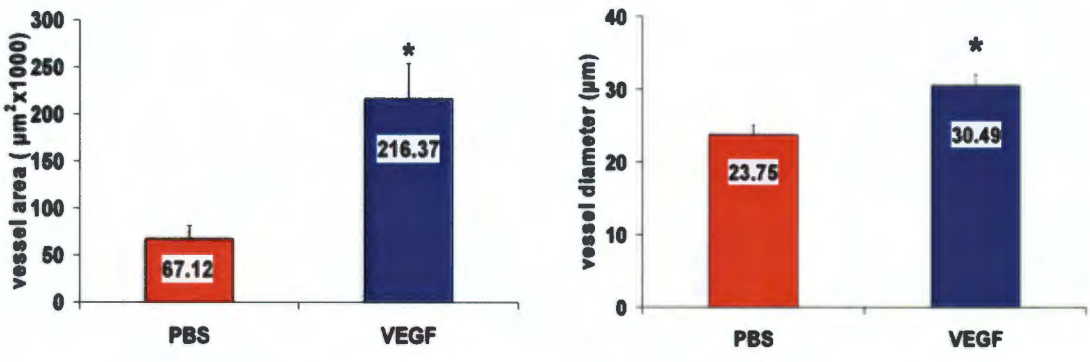

A B

Figure 42: CD31 immunohistochemical staining of micro vascular network created in "Neovascularisation Constructs" by PBS (red columns) vs. $VEGF_{165}$ delivery (blue columns) for 10 days. Histo-morphometric analysis of CD31 positive luminal structures for area (A) and diameter (B) (n=4). Data is presented as vessel area (μm^2) per cross section and as vessel diameter (µm). * indicates a 222.36 % increase in vascular area as well as a 28.38 % increase in vessel diameter by $VEGF_{165}$ delivery compared to PBS ($p<0.05$ in both cases).

	PBS	$VEGF_{165}$	p-value
CD31	67.12 ± 14.37	216.37 ± 37.28	p<0.05
Lectin	9.75 ± 1.83	196.09 ± 40.56	p<0.05
Corrosion cast	22.06 ± 7.1	229.7 ± 19.54	p<0.05
Micro-CT	0.16 ± 0.06 mm^3	2.77 ± 0.67 mm^3	p<0.05

Table 4: Analysis of vascular areas of micro-vascular network created in "Neovascularisation Constructs" by PBS vs. $VEGF_{165}$ delivery for 10 days. Assessed by CD31, lectin perfusion, SEM analysis of vascular corrosion casts and by micro-CT scanning. Data is presented as vessel area x 10^3 (μm^2) per cross section or as vascular volume in mm^3 (micro-CT). The p-value indicates the comparison of PBS vs. $VEGF_{165}$ within each analysis subgroup.

7.3.2 Lectin perfusion of $VEGF_{165}$ stimulated neovascularisation in PU

In initial experiments, FITC-labeled lycopersicon esculentum lectin was successfully tested as intravital marker of perfused capillaries as demonstrated on tracheal vascular network of rats (Figure 43 A). In the same animals, neovascularisation into porous PU constructs after 10 day delivery of $VEGF_{165}$ could be detected as well (Figure 43 B). To increase the detection sensitivity of perfused vascular networks, biotinylated lycopersicon esculentum lectin was used thereafter (Figure 43 C, D). Sustained $VEGF_{165}$ delivery increased neovascularisation compared to PBS control significantly. Mean vessel density of lectin positive stained vessels increased 7.3 fold from 53.25 ± 3.64 vessels / cross section (PBS) to 389 ± 51.73 vessels / cross section ($VEGF_{165}$, p<0.05) (Table 2). Vascular area increased in parallel from 9.75 x 10^3 ± 1.83 x 10^3 μm^2 to 196.09 x 10^3 ± 40.56 x 10^3 μm^2, (p<0.05) (Table 4 and Figure 44 A). Overall, this translates to a 20.1 fold increase in vascular perfusion in $VEGF_{165}$ treated samples compared to PBS. Mean vessel diameter increased insignificantly by 15.43 % (28.12 ± 4.44 µm to 32.46 ± 8.9 µm, p=n.s.) (Table 3 and Figure 44 B). If the vessel density of lectin perfused vessels is compared to the CD31 positive stained vessels, the following becomes apparent: only 14.15 % of CD31 positive stained vessels in the PBS group showed signs of lectin perfusion (53.25 ± 3.64 vessels / cross section compared to 376.25 ± 108.48 vessels / cross section) Continuous delivery of $VEGF_{165}$ for 10 days increased this "relative" vessel density to 47.41 % (389 ± 51.73 vessels / cross section vs. 820.5 ± 92.34 vessels / cross section). Therefore, $VEGF_{165}$ delivery not only increased absolute vessel density, but also seems to have increased perfusion above the expected level. Perfusion of kidneys as control for adequate systemic perfusion was positive in all samples and showed no difference between PBS and $VEGF_{165}$ (Figure 43 E, F).

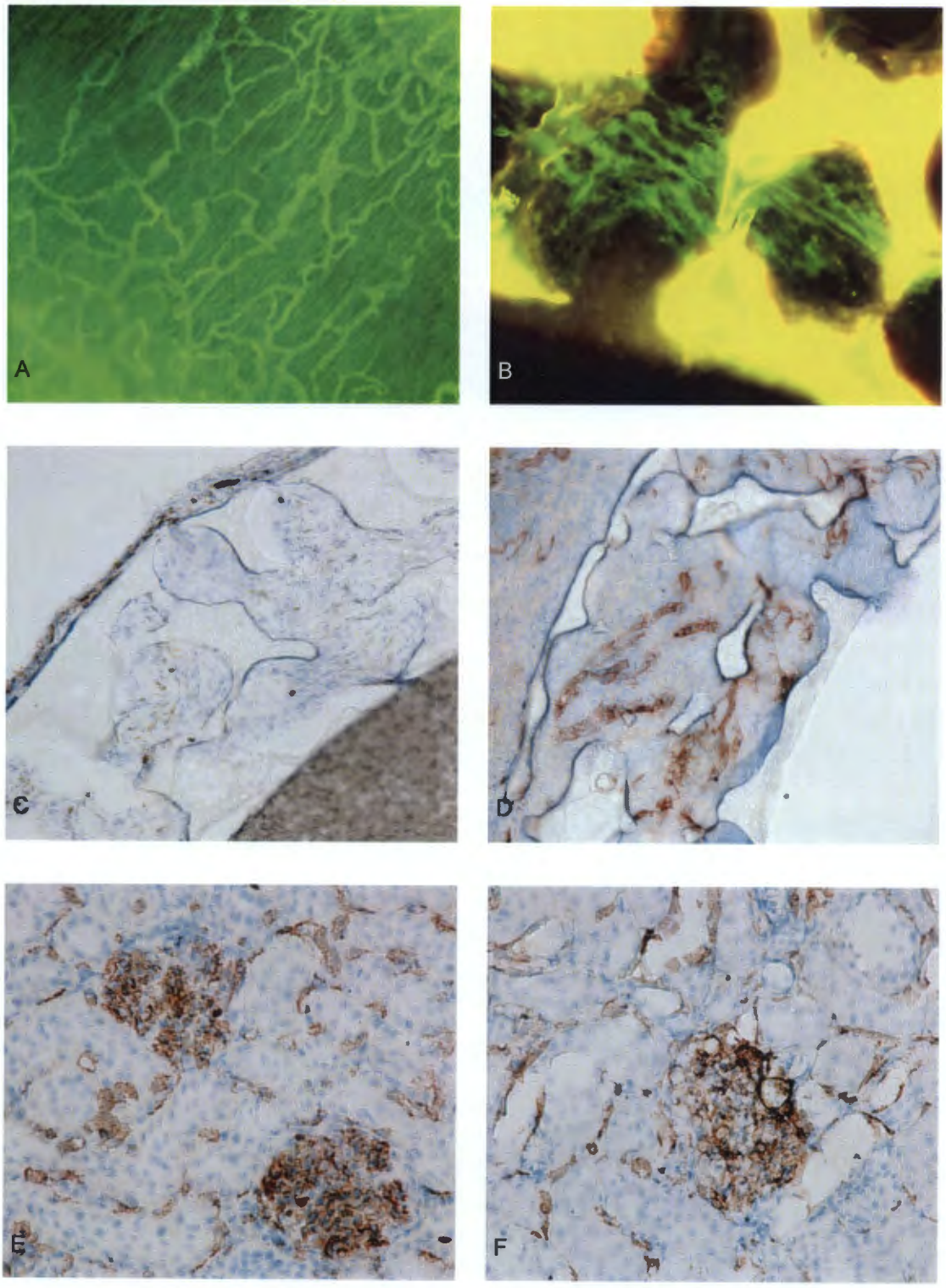

Figure 43: Perfusion of tracheal capillary network with FITC-labeled lycopersicon esculentum lectin (green color) as proof of adequate capillary perfusion (A, 15 x magnification) and neovascularisation of porous PU (B, 15 x magnification) after 10 days delivery of $VEGF_{165}$. Poor perfusion of PBS delivered PU constructs (C), but well perfused micro vascular network in $VEGF_{165}$ delivered constructs after perfusion with biotinylated lycopersicon esculentum lectin (brown color) (D, 10 x magnification). No difference between PBS (E) and $VEGF_{165}$ (F) group in kidney perfusion by biotinylated lycopersicon esculentum lectin perfusion (20 x magnification).

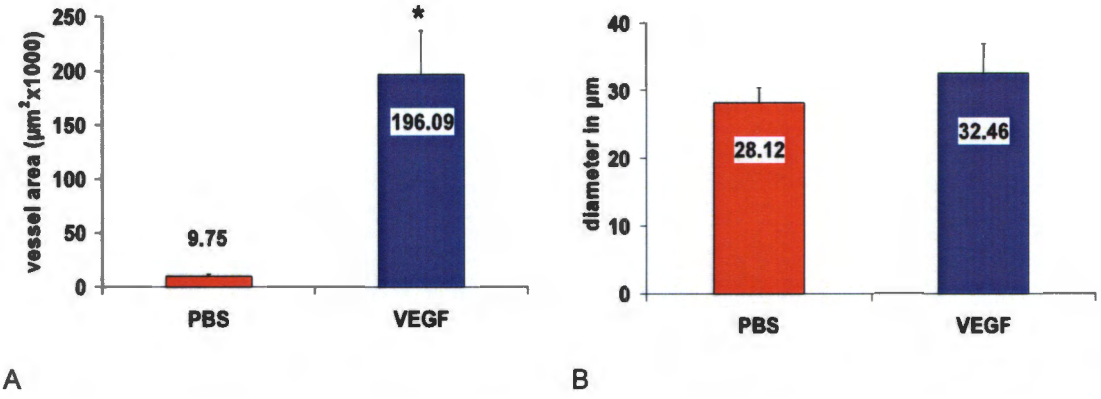

A B

Figure 44: Lycopersicon esculentum lectin perfusion of micro-vascular network created in "Neovascularisation Construct" by PBS (red columns) vs. $VEGF_{165}$ delivery (blue columns) for 10 days. Histomorphometric analysis of lectin positive luminal structures for vessel area (A) and diameter (B) (n=4). Data is presented as total vessel number and vessel area (μm^2) per cross section as well as vessel diameter (µm). * indicates a 20.1 fold increase in vascular area by $VEGF_{165}$ delivery compared to PBS ($p<0.05$). Vessel diameter was not significantly different.

7.3.3 Vascular corrosion casting of $VEGF_{165}$ stimulated neovascularisation in PU

To obtain a quasi three dimensional aspect of the vascular network created through continuous delivery of $VEGF_{165}$ in comparison to PBS, the whole animal was casted using methyl-methacrylate (7.2.5), the "Neovascularisation Constructs" were explanted and surrounding soft tissue was corroded. Remaining vascular casts were analyzed quantitatively by scanning electron microscopy (7.2.6) followed by image analysis, which confirmed the results obtained by lectin perfusion, and provided additional information about the spatial distribution of the microvascular network (Figure 45 A - D). SEM analysis of corrosion casts showed that continuous PBS delivery via osmotic mini pumps for 10 days created 55.75 ± 10.51 vessels / cross section. $VEGF_{165}$ for 10 days increased the vessel density 4.13 fold (230.5 ± 30.17 vessels / cross section), ($p<0.05$) (Table 2). Vascular area increased 10.42 fold ($22.06 \times 10^3 \pm 7.1 \times 10^3$ μm^2 vs. $229.7 \times 10^3 \pm 19.54 \times 10^3$ μm^2, $p<0.05$) (Table 3 and Figure 46 A) and vessel diameter increased 1.91 fold (16.58 ± 0.75 vs. 31.73 ± 1.87 µm, $p<0.05$) (Table 4 and Figure 46 B).

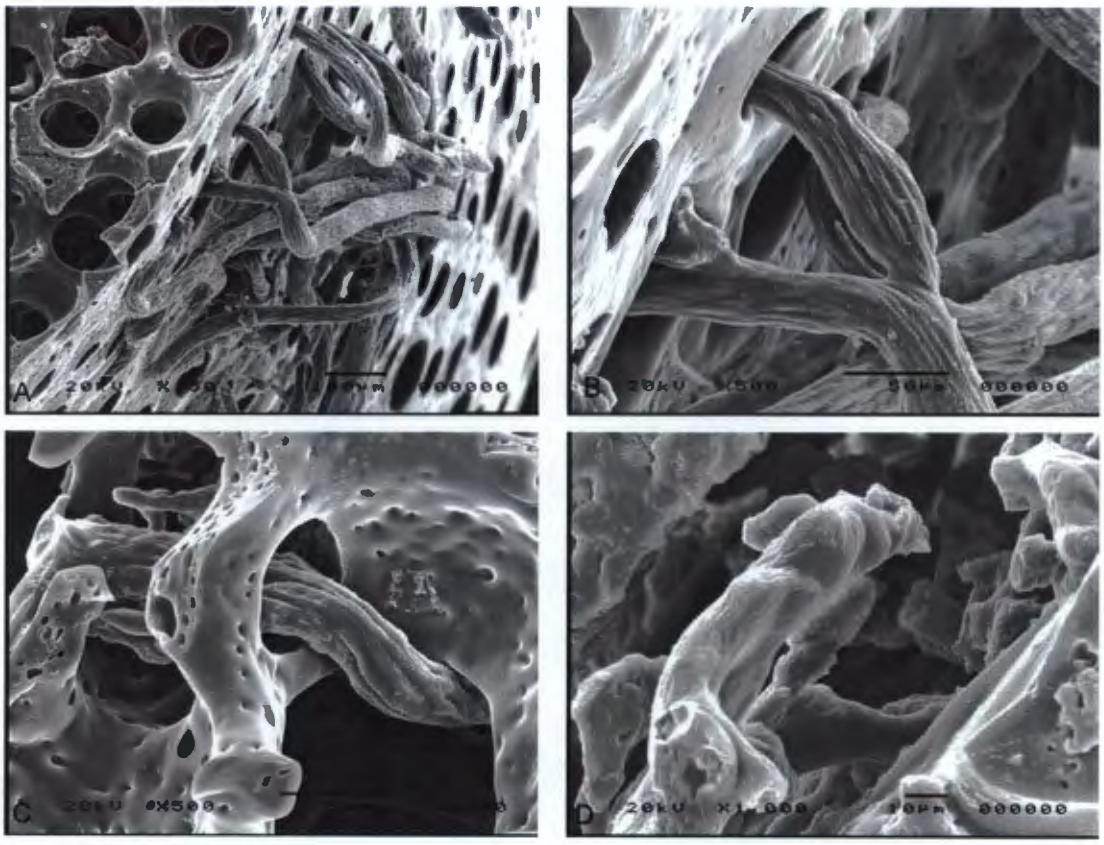

Figure 45: Scanning electron microscopical (SEM) images of neovascularisation of PU constructs after 10 days of continuous $VEGF_{165}$ delivery. Micro vascular network has been casted using methyl-methacylate and surrounding tissue has been corroded. (A) Vascular network was infiltrating the PU through the pores (150 x magnification). Higher magnification in B and C (500 x) reveals spatial relationship between neovascularisation and porous structure of PU. C indicates that vessels were growing through the entire PU graft wall (350 µm), until ePTFE lining prevented further ingrowth towards the lumen of the construct (D, 1000 x magnification).

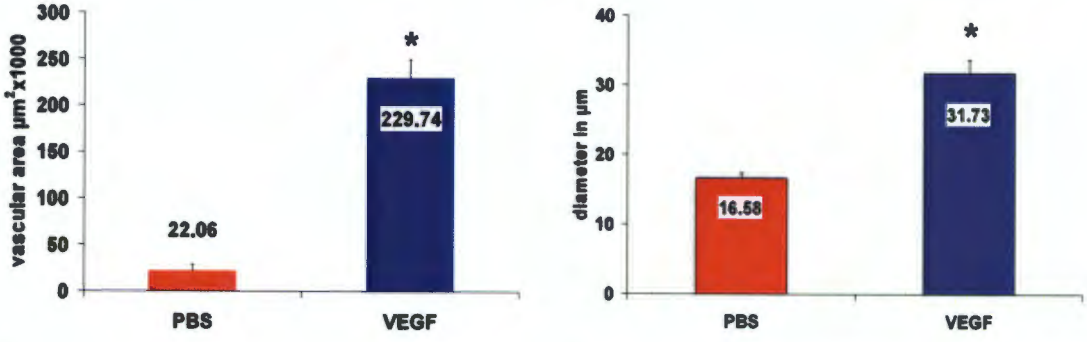

Figure 46: Scanning electron microscopical (SEM) analysis of microvascular corrosion casts of neovascularisation induced by continuous 10 day PBS (red columns) vs. $VEGF_{165}$ delivery (blue columns). Analysis of vascular area (μm^2) (A) and diameter (µm) (B) (n=4). * indicates a 10.42 fold increase in vascular area as well as a 1.91 fold increase of vessel diameter by $VEGF_{165}$ delivery compared to PBS ($p<0.05$).

7.3.4. Micro-CT analysis of neovascularisation

Threshold setting

In vitro experiments involving micro-CT scanning of the "Neovascularisation Construct" showed a threshold of 60 (6 % of maximal grey scale value) for PU and a threshold of 90 (9 % of maximal grey scale value) for ePTFE. For in vivo experiments the threshold was set to 220 (22 % of maximal grey scale value) for the measurements of vessels which were filled with lead chromate containing silicone rubber (Microfil® MV-122, Flow Tech; Carver, MA, USA). Therefore, vessel measurement did not overlap or interfere with false positive detection of PU.

Vascularisation parameters

Neo-vessels of the PU of the "Neovascularisation Construct" (planimetric poresize of 157 ± 1 µm) were detected by micro-CT scanning between sizes of 6 µm and 144 µm. Micro CT determined a vessel density of 0.93 ± 0.1 vessels / mm in PBS perfused constructs. $VEGF_{165}$ for 10 days increased vessel density 3.64 fold (3.37 ± 0.58 vessels / mm, $p<0.05$) (Table 2). Vascular volume increased 17.38 fold from 0.16 ± 0.06 mm^3 (PBS) to 2.77 ± 0.67 mm^3 ($VEGF_{165}$, $p<0.05$) (Table 4 and Figure 47 A). Average vessel diameter increased by 1.47 fold from 44.5 ± 1.73 µm (PBS) to 65.6 ± 4.03 µm ($VEGF_{165}$, $p<0.05$) (Table 3 and Figure 48 A). Due to the 3-dimensional quantification capabilities, µ-CT provided as well vessel-connectivity data: mean vessel connectivity increased significantly from 0.3 ± 0.074 / mm^3 (PBS) to 62.34 ± 18.75 / mm^3 ($VEGF_{165}$, $p<0.05$) (Figure 47 B). Apart from increases in vessel number, vascular volume, diameters and connectivity, image analysis indicated an even distribution of neovascularisation throughout the whole porous construct in the $VEGF_{165}$ treated group (Figure 49 B). The PBS treated constructs, however, were less vascularized and the distribution of neo-vessels appeared to be uneven, including areas without any vascularisation apparent (Figure 49 A). Furthermore, analysis of the distribution of vessel sizes revealed, that $VEGF_{165}$ treated constructs showed a high percentage of 40 µm to 80 µm sized vessels reflecting growth of arterioles and venules, vessels of superior importance for a high level of blood flow (Figure 48 B).

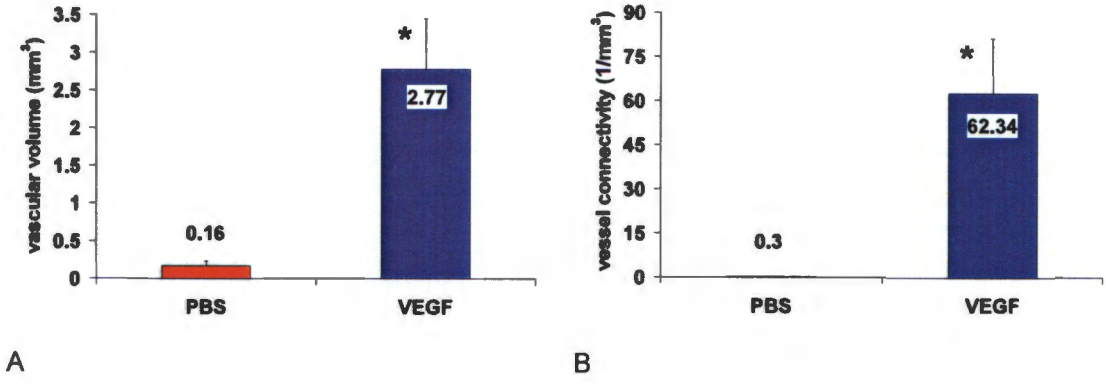

A B

Figure 47: Micro-CT analysis of silicon rubber filled micro vascular network growing into the "Neovascularisation Constructs" (n=4). Vascular volume (A), and vascular connectivity (B) of micro vessels created by continuous 10 day delivery of PBS (red columns) vs. $VEGF_{165}$ (blue columns). * indicates significant effect of $VEGF_{165}$ in both subgroups, $p<0.05$. Data is presented as total vessel volume in mm^3 and connectivity as $1 / mm^3$.

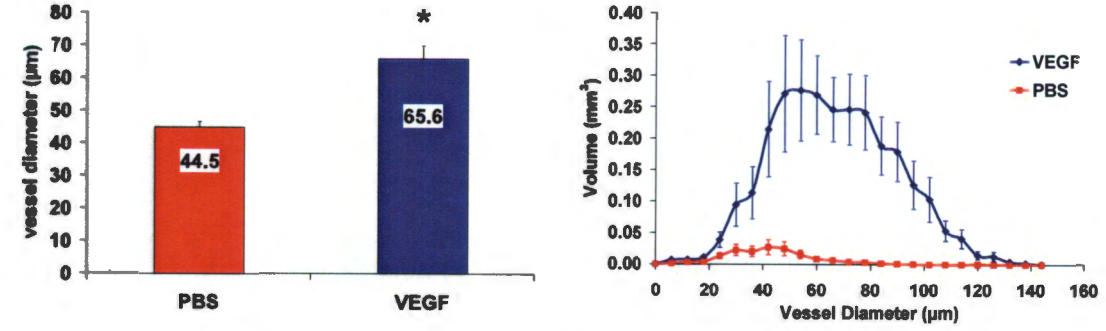

A B

Figure 48: Mean vessel diameter (A) and distribution of vessel diameters (B) into porous PU created by continuous 10 day delivery of PBS (red) and $VEGF_{165}$ (blue). Quantitative analysis of lead chromate containing silicone rubber filled micro vessels by micro-CT. Vessel diameters are presented in µm (n=4). A: Micro-CT determined vessel sizes were significantly larger in the $VEGF_{165}$ group compared to PBS, as indicated by * (44.29 ± 1.73 µm vs. 65.60 ± 4.03 µm, $p<0.05$). Note the large amount of vessels between 40 µm and 100 µm in the $VEGF_{165}$ group, as shown in (B).

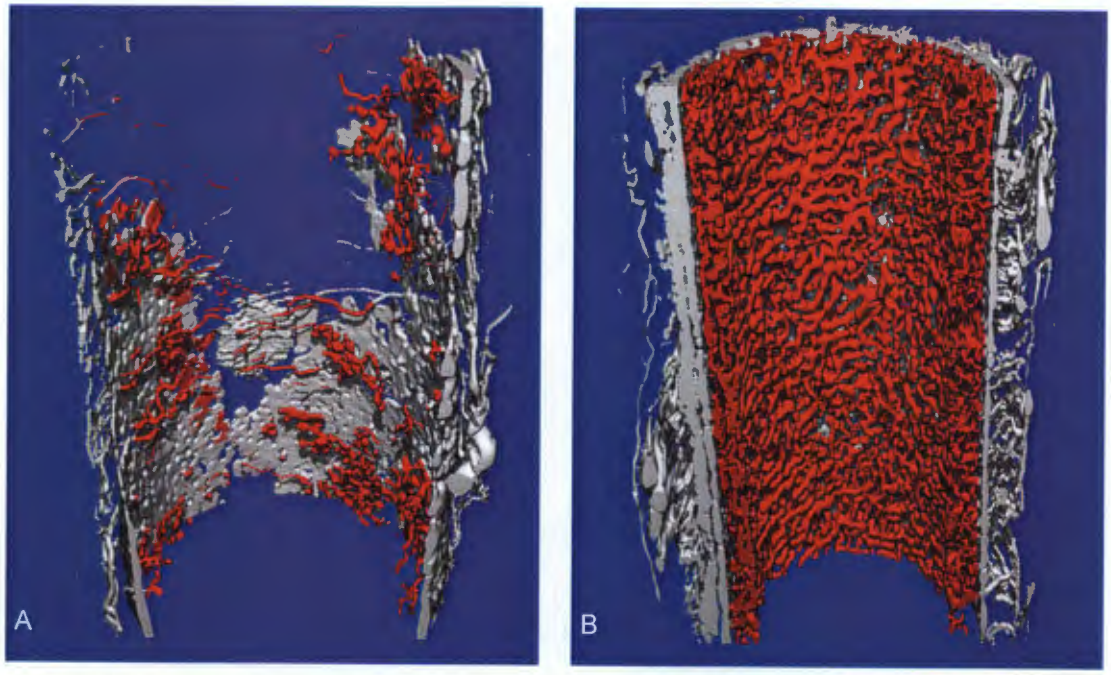

Figure 49: Representative micro-CT images of neovascularisation of polyurethane constructs after 10 days of PBS (A) or $VEGF_{165}$ (B) deliver. "Neovascularisation Constructs" were cut in half by computational image analysis; the views show the inside of the construct. Red color represents the micro vascular network within the defined area of interest (n=4). Grey color represents the micro vascular network outside the construct. PU and ePTFE are invisible due to threshold elimination. Note the significantly increased neovascularisation in the $VEGF_{165}$ group (B) compared to PBS (A).

In order to evaluate the capability of Microfil® to perfuse capillaries, we examined Microfil® filled "Neovascularisation Constructs" after micro-CT scanning histologically (n=4). Light microscopical analysis showed, that capillaries as small as 7.07 µm were filled with Microfil®. Mean vessel density of PBS perfused constructs was 57.67 ± 19.19 vessels / cross section and increased significantly by 2.4 fold, when $VEGF_{165}$ was delivered for 10 days (139.67 ± 19.68 vessels / cross section), ($p<0.05$) (Figure 50 A). Mean vessel diameter increased by 1.78 fold from 23.34 ± 5.67 µm to 41.55 ± 9.63 µm ($p<0.05$) (Figure 50 B). The same vessels measured histologically had therefore 1.91 fold (PBS) and 1.58 fold ($VEGF_{165}$) smaller diameters compared to micro-CT determined vessel diameters, but the relative increase induced by $VEGF_{165}$ in comparison to PBS was similar (1.47 fold by micro-CT and 1.78 fold by histology). Taking histological measurements as the "Gold-standard", micro-CT overestimated micro vessel size 1.5 to 2 fold. In parallel, increases in vessel density were 3.64 fold by micro-CT and 2.4 fold on histology. Interestingly, of all vessels filled with Microfil® and evaluated histologically, only 2.53 % ($VEGF_{165}$) and 5.21 % (PBS) were smaller than 12 µm, which equals the size of 2 micro-CT voxels and the best resolution achievable with commercially

available benchtop CT scanners (Figure 51). If the detection threshold would be set to 18 µm (3 voxels), substantially more micro vessels would be "lost" on analysis (8.51 % and 29.2 %, respectively).

This underscores the critical need for the best possible resolution of micro-CT scanning for the detection of micro vascular networks in biomaterials.

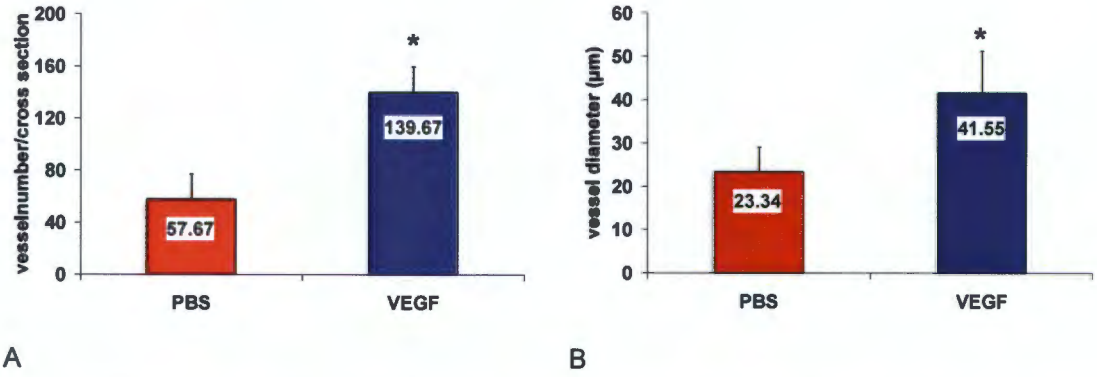

Figure 50: Microscopical analysis of histological sections of silicone rubber perfused "Neovascularisation Constructs" after micro-CT scanning (n=4): * indicates significant increase in vessel density (A) in $VEGF_{165}$ vs. PBS perfused constructs (57.67 ± 19.19 vessels / cross section vs. 139.67 ± 19.68 vessels / cross section) ($p<0.05$). Vessel size (B) increased from 23.34 ± 5.67 µm to 41.55 ± 9.63 µm ($p<0.05$). Therefore, histological results of Microfil® perfused constructs paralleled results obtained by micro-CT scanning (Figure 46, 47).

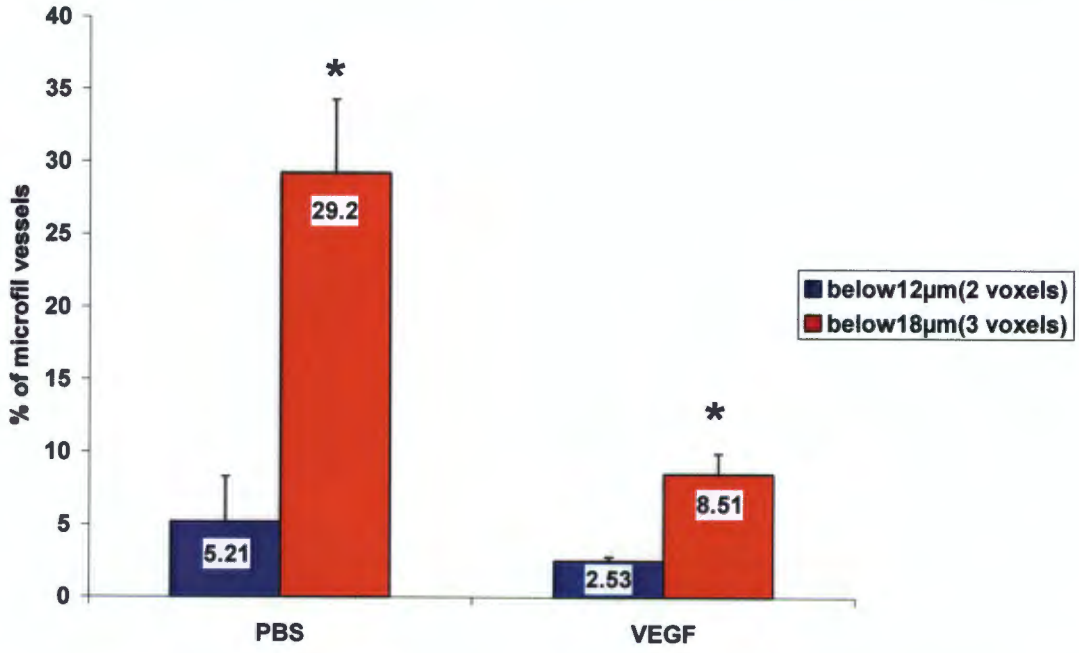

Figure 51: Importance of high resolution of micro-CT scanning: 5.21 % (PBS) and 2.53 % ($VEGF_{165}$) of all Microfil® filled vessels were on histological examination smaller than 12 µm (2 voxels) and were likely to be missed or misinterpreted by micro-CT scanning. If resolution would be set to 18 µm (3 voxels), significantly more vessels would be affected, as indicated by * ($p<0.05$ for PBS and $VEGF_{165}$, respectively, n=4).

7.3.5 Comparison between CD31, lectin perfusion, corrosion casting and micro-CT scanning

All techniques which rely on a intravitally, physiologically perfused micro vascular network such as lectin perfusion or at least on patent microvessels, as shown by perfusion techniques such as corrosion casting and Microfil® perfusion showed significantly less vessels in PBS and $VEGF_{165}$ delivered constructs compared to immunhistochemical CD31 analysis (Figure 52). CD31 detected a high number of small, poorly perfused or non-perfused vessels (vessel density). Only 14.15 % of CD31 positive stained vessels in the PBS group showed signs of lectin perfusion (53.25 ± 3.64 vessels / cross section compared to 376.25 ± 108.48 vessels / cross section). Continuous delivery of $VEGF_{165}$, however, increased perfusion substantially. Therefore, vessel density increased 7.3 fold on lectin perfusion, 4.13 fold using corrosion casting technique and 3.64 fold after Microfil® perfusion followed by micro-CT analysis after $VEGF_{165}$ delivery. This resulted in 47.41 % lectin perfusion of all CD31 positive vessels after $VEGF_{165}$ delivery (389 ± 51.73 vessels / cross section vs. 820.5 ± 92.34 vessels / cross section). The finding, that CD31 showed a substantial amount of non perfused vessels in PBS delivered PU constructs was reflected by the comparison of vessel areas as well (Figure 53). Vessel area of $VEGF_{165}$ delivered PU constructs however, showed no difference between perfusion methods and CD31 because $VEGF_{165}$ created more, larger, well perfused vessels. Therefore, the amount of small, poorly or non-perfused vessels detected by CD 31 did not contribute substantially to the overall vascular area anymore (Figure 53). Vascular area as a relevant indicator for vascular flow reflected functional neovascularisation for $VEGF_{165}$ delivered constructs very well.
In contrast to all other methods, micro-CT scanning was the only method able to evaluate the whole "Neovascularisation Construct" in a reasonable amount of time (6 – 12 hours). Furthermore, three dimensional images and data were provided by micro-CT without destruction of the construct. However, limitations in resolution using the minimal voxel size of 6 µm became apparent, as vessel sizes of the microvascular network were analyzed. PBS delivered constructs showed mean vessel diameters of 16.58 µm (corrosion casting), 23.75 µm (CD31) and 28.12 µm (lectin). Mean vessel diameters determined by micro-CT was significantly larger (61 µm, $p<0.05$ compared to CD31) (Figure 54). Delivery of $VEGF_{165}$ increased vessel sizes to 31.73 µm (corrosion cast), 30.49 µm (CD31) and 32.46 µm (lectin). Again vessel diamters determined by micro-CT scanning was larger (65.6 µm, $p<0.05$ compared to CD31) (Figure 54).

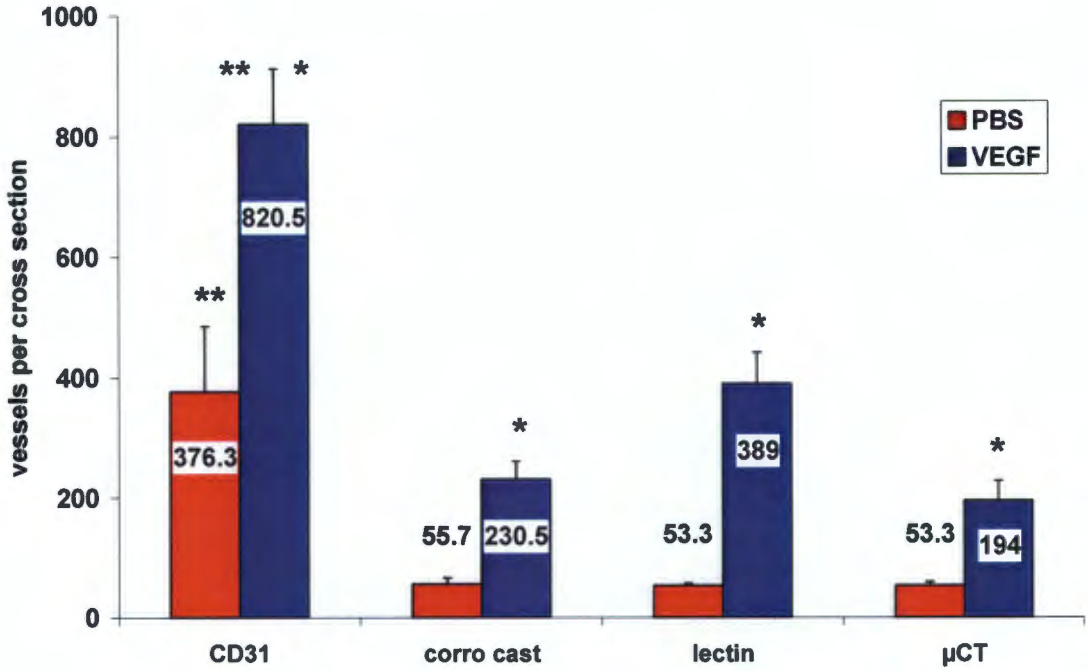

Figure 52: Vessel density created in "Neovascularisation Constructs" by continuous delivery of PBS (red columns) or 1 µg / day $VEGF_{165}$ (blue columns) for 10 days (n=4). Microscopical analysis of CD31 immunostaining (CD31), lectin perfused vessels (lectin), SEM analysis of Mercox® casted and corroded microvessels (corro cast), as well as µ-CT analysis of Microfil® perfused vessels (µCT) (n=4 in all subgroups). * indicates increased neovascularisation after $VEGF_{165}$ delivery compared to PBS ($p<0.05$). ** indicates higher density of CD31 stained vessels compared to corrosion casting, lectin perfusion and µ-CT scanning in each subgroup ($p<0.05$). Data is presented as total vessels per cross section.

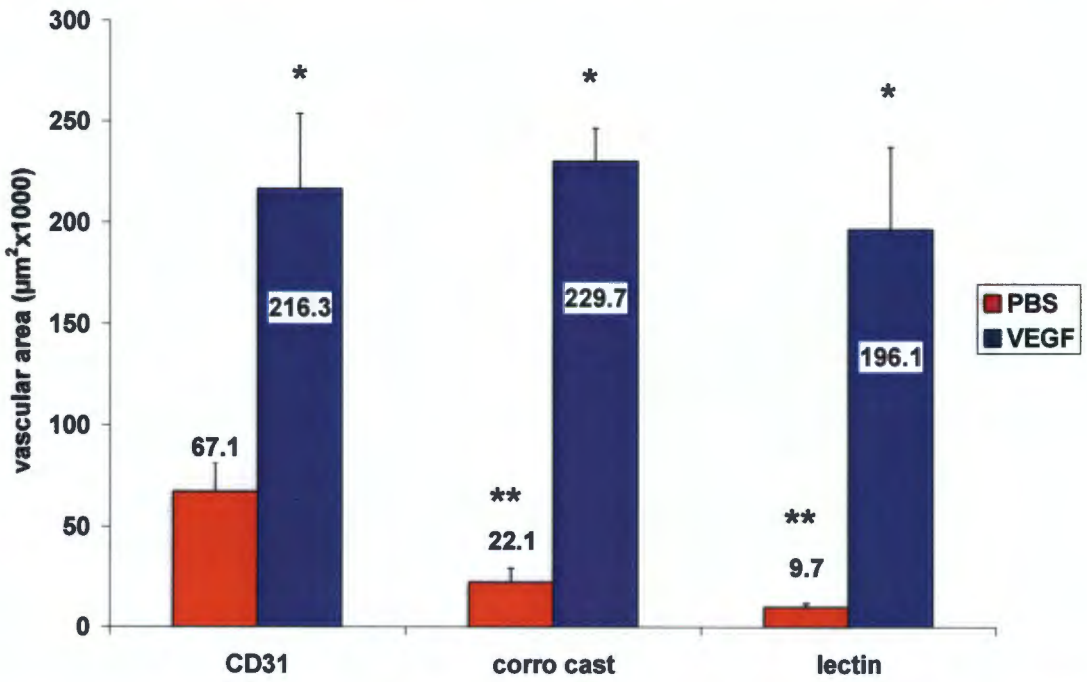

Figure 53: Comparison of vascular areas in "Neovascularisation Constructs" by different quantification methods (n=4 in all groups). * indicates increased vascular area after $VEGF_{165}$ delivery compared to PBS ($p<0.05$). ** indicates smaller vessel area of corrosion casted as well as lectin perfused vessels compared to CD31 immunostained vessels ($p<0.05$). Data is presented as total vessel area per cross section in μm^2 x 1000.

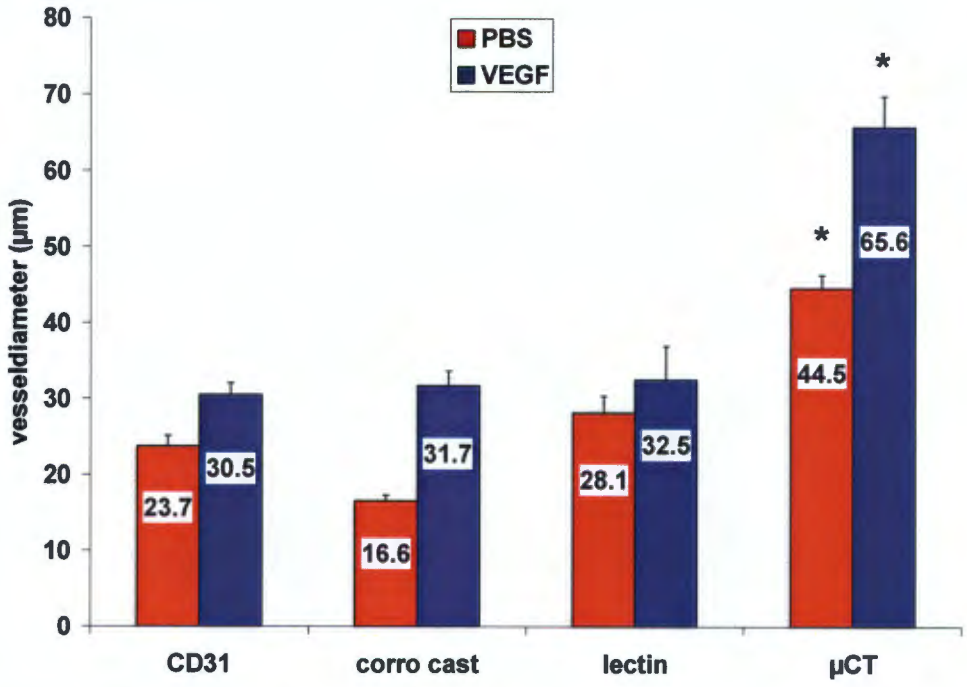

Figure 54: Comparison of vessel diameters in "Neovascularisation Constructs" by different quantification methods (n=4 in all groups). Micro-CT scanned vessels overestimated vessel size compared to CD31 control in the PBS and $VEGF_{165}$ delivered subgroups, as indicated by * and **, respectively ($p<0.05$). Vessel size is presented in µm.

7.4 Discussion

Vascularisation of implants using tissue engineering strategies is considered as critical for achieving the full range of functionality, if the goal is tissue regeneration rather than repair (26). To study vascular ingrowth into porous biomaterials such as polyurethane, we developed a novel "Neovascularisation Construct" consisting of an ePTFE lined porous polyurethane tube, into which PBS or $VEGF_{165}$ was delivered via an osmotic mini-pump, as described in chapter 6 of this PhD thesis. Considering the spatial, three dimensional distribution of newly formed blood vessels into porous biomaterials, conventional histological sections often represent an immense loss of information and data, even when labor intensive serial sections are used. As an additional challenge in characterizing vascular networks, the morphological aspect determined by conventional immunhistochemistry such as CD31, CD34 and von Willebrand factor does not reflect the functional perfusion status (359). Truly functional, real time techniques such as ultrasound doppler on the other hand lack the required penetration depth of tissues at high resolution and are physically of limited value in imaging vascular networks grown into hydrophobic biomaterials (365). Magnetic Resonance Angiography (MRA) and Positron Emission

Tomography (PET) are methods used in clinical medicine and research to evaluate blood flow and blood volume, but up to date, the resolution of 200 µm and 1.5 mm respectively, are not suitable for microvascular imaging (366), (367).

In view of these limitations in quantifying minute vascular networks in biomaterials using conventional methods, we chose to use a combined approach including two dimensional CD31 immunhistochemical staining of blood vessels, intravital perfusion of the vascular network by lycopersicon esculentum lectin as well as postmortal perfusion of the vascular system with lead chromate containing silicone rubber followed by micro-CT scanning. Furthermore, methyl-methacrylate was used for corrosion casting followed by scanning electron microscopical (SEM) analysis. CD31 immunhistochemistry as endothelial marker is widely used and accepted for the quantification of microvascular structures (389). Lectin binding to endothelial cells reflects the intravital, physiological perfusion of a vascular network and has been shown to be a sensitive marker in angiogenesis and vessel regression (362), (328). Vascular corrosion casting allows to study the exact three dimensional structure of a perfused micro vascular network and has been used for visualization and quantification of micro vessels extensively (361). As a novel method to quantify micro vessels three dimensionally, objectively and reproducibly, micro-CT has been introduced recently (368), (378). The aim of this study was to determine the perfusion status of the neovascularisation construct as well as to investigate the capabilities and limitations of micro-CT scanning to quantify neovascularisation into biomaterials such as porous PU.

Our results showed that $VEGF_{165}$ delivered via an osmotic mini-pump for 10 days into a porous PU increased vessel density, size, area, volume and connectivity significantly irrespective of the quantification method used. Direct comparison of the 4 different quantification techniques revealed however, that immunhistochemical staining of endothelial cells such as CD31 antibody overestimated functional micro vessels in PBS treated PU by three fold with regards to vascular area. With regards to vessel density, only 14.15 % of CD31 positive vessels in the PBS group showed signs of lectin perfusion. Since the tracheal- as well as the kidney capillary network was adequately perfused with lectin, it seems unlikely, that results obtained on perfusion of porous PU were false negative. Furthermore, corrosion casting as additional perfusion technique for patent vessels confirmed lectin results with respect to vessel density and area in PBS. These findings indicated that quantification of micro vascular networks exclusively based on immunhistochemistry might show a significant percentage of non-functional vessels and thereby overestimate perfusion and oxygen as well as nutrient delivery to tissue growing into

porous PU. Functional vascular quantification methods such as lectin perfusion, corrosion casting and micro-CT scanning are clearly necessary to obtain a reasonable reflection of tissue perfusion within a biomaterial.

A second interesting finding was the pronounced effect of 10 day $VEGF_{165}$ delivery on the perfusion of the micro vascular networks inside the PU. Lectin perfusion indicated a striking 20.11 fold increase of perfusion and micro-CT scanning showed a 10.42 fold increase as a postmortal perfusion method. In contrast, due to the large vessel area of PBS delivered constructs on CD31 immunhistochemistry apparently without adequate perfusion, the increase in vessel area by $VEGF_{165}$ delivery on CD31 was only 3.22 fold. The reason for the strong $VEGF_{165}$ effect on perfusion might be twofold: firstly, mean vessel size increased by 15.43 % (lectin), 28.38 % (CD31), 41.41 % (micro-CT) and 91.39 % using SEM on corrosion cast specimens. According to "Hagen-Poiseuille's Law", resistance to flow $R = (8 \times \eta \times L) / (\pi \times r^4)$, an increase in diameter of 30 - 40 % would account for a 2.8 to 3.8 times decrease in resistance and thus increase flow rate and perfusion by the same factor. Since $VEGF_{165}$ not only enlarges preexisting vessels and creates new vessels, but also increases vascular permeability and is also known as vascular permeability factor (390), resistance is further reduced and allows for additional increase of perfusion. The increase in vessel diameter might be due in part to a direct vasodilatory effect of $VEGF_{165}$ via NO release (390), and additionally via a direct effect on endothelial proliferation and migration. The ability of $VEGF_{165}$ to improve blood flow has been described in pig coronary artery models (391), (392). In the model used by Lopez et al., $VEGF_{165}$ produced a significant, dose-dependent 3.5 fold increase in coronary blood flow measured by intracoronary doppler ultrasound (391). This effect was explained exclusively by vasodilatation of micro vessels, since $VEGF_{165}$ was administered as intracoronary infusion over a few minutes and did not contribute to any neoangiogenic effect. Future experiments on the effect of long term $VEGF_{165}$ delivery on tissue perfusion would be clearly useful and indicated.

In comparison to CD31 immunohistochemistry as a morphological marker, lectin perfusion and corrosion casting as functional markers, micro-CT scanning of silicone rubber filled micro vessels proved to be an excellent method to study the three dimensional vascular network across the whole length of the "Neovascularisation Construct". Micro-CT enabled us to quantify complex parameters such as vessel density, vessel size and –distribution, vascular volume and connectivity relatively rapidly. Furthermore, it allowed the quantification of functional angiogenesis in intact biomaterials impenetrable for other techniques such as doppler ultrasound. In comparison to CD31, lectin and corrosion casting, micro-CT overestimated average

vessel size in our hands in the $VEGF_{165}$ group by 1.58 times and in the PBS group by 1.91 times, presumably due to a merging effect (partial volume effect) of small vessels lying next to each other with an inter-vessel distance of less than 12 µm. The relative increase of vessel diameter as well as vessel density induced by $VEGF_{165}$ was however, similar on histology and on micro-CT (1.47 fold and 3.64 fold by micro-CT and 1.78 fold and 3.1 fold by histology, respectively). An excellent agreement between micro-CT and histology was described by Duvall et al., who analyzed collateral vessel development after ischemic injury in a mouse model (377). He regarded a voxel size of 36 µm as optimal to determine collateral growth of larger, arteriole sized vessels. Since we were interested in neovascularisation into the porous construct including capillaries, small arterioles and venules, we chose the minimal voxel size of 6 µm. Because the best possible resolution of the micro-CT system we used was limited to 2 voxels, structures below 12 µm were most likely not recognized and quantified exactly. Our findings, that 8.51 % (PBS) and 29.2 %, ($VEGF_{165}$) of all Microfil® filled vessels would be missed or misinterpreted, if resolution would be set to 18 µm (3 voxels), underscored the critical need for the best possible resolution of micro-CT scanning for the evaluation of micro vascular networks growing into biomaterials. Data obtained on vessel connectivity by Duvall et al. (377) in a mouse ischemic hindlimb model is very similar our data of PBS perfused "Neovascularisation Constructs" (0.3 ± 0.074 / mm^3). Micro-CT scanning has been described to provide reliable data on vessel connectivity (388), (396), which has been shown to be dependent on VEGF (397).

The limitations of micro-CT in terms of exact resolution of vascular structures of less than 12 µm, which allows for the study of angiogenesis at the capillary level, has been overcome technically already by the use of synchrotron as radiation source (369), (393). However, this highly specialized technical equipment is generally not easily accessible and therefore, development of a commercially available bench top micro-CT scanner, which scans samples of several centimeters in a few hours with increasing resolution, will be a technical challenge for the future. Furthermore, the demand for in vivo micro-CT systems for animal micro tissue imaging will surely increase to study different time points in the same organism and thus reduce the use of animals for medical research (377). As for today, in conjunction with other functional and morphological methods to quantify vascularisation such as lectin perfusion, corrosion casting and CD31 immunhistochemistry, micro-CT promises to be an invaluable tool to study neovascularisation of porous biomaterials (382).

8. Conclusions

The concept of transmural in vivo endothelialisation of vascular grafts holds great promise for increased long term patency. To achieve complete luminal endothelial cell coverage and optimal integration of the porous synthetic graft material into the host tissue, transmural ingrowth of tissue and vasa vasorum might have to be facilitated. Since $VEGF_{165}$ and PDGF-BB are growth factors known to stimulate and consolidate angiogenesis, this PhD thesis hypothesised, that neovascularisation of porous polyurethane can be increased by delivery of vascular endothelial growth factor ($VEGF_{165}$) and platelet derived growth factor (PDGF-BB). To prove or disprove this hypothesis, four main project aims were addressed

1. A valid, reproducible, simple and quantifiable neovascularisation model was established
2. Different ways of growth factor delivery were investigated.
3. The induction as well as the stability of neovascularisation into porous polyurethane was investigated.
4. Functionality of the newly created vascular network was shown

Three different ways of growth factor delivery were specifically evaluated:

1. Growth factor delivery to porous polyurethane by adeno-associated viruses
2. Growth factor delivery to porous polyurethane by heparin surface modification
3. Continuous growth factor delivery by osmotic mini pumps into a "Neovascularisation Construct"

AAV as a small, single stranded non human pathogenic parvo-virus has been shown to efficiently transduce dividing as well as non-dividing cells. We used genetic modification of AAV by cloning the gene encoding for β-galactosidase (LacZ) and the gene encoding for human $VEGF_{165}$ into the viral genome of AAV. In order to achieve a sustained, localized and controllable growth factor production, the concept of a "Gene Activated Matrix" (GAM) was applied by loading genetically modified AAV into porous PU discs which allows for the transduction of autologous ingrowing wound cells after subcutaneous implantation. Highly infective viruses of up to 5.4 x 10^{11} gc AAV / ml with an infectivity ratio of 1:120 were produced using Stratagene's

"AAV helper-free production system" and a novel AAV single step heparin purification method.

AAV elution from different embedding matrices such as fibrin 10 mg / ml, 25 mg / ml, 50 mg / ml, collagen 0.4 % and PEG 3 % was evaluated and resulted in increasing virus retention with increasing matrix concentrations. In terms of virus retention fibrin 50 mg / ml with only 25.08 % AAV-LacZ release after 24 hours was superior to other matrices tested. In vivo studies involving subcutaneous implantation of matrix embedded AAV showed a sufficient tissue ingrowth after 20 days in to fibrin 50 mg / ml loaded discs (70.95 % ingrowth), which is a prerequisite for the successful application of the "Gene Activated Matrix" approach. AAV-LacZ injected directly into tibialis anterior muscles of rats indicated successful transduction and confirmed the previously known tropism for myocytes. LacZ transgene expression started as early as 3 days after injection and lasted for at least 28 days. AAV was also capable of $VEGF_{165}$ gene transfer in vivo. A 5.75 fold increase in $VEGF_{165}$ concentration was measured by ELISA in muscle tissue 10 days after AAV-$VEGF_{165}$ injection compared to AAV-LacZ control. However, transduction efficiency of AAV-$VEGF_{165}$ for granulation tissue was relatively poor. After subcutaneous implantation of fibrin embedded AAV-LacZ loaded PU discs, ingrowing tissue was visibly transduced by AAV-LacZ, the amount of $VEGF_{165}$ expression following AAV-$VEGF_{165}$ transduction was, however, not detectable by $VEGF_{165}$ ELISA after protein extraction from PU discs. The future direction of AAV gene delivery leads towards a genetically altered tropism of AAV to generate vectors that are more efficient, and even selective for specific tissues, such as vasculature. As this was beyond the scope of this PhD thesis, we evaluated heparin surface modification as a second modality to increase neovascularisation into porous polyurethane.

PU discs were coated with heparin by cerium-ion initiated graft co-polymerization with acrylic acid and acrylamide, covalent attachment of ethylene diamine and immobilization of nitrous acid degraded (NAD) heparin via reductive amination. Subsequently, $VEGF_{165}$ and / or PDGF-BB was absorbed passively onto heparin coated PU discs. In vitro elution experiments indicated that a maximum of 1.2 µg $VEGF_{165}$ was adsorbed per disc and took 48 hours to elute into PBS at 37°C with continuous agitation. 3.5 µg PDGF-BB was loaded as well onto PU discs and only 3.04 % was eluted after 7 days. This indicated a higher affinity of PDGF-BB for heparin compared to $VEGF_{165}$ and warranted further analysis as a dual growth factor delivery system. Implantation of heparin coated PU discs with and without addition of $VEGF_{165}$ as well as PDGF-BB alone and in combination revealed a significant effect on neovascularisation of the PU discs. Surface modification with heparin

alone increased average vessel density by 77.64 % compared to uncoated control PU at 10 days. The delivery of $VEGF_{165}$ alone and in combination with PDGF-BB increased vessel density by up to 115 %. At 2 months implantation time heparin surface modification still had a significant effect on vessel density (41.91 % increase in comparison to non coated control PU). However, plain PU discs, heparin coated PU discs and heparin coated PU discs loaded with $VEGF_{165}$ showed signs of significant vessel regression after 2 months. In contrast, PDGF-BB supplemented discs stabilized neovascularisation at a 2 - 3 fold increased level compared to control discs. Therefore, $VEGF_{165}$ initiated neovascularisation, whereas PDGF-BB had an angiogenic as well as a stabilizing effect. The dual growth factor delivery approach resulted in a stable level of increased neovascularisation over a long period of time and from early on after implantation. To evaluate the role of PDGF-BB on angiogenesis and vessel stabilization in more detail, we are currently investigating smooth muscle cell coverage of microvascular networks.

Because healing of vascular grafts and tissue replacements usually occurs in a hypoxic wound healing situation, we were interested to evaluate, whether chronic whole body hypobaric hypoxia has an effect on heparin-induced angiogenesis into heparin coated polyurethane discs in a wound model. As an unexpected finding, whole body hypobaric hypoxia (11 % O_2) did not increase neovascularisation into porous PU discs implanted subcutaneously in rats, but rather had a distinctive counter-effect on the angiogenic effect of covalent heparin coating. In accordance with our previous results, heparin surface modification increased vessel density by 61.25 % compared to baseline under normoxic conditions. Addition of $VEGF_{165}$ had an additive effect up to 111.71 %. In hypoxia, however, the pro-angiogenic effect of heparin was completely absent, and additional $VEGF_{165}$ was necessary to increase vessel density by only 28.59 % compared to control. Clearly, this complex issue of hypoxic wound healing involving biomaterials needs further investigations on a molecular level to fully understand the mechanisms involved in wound healing and thus create the basis for applied research into wound / biomaterial interactions.

As an approach to study the effects of a sustained growth factor delivery on neovascularisation into porous PU, a novel "Neovascularisation Construct" was developed consisting of an osmotic mini-pump delivering $VEGF_{165}$ or PBS into a tube of porous PU lined with ePTFE on the inside. After subcutaneous implantation, granulation tissue was growing into the porous PU towards the growth factor gradient. Delivery of $VEGF_{165}$ appeared to be safe and effective. Quantification of neovascularisation showed an increase in vessel density after 10 days of continuous $VEGF_{165}$ delivery (1000 ng / day) by 75.19 %. A study involving different dosages of

$VEGF_{165}$ (10 ng / day, 100 ng / day and 1000 ng / day) showed a linear increase in vascular area by increasing $VEGF_{165}$ concentrations up to 265.1 % compared to control. Neovascularisation appeared to be localized without any signs of a distant or systemic angiogenic response. Therefore, continuous delivery of $VEGF_{165}$ into the porous PU "Neovascularisation Construct" appeared to be a reliable model to induce neovascularisation within a biomaterial and a useful tool to study different growth factor combinations for variable lengths of time.

Since vascularisation of implants using tissue engineering strategies is considered as critical for achieving the full range of functionality, but the traditional quantification method of endothelial cell immunostaining usually lacks information about the three dimensional structure of vessels and furthermore provides no sufficient information on vascular perfusion, we evaluated four different techniques to quantify micro vascular networks growing into the "Neovascularisation Construct" and to assess their perfusion. CD31 immunostaining, lectin perfusion, scanning electron microscopy of vascular corrosion casts and micro-CT scanning of silicone rubber perfused micro vessels growing into the "Neovascularisation Construct" all showed a significant increase in vessel density, area and diameter after delivery of $VEGF_{165}$ for 10 days compared to PBS control. Absolute values however, showed distinctive differences. CD31 immunostaining showed a 3 times higher vascular area per cross section in the PBS delivered constructs compared to the perfusion methods such as lectin perfusion and corrosion casts. These findings indicated, that a substantial amount of capillaries which were stained positive by CD31 because of endothelial lining, did not contribute to tissue perfusion in a biomaterial such as polyurethane. In contrast, after delivery of $VEGF_{165}$ to the "Neovascularisation Constructs" all CD31 stained micro vessels seemed to be adequately perfused. Micro-CT scanning of silicone rubber perfused micro vessels has, so far, never been used to analyze micro vascular networks growing into a biomaterial. We evaluated this new diagnostic instrument and found several advantages. Micro vessels were detected and analyzed across the whole length of the "Neovascularisation Construct" within 6 - 12 hours. Polyurethane did not interfere with detection, because threshold levels were different between perfused mico vessels and biomaterial. Three dimensional data including total vascular volume and vessel connectivity were obtained and visualized. And finally, for the scanning process, samples did not have to be sectioned or manipulated in any other way. Resolution was however, still a limiting factor using a commercially available bench top scanner (about 10 µm with a nominal voxel size of 6 µm). This resulted in a two fold overestimation of average vessel diameters due to a merging or "partial volume effect". At the present stage,

when micro vascular networks down to the capillary level are to be analyzed and quantified, micro CT-scanning needs to be complemented by immunhistochemistry and perfusion studies such as lectin perfusion and corrosion casting. As a future perspective, however, increasing technical potential with regards to the improvement of resolution and computational processing might even allow for non-invasive quantitative flow analysis using computational fluid dynamics (CFD) involving numerical modeling.

In conclusion, the subcutaneous implantation of porous PU discs as well as the "Neovascularisation Constructs" established a valid, reproducible, relatively simple and quantifiable neovascularisation model. The induction of neovascularisation was achieved by heparin surface modification alone as well as by additional delivery of growth factors. Furthermore, prolonged growth factor delivery by osmotic pumps induced neovascularisation into PU as a biomaterial. The creation of a stable microvascular network at 2 months was achieved and the functionality was shown 10 days after implantation using four different, independent techniques including the novel micro-CT scanning of neovascularisation into biomaterials.
Towards the development of an in vivo, spontaneously and transmurally endothelializing vascular graft with superior long term patency future experimental and clinical studies are clearly indicated. As a first step, increased spontaneous neovascularisation of the possible graft material polyurethane was achieved by heparin surface modification and growth factor delivery. Other growth factor combinations such as Angiopoietin-1 and VEGF might have to be studied for their angiogenic potential. With respect to the stabilizing effect of mural cells, immunhistochemistry of vessels needs to be improved. A reliable mural cell staining would contribute substantially towards a better insight into the effect of PDGF-BB we observed regarding maturation of neovascularisation into a biomaterial. Future investigations need to study the translation of increased neovascularisation of the subcutaneously implanted biomaterial polyurethane towards increased endothelialisation in a vascular graft model. The rat infrarenal aortic replacement could be a suitable animal model as an indicator of the safety and feasibility of this approach. Subsequently, as the animal model closest to the human situation, a baboon graft model using heparinised porous PU grafts might be beneficial. Anticoagulant properties of heparin surface modified PU could thereby be addressed by decreasing PU pore size to below 100 µm and by the surgical technique of "pre-clotting" of macro porous grafts. In conclusion, a promising first step has been done, but many questions still need to be answered.

9. References

1. Drouet L. Atherothrombosis as a systemic disease. Cerebrovasc Dis 2002;13 Suppl 1:1-6.
2. Ross R. Atherosclerosis--an inflammatory disease. N Engl J Med 1999;340(2):115-26.
3. Bakhai A. The burden of coronary, cerebrovascular and peripheral arterial disease. Pharmacoeconomics 2004;22 Suppl 4:11-8.
4. AHA. Heart disease and stroke statistics - 2004 update. Dallas, Texas: American Heart Association 2004.
5. Hirsch A, Criqui M, Treat -JD, Regensteiner J, Creager M, Olin J, et al. Peripheral arterial disease detection, awareness, and treatment in primary care. JAMA 2001;286(11):1317-24.
6. Meijer W, Hoes A, Rutgers D, Bots M, Hofman A, Grobbee D. Peripheral arterial disease in the elderly: The Rotterdam Study. Arterioscler Thromb Vasc Biol 1998;18(2):185-92.
7. Murray C, Lopez A. Alternative projections of mortality and disability by cause 1990-2020: Global Burden of Disease Study. Lancet 1997;349(9064):1498-504.
8. Bradshaw D, Groenewald P, Laubscher R, Nannan N, Nojilana B, Norman R, et al. Initial burden of disease estimates for South Africa, 2000. S Afr Med J 2003;93(9):682-8.
9. Leeder S RS, Greenberg H, Liu H, Esson KA. Race Against Time: The Challenge of Cardiovascular Disease in Developing Economies. New York: Columbia University; 2004.
10. Niklason L, Langer R. Advances in tissue engineering of blood vessels and other tissues. Transpl Immunol 1997;5(4):303-6.
11. Grondin C, Campeau L, Lesperance J, Enjalbert M, Bourassa M. Comparison of late changes in internal mammary artery and saphenous vein grafts in two consecutive series of patients 10 years after operation. Circulation 1984;70(3 Pt 2):I208-12.
12. Szilagyi D, Hageman J, Smith R, Elliott J, Brown F, Dietz P. Autogenous vein grafting in femoropopliteal atherosclerosis: the limits of its effectiveness. Surgery 1979;86(6):836-51.
13. Sladen J, Gilmour J, Wong R. Cumulative patency and actual palliation in patients with claudication after aortofemoral bypass. Prospective long-term follow-up of 100 patients. Am J Surg 1986;152(2):190-5.
14. Veith F, Gupta S, Ascer E, White -FS, Samson R, Scher L, et al. Six-year prospective multicenter randomized comparison of autologous saphenous vein and expanded polytetrafluoroethylene grafts in infrainguinal arterial reconstructions. J Vasc Surg 1986;3(1):104-14.
15. Brewster D, LaSalle A, Robison J, Strayhorn E, Darling R. Femoropopliteal graft failures. Clinical consequences and success of secondary reconstructions. Arch Surg 1983;118(9):1043-7.
16. Belkin M, Knox J, Donaldson M, Mannick J, Whittemore A. Infrainguinal arterial reconstruction with nonreversed greater saphenous vein. J Vasc Surg 1996;24(6):957-62.
17. Renwick P, Johnson B, Wilkinson A, Galloway J, McCollum P. Vascular surgical society of great britain and ireland: limb outcome following failed femoropopliteal polytetrafluoroethylene bypass for intermittent claudication. Br J Surg 1999;86(5):693.
18. Domenig C, Hamdan A, Holzenbein T, Kansal N, Aulivola B, Skillman J, et al. Timing of pedal bypass failure and its impact on the need for amputation. Ann Vasc Surg 2005;19(1):56-62.

19. Saifalian A, Giudiceandrea A, Schmitz-Rixen T, Hamilton G. Noncomliance: the silent accepatance of a villain. In: Zilla P, Greissler H, editors. Tissue engineering of vascular prosthetic grafts. Austin, Texas: R.G.Landes Company; 1999.
20. Wesolow A. Biological behaviour of tissue and prosthetic grafts. In: Haimovoci H, editor. Vascular surgery. Principles and techniques. Norwark,Conneticut: Appleton-Century-Crofts; 1984. p. 93-118.
21. Davids L, Dower T, Zilla P. The lack of healing in conventional vasculargrafts. In: Zilla P, Greissler H, editors. Tissue engineering of vascular prosthetic grafts. Austin, Texas: R.G.Landes Company; 1999.
22. Sottiurai V, Yao J, Flinn W, Batson R. Intimal hyperplasia and neointima: An ultrastructural analysis of thrombosed grafts in humans. Surgery 1983;93(6):809-17.
23. Shi Q, Wu M, Onuki Y, Ghali R, Hunter G, Johansen K, et al. Endothelium on the flow surface of human aortic Dacron vascular grafts. J Vasc Surg 1997;25(4):736-42.
24. Zilla P, Deutsch M, Meinhart J. Endothelial cell transplantation. Semin Vasc Surg 1999;12(1):52-63.
25. Langer R, Vacanti J. Tissue engineering. Science 1993;260(5110):920-6.
26. Williams DF. To engineer is to create: the link between engineering and regeneration. Trends Biotechnol 2006;24(1):4-8.
27. Weinberg C, Bell E. A blood vessel model constructed from collagen and cultured vascular cells. Science 1986;231(4736):397-400.
28. L HN, Germain L, Labbe R, Auger F. In vitro construction of a human blood vessel from cultured vascular cells: a morphologic study. J Vasc Surg 1993;17(3):499-509.
29. Hirai J, Matsuda T. Venous reconstruction using hybrid vascular tissue composed of vascular cells and collagen: tissue regeneration process. Cell Transplant 1996;5(1):93-105.
30. L HN, Paquet S, Labbe R, Germain L, Auger F. A completely biological tissue-engineered human blood vessel. FASEB J 1998;12(1):47-56.
31. Niklason LE, Gao J, Abbott WM, Hirschi KK, Houser S, Marini R, et al. Functional arteries grown in vitro. Science 1999;284(5413):489-93.
32. Herring M, Gardner A, Glover J. A single-staged technique for seeding vascular grafts with autogenous endothelium. Surgery 1978;84(4):498-504.
33. Herring M, Compton R, LeGrand D, Gardner A, Madison D, Glover J. Endothelial seeding of polytetrafluoroethylene popliteal bypasses. A preliminary report. J Vasc Surg 1987;6(2):114-8.
34. Jarrell B, Levine E, Shapiro S, Williams S, Carabasi R, Mueller S, et al. Human adult endothelial cell growth in culture. J Vasc Surg 1984;1(6):757-64.
35. Williams S, Wang T, Castrillo R, Jarrell B. Liposuction-derived human fat used for vascular graft sodding contains endothelial cells and not mesothelial cells as the major cell type. J Vasc Surg 1994;19(5):916-23.
36. Greisler H, Klosak J, Dennis J, Ellinger J, Un KD, Burgess W, et al. Endothelial cell growth factor attachment to biomaterials. ASAIO Trans 1986;32(1):346-9.
37. Greisler H, Klosak J, Dennis J, Karesh S, Ellinger J, Kim D. Biomaterial pretreatment with ECGF to augment endothelial cell proliferation. J Vasc Surg 1987;5(2):393-9.
38. Greisler H, Schwarcz T, Ellinger J, Kim D. Dacron inhibition of arterial regenerative activities. J Vasc Surg 1986;3(5):747-56.
39. Gosselin C, Vorp D, Warty V, Severyn D, Dick E, Borovetz H, et al. ePTFE coating with fibrin glue, FGF-1, and heparin: effect on retention of seeded endothelial cells. J Surg Res 1996;60(2):327-32.

40. Zilla P, Fasol R, Deutsch M, Fischlein T, Minar E, Hammerle A, et al. Endothelial cell seeding of polytetrafluoroethylene vascular grafts in humans: a preliminary report. J Vasc Surg 1987;6(6):535-41.
41. Deutsch M, Meinhart J, Fischlein T, Preiss P, Zilla P. Clinical autologous in vitro endothelialization of infrainguinal ePTFE grafts in 100 patients: a 9-year experience. Surgery 1999;126(5):847-55.
42. Meinhart J, Deutsch M, Fischlein T, Howanietz N, Froschl A, Zilla P. Clinical autologous in vitro endothelialization of 153 infrainguinal ePTFE grafts. Ann Thorac Surg 2001;71(5 Suppl):S327-31.
43. Sottiurai V, Sue S, Rau D, Tran A. Comparative analysis of pseudointima biogenesis in Gelseal coated Dacron knitted graft versus crimped and noncrimped graft. J Cardiovasc Surg (Torino) 1989;30(6):902-9.
44. Stewart G, Essa N, Chang K, Reichle F. A scanning and transmission electron microscope study of the luminal coating on Dacron prostheses in the canine thoracic aorta. J Lab Clin Med 1975;85(2):208-26.
45. Bull D, Hunter G, Holubec H, Aguirre M, Rappaport W, Putnam C. Cellular origin and rate of endothelial cell coverage of PTFE grafts. J Surg Res 1995;58(1):58-68.
46. Hertzer N. Regeneration of endothelium in knitted and velour dacron vascular grafts in dogs. J Cardiovasc Surg (Torino) 1981;22(3):223-30.
47. Bezuidenhout D. Porous polymeric superstructures as in-growth scaffolds for tissue-engineered vascular prostheses [PhD Thesis]. Cape Town: University of Stellenbosch; 2001.
48. Szilagyi D, Smith R, Elliott J, Allen H. Long-term behavior of a dacron arterial substitute: clinical, roentgenologic and histologic correlations. Ann Surg 1965;162(3):453-77.
49. Stumb M, Jordan G, DeBakey M. Endothelium growth from circulating blood on isolated intravascular Dacron hub. Am J Path 1963;43:361-68.
50. Bossart M, Turner S, Milam J, Connor D, Urrutia C, Frazier O. Multipotential cells in the circulating blood: ultrastructural evidence in the calf. Trans Am Soc Artif Intern Organs 1982;28:185-9.
51. Shi Q, Wu M, Hayashida N, Wechezak A, Clowes A, Sauvage L. Proof of fallout endothelialization of impervious Dacron grafts in the aorta and inferior vena cava of the dog. J Vasc Surg 1994;20(4):546-56; discussion 556-7.
52. Asahara T, Murohara T, Sullivan A, Silver M, van dZR, Li T, et al. Isolation of putative progenitor endothelial cells for angiogenesis. Science 1997;275(5302):964-7.
53. Asahara T, Masuda H, Takahashi T, Kalka C, Pastore C, Silver M, et al. Bone marrow origin of endothelial progenitor cells responsible for postnatal vasculogenesis in physiological and pathological neovascularization. Circ Res 1999;85(3):221-8.
54. Clowes A, Kirkman T, Reidy M. Mechanisms of arterial graft healing. Rapid transmural capillary ingrowth provides a source of intimal endothelium and smooth muscle in porous PTFE prostheses. Am J Pathol 1986;123(2):220-30.
55. Clowes A, Zacharias R, Kirkman T. Early endothelial coverage of synthetic arterial grafts: porosity revisited. Am J Surg 1987;153(5):501-4.
56. Greisler H, Cziperle D, Kim D, Garfield J, Petsikas D, Murchan P, et al. Enhanced endothelialization of expanded polytetrafluoroethylene grafts by fibroblast growth factor type 1 pretreatment. Surgery 1992;112(2):244-54; discussion 254-5.
57. Sauvage L, Berger K, Wood S, Nakagawa Y, Mansfield P. An external velour surface for porous arterial prostheses. Surgery 1971;70(6):940-53.

58. Debakey M, Jordan GJ, Beall AJ, O NR, Abbott J, Halpert B. Basic biologic reactions to vascular grafts an prosthesis. Surg Clin North Am 1965;45:477-97.
59. Berger K, Sauvage L, Rao A, Wood S. Healing of arterial prostheses in man: its incompleteness. Ann Surg 1972;175(1):118-27.
60. Bezuidenhout D, Davies N, Zilla P. Effect of well defined dodecahedral porosity on inflammation and angiogenesis. ASAIO J 2002;48(5):465-71.
61. Folkman J, D AP. Blood vessel formation: what is its molecular basis? Cell 1996;87(7):1153-5.
62. Risau W. Mechanisms of angiogenesis. Nature 1997;386(6626):671-4.
63. Reyes M, Dudek A, Jahagirdar B, Koodie L, Marker P, Verfaillie C. Origin of endothelial progenitors in human postnatal bone marrow. J Clin Invest 2002;109(3):337-46.
64. Luttun A, Carmeliet G, Carmeliet P. Vascular progenitors: from biology to treatment. Trends Cardiovasc Med 2002;12(2):88-96.
65. Shi Q, Rafii S, Wu M, Wijelath E, Yu C, Ishida A, et al. Evidence for circulating bone marrow-derived endothelial cells. Blood 1998;92(2):362-7.
66. Takahashi T, Kalka C, Masuda H, Chen D, Silver M, Kearney M, et al. Ischemia- and cytokine-induced mobilization of bone marrow-derived endothelial progenitor cells for neovascularization. Nat Med 1999;5(4):434-8.
67. Peichev M, Naiyer A, Pereira D, Zhu Z, Lane W, Williams M, et al. Expression of VEGFR-2 and AC133 by circulating human CD34(+) cells identifies a population of functional endothelial precursors. Blood 2000;95(3):952-8.
68. Hattori K, Dias S, Heissig B, Hackett N, Lyden D, Tateno M, et al. Vascular endothelial growth factor and angiopoietin-1 stimulate postnatal hematopoiesis by recruitment of vasculogenic and hematopoietic stem cells. J Exp Med 2001;193(9):1005-14.
69. Hattori K, Heissig B, Wu Y, Dias S, Tejada R, Ferris B, et al. Placental growth factor reconstitutes hematopoiesis by recruiting VEGFR1(+) stem cells from bone-marrow microenvironment. Nat Med 2002;8(8):841-9.
70. Folkman J, Klagsbrun M. Angiogenic factors. Science 1987;235(4787):442-7.
71. Folkman J. Angiogenesis in cancer, vascular, rheumatoid and other disease. Nat Med 1995;1(1):27-31.
72. Carmeliet P. Angiogenesis in health and disease. Nat Med 2003;9(6):653-60.
73. Rupnick M, Panigrahy D, Zhang C, Dallabrida S, Lowell B, Langer R, et al. Adipose tissue mass can be regulated through the vasculature. Proc Natl Acad Sci U S A 2002;99(16):10730-5.
74. Harada K, Lu S, Chisholm D, Syrjanen S, Schor A. Angiogenesis and vasodilation in skin warts. Association with HPV infection. Anticancer Res 2000;20(6B):4519-23.
75. Vikkula M, Boon L, Carraway Kr, Calvert J, Diamonti A, Goumnerov B, et al. Vascular dysmorphogenesis caused by an activating mutation in the receptor tyrosine kinase TIE2. Cell 1996;87(7):1181-90.
76. de ITJ. Alzheimer's disease: how does it start? J Alzheimers Dis 2002;4(6):497-512.
77. Van BE, Rivard A, Chen D, Silver M, Bunting S, Ferrara N, et al. Hypercholesterolemia attenuates angiogenesis but does not preclude augmentation by angiogenic cytokines. Circulation 1997;96(8):2667-74.
78. Boudier H. Arteriolar and capillary remodelling in hypertension. Drugs 1999;58 Spec No 1:37-40.
79. Krupinski J, Kaluza J, Kumar P, Kumar S, Wang J. Role of angiogenesis in patients with cerebral ischemic stroke. Stroke 1994;25(9):1794-8.

80. Waltenberger J. Impaired collateral vessel development in diabetes: potential cellular mechanisms and therapeutic implications. Cardiovasc Res 2001;49(3):554-60.
81. Martinez P, Esbrit P, Rodrigo A, Alvarez -AM, Martinez M. Age-related changes in parathyroid hormone-related protein and vascular endothelial growth factor in human osteoblastic cells. Osteoporos Int 2002;13(11):874-81.
82. Kimura H, Weisz A, Kurashima Y, Hashimoto K, Ogura T, D AF, et al. Hypoxia response element of the human vascular endothelial growth factor gene mediates transcriptional regulation by nitric oxide: control of hypoxia-inducible factor-1 activity by nitric oxide. Blood 2000;95(1):189-97.
83. Gale N, Yancopoulos G. Growth factors acting via endothelial cell-specific receptor tyrosine kinases: VEGFs, angiopoietins, and ephrins in vascular development. Genes Dev 1999;13(9):1055-66.
84. Maisonpierre P, Suri C, Jones P, Bartunkova S, Wiegand S, Radziejewski C, et al. Angiopoietin-2, a natural antagonist for Tie2 that disrupts in vivo angiogenesis. Science 1997;277(5322):55-60.
85. Nelson A, Fingleton B, Rothenberg M, Matrisian L. Matrix metalloproteinases: biologic activity and clinical implications. J Clin Oncol 2000;18(5):1135-49.
86. Kim I, Kim H, Moon S, Chae S, So J, Koh K, et al. Angiopoietin-1 induces endothelial cell sprouting through the activation of focal adhesion kinase and plasmin secretion. Circ Res 2000;86(9):952-9.
87. Pozzi A, Moberg P, Miles L, Wagner S, Soloway P, Gardner H. Elevated matrix metalloprotease and angiostatin levels in integrin alpha 1 knockout mice cause reduced tumor vascularization. Proc Natl Acad Sci U S A 2000;97(5):2202-7.
88. Carmeliet P. Fibroblast growth factor-1 stimulates branching and survival of myocardial arteries: a goal for therapeutic angiogenesis? Circ Res 2000;87(3):176-8.
89. Fredriksson L, Li H, Eriksson U. The PDGF family: four gene products form five dimeric isoforms. Cytokine Growth Factor Rev 2004;15(4):197-204.
90. Lindahl P, Hellstrom M, Kalen M, Betsholtz C. Endothelial-perivascular cell signaling in vascular development: lessons from knockout mice. Curr Opin Lipidol 1998;9(5):407-11.
91. Lindahl P, Bostrom H, Karlsson L, Hellstrom M, Kalen M, Betsholtz C. Role of platelet-derived growth factors in angiogenesis and alveogenesis. Curr Top Pathol 1999;93:27-33.
92. Hellstrom M, Gerhardt H, Kalen M, Li X, Eriksson U, Wolburg H, et al. Lack of pericytes leads to endothelial hyperplasia and abnormal vascular morphogenesis. J Cell Biol 2001;153(3):543-53.
93. Abramsson A, Berlin O, Papayan H, Paulin D, Shani M, Betsholtz C. Analysis of mural cell recruitment to tumor vessels. Circulation 2002;105(1):112-7.
94. Dinehart S, Kincannon J, Geronemus R. Hemangiomas: evaluation and treatment. Dermatol Surg 2001;27(5):475-85.
95. Richardson T, Peters M, Ennett A, Mooney D. Polymeric system for dual growth factor delivery. Nat Biotechnol 2001;19(11):1029-34.
96. Cao R, Brakenhielm E, Li X, Pietras K, Widenfalk J, Ostman A, et al. Angiogenesis stimulated by PDGF-CC, a novel member in the PDGF family, involves activation of PDGFR-alphaalpha and -alphabeta receptors. FASEB J 2002;16(12):1575-83.
97. Thurston G, Rudge J, Ioffe E, Zhou H, Ross L, Croll S, et al. Angiopoietin-1 protects the adult vasculature against plasma leakage. Nat Med 2000;6(4):460-3.

98. Carmeliet P. Mechanisms of angiogenesis and arteriogenesis. Nat Med 2000;6(4):389-95.
99. Conway E, Collen D, Carmeliet P. Molecular mechanisms of blood vessel growth. Cardiovasc Res 2001;49(3):507-21.
100. O RM, Holmgren L, Shing Y, Chen C, Rosenthal R, Moses M, et al. Angiostatin: a novel angiogenesis inhibitor that mediates the suppression of metastases by a Lewis lung carcinoma. Cell 1994;79(2):315-28.
101. O RM, Boehm T, Shing Y, Fukai N, Vasios G, Lane W, et al. Endostatin: an endogenous inhibitor of angiogenesis and tumor growth. Cell 1997;88(2):277-85.
102. Hirschi K, D AP. Pericytes in the microvasculature. Cardiovasc Res 1996;32(4):687-98.
103. Schaper W, Ito W. Molecular mechanisms of coronary collateral vessel growth. Circ Res 1996;79(5):911-9.
104. Schaper W PJ, Munoz-Chapuli R, Wolf C, Ito W. Collateral circulation of the heart. In: Ware JA SM, editor. Angiogenesis and cardiovascular disease. New York: Oxford:Oxford University Press; 1999. p. 159-198.
105. Pipp F, Boehm S, Cai W, Adili F, Ziegler B, Karanovic G, et al. Elevated fluid shear stress enhances postocclusive collateral artery growth and gene expression in the pig hind limb. Arterioscler Thromb Vasc Biol 2004;24(9):1664-8.
106. Szuba A, Skobe M, Karkkainen M, Shin W, Beynet D, Rockson N, et al. Therapeutic lymphangiogenesis with human recombinant VEGF-C. FASEB J 2002;16(14):1985-7.
107. Jeltsch M, Kaipainen A, Joukov V, Meng X, Lakso M, Rauvala H, et al. Hyperplasia of lymphatic vessels in VEGF-C transgenic mice. Science 1997;276(5317):1423-5.
108. Karpanen T, Egeblad M, Karkkainen M, Kubo H, Yla -HS, Jaattela M, et al. Vascular endothelial growth factor C promotes tumor lymphangiogenesis and intralymphatic tumor growth. Cancer Res 2001;61(5):1786-90.
109. Karkkainen M, Haiko P, Sainio K, Partanen J, Taipale J, Petrova T, et al. Vascular endothelial growth factor C is required for sprouting of the first lymphatic vessels from embryonic veins. Nat Immunol 2004;5(1):74-80.
110. Stacker S, Caesar C, Baldwin M, Thornton G, Williams R, Prevo R, et al. VEGF-D promotes the metastatic spread of tumor cells via the lymphatics. Nat Med 2001;7(2):186-91.
111. Tammela T, Saaristo A, Lohela M, Morisada T, Tornberg J, Norrmen C, et al. Angiopoietin-1 promotes lymphatic sprouting and hyperplasia. Blood 2005;105(12):4642-8.
112. Bjorndahl M, Cao R, Nissen LJ, Clasper S, Johnson LA, Xue Y, et al. Insulin-like growth factors 1 and 2 induce lymphangiogenesis in vivo. Proc Natl Acad Sci U S A 2005;102(43):15593-8.
113. Kajiya K, Hirakawa S, Ma B, Drinnenberg I, Detmar M. Hepatocyte growth factor promotes lymphatic vessel formation and function. EMBO J 2005;24(16):2885-95.
114. Breier G. Lymphangiogenesis in regenerating tissue: is VEGF-C sufficient? Circ Res 2005;96(11):1132-4.
115. Wang G, Jiang B, Rue E, Semenza G. Hypoxia-inducible factor 1 is a basic-helix-loop-helix-PAS heterodimer regulated by cellular O2 tension. Proc Natl Acad Sci U S A 1995;92(12):5510-4.
116. Wenger R. Cellular adaptation to hypoxia: O2-sensing protein hydroxylases, hypoxia-inducible transcription factors, and O2-regulated gene expression. FASEB J 2002;16(10):1151-62.

117. Makino Y, Cao R, Svensson K, Bertilsson G, Asman M, Tanaka H, et al. Inhibitory PAS domain protein is a negative regulator of hypoxia-inducible gene expression. Nature 2001;414(6863):550-4.
118. Semenza G. Hypoxia-inducible factor 1: master regulator of O2 homeostasis. Curr Opin Genet Dev 1998;8(5):588-94.
119. Leung D, Cachianes G, Kuang W, Goeddel D, Ferrara N. Vascular endothelial growth factor is a secreted angiogenic mitogen. Science 1989;246(4935):1306-9.
120. Veikkola T, Alitalo K. VEGFs, receptors and angiogenesis. Semin Cancer Biol 1999;9(3):211-20.
121. Ferrara N, Davis -ST. The biology of vascular endothelial growth factor. Endocr Rev 1997;18(1):4-25.
122. Ferrara N, Gerber H, LeCouter J. The biology of VEGF and its receptors. Nat Med 2003;9(6):669-76.
123. Ferrara N, Carver -MK, Chen H, Dowd M, Lu L, O SK, et al. Heterozygous embryonic lethality induced by targeted inactivation of the VEGF gene. Nature 1996;380(6573):439-42.
124. Carmeliet P, Ferreira V, Breier G, Pollefeyt S, Kieckens L, Gertsenstein M, et al. Abnormal blood vessel development and lethality in embryos lacking a single VEGF allele. Nature 1996;380(6573):435-9.
125. Ferrara N. Vascular endothelial growth factor: basic science and clinical progress. Endocr Rev 2004;25(4):581-611.
126. Shibuya M. Role of VEGF-flt receptor system in normal and tumor angiogenesis. Adv Cancer Res 1995;67:281-316.
127. Dimmeler S, Zeiher A. Akt takes center stage in angiogenesis signaling. Circ Res 2000;86(1):4-5.
128. Shweiki D, Itin A, Soffer D, Keshet E. Vascular endothelial growth factor induced by hypoxia may mediate hypoxia-initiated angiogenesis. Nature 1992;359(6398):843-5.
129. Dvorak H, Brown L, Detmar M, Dvorak A. Vascular permeability factor/vascular endothelial growth factor, microvascular hyperpermeability, and angiogenesis. Am J Pathol 1995;146(5):1029-39.
130. Houck K, Ferrara N, Winer J, Cachianes G, Li B, Leung D. The vascular endothelial growth factor family: identification of a fourth molecular species and characterization of alternative splicing of RNA. Mol Endocrinol 1991;5(12):1806-14.
131. Keyt B, Berleau L, Nguyen H, Chen H, Heinsohn H, Vandlen R, et al. The carboxyl-terminal domain (111-165) of vascular endothelial growth factor is critical for its mitogenic potency. J Biol Chem 1996;271(13):7788-95.
132. Soker S, Takashima S, Miao H, Neufeld G, Klagsbrun M. Neuropilin-1 is expressed by endothelial and tumor cells as an isoform-specific receptor for vascular endothelial growth factor. Cell 1998;92(6):735-45.
133. Park J, Keller G, Ferrara N. The vascular endothelial growth factor (VEGF) isoforms: differential deposition into the subepithelial extracellular matrix and bioactivity of extracellular matrix-bound VEGF. Mol Biol Cell 1993;4(12):1317-26.
134. Olofsson B, Pajusola K, Kaipainen A, von EG, Joukov V, Saksela O, et al. Vascular endothelial growth factor B, a novel growth factor for endothelial cells. Proc Natl Acad Sci U S A 1996;93(6):2576-81.
135. Olofsson B, Korpelainen E, Pepper M, Mandriota S, Aase K, Kumar V, et al. Vascular endothelial growth factor B (VEGF-B) binds to VEGF receptor-1 and regulates plasminogen activator activity in endothelial cells. Proc Natl Acad Sci U S A 1998;95(20):11709-14.

136. Silvestre J, Tamarat R, Ebrahimian T, Le -RA, Clergue M, Emmanuel F, et al. Vascular endothelial growth factor-B promotes in vivo angiogenesis. Circ Res 2003;93(2):114-23.
137. Joukov V, Pajusola K, Kaipainen A, Chilov D, Lahtinen I, Kukk E, et al. A novel vascular endothelial growth factor, VEGF-C, is a ligand for the Flt4 (VEGFR-3) and KDR (VEGFR-2) receptor tyrosine kinases. EMBO J 1996;15(7):1751.
138. Cao Y, Linden P, Farnebo J, Cao R, Eriksson A, Kumar V, et al. Vascular endothelial growth factor C induces angiogenesis in vivo. Proc Natl Acad Sci U S A 1998;95(24):14389-94.
139. Orlandini M, Marconcini L, Ferruzzi R, Oliviero S. Identification of a c-fos-induced gene that is related to the platelet-derived growth factor/vascular endothelial growth factor family. Proc Natl Acad Sci U S A 1996;93(21):11675-80.
140. Achen M, Jeltsch M, Kukk E, Makinen T, Vitali A, Wilks A, et al. Vascular endothelial growth factor D (VEGF-D) is a ligand for the tyrosine kinases VEGF receptor 2 (Flk1) and VEGF receptor 3 (Flt4). Proc Natl Acad Sci U S A 1998;95(2):548-53.
141. Lyttle D, Fraser K, Fleming S, Mercer A, Robinson A. Homologs of vascular endothelial growth factor are encoded by the poxvirus orf virus. J Virol 1994;68(1):84-92.
142. Maglione D, Guerriero V, Viglietto G, Delli -BP, Persico M. Isolation of a human placenta cDNA coding for a protein related to the vascular permeability factor. Proc Natl Acad Sci U S A 1991;88(20):9267-71.
143. Carmeliet P, Moons L, Luttun A, Vincenti V, Compernolle V, De MM, et al. Synergism between vascular endothelial growth factor and placental growth factor contributes to angiogenesis and plasma extravasation in pathological conditions. Nat Med 2001;7(5):575-83.
144. Luttun A, Tjwa M, Moons L, Wu Y, Angelillo -SA, Liao F, et al. Revascularization of ischemic tissues by PlGF treatment, and inhibition of tumor angiogenesis, arthritis and atherosclerosis by anti-Flt1. Nat Med 2002;8(8):831-40.
145. Pipp F, Heil M, Issbrucker K, Ziegelhoeffer T, Martin S, van dHJ, et al. VEGFR-1-selective VEGF homologue PlGF is arteriogenic: evidence for a monocyte-mediated mechanism. Circ Res 2003;92(4):378-85.
146. Folkman J. Tumor angiogenesis: therapeutic implications. N Engl J Med 1971;285(21):1182-6.
147. Shing Y, Folkman J, Sullivan R, Butterfield C, Murray J, Klagsbrun M. Heparin affinity: purification of a tumor-derived capillary endothelial cell growth factor. Science 1984;223(4642):1296-9.
148. Baffour R, Berman J, Garb J, Rhee S, Kaufman J, Friedmann P. Enhanced angiogenesis and growth of collaterals by in vivo administration of recombinant basic fibroblast growth factor in a rabbit model of acute lower limb ischemia: dose-response effect of basic fibroblast growth factor. J Vasc Surg 1992;16(2):181-91.
149. Pu L, Sniderman A, Brassard R, Lachapelle K, Graham A, Lisbona R, et al. Enhanced revascularization of the ischemic limb by angiogenic therapy. Circulation 1993;88(1):208-15.
150. Yanagisawa -MA, Uchida Y, Nakamura F, Tomaru T, Kido H, Kamijo T, et al. Salvage of infarcted myocardium by angiogenic action of basic fibroblast growth factor. Science 1992;257(5075):1401-3.
151. Isner J, Walsh K, Symes J, Pieczek A, Takeshita S, Lowry J, et al. Arterial gene transfer for therapeutic angiogenesis in patients with peripheral artery disease. Hum Gene Ther 1996;7(8):959-88.

152. Stein I, Neeman M, Shweiki D, Itin A, Keshet E. Stabilization of vascular endothelial growth factor mRNA by hypoxia and hypoglycemia and coregulation with other ischemia-induced genes. Mol Cell Biol 1995;15(10):5363-8.
153. Simons M, Bonow R, Chronos N, Cohen D, Giordano F, Hammond H, et al. Clinical trials in coronary angiogenesis: issues, problems, consensus: An expert panel summary. Circulation 2000;102(11):E73-86.
154. Daniel T, Fen Z. Distinct pathways mediate transcriptional regulation of platelet-derived growth factor B/c-sis expression. J Biol Chem 1988;263(36):19815-20.
155. Zhu G, Mallery S, Schwendeman S. Stabilization of proteins encapsulated in injectable poly (lactide-co-glycolide). Nat Biotechnol 2000;18(1):52-7.
156. Hosaka A, Koyama H, Kushibiki T, Tabata Y, Nishiyama N, Miyata T, et al. Gelatin hydrogel microspheres enable pinpoint delivery of basic fibroblast growth factor for the development of functional collateral vessels. Circulation 2004;110(21):3322-8.
157. Gu F, Amsden B, Neufeld R. Sustained delivery of vascular endothelial growth factor with alginate beads. J Control Release 2004;96(3):463-72.
158. Bonadio J. Tissue engineering via local gene delivery: update and future prospects for enhancing the technology. Adv Drug Deliv Rev 2000;44(2-3):185-94.
159. Cleland J, Duenas E, Park A, Daugherty A, Kahn J, Kowalski J, et al. Development of poly-(D,L-lactide--coglycolide) microsphere formulations containing recombinant human vascular endothelial growth factor to promote local angiogenesis. J Control Release 2001;72(1-3):13-24.
160. Davies N. Gene-activated matrix. In: Bowlin G, Wnek G, editors. Encyclopedia of Biomaterials and Biomedical Engineering. New York: Marcel Dekker Inc.; 2004. p. 662-669.
161. Bonadio J. Tissue engineering via local gene delivery. J Mol Med 2000;78(6):303-11.
162. Baumgartner I, Pieczek A, Manor O, Blair R, Kearney M, Walsh K, et al. Constitutive expression of phVEGF165 after intramuscular gene transfer promotes collateral vessel development in patients with critical limb ischemia. Circulation 1998;97(12):1114-23.
163. Bonadio J, Smiley E, Patil P, Goldstein S. Localized, direct plasmid gene delivery in vivo: prolonged therapy results in reproducible tissue regeneration. Nat Med 1999;5(7):753-9.
164. Ochiya T, Takahama Y, Nagahara S, Sumita Y, Hisada A, Itoh H, et al. New delivery system for plasmid DNA in vivo using atelocollagen as a carrier material: the Minipellet. Nat Med 1999;5(6):707-10.
165. Fang J, Zhu Y, Smiley E, Bonadio J, Rouleau J, Goldstein S, et al. Stimulation of new bone formation by direct transfer of osteogenic plasmid genes. Proc Natl Acad Sci U S A 1996;93(12):5753-8.
166. Brunner S, Sauer T, Carotta S, Cotten M, Saltik M, Wagner E. Cell cycle dependence of gene transfer by lipoplex, polyplex and recombinant adenovirus. Gene Ther 2000;7(5):401-7.
167. Bebok Z, Abai A, Dong J, King S, Kirk K, Berta G, et al. Efficiency of plasmid delivery and expression after lipid-mediated gene transfer to human cells in vitro. J Pharmacol Exp Ther 1996;279(3):1462-9.
168. Deng G, Nilsson I, Verdrengh M, Collins L, Tarkowski A. Intra-articularly localized bacterial DNA containing CpG motifs induces arthritis. Nat Med 1999;5(6):702-5.
169. Kay M, Glorioso J, Naldini L. Viral vectors for gene therapy: the art of turning infectious agents into vehicles of therapeutics. Nat Med 2001;7(1):33-40.

170. Kay M, Liu D, Hoogerbrugge P. Gene therapy. Proc Natl Acad Sci U S A 1997;94(24):12744-6.
171. Marshall E. Gene therapy. Second child in French trial is found to have leukemia. Science 2003;299(5605):320.
172. Mesri E, Federoff H, Brownlee M. Expression of vascular endothelial growth factor from a defective herpes simplex virus type 1 amplicon vector induces angiogenesis in mice. Circ Res 1995;76(2):161-7.
173. Yla -HS, Alitalo K. Gene transfer as a tool to induce therapeutic vascular growth. Nat Med 2003;9(6):694-701.
174. Yang Y, Nunes F, Berencsi K, Furth E, Gonczol E, Wilson J. Cellular immunity to viral antigens limits E1-deleted adenoviruses for gene therapy. Proc Natl Acad Sci U S A 1994;91(10):4407-11.
175. Lehrman S. Virus treatment questioned after gene therapy death. Nature 1999;401(6753):517-8.
176. Monahan P, Samulski R. AAV vectors: is clinical success on the horizon? Gene Ther 2000;7(1):24-30.
177. Xiao X, Li J, Samulski R. Efficient long-term gene transfer into muscle tissue of immunocompetent mice by adeno-associated virus vector. J Virol 1996;70(11):8098-108.
178. Summerford C, Samulski R. Viral receptors and vector purification: new approaches for generating clinical-grade reagents. Nat Med 1999;5(5):587-8.
179. Snyder R, Spratt S, Lagarde C, Bohl D, Kaspar B, Sloan B, et al. Efficient and stable adeno-associated virus-mediated transduction in the skeletal muscle of adult immunocompetent mice. Hum Gene Ther 1997;8(16):1891-900.
180. Su H, Lu R, Kan Y. Adeno-associated viral vector-mediated vascular endothelial growth factor gene transfer induces neovascular formation in ischemic heart. Proc Natl Acad Sci U S A 2000;97(25):13801-6.
181. Xiao W, Berta S, Lu M, Moscioni A, Tazelaar J, Wilson J. Adeno-associated virus as a vector for liver-directed gene therapy. J Virol 1998;72(12):10222-6.
182. Kaplitt M, Leone P, Samulski R, Xiao X, Pfaff D, O MK, et al. Long-term gene expression and phenotypic correction using adeno-associated virus vectors in the mammalian brain. Nat Genet 1994;8(2):148-54.
183. Herzog R, Yang E, Couto L, Hagstrom J, Elwell D, Fields P, et al. Long-term correction of canine hemophilia B by gene transfer of blood coagulation factor IX mediated by adeno-associated viral vector. Nat Med 1999;5(1):56-63.
184. Kay M, Manno C, Ragni M, Larson P, Couto L, McClelland A, et al. Evidence for gene transfer and expression of factor IX in haemophilia B patients treated with an AAV vector. Nat Genet 2000;24(3):257-61.
185. Williams D. Definitions in Biomaterials: Elsevier Science LTD.; 1987.
186. Lamba N, Woodhouse K, Cooper S. Polyurethanes in Biomedical Applications. Boca Raton: CRC Press; 1998.
187. Hoffman A. Hydrogels for biomedical applications. Adv Drug Deliv Rev 2002;54(1):3-12.
188. West J, Hubbell J. Polymeric biomaterials with degradation sites for proteases involved in cell migration. macromolecules 1999(32):241-4.
189. Jeong B, Bae Y, Lee D, Kim S. Biodegradable block copolymers as injectable drug-delivery systems. Nature 1997;388(6645):860-2.
190. Lee K, Mooney D. Hydrogels for tissue engineering. Chem Rev 2001;101(7):1869-79.
191. Lee C, Singla A, Lee Y. Biomedical applications of collagen. Int J Pharm 2001;221(1-2):1-22.
192. Zisch A, Lutolf M, Hubbell J. Biopolymeric delivery matrices for angiogenic growth factors. Cardiovasc Pathol 2003;12(6):295-310.

193. Shireman P, Greisler H. Fibrin sealant in vascular surgery: a review. J Long Term Eff Med Implants 1998;8(2):117-32.
194. Fasol R, Schumacher B, Schlaudraff K, Hauenstein K, Seitelberger R. Experimental use of a modified fibrin glue to induce site-directed angiogenesis from the aorta to the heart. J Thorac Cardiovasc Surg 1994;107(6):1432-9.
195. Bach A, Bannasch H, Galla T, Bittner K, Stark G. Fibrin glue as matrix for cultured autologous urothelial cells in urethral reconstruction. Tissue Eng 2001;7(1):45-53.
196. Andree C, Voigt M, Wenger A, Erichsen T, Bittner K, Schaefer D, et al. Plasmid gene delivery to human keratinocytes through a fibrin-mediated transfection system. Tissue Eng 2001;7(6):757-66.
197. Zisch A, Schenk U, Schense J, Sakiyama -ES, Hubbell J. Covalently conjugated VEGF--fibrin matrices for endothelialization. J Control Release 2001;72(1-3):101-13.
198. Deutsch M, Meinhart J, Vesely M, Fischlein T, Groscurth P, von OU, et al. In vitro endothelialization of expanded polytetrafluoroethylene grafts: a clinical case report after 41 months of implantation. J Vasc Surg 1997;25(4):757-63.
199. Smidsrod O, Skjak -BG. Alginate as immobilization matrix for cells. Trends Biotechnol 1990;8(3):71-8.
200. Peters M, Isenberg B, Rowley J, Mooney D. Release from alginate enhances the biological activity of vascular endothelial growth factor. J Biomater Sci Polym Ed 1998;9(12):1267-78.
201. Lee K, Yoon J, Lee J, Kim S, Jung H, Kim S, et al. Sustained release of vascular endothelial growth factor from calcium-induced alginate hydrogels reinforced by heparin and chitosan. Transplant Proc 2004;36(8):2464-5.
202. Drury J, Mooney D. Hydrogels for tissue engineering: scaffold design variables and applications. Biomaterials 2003;24(24):4337-51.
203. Lutolf M, Hubbell J. Synthetic biomaterials as instructive extracellular microenvironments for morphogenesis in tissue engineering. Nat Biotechnol 2005;23(1):47-55.
204. Harris L, Kim B, Mooney D. Open pore biodegradable matrices formed with gas foaming. J Biomed Mater Res 1998;42(3):396-402.
205. Sheridan M, Shea L, Peters M, Mooney D. Bioabsorbable polymer scaffolds for tissue engineering capable of sustained growth factor delivery. J Control Release 2000;64(1-3):91-102.
206. Kidane A, Szabocsik J, Park K. Accelerated study on lysozyme deposition on poly(HEMA) contact lenses. Biomaterials 1998;19(22):2051-5.
207. Oxley H, Corkhill P, Fitton J, Tighe B. Macroporous hydrogels for biomedical applications: methodology and morphology. Biomaterials 1993;14(14):1064-72.
208. Lu S, Anseth K. Photopolymerization of multilaminated poly(HEMA) hydrogels for controlled release. J Control Release 1999;57(3):291-300.
209. Meyvis T, De SS, Stubbe B, Hennink W, Demeester J. On the release of proteins from degrading dextran methacrylate hydrogels and the correlation with the rheologic properties of the hydrogels. Pharm Res 2001;18(11):1593-9.
210. Serres A, Baudys M, Kim S. Temperature and pH-sensitive polymers for human calcitonin delivery. Pharm Res 1996;13(2):196-201.
211. Kwon O, Kikuchi A, Yamato M, Sakurai Y, Okano T. Rapid cell sheet detachment from poly(N-isopropylacrylamide)-grafted porous cell culture membranes. J Biomed Mater Res 2000;50(1):82-9.
212. Orienti, Trere R, Zecchi V. Hydrogels formed by cross-linked polyvinylalcohol as colon-specific drug delivery systems. Drug Dev Ind Pharm 2001;27(8):877-84.

213. Taguchi T, Kishida A, Akashi M. Apatite formation on/in hydrogel matrices using an alternate soaking process: II. Effect of swelling ratios of poly(vinyl alcohol) hydrogel matrices on apatite formation. J Biomater Sci Polym Ed 1999;10(3):331-9.
214. Burczak K, Gamian E, Kochman A. Long-term in vivo performance and biocompatibility of poly(vinyl alcohol) hydrogel macrocapsules for hybrid-type artificial pancreas. Biomaterials 1996;17(24):2351-6.
215. Laurencin C, El -AS, Ibim S, Willoughby D, Attawia M, Allcock H, et al. A highly porous 3-dimensional polyphosphazene polymer matrix for skeletal tissue regeneration. J Biomed Mater Res 1996;30(2):133-8.
216. Carmen BM, Cohen S, Visscher K, Allcock H, Langer R. A novel synthetic method for hybridoma cell encapsulation. Biotechnology (N Y) 1991;9(5):468-71.
217. Sawhney A, Pathak C, van RJ, Dunn R, Hubbell J. Optimization of photopolymerized bioerodible hydrogel properties for adhesion prevention. J Biomed Mater Res 1994;28(7):831-8.
218. Lutolf M, Tirelli N, Cerritelli S, Cavalli L, Hubbell J. Systematic modulation of Michael-type reactivity of thiols through the use of charged amino acids. Bioconjug Chem 2001;12(6):1051-6.
219. West J, Hubbell J. Comparison of covalently and physically cross-linked polyethylene glycol-based hydrogels for the prevention of postoperative adhesions in a rat model. Biomaterials 1995;16(15):1153-6.
220. Mann B, West J. Cell adhesion peptides alter smooth muscle cell adhesion, proliferation, migration, and matrix protein synthesis on modified surfaces and in polymer scaffolds. J Biomed Mater Res 2002;60(1):86-93.
221. Lutolf M, Lauer -FJ, Schmoekel H, Metters A, Weber F, Fields G, et al. Synthetic matrix metalloproteinase-sensitive hydrogels for the conduction of tissue regeneration: engineering cell-invasion characteristics. Proc Natl Acad Sci U S A 2003;100(9):5413-8.
222. Lutolf M, Weber F, Schmoekel H, Schense J, Kohler T, Muller R, et al. Repair of bone defects using synthetic mimetics of collagenous extracellular matrices. Nat Biotechnol 2003;21(5):513-8.
223. Zisch A, Lutolf M, Ehrbar M, Raeber G, Rizzi S, Davies N, et al. Cell-demanded release of VEGF from synthetic, biointeractive cell ingrowth matrices for vascularized tissue growth. FASEB J 2003;17(15):2260-2.
224. Bayer O. The diisocyanate polyaddition process (polyurethanes). Description of a new principle for builing up high-molecular compounds. Angewandte Chemie 1937;A 59:257.
225. Auerbach R, Lewis R, Shinners B, Kubai L, Akhtar N. Angiogenesis assays: a critical overview. Clin Chem 2003;49(1):32-40.
226. Staton C, Stribbling S, Tazzyman S, Hughes R, Brown N, Lewis C. Current methods for assaying angiogenesis in vitro and in vivo. Int J Exp Pathol 2004;85(5):233-48.
227. Freshney RI. Culture of Animal Cells. 3rd edn. ed. New York: Wiley-Lisds.; 1994.
228. Alessandri G, Raju K, Gullino P. Mobilization of capillary endothelium in vitro induced by effectors of angiogenesis in vivo. Cancer Res 1983;43(4):1790-7.
229. Zetter B. Assay of capillary endothelial cell migration. Methods Enzymol 1987;147:135-44.
230. Pepper M, Belin D, Montesano R, Orci L, Vassalli J. Transforming growth factor-beta 1 modulates basic fibroblast growth factor-induced proteolytic and angiogenic properties of endothelial cells in vitro. J Cell Biol 1990;111(2):743-55.

231. Lawley T, Kubota Y. Induction of morphologic differentiation of endothelial cells in culture. J Invest Dermatol 1989;93(2 Suppl):59S-61S.
232. Zimrin A, Villeponteau B, Maciag T. Models of in vitro angiogenesis: endothelial cell differentiation on fibrin but not matrigel is transcriptionally dependent. Biochem Biophys Res Commun 1995;213(2):630-8.
233. Donovan D, Brown N, Bishop E, Lewis C. Comparison of three in vitro human 'angiogenesis' assays with capillaries formed in vivo. Angiogenesis 2001;4(2):113-21.
234. Nicosia R, Ottinetti A. Growth of microvessels in serum-free matrix culture of rat aorta. A quantitative assay of angiogenesis in vitro. Lab Invest 1990;63(1):115-22.
235. Jung S, Siegrist B, Wade M, Anthony C, Woltering E. Inhibition of human angiogenesis with heparin and hydrocortisone. Angiogenesis 2001;4(3):175-86.
236. Deckers M, van dPG, Dooijewaard S, Kroon M, van HV, Papapoulos S, et al. Effect of angiogenic and antiangiogenic compounds on the outgrowth of capillary structures from fetal mouse bone explants. Lab Invest 2001;81(1):5-15.
237. Liekens S, De CE, Neyts J. Angiogenesis: regulators and clinical applications. Biochem Pharmacol 2001;61(3):253-70.
238. Nguyen M, Shing Y, Folkman J. Quantitation of angiogenesis and antiangiogenesis in the chick embryo chorioallantoic membrane. Microvasc Res 1994;47(1):31-40.
239. Auerbach R, Kubai L, Knighton D, Folkman J. A simple procedure for the long-term cultivation of chicken embryos. Dev Biol 1974;41(2):391-4.
240. Fuchs A, Lindenbaum E. The two- and three-dimensional structure of the microcirculation of the chick chorioallantoic membrane. Acta Anat (Basel) 1988;131(4):271-5.
241. Taylor CM, Weiss JB. The chick vitelline membrane as a test system for angiogenesis and antiangiogenesis. Int. J. microsurc. clin. exp. 1984;3:337.
242. Gimbrone MJ, Cotran R, Leapman S, Folkman J. Tumor growth and neovascularization: an experimental model using the rabbit cornea. J Natl Cancer Inst 1974;52(2):413-27.
243. Muthukkaruppan V, Auerbach R. Angiogenesis in the mouse cornea. Science 1979;205(4413):1416-8.
244. Kenyon B, Voest E, Chen C, Flynn E, Folkman J, D AR. A model of angiogenesis in the mouse cornea. Invest Ophthalmol Vis Sci 1996;37(8):1625-32.
245. Jain R, Schlenger K, Hockel M, Yuan F. Quantitative angiogenesis assays: progress and problems. Nat Med 1997;3(11):1203-8.
246. Hu D, Hiley C, Smither R, Gresham G, Fan T. Correlation of 133Xe clearance, blood flow and histology in the rat sponge model for angiogenesis. Further studies with angiogenic modifiers. Lab Invest 1995;72(5):601-10.
247. Plunkett M, Hailey J. An in vivo quantitative angiogenesis model using tumor cells entrapped in alginate. Lab Invest 1990;62(4):510-7.
248. Dellian M, Witwer B, Salehi H, Yuan F, Jain R. Quantitation and physiological characterization of angiogenic vessels in mice: effect of basic fibroblast growth factor, vascular endothelial growth factor/vascular permeability factor, and host microenvironment. Am J Pathol 1996;149(1):59-71.
249. Passaniti A, Taylor R, Pili R, Guo Y, Long P, Haney J, et al. A simple, quantitative method for assessing angiogenesis and antiangiogenic agents using reconstituted basement membrane, heparin, and fibroblast growth factor. Lab Invest 1992;67(4):519-28.

250. Shea L, Smiley E, Bonadio J, Mooney D. DNA delivery from polymer matrices for tissue engineering. Nat Biotechnol 1999;17(6):551-4.
251. Chandler L, Doukas J, Gonzalez A, Hoganson D, Gu D, Ma C, et al. FGF2-Targeted adenovirus encoding platelet-derived growth factor-B enhances de novo tissue formation. Mol Ther 2000;2(2):153-60.
252. Matsushita T, Elliger S, Elliger C, Podsakoff G, Villarreal L, Kurtzman G, et al. Adeno-associated virus vectors can be efficiently produced without helper virus. Gene Ther 1998;5(7):938-45.
253. Xiao X, Li J, Samulski R. Production of high-titer recombinant adeno-associated virus vectors in the absence of helper adenovirus. J Virol 1998;72(3):2224-32.
254. Auricchio A, Hildinger M, O CE, Gao G, Wilson J. Isolation of highly infectious and pure adeno-associated virus type 2 vectors with a single-step gravity-flow column. Hum Gene Ther 2001;12(1):71-6.
255. Mercer EH, Hoyle GW, Kapur RP, Brinster RL, Palmiter RD. The dopamine beta-hydroxylase gene promoter directs expression of E. coli lacZ to sympathetic and other neurons in adult transgenic mice. Neuron 1991;7(5):703-16.
256. Shimpo M, Ikeda U, Maeda Y, Takahashi M, Miyashita H, Mizukami H, et al. AAV-mediated VEGF gene transfer into skeletal muscle stimulates angiogenesis and improves blood flow in a rat hindlimb ischemia model. Cardiovasc Res 2002;53(4):993-1001.
257. Gamble M, Wilson I. The Hemantoxylins and Eosin. In: Bankroft JD, Gamble M, editors. Theory and Practice of Histological Techniques. London: Churchill Livingstone; 2002. p. 125-139.
258. Rohr U, Wulf M, Stahn S, Steidl U, Haas R, Kronenwett R. Fast and reliable titration of recombinant adeno-associated virus type-2 using quantitative real-time PCR. J Virol Methods 2002;106(1):81-8.
259. Summerford C, Samulski R. Membrane-associated heparan sulfate proteoglycan is a receptor for adeno-associated virus type 2 virions. J Virol 1998;72(2):1438-45.
260. Richter M, Iwata A, Nyhuis J, Nitta Y, Miller A, Halbert C, et al. Adeno-associated virus vector transduction of vascular smooth muscle cells in vivo. Physiol Genomics 2000;2(3):117-27.
261. Wang Z, Ma H, Li J, Sun L, Zhang J, Xiao X. Rapid and highly efficient transduction by double-stranded adeno-associated virus vectors in vitro and in vivo. Gene Ther 2003;10(26):2105-11.
262. Doukas J, Chandler L, Gonzalez A, Gu D, Hoganson D, Ma C, et al. Matrix immobilization enhances the tissue repair activity of growth factor gene therapy vectors. Hum Gene Ther 2001;12(7):783-98.
263. Jooss K, Yang Y, Fisher K, Wilson J. Transduction of dendritic cells by DNA viral vectors directs the immune response to transgene products in muscle fibers. J Virol 1998;72(5):4212-23.
264. Gao G, Qu G, Burnham M, Huang J, Chirmule N, Joshi B, et al. Purification of recombinant adeno-associated virus vectors by column chromatography and its performance in vivo. Hum Gene Ther 2000;11(15):2079-91.
265. Zolotukhin S, Byrne B, Mason E, Zolotukhin I, Potter M, Chesnut K, et al. Recombinant adeno-associated virus purification using novel methods improves infectious titer and yield. Gene Ther 1999;6(6):973-85.
266. Bacilious N, Kulber D, Peters E, Gayle L, Chen M, Harper A, et al. Harvesting of the latissimus dorsi muscle: a small animal model for seroma formation. Microsurgery 1995;16(9):646-9.
267. Fisher K, Jooss K, Alston J, Yang Y, Haecker S, High K, et al. Recombinant adeno-associated virus for muscle directed gene therapy. Nat Med 1997;3(3):306-12.

268. Deodato B, Arsic N, Zentilin L, Galeano M, Santoro D, Torre V, et al. Recombinant AAV vector encoding human VEGF165 enhances wound healing. Gene Ther 2002;9(12):777-85.
269. Galeano M, Deodato B, Altavilla D, Cucinotta D, Arsic N, Marini H, et al. Adeno-associated viral vector-mediated human vascular endothelial growth factor gene transfer stimulates angiogenesis and wound healing in the genetically diabetic mouse. Diabetologia 2003;46:546-555.
270. Galeano M, Deodato B, Altavilla D, Squadrito G, Seminara P, Marini H, et al. Effect of recombinant adeno-associated virus vector-mediated vascular endothelial growth factor gene transfer on wound healing after burn injury. Crit Care Med 2003;31(4):1017-25.
271. Paterna J, Bueler H. Recombinant adeno-associated virus vector design and gene expression in the mammalian brain. Methods 2002;28(2):208-18.
272. Nicklin S, Buening H, Dishart K, de AM, Girod A, Hacker U, et al. Efficient and selective AAV2-mediated gene transfer directed to human vascular endothelial cells. Mol Ther 2001;4(3):174-81.
273. Pajusola K, Gruchala M, Joch H, Luscher T, Yla -HS, Bueler H. Cell-type-specific characteristics modulate the transduction efficiency of adeno-associated virus type 2 and restrain infection of endothelial cells. J Virol 2002;76(22):11530-40.
274. Hansen J, Qing K, Kwon H, Mah C, Srivastava A. Impaired intracellular trafficking of adeno-associated virus type 2 vectors limits efficient transduction of murine fibroblasts. J Virol 2000;74(2):992-6.
275. Qing K, Mah C, Hansen J, Zhou S, Dwarki V, Srivastava A. Human fibroblast growth factor receptor 1 is a co-receptor for infection by adeno-associated virus 2. Nat Med 1999;5(1):71-7.
276. Summerford C, Bartlett J, Samulski R. AlphaVbeta5 integrin: a co-receptor for adeno-associated virus type 2 infection. Nat Med 1999;5(1):78-82.
277. Denby L, Nicklin S, Baker A. Adeno-associated virus (AAV)-7 and -8 poorly transduce vascular endothelial cells and are sensitive to proteasomal degradation. Gene Ther 2005;12(20):1534-8.
278. Virella -LI, Poirier A, Chesnut K, Brantly M, Flotte T. Inhibition of recombinant adeno-associated virus (rAAV) transduction by bronchial secretions from cystic fibrosis patients. Gene Ther 2000;7(20):1783-9.
279. White S, Nicklin S, Buning H, Brosnan M, Leike K, Papadakis E, et al. Targeted gene delivery to vascular tissue in vivo by tropism-modified adeno-associated virus vectors. Circulation 2004;109(4):513-9.
280. Buning H, Braun -FM, Hallek M. Progress in the use of adeno-associated viral vectors for gene therapy. Cells Tissues Organs 2004;177(3):139-50.
281. Sasisekharan R, Venkataraman G. Heparin and heparan sulfate: biosynthesis, structure and function. Curr Opin Chem Biol 2000;4(6):626-31.
282. McLean J. The thromboplastic action of cephalin. Am J Physiol 1916;41:250-257.
283. Petitou M, Herault J, Bernat A, Driguez P, Duchaussoy P, Lormeau J, et al. Synthesis of thrombin-inhibiting heparin mimetics without side effects. Nature 1999;398(6726):417-22.
284. Perrimon N, Bernfield M. Specificities of heparan sulphate proteoglycans in developmental processes. Nature 2000;404(6779):725-8.
285. Chen Y, Maguire T, Hileman R, Fromm J, Esko J, Linhardt R, et al. Dengue virus infectivity depends on envelope protein binding to target cell heparan sulfate. Nat Med 1997;3(8):866-71.
286. Folkman J, Shing Y. Control of angiogenesis by heparin and other sulfated polysaccharides. Adv Exp Med Biol 1992;313:355-64.

287. Folkman J, Langer R, Linhardt R, Haudenschild C, Taylor S. Angiogenesis inhibition and tumor regression caused by heparin or a heparin fragment in the presence of cortisone. Science 1983;221(4612):719-25.
288. Soker S, Goldstaub D, Svahn C, Vlodavsky I, Levi B, Neufeld G. Variations in the size and sulfation of heparin modulate the effect of heparin on the binding of VEGF165 to its receptors. Biochem Biophys Res Commun 1994;203(2):1339-47.
289. Kan M, Wang F, Xu J, Crabb J, Hou J, McKeehan W. An essential heparin-binding domain in the fibroblast growth factor receptor kinase. Science 1993;259(5103):1918-21.
290. Marikovsky M, Breuing K, Liu P, Eriksson E, Higashiyama S, Farber P, et al. Appearance of heparin-binding EGF-like growth factor in wound fluid as a response to injury. Proc Natl Acad Sci U S A 1993;90(9):3889-93.
291. Chen B, Arakawa T. Stabilization of recombinant human keratinocyte growth factor by osmolytes and salts. J Pharm Sci 1996;85(4):419-26.
292. McCaffrey T, Falcone D, Vicente D, Du B, Consigli S, Borth W. Protection of transforming growth factor-beta 1 activity by heparin and fucoidan. J Cell Physiol 1994;159(1):51-9.
293. Simons M, Horowitz A. Syndecan-4-mediated signalling. Cell Signal 2001;13(12):855-62.
294. Ashikari-Hada S, Habuchi H, Kariya Y, Kimata K. Heparin regulates vascular endothelial growth factor165-dependent mitogenic activity, tube formation, and its receptor phosphorylation of human endothelial cells. Comparison of the effects of heparin and modified heparins. J Biol Chem 2005;280(36):31508-15.
295. Wissink M, Beernink R, Pieper J, Poot A, Engbers G, Beugeling T, et al. Binding and release of basic fibroblast growth factor from heparinized collagen matrices. Biomaterials 2001;22(16):2291-9.
296. Pieper J, Hafmans T, van WP, van LM, Brouwer L, Veerkamp J, et al. Loading of collagen-heparan sulfate matrices with bFGF promotes angiogenesis and tissue generation in rats. J Biomed Mater Res 2002;62(2):185-94.
297. Tabata Y, Miyao M, Ozeki M, Ikada Y. Controlled release of vascular endothelial growth factor by use of collagen hydrogels. J Biomater Sci Polym Ed 2000;11(9):915-30.
298. Tanihara M, Suzuki Y, Yamamoto E, Noguchi A, Mizushima Y. Sustained release of basic fibroblast growth factor and angiogenesis in a novel covalently crosslinked gel of heparin and alginate. J Biomed Mater Res 2001;56(2):216-21.
299. Sakiyama -ES, Hubbell J. Development of fibrin derivatives for controlled release of heparin-binding growth factors. J Control Release 2000;65(3):389-402.
300. Knighton D, Hunt T, Scheuenstuhl H, Halliday B, Werb Z, Banda M. Oxygen tension regulates the expression of angiogenesis factor by macrophages. Science 1983;221(4617):1283-5.
301. Kuwabara K, Ogawa S, Matsumoto M, Koga S, Clauss M, Pinsky D, et al. Hypoxia-mediated induction of acidic/basic fibroblast growth factor and platelet-derived growth factor in mononuclear phagocytes stimulates growth of hypoxic endothelial cells. Proc Natl Acad Sci U S A 1995;92(10):4606-10.
302. Kourembanas S, Hannan R, Faller D. Oxygen tension regulates the expression of the platelet-derived growth factor-B chain gene in human endothelial cells. J Clin Invest 1990;86(2):670-4.
303. Krikun G, Schatz F, Finlay T, Kadner S, Mesia A, Gerrets R, et al. Expression of angiopoietin-2 by human endometrial endothelial cells:

regulation by hypoxia and inflammation. Biochem Biophys Res Commun 2000;275(1):159-63.
304. Mandriota S, Pepper M. Regulation of angiopoietin-2 mRNA levels in bovine microvascular endothelial cells by cytokines and hypoxia. Circ Res 1998;83(8):852-9.
305. Minchenko A, Bauer T, Salceda S, Caro J. Hypoxic stimulation of vascular endothelial growth factor expression in vitro and in vivo. Lab Invest 1994;71(3):374-9.
306. Marti H, Risau W. Systemic hypoxia changes the organ-specific distribution of vascular endothelial growth factor and its receptors. Proc Natl Acad Sci U S A 1998;95(26):15809-14.
307. Diemer K, Henn R. Kapillarvermehrung in der hirnrinde der ratte unter chronischem sauerstoffmangel. Die Natur 1965;52:135-136.
308. Harik S, Hritz M, LaManna J. Hypoxia-induced brain angiogenesis in the adult rat. J Physiol 1995;485 (Pt 2):525-30.
309. LaManna J, Vendel L, Farrell R. Brain adaptation to chronic hypobaric hypoxia in rats. J Appl Physiol 1992;72(6):2238-43.
310. Boero J, Ascher J, Arregui A, Rovainen C, Woolsey T. Increased brain capillaries in chronic hypoxia. J Appl Physiol 1999;86(4):1211-9.
311. Smith K, Marshall J. Physiological adjustments and arteriolar remodelling within skeletal muscle during acclimation to chronic hypoxia in the rat. J Physiol 1999;521 Pt 1:261-72.
312. Howell K, Preston R, McLoughlin P. Chronic hypoxia causes angiogenesis in addition to remodelling in the adult rat pulmonary circulation. J Physiol 2003;547(Pt 1):133-45.
313. Beckstead J. A simple technique for preservation of fixation-sensitive antigens in paraffin-embedded tissues. J Histochem Cytochem 1994;42(8):1127-34.
314. Fujita M, Ishihara M, Simizu M, Obara K, Ishizuka T, Saito Y, et al. Vascularization in vivo caused by the controlled release of fibroblast growth factor-2 from an injectable chitosan/non-anticoagulant heparin hydrogel. Biomaterials 2004;25(4):699-706.
315. Ishihara M, Obara K, Ishizuka T, Fujita M, Sato M, Masuoka K, et al. Controlled release of fibroblast growth factors and heparin from photocrosslinked chitosan hydrogels and subsequent effect on in vivo vascularization. J Biomed Mater Res 2003;64A(3):551-9.
316. Doi K, Matsuda T. Enhanced vascularization in a microporous polyurethane graft impregnated with basic fibroblast growth factor and heparin. J Biomed Mater Res 1997;34(3):361-70.
317. Masuda S, Doi K, Satoh S, Oka T, Matsuda T. Vascular endothelial growth factor enhances vascularization in microporous small caliber polyurethane grafts. ASAIO J 1997;43(5):M530-4.
318. Steffens G, Yao C, Prevel P, Markowicz M, Schenck P, Noah E, et al. Modulation of angiogenic potential of collagen matrices by covalent incorporation of heparin and loading with vascular endothelial growth factor. Tissue Eng 2004;10(9-10):1502-9.
319. Chen RR, Silva EA, Yuen WW, Mooney DJ. Spatio-temporal VEGF and PDGF Delivery Patterns Blood Vessel Formation and Maturation. Pharm Res 2006.
320. Cao R, Brakenhielm E, Pawliuk R, Wariaro D, Post M, Wahlberg E, et al. Angiogenic synergism, vascular stability and improvement of hind-limb ischemia by a combination of PDGF-BB and FGF-2. Nat Med 2003;9(5):604-13.
321. Baumgartner I, Isner J. Stimulation of peripheral angiogenesis by vascular endothelial growth factor (VEGF). Vasa 1998;27(4):201-6.

322. Lindahl P, Johansson BR, Leveen P, Betsholtz C. Pericyte loss and microaneurysm formation in PDGF-B-deficient mice. Science 1997;277(5323):242-5.
323. Heldin CH, Westermark B. Mechanism of action and in vivo role of platelet-derived growth factor. Physiol Rev 1999;79(4):1283-316.
324. Abramsson A, Lindblom P, Betsholtz C. Endothelial and nonendothelial sources of PDGF-B regulate pericyte recruitment and influence vascular pattern formation in tumors. J Clin Invest 2003;112(8):1142-51.
325. Benjamin LE, Hemo I, Keshet E. A plasticity window for blood vessel remodelling is defined by pericyte coverage of the preformed endothelial network and is regulated by PDGF-B and VEGF. Development 1998;125(9):1591-8.
326. Benjamin LE, Golijanin D, Itin A, Pode D, Keshet E. Selective ablation of immature blood vessels in established human tumors follows vascular endothelial growth factor withdrawal. J Clin Invest 1999;103(2):159-65.
327. Alon T, Hemo I, Itin A, Pe eJ, Stone J, Keshet E. Vascular endothelial growth factor acts as a survival factor for newly formed retinal vessels and has implications for retinopathy of prematurity. Nat Med 1995;1(10):1024-8.
328. Baffert F, Le T, Sennino B, Thurston G, Kuo CJ, Hu-Lowe D, et al. Cellular changes in normal blood capillaries undergoing regression after inhibition of VEGF signaling. Am J Physiol Heart Circ Physiol 2006;290(2):H547-59.
329. Li H, Fredriksson L, Li X, Eriksson U. PDGF-D is a potent transforming and angiogenic growth factor. Oncogene 2003;22(10):1501-10.
330. Brown DM, Hong SP, Farrell CL, Pierce GF, Khouri RK. Platelet-derived growth factor BB induces functional vascular anastomoses in vivo. Proc Natl Acad Sci U S A 1995;92(13):5920-4.
331. Betsholtz C. Insight into the physiological functions of PDGF through genetic studies in mice. Cytokine Growth Factor Rev 2004;15(4):215-28.
332. Humphries D, Lee S, Fanburg B, Silbert J. Effects of hypoxia and hyperoxia on proteoglycan production by bovine pulmonary artery endothelial cells. J Cell Physiol 1986;126(2):249-53.
333. Kittlick PD. Hypoxia in fibroblast cultures. 3. 35S-sulfate incorporation into acid mucopolysaccharides as influenced by 5% O2 hypoxia with simultaneous changes in the lactate-and H-ion concentrations. Exp Pathol (Jena) 1977;13(4-5):213-6.
334. Ruscher K, Isaev N, Trendelenburg G, Weih M, Iurato L, Meisel A, et al. Induction of hypoxia inducible factor 1 by oxygen glucose deprivation is attenuated by hypoxic preconditioning in rat cultured neurons. Neurosci Lett 1998;254(2):117-20.
335. Levy A. A cellular paradigm for the failure to increase vascular endothelial growth factor in chronically hypoxic states. Coron Artery Dis 1999;10(6):427-30.
336. Gordillo G, Sen C. Revisiting the essential role of oxygen in wound healing. Am J Surg 2003;186(3):259-63.
337. Snyder GK, Wilcox EE, Burnham EW. Effects of hypoxia on muscle capillarity in rats. Respir Physiol 1985;62(1):135-40.
338. Sillau AH, Banchero N. Effects of hypoxia on capillary density and fiber composition in rat skeletal muscle. Pflugers Arch 1977;370(3):227-32.
339. Lundby C, Pilegaard H, Andersen J, van HG, Sander M, Calbet J. Acclimatization to 4100 m does not change capillary density or mRNA expression of potential angiogenesis regulatory factors in human skeletal muscle. J Exp Biol 2004;207(Pt 22):3865-71.
340. Ninikoski J, Heughan C, Hunt T. Oxygen and carbon dioxide tensions in experimental wounds. Surg Gynecol Obstet 1971;133(6):1003-7.

341. Chang N, Goodson Wr, Gottrup F, Hunt T. Direct measurement of wound and tissue oxygen tension in postoperative patients. Ann Surg 1983;197(4):470-8.
342. Haroon Z, Raleigh J, Greenberg C, Dewhirst M. Early wound healing exhibits cytokine surge without evidence of hypoxia. Ann Surg 2000;231(1):137-47.
343. Howdieshell T, Riegner C, Gupta V, Callaway D, Grembowicz K, Sathyanarayana, et al. Normoxic wound fluid contains high levels of vascular endothelial growth factor. Ann Surg 1998;228(5):707-15.
344. Knighton D, Silver I, Hunt T. Regulation of wound-healing angiogenesis-effect of oxygen gradients and inspired oxygen concentration. Surgery 1981;90(2):262-70.
345. Gibson J, Angeles A, Hunt T. Increased Oxygen Tension Potentiates Angiogenesis. Surgical Forum 1997;48:696-699.
346. Sheikh A, Gibson J, Rollins M, Hopf H, Hussain Z, Hunt T. Effect of hyperoxia on vascular endothelial growth factor levels in a wound model. Arch Surg 2000;135(11):1293-7.
347. Roy S, Khanna S, Nallu K, Hunt TK, Sen CK. Dermal wound healing is subject to redox control. Mol Ther 2006;13(1):211-20.
348. Sen C, Khanna S, Babior B, Hunt T, Ellison E, Roy S. Oxidant-induced vascular endothelial growth factor expression in human keratinocytes and cutaneous wound healing. J Biol Chem 2002;277(36):33284-90.
349. Niinikoski J. Effect of oxygen supply on wound healing and formation of experimental granulation tissue. Acta Physiol Scand Suppl 1969;334:1-72.
350. Roguin A, Avivi A, Nitecki S, Rubinstein I, Levy N, Abassi Z, et al. Restoration of blood flow by using continuous perimuscular infiltration of plasmid DNA encoding subterranean mole rat Spalax ehrenbergi VEGF. Proc Natl Acad Sci U S A 2003;100(8):4644-8.
351. Sellke F, Wang S, Friedman M, Dai H, Harada K, Lopez J, et al. Beta-adrenergic modulation of the collateral-dependent coronary microcirculation. J Surg Res 1995;59(1):185-90.
352. Efron D, Most D, Shi H, Tantry U, Barbul A. A novel method of studying wound healing. J Surg Res 2001;98(1):16-20.
353. Croll SD, Ransohoff RM, Cai N, Zhang Q, Martin FJ, Wei T, et al. VEGF-mediated inflammation precedes angiogenesis in adult brain. Exp Neurol 2004;187(2):388-402.
354. Ozawa CR, Banfi A, Glazer NL, Thurston G, Springer ML, Kraft PE, et al. Microenvironmental VEGF concentration, not total dose, determines a threshold between normal and aberrant angiogenesis. J Clin Invest 2004;113(4):516-27.
355. Ward W, Quinn M, Wood M, Tiekotter K, Pidikiti S, Gallagher J. Vascularizing the tissue surrounding a model biosensor: how localized is the effect of a subcutaneous infusion of vascular endothelial growth factor (VEGF)? Biosens Bioelectron 2003;19(3):155-63.
356. Lee H, Cusick R, Browne F, Ho KT, Ma P, Utsunomiya H, et al. Local delivery of basic fibroblast growth factor increases both angiogenesis and engraftment of hepatocytes in tissue-engineered polymer devices. Transplantation 2002;73(10):1589-93.
357. Perets A, Baruch Y, Weisbuch F, Shoshany G, Neufeld G, Cohen S. Enhancing the vascularization of three-dimensional porous alginate scaffolds by incorporating controlled release basic fibroblast growth factor microspheres. J Biomed Mater Res 2003;65A(4):489-97.
358. Patel Z, Mikos A. Angiogenesis with biomaterial-based drug- and cell-delivery systems. J Biomater Sci Polym Ed 2004;15(6):701-26.

359. Hashizume H, Baluk P, Morikawa S, McLean J, Thurston G, Roberge S, et al. Openings between defective endothelial cells explain tumor vessel leakiness. Am J Pathol 2000;156(4):1363-80.
360. Bowman W. On the structure and use of the malpighian bodies of the kidney with observations on the circulation through that gland. Phil Trans Roy Soc (London) 1842;Part I(132):57-80.
361. Lametschwandtner A, Lametschwandtner U, Weiger T. Scanning electron microscopy of vascular corrosion casts--technique and applications. In: Scan Electron Microsc; 1984; UNITED STATES; 1984. p. 663-95.
362. Alroy J, Goyal V, Skutelsky E. Lectin histochemistry of mammalian endothelium. Histochemistry 1987;86(6):603-7.
363. Couffinhal T, Silver M, Zheng L, Kearney M, Witzenbichler B, Isner J. Mouse model of angiogenesis. Am J Pathol 1998;152(6):1667-79.
364. Scholz D, Ziegelhoeffer T, Helisch A, Wagner S, Friedrich C, Podzuweit T, et al. Contribution of arteriogenesis and angiogenesis to postocclusive hindlimb perfusion in mice. J Mol Cell Cardiol 2002;34(7):775-87.
365. Fleischer A, Wojcicki W, Donnelly E, Pickens D, Thirsk G, Thurman G, et al. Quantified color Doppler sonography of tumor vascularity in an animal model. J Ultrasound Med 1999;18(8):547-51.
366. Kobayashi H, Sato N, Hiraga A, Saga T, Nakamoto Y, Ueda H, et al. 3D-micro-MR angiography of mice using macromolecular MR contrast agents with polyamidoamine dendrimer core with reference to their pharmacokinetic properties. Magn Reson Med 2001;45(3):454-60.
367. Budinger T. PET instrumentation: what are the limits? Semin Nucl Med 1998;28(3):247-67.
368. Feldkamp L, Goldstein S, Parfitt A, Jesion G, Kleerekoper M. The direct examination of three-dimensional bone architecture in vitro by computed tomography. J Bone Miner Res 1989;4(1):3-11.
369. Garcia -SA, Rodriguez -BA, Bentley M, Ritman E, Romero J. Three-dimensional microcomputed tomography of renal vasculature in rats. Hypertension 1998;31(1 Pt 2):440-4.
370. Jorgensen S, Demirkaya O, Ritman E. Three-dimensional imaging of vasculature and parenchyma in intact rodent organs with X-ray micro-CT. Am J Physiol 1998;275(3 Pt 2):H1103-14.
371. Lerman A, Ritman E. Evaluation of microvascular anatomy by micro-CT. Herz 1999;24(7):531-3.
372. Beighley P, Thomas P, Jorgensen S, Ritman E. 3D architecture of myocardial microcirculation in intact rat heart: a study with micro-CT. Adv Exp Med Biol 1997;430:165-75.
373. Johnson R, Hu H, Haworth S, Cho P, Dawson C, Linehan J. Feldkamp and circle-and-line cone-beam reconstruction for 3D micro-CT of vascular networks. Phys Med Biol 1998;43(4):929-40.
374. Kwon H, Sangiorgi G, Ritman E, Lerman A, McKenna C, Virmani R, et al. Adventitial vasa vasorum in balloon-injured coronary arteries: visualization and quantitation by a microscopic three-dimensional computed tomography technique. J Am Coll Cardiol 1998;32(7):2072-9.
375. Wan S, Kiraly A, Ritman E, Higgins W. Extraction of the hepatic vasculature in rats using 3-D micro-CT images. IEEE Trans Med Imaging 2000;19(9):964-71.
376. Maehara N. Experimental microcomputed tomography study of the 3D microangioarchitecture of tumors. Eur Radiol 2003;13(7):1559-65.
377. Duvall C, Robert TW, Weiss D, Guldberg R. Quantitative microcomputed tomography analysis of collateral vessel development after ischemic injury. Am J Physiol Heart Circ Physiol 2004;287(1):H302-10.

378. Bentley M, Ortiz M, Ritman E, Romero J. The use of microcomputed tomography to study microvasculature in small rodents. Am J Physiol Regul Integr Comp Physiol 2002;282(5):R1267-79.
379. Lin A, Barrows T, Cartmell S, Guldberg R. Microarchitectural and mechanical characterization of oriented porous polymer scaffolds. Biomaterials 2003;24(3):481-9.
380. Cartmell S, Huynh K, Lin A, Nagaraja S, Guldberg R. Quantitative microcomputed tomography analysis of mineralization within three-dimensional scaffolds in vitro. J Biomed Mater Res 2004;69A(1):97-104.
381. Gauthier O, Muller R, von SD, Lamy B, Weiss P, Bouler J, et al. In vivo bone regeneration with injectable calcium phosphate biomaterial: a three-dimensional micro-computed tomographic, biomechanical and SEM study. Biomaterials 2005;26(27):5444-53.
382. Ho ST, Hutmacher DW. A comparison of micro CT with other techniques used in the characterization of scaffolds. Biomaterials 2006;27(8):1362-76.
383. Bankston P, Porter G, Milici A, Palade G. Differential and specific labeling of epithelial and vascular endothelial cells of the rat lung by Lycopersicon esculentum and Griffonia simplicifolia I lectins. Eur J Cell Biol 1991;54(2):187-95.
384. Thurston G, Baluk P, Hirata A, McDonald D. Permeability-related changes revealed at endothelial cell borders in inflamed venules by lectin binding. Am J Physiol 1996;271(6 Pt 2):H2547-62.
385. Feldkamp L. Practical cone-beam algorithm. J Opt Soc Am A 1984;1:612-619.
386. Hildebrand T, Laib A, Muller R, Dequeker J, Ruegsegger P. Direct three-dimensional morphometric analysis of human cancellous bone: microstructural data from spine, femur, iliac crest, and calcaneus. J Bone Miner Res 1999;14(7):1167-74.
387. Hildebrand T, Ruegsegger P. A new method for the model-independent assessment of thickness in three-dimensional images. J Microsc 1997;185:67-75.
388. Odgaard A, Gundersen H. Quantification of connectivity in cancellous bone, with special emphasis on 3-D reconstructions. Bone 1993;14(2):173-82.
389. McDonald D, Choyke P. Imaging of angiogenesis: from microscope to clinic. Nat Med 2003;9(6):713-25.
390. Murohara T, Horowitz J, Silver M, Tsurumi Y, Chen D, Sullivan A, et al. Vascular endothelial growth factor/vascular permeability factor enhances vascular permeability via nitric oxide and prostacyclin. Circulation 1998;97(1):99-107.
391. Lopez J, Laham R, Carrozza J, Tofukuji M, Sellke F, Bunting S, et al. Hemodynamic effects of intracoronary VEGF delivery: evidence of tachyphylaxis and NO dependence of response. Am J Physiol 1997;273(3 Pt 2):H1317-23.
392. Hariawala MD, Horowitz JR, Esakof D, Sheriff DD, Walter DH, Keyt B, et al. VEGF improves myocardial blood flow but produces EDRF-mediated hypotension in porcine hearts. J Surg Res 1996;63(1):77-82.
393. Heinzer S, Krucker T, Stampanoni M, Abela R, Meyer EP, Schuler A, et al. Hierarchical microimaging for multiscale analysis of large vascular networks. Neuroimage 2006;32(2):626-36.
394. WHO The world health report 2004 - changing history Geneva: World Health Organisation World Health 2004
395. WHO World Health Statistics Annual 2001 Geneva: World Health Organisation World Health 2002

396. Jackowski M, Papademetris X, Dobrucki LW, Sinusas AJ, Staib LH Characterizing vascular connectivity from microCT images. Med Image 2005;8(2):701-08
397. Kutcher ME, Klagsbrun M, Mamluk R VEGF is required for the maintanance of dorsal root ganglia blood vessels but not neurons during development FASEB J. 2004;18(15):1952-54